

Analysis of the toxicity mechanism of zinc oxide nanoparticles aiming at their application as innovative anti-tumor agent

Dissertation

for attaining the academic degree of

Doctor rerum naturalium (Dr. rer. nat.)

in accordance with regulations of the **Max Planck Graduate Center**

of the departments

08 – Physics, Mathematics, and Computer Science,

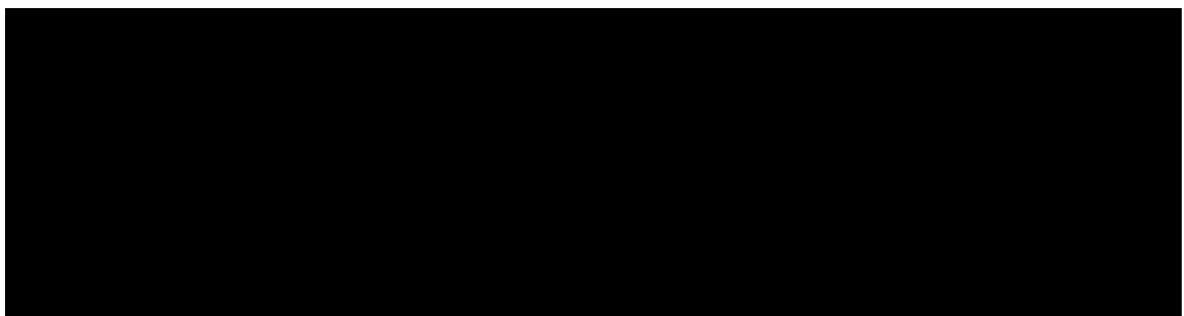
09 – Chemistry, Pharmaceutics, and Geoscience,

10 – Biology, and the University Medicine

of the Johannes Gutenberg University

submitted by

Nadine Wiesmann



Mainz, March 2019

Declaration

I hereby declare that I wrote the dissertation submitted without any unauthorized external assistance and used only sources acknowledged in the work. All textual passages which are appropriated verbatim or paraphrased from published and unpublished texts as well as all information obtained from oral sources are duly indicated and listed in accordance with bibliographical rules.

In carrying out this research, I complied with the rules of standard scientific practice as formulated in the statutes of Johannes Gutenberg University Mainz to insure standard scientific practice.

Here I declare that the scientific thesis I am now handing in has not yet been published at any other German University, or any university abroad, or any comparable institution, with the aim of attaining a scientific degree.

Here I also declare that I have not yet finished any other doctoral PhD or any similar graduation program in any of the subjects represented by the MPGC-JOGU without success.

.....
Place

Date

Nadine Wiesmann

Dedicated in gratitude to my family and friends

Zusammenfassung

Die Entwicklung innovativer nanopartikelbasierter Therapeutika ist gegenwärtig in der Medizin ein großes Thema und auch in der Tumorthherapie ruhen viele Hoffnungen auf der Nanomedizin. Gleichzeitig ist die Beurteilung unerwünschter Nebenwirkungen bei nanomedizinischen Therapeutika jedoch eine große Herausforderung, da zwischen Nanopartikeln und dem menschlichen Körper vollkommen neue Interaktionsmöglichkeiten bestehen.

Diese Doktorarbeit befasst sich mit dem Toxizitätsmechanismus von Zinkoxid-Nanopartikeln (ZnO NP) und ihrer potenziellen Anwendung als innovatives Krebstherapeutikum. Metalloxid-Nanopartikel wie ZnO NP stellen eine besondere Herausforderung dar, da sie in der Lage sind Metallionen frei zu setzen und so über viele unterschiedliche Mechanismen mit dem Körper zu interagieren. Um eine Translation dieser Partikel in die klinische Praxis zu ermöglichen ist es fundamental wichtig ihr Verhalten in biologischen Systemen im Detail zu verstehen, um so ihre Toxizität genau kontrollieren zu können.

Diese Studie wurde mit ZnO NP einer Größe von 5-22 nm durchgeführt, die ein Zeta-Potential von 20-30 mV aufwiesen. In wässrigem Medium bildeten sie schnell Agglomerate und Präzipitate. Zudem kam es zur Auflösung der Partikel und zur Freisetzung von Zinkionen (Zn^{2+}). Etwa ein Viertel aller in den Partikeln enthaltenen Zn^{2+} wurden innerhalb von vier Stunden freigesetzt. Extrazellulär frei gesetzte Zn^{2+} sind in der Lage toxische Effekte hervor zu rufen, wie Versuch mit Zinkchlorid ($ZnCl_2$) zeigen konnten. Gleichzeitig beruht die Toxizität von ZnO NP jedoch nicht allein auf der Freisetzung von Zn^{2+} , vielmehr ist auch eine direkte Interaktion der Nanopartikel mit humanen Tumorzellen vonnöten.

Wir konnten zeigen, dass es mit Hilfe einer Silikahülle ($ZnO@SiO_2$ NP) möglich ist, die Freisetzung von Zn^{2+} aus den Partikeln zu verzögern, sodass ein sicherer Transport im Blutgefäßsystem möglich wäre. Zudem könnte mit Hilfe von speziellen Liganden ein gezieltes Ansteuern des Tumors im menschlichen Körper erfolgen. Wir konnten nachzuweisen, dass $ZnO@SiO_2$ NP innerhalb von vier Stunden auf der Membran verschiedener Tumorzellen zu liegen kamen und von diesen aufgenommen wurden. Dies zeigt, dass die Synthese solcher Partikel im Prinzip möglich ist, allerdings braucht das System noch weiteren Feinschliff.

Um die Toxizität im Körper optimal kontrollieren zu können, ist es enorm wichtig zu wissen, auf welche Weise Zellen mit den Nanopartikeln interagieren und wie toxische

Effekte zustande kommen. Mit verschiedenen Tumorzelllinien konnten wir zeigen, dass sowohl nekrotischer als auch apoptotischer Zelltod vermittelt werden können.

In einem einfachen Experiment mit Plasmid-DNA in einer zellfreien Umgebung konnte gezeigt werden, dass ZnO NP in der Lage sind, Einzelstrangbrüche der DNA zu induzieren und, dass zusammen mit H₂O₂ als repräsentativer Vertreter von reaktiven Sauerstoffspezies (ROS) auch Doppelstrangbrüche entstehen, die über den alleinigen Effekt von H₂O₂ deutlich hinaus gehen. Somit sind ZnO NP auch in der Lage Tumorzellen über die DNA zu schädigen.

Es ist wohlbekannt, dass die Entstehung von ROS an der Toxizität von ZnO NP beteiligt ist, jedoch ist es Gegenstand von Diskussionen ob die ROS direkt an der Oberfläche der Partikel entstehen oder erst bei Interaktion mit einem biologischen System. Für die hier verwendeten ZnO NP konnten wir nachweisen, dass ROS nicht direkt an den Nanopartikeln entstehen, die Inkubation mit ZnO NP konnte jedoch das Superoxid-Level in den Mitochondrien anheben und zu einer Freisetzung von Cytochrom C führen. Dies deutet darauf hin, dass sowohl ROS als auch eine Schädigung der Mitochondrien eine zentrale Rolle im Toxizitätsmechanismus von ZnO NP spielen. Das Auslösen von Apoptose über den intrinsischen Weg über die Mitochondrien ist denkbar sowie eine Vermittlung des Tumorzelltods über die oben genannten DNA-Schäden.

Um zu untersuchen, ob ZnO NP eine selektive Toxizität gegenüber Tumorzellen aufweisen wurden die Effekte der Nanopartikel auf Tumorzellen mit jenen auf Fibroblasten und endotheliale Zellen verglichen. Bei einer mittleren Konzentration von 50 µg/mL ZnO NP wurden zwar die Fibroblasten weniger geschädigt als die Tumorzellen, jedoch reagierten die endothelialen Zellen sehr empfindlich. Dies zeigt, dass für eine sichere Anwendung der Nanopartikel auf jeden Fall eine entsprechende Hülle vonnöten ist, um die Partikel im Blutgefäßsystem transportieren zu können, sowie um ein aktives *Targeting* zum Tumor zu ermöglichen.

Nicht nur als alleinstehendes Tumorthapeutikum sind ZnO NP denkbar, sondern auch in Kombination mit Strahlentherapie. Hier konnten wir zeigen, dass die Nanopartikel in der Lage sind den Erfolg der Radiotherapie zu verbessern, was besonders im Licht von häufig während der Therapie entstehenden Strahlenresistenzen interessant ist.

Zusammenfassend lässt sich sagen, dass viele Details des Toxizitätsmechanismus von ZnO NP aufgedeckt werden konnten. Dies ist wichtig um diese Nanopartikel in der Zukunft sicher als innovatives Therapeutikum einsetzen zu können.

Abstract

Currently, nanomedicine is a hot topic in the development of new therapeutic agents and great hopes have been placed on nanoparticulate formulations to revolutionise tumor therapy. However, risk assessment in the field of nanomedicine constitutes a major challenge since completely new interactions between the therapeutic agent and the human body must be considered.

The aim of this study was to unveil the concepts underlying the toxicity of zinc oxide nanoparticles (ZnO NP) to be able to precisely control their behaviour in an *in vivo* setting and thus paving the way for their application as innovative anti-tumor agent. The work with ZnO NP and zinc ions released by them is particularly challenging since metal ions intervene with many signalling pathways and can elicit toxicities via a multitude of mechanisms.

We used ZnO NP of spherical shape with a size of 5–22 nm and a zeta potential of +20–30 mV. They readily formed agglomerates in aqueous solution, and they were prone to dissolution. About one fourth of the contained amount of zinc ions may be released extracellularly. Experiments with ZnCl₂—as representative of the extracellularly released zinc ions—showed that zinc ions can exert cytotoxicity once the buffer capacity of the cell culture medium is exhausted. The cytotoxicity of ZnO NP was not only attributable to the extracellular release of zinc ions but rather additionally to direct interaction with the nanoparticulate matter.

Enclosing zinc oxide nanoparticles into a silica shell (ZnO@SiO₂ NP) served the triple purposes of preventing them from premature dissolution, enabling the attachment of targeting moieties, and tracking the nanoparticles via incorporated dyes. Experiments with ZnO@SiO₂ NP showed attachment of the particles to the outer membrane of different tumor cells as well as uptake within four hours. Additionally, the silica coating delayed onset of cytotoxicity. This shows that nanoparticles with these favourable properties are technically possible, even though requiring further fine-tuning.

It is of great importance to understand the cellular reactions to treatment with ZnO NP to optimally control their toxicity in the human body. We found that ZnO NP were able to convey apoptotic and necrotic cell death to different human tumor cells. An experiment with plasmids as DNA representatives in a cell-free environment showed that ZnO NP were able to induce single strand breaks (SSB) of the DNA. Together with H₂O₂ as a representative reactive oxygen species (ROS) they additionally induced

huge amounts of double strand breaks (DSB), which surpassed the effect of treatment with H₂O₂ alone.

ROS generation is a well-established part of the mechanism of ZnO NP's cytotoxicity. However, there are still ongoing debates on whether ROS are generated directly on the surface of ZnO NP or whether they are triggered intracellularly. We showed that the ZnO NP used in this study were not able to generate ROS at their surface, but they did elevate superoxide levels in the mitochondria. Furthermore, we showed that mitochondria release cytochrome c upon treatment. Thus, damaging of the mitochondria and generation of ROS are most likely central elements of the toxicity of ZnO NP. Induction of apoptosis may occur via the mitochondrial signalling pathway. Alternatively, also above-mentioned DNA damage may play a role in induction of apoptosis.

To test for tumor-specific toxicity, we treated A549 tumor cells as well as non-malignant fibroblasts and endothelial cells with ZnO NP of different concentrations. Treatment with an intermediate concentration of 50 µg/mL revealed that fibroblasts were less affected by the treatment compared to tumor cells, but endothelial cells reacted very sensitive. Thus, treatment with ZnO NP is a double-edged sword. This means we need to prevent premature dissolution of ZnO NP in the bloodstream and add active targeting to the NP, to safely direct them to the tumor.

ZnO NP are discussed as a stand-alone treatment against cancer and as adjuvant for other therapies, for example radiotherapy. We were able to show that ZnO NP in combination with irradiation significantly reduced tumor cell survival. This demonstrates the potential of ZnO NP to improve the radiotherapeutic outcome.

We unveiled some details of the toxicity mechanism of ZnO NP. It is of great importance to truly understand the interaction between these nanoparticles and human cells in order to be able to safely apply them in an *in vivo* setting. Nanoparticulate anti-tumor agents such as ZnO NP have the potential to overcome current therapeutic hurdles in tumor treatment.

1 Table of contents

DECLARATION	I
ZUSAMMENFASSUNG	III
ABSTRACT	V
1 TABLE OF CONTENTS	VII
2 LIST OF ABBREVIATIONS	XI
3 LIST OF FIGURES	XIV
4 LIST OF TABLES	XVI
5 INTRODUCTION	1
5.1 Zinc as trace element in the human body	1
5.1.1 Body zinc content and zinc distribution	2
5.1.2 Zinc proteins	3
5.1.3 Intracellular zinc homeostasis	5
5.1.3.1 Zinc transport	6
5.1.3.2 Metallothionein and redox signalling	7
5.1.3.3 Zinc as a signalling ion	9
5.1.4 Pathological dyshomeostasis of zinc	9
5.1.4.1 Zinc intoxication and zinc deficiency	11
5.1.4.2 Zinc in tumorigenesis and tumor progression	12
5.2 Nanomedicine	15
5.2.1 Nanotechnology in tumor therapy	17
5.2.2 Nanoparticles as radiosensitizer	18
5.3 Zinc oxide nanoparticles (ZnO NP)	19
5.3.1 Biomedical application of ZnO NP	20
5.3.2 Characteristics and <i>in vitro</i> cytotoxicity mechanism of ZnO NP	21
5.3.2.1 Coatings, stability against dissolution, and protein corona	22
5.3.2.2 Cytoskeletal damage, cellular integrity, and cellular uptake	25
5.3.2.3 Generation of reactive oxygen species (ROS)	26
5.3.2.3.1 Photocatalytic activity of zinc oxide nanoparticles	27

5.3.2.3.2	ROS and mitochondrial damage—cause or effect?	28
5.3.2.4	Genotoxicity and epigenetic changes	31
5.3.2.5	Cellular fate after treatment with ZnO NP	33
5.3.3	Zinc oxide nanoparticles as innovative anti-tumor agents	34
6	AIM OF THE WORK	41
7	MATERIALS AND METHODS	42
7.1	Materials	42
7.1.1	Chemicals	42
7.1.2	Equipment	42
7.1.3	Consumables	44
7.1.4	Buffers, solutions, and cell culture medium	45
7.2	Methods	47
7.2.1	Synthesis of zinc oxide nanoparticle (ZnO and ZnO@SiO ₂ NP)	47
7.2.1.1	Characterization of the nanoparticles	48
7.2.1.1.1	Atomic absorption spectroscopy	48
7.2.1.1.2	Measurement of reactive oxygen species (ROS) at the NP	49
7.2.2	Cells, cell culture, and nanoparticle treatment	49
7.2.2.1	Cells	49
7.2.2.2	Cell culture	50
7.2.2.3	Nanoparticle treatment conditions	50
7.2.3	Viability measurement	51
7.2.4	<i>In vitro</i> DNA damage analysis	52
7.2.5	Microscopy	52
7.2.5.1	Light Microscopy	52
7.2.5.2	Confocal laser scanning microscopy (CLSM)	52
7.2.5.3	Immunofluorescence	53
7.2.6	Flow cytometry	53
7.2.6.1	Apoptosis assay	54
7.2.6.2	Cell cycle analysis	55
7.2.6.3	MitoSOX™ Red mitochondrial superoxide indicator assay	56
7.2.6.4	Cytochrome c release assay	57
7.2.7	Colony formation assay (CFA)	58
7.2.8	Expression analysis by SDS-PAGE and western blotting	59
7.2.8.1	Harvesting of the cells	59
7.2.8.2	Preparation of the lysates for the SDS-PAGE	59
7.2.8.3	Running of the SDS-PAGE	60
7.2.8.4	Western blotting by wet-tank method	60
7.2.9	Statistical evaluation	61

8	RESULTS	63
8.1	Characterization of ZnO NP	65
8.2	What causes the toxicity of ZnO NP?	66
8.2.1	Zinc ion release from ZnO NP	66
8.2.2	Toxicity of released zinc ions	67
8.2.3	Influence of changes in pH value and ionic strength	68
8.2.4	Particles vs. ions—how do the NP contribute to the toxicity?	70
8.3	ZnO@SiO ₂ NP—ZnO NP covered by a silica coating	71
8.3.1	Transmission electron microscopy	71
8.3.2	Comparative toxicity analysis of ZnO@SiO ₂ NP and ZnO NP	72
8.3.3	Cellular uptake	72
8.4	Cellular reaction to treatment with ZnO NP	74
8.4.1	Morphology	74
8.4.2	Apoptosis and necrosis	75
8.4.3	Cell cycle distribution	78
8.5	Genotoxic effects of ZnO NP	79
8.5.1	<i>In vitro</i> DNA damage analysis	79
8.6	The role of mitochondria and reactive oxygen species (ROS)	80
8.6.1	MitoSOX™ Red assay	80
8.6.2	Cytochrome c release assay	81
8.6.3	Western blot analysis of p53, bax, bcl-xL, and caspase-9	81
8.7	Toxicity of ZnO NP against malignant and non-malignant cells	84
8.8	ZnO NP as a radiosensitizer	86
9	DISCUSSION	89
9.1	The nature of ZnO NP used in this study	89
9.2	Toxicity of ZnO NP is not solely based on release of zinc ions	90
9.3	Zinc oxide nanoparticles covered by a silica shell	92
9.4	ZnO NP can convey apoptotic and necrotic cell death	93
9.5	ZnO NP induce DNA damage	95
9.6	Mitochondria are central for the toxicity of ZnO NP	96

9.7 ZnO NP can damage malignant and non-malignant cells	99
9.8 ZnO NP can reduce survival of tumor cells after irradiation	99
10 CONCLUSIONS	100
11 REFERENCES	101
12 APPENDIX	129
13 ACKNOWLEDGEMENT	148
14 CONFERENCE CONTRIBUTIONS	150
15 PUBLICATIONS	151
16 CURRICULUM VITAE	152

2 List of abbreviations

8-oxo-dG	8-Oxo-2'-deoxyguanosine, oxidized derivative of deoxyguanosine
AAS	atomic absorption spectroscopy
ANOVA	analysis of variance
APTES	(3-aminopropyl)triethoxysilane
ATP	adenosine triphosphate
ATPase	adenosine triphosphatase
AU	arbitrary units
BMSC	bone-marrow derived mesenchymal stem cells
bp	base pair
BPB	bromophenol blue
BSA	bovine serum albumin
C	complex
CB	conduction band
CFA	colony formation assay
CLSM	confocal laser scanning microscopy
CMA	cellular metabolic activity
CMV	cytomegalovirus
Cyt C	cytochrome c
DEPC	diethyl pyrocarbonate
DMEM	Dulbecco's Modified Eagle Medium
DMSO	dimethyl sulfoxide
DNA	deoxyribonucleic acid
DSB	double strand break
dsDNA	double stranded DNA
DSMZ	German Collection of Microorganisms and Cell Cultures
ECD	extracellular domain
EPR effect	enhanced permeability and retention effect
ESCC	oesophageal squamous-cell carcinoma
ETC	electron transport chain
FAD / FADH ₂	flavin adenine dinucleotide
FCS	fetal calf serum
FDA	Food and Drug Administration
FITC	fluorescein isothiocyanate
FSC	forward scatter
GOF	gain-of-function
GRAS	Generally Recognized As Safe
HBSS	Hanks' balanced salt solution
HCC	hepatocellular carcinoma

HEPES	4-(2-hydroxyethyl)-1-piperazineethanesulfonic acid
HNSCC	head and neck squamous cell carcinoma
HRP	horseradish peroxidase
HU	heat up
HUVEC	human umbilical vein endothelial cell
IC ₅₀	half maximal inhibitory concentration
INT	iodonitrotetrazolium chloride
ISO	International Organization for Standardization
kB	kilobases
LD ₅₀	median lethal dose
LDH	lactate dehydrogenase
MDCK	Madin-Darby canine kidney cells
MOMP	mitochondrial outer membrane permeabilization
MP	milk powder
MPGC	Max Planck Graduate Center
MRE	metal response element
mRNA	messenger RNA (ribonucleic acid)
MT	metallothionein
MTF 1	metal regulatory transcription factor 1
NAC	N-acetylcysteine
NAD ⁺ / NADH	nicotinamide adenine dinucleotide
NHDF	normal human dermal fibroblasts
NK cells	natural killer cells
NP	nanoparticles
NSCLC	non-small cell lung cancer
PAA	polyacrylic acid
PAL	proline-alanine-leucine-containing
PBMC	peripheral blood mononuclear cells
PBS	phosphate buffered saline
PCR	polymerase chain reaction
PDT	photodynamic therapy
PEG	polyethylene glycol
PEGTES	trimethoxysilane functionalized polyethyleneglycol
PI	propidium iodide
pOMC	primary oral mucosa cells
PVDF membrane	polyvinylidene fluoride membrane
Q	ubiquinone
ROS	reactive oxygen species
RT	room temperature
SCC	squamous cell carcinoma
SCOGS	Select Committee on GRAS Substances

SD	standard deviation
SDS	sodium dodecyl sulphate
SDS-PAGE	sodium dodecyl sulphate polyacrylamide gel electrophoresis
SF	surviving fraction
SG	space group
SLN	solid lipid nanoparticles
SOD	superoxide dismutase
SSB	single strand break
SSC	side scatter
ssDNA	single stranded DNA
STR	short tandem repeats
TBS	Tris buffered saline
TBST ₂₀	Tris buffered saline with Tween ₂₀
TCA cycle	tricarboxylic acid cycle
TEM	transmission electron microscopy
TEOS	tetraethyl orthosilicate
TFIIIA	transcription factor IIIA
TMB	3,3',5,5'-tetramethylbenzidine
Tris	tris(hydroxymethyl)aminomethane
VB	valence band
WHO	World Health Organization
XRD	x-ray diffraction
ZIP	Zrt- and Irt-like protein
ZnO NP	zinc oxide nanoparticles
ZnO@SiO ₂ NP	zinc oxide nanoparticles with silica coating
ZnT	zinc transporter
γH2AX	H2A histone family member X phosphorylated on serine 139

3 List of figures

Figure 1: Chemical elements of the human body	1
Figure 2: Zinc distribution in the human body.....	2
Figure 3: Carbonic anhydrase as a zinc protein	3
Figure 4: Structural features of zinc-finger proteins.....	4
Figure 5: Intracellular concentration of unbound divalent metal ions and Irving-Williams series	5
Figure 6: Putative structure of ZIP and ZnT zinc transporters	6
Figure 7: Structure of metallothionein.....	7
Figure 8: Cellular zinc and redox buffering capacity of metallothionein.....	8
Figure 9: Insulin hexamer with central zinc atoms.....	10
Figure 10: Clinical symptoms of zinc excess and zinc deficiency.....	12
Figure 11: Scale of nanomaterials.....	15
Figure 12: Different nanotherapeutic platforms	16
Figure 13: Zinc oxide nanostructures	19
Figure 14: Overview over the most important characteristics which contribute to the cytotoxicity of ZnO NP	21
Figure 15: Transition of NP from their synthetic to the biological identity	23
Figure 16: Cell-nanoparticle interactions	24
Figure 17: Nanotoxicity conveyed by the generation of ROS	26
Figure 18: Photocatalytic activity of zinc oxide nanoparticles	27
Figure 19: Mitochondrial tricarboxylic acid cycle and electron transport chain	29
Figure 20: Interaction of zinc ions with the nucleobases in the DNA.....	31
Figure 21: Cell death mechanisms.....	33
Figure 22: Principle of flow cytometry.....	54
Figure 23: Graphical representation of the different aspects of the cell–nanoparticle interaction.....	64
Figure 24: Characterization of ZnO NP by TEM and x-ray diffraction.....	65
Figure 25: Zinc ions released from ZnO NP	66
Figure 26: Toxicity of released zinc ions	67
Figure 27: Comparative analysis of the toxicity of MgCl ₂ , ZnCl ₂ , and ZnO NP	68
Figure 28: Dose-response curves for the inhibition of the cellular metabolic activity (CMA) by treatment with ZnO NP (A) or ZnCl ₂ (B), respectively	69
Figure 29: Cellular viability after treatment with ZnO NP or released zinc ions	70

Figure 30: TEM imaging of ZnO@SiO ₂ NP	71
Figure 31: Comparison of the toxicity of ZnO NP and ZnO@SiO ₂ NP	72
Figure 32: Fluorescent imaging of ZnO@SiO ₂ NP	73
Figure 33: CLSM imaging of cells treated with ZnO@SiO ₂ NP	73
Figure 34: Morphology of different tumor cell lines after treatment with ZnO NP	74
Figure 35: Analysis of necrotic and apoptotic cell death in A549 cells	75
Figure 36: Analysis of the mechanism of cell death in A549, HNSCCUM-02T, HeLa, and T24 cells	77
Figure 37: Distribution between the cell cycle phases after ZnO NP treatment.....	78
Figure 38: DNA damage analysis in cell-free environment using plasmids	79
Figure 39: Assessment of the mitochondrial superoxide level.....	80
Figure 40: Cytochrome c release assay	81
Figure 41: Relative expression levels of p53, bax, bcl-xL, and caspase-9 in untreated A549, HeLa, HNSCCUM-02T, and T24 cells.....	82
Figure 42: Expression of p53, caspase-9, bax, and bcl-xL 4 h and 20 h after treatment with ZnO NP	83
Figure 43: Toxicity of ZnO NP towards malignant and non-malignant cells	85
Figure 44: Colony formation assay (CFA) after ZnO NP treatment	86
Figure 45: Part of the intrinsic / mitochondrial pathway of apoptosis.....	97

4 List of tables

Table 1: Association between deregulated zinc transporters and tumorigenesis	13
Table 2: Selective anti-cancer activity of zinc, zinc compounds, and ZnO NP	35
Table 3: Equipment	42
Table 4: Consumables	44
Table 5: Treatment groups for the colony formation assay	58
Table 6: Antibodies and corresponding incubation strategies	61
Table 7: Treatment groups for the colony formation assay	86
Table 8 corresponding to Figure 25.....	129
Table 9 corresponding to Figure 26.....	129
Table 10 corresponding to Figure 27.....	130
Table 11 corresponding to Figure 29.....	131
Table 12 corresponding to Figure 31.....	131
Table 13 corresponding to Figure 35.....	132
Table 14 corresponding to Figure 36.....	139
Table 15 corresponding to Figure 37.....	141
Table 16 corresponding to Figure 39.....	142
Table 17 corresponding to Figure 40.....	143
Table 18 corresponding to Figure 41.....	143
Table 19 corresponding to Figure 42.....	143
Table 20 corresponding to Figure 43.....	144
Table 21 corresponding to Figure 44.....	145

5 Introduction

This chapter serves to guide the reader into the topic of this doctoral thesis. We begin with an overview over the role of zinc in the human body (5.1) in general. Then I will provide an introduction into the application of nanomaterials in modern medicine in general (5.2), and in tumor therapy (5.2.1), and in radiation therapy (5.2.2). This leads over to the introduction of zinc oxide nanoparticles (5.3), their biomedical application (5.3.1), and their characteristics which can convey cytotoxicity (5.3.2). Finally, I will provide an overview over the state of research concerning the application of zinc oxide nanoparticles as innovative antitumor agent (5.3.3).

5.1 Zinc as trace element in the human body

Our knowledge of the chemical elements of life is rather new. A hundred years ago chemistry was strictly divided into “inorganic” and “organic” chemistry believing that the latter does suffice to describe the main chemical processes in living organisms. This resulted in almost complete disappearance of teaching of inorganic chemistry from the curriculum of medicine and biology students. In the last decades we learned that this division of chemistry does not represent living systems accurately as the name implies. (Robert J. P. Williams 1991) Figure 1 shows the essential chemical elements of the human body.

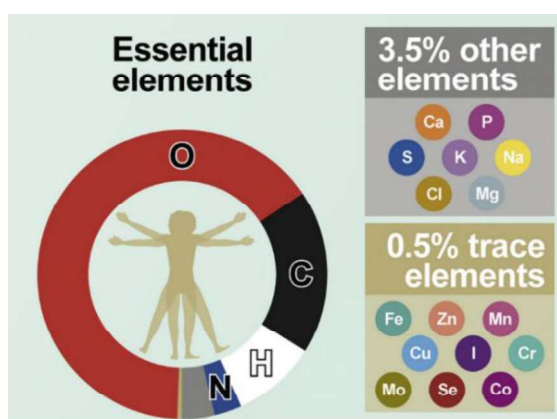


Figure 1: Chemical elements of the human body

The four chemical elements oxygen, carbon, hydrogen, and nitrogen make about 96% of the mass of the human body. Further 3.5% of body is composed of seven chemical elements, namely calcium, phosphorus, sulphur, potassium, sodium, chlorine, and magnesium. The remaining constituents of the body are trace elements, among them zinc. Modified according to (Huat et al. 2019).

Those elements which are present in only small amounts turned out to be also of utmost importance for many body functions. (Prashanth et al. 2015; Huat et al. 2019)

5.1.1 Body zinc content and zinc distribution

Essential trace elements are understood to be chemical elements that are needed in very minute quantities for proper growth, development, and physiology of the organism. Only in the sixties of the last century the essentiality of zinc as a trace element for humans was established. Hitherto significant clinical problems stemming from zinc deficiency were considered improbable. (Prasad 2013; Roohani et al. 2013; Al-Fartusie et al. 2017)

Zinc is a chemical element with the symbol “Zn”, the proton number $Z = 30$, an atomic weight of 65.4, and it is the first element of group 12 of the periodic table. Zinc is the second most common metal present in the human body at about 2–4 g, after iron at about 3–5 g but before copper at about 0.1–0.2 g. (Kloubert et al. 2015; Prashanth et al. 2015; Ollig et al. 2016; Al-Fartusie et al. 2017) In contrast to iron, which is predominantly found in red blood cells, zinc is distributed throughout the entire human body, mostly intracellularly. The plasma concentrations of zinc range only from 12-16 μM . In the blood it is mostly bound to albumin (60%) and to a lesser extent to transferrin (10%). (Osredkar 2011; Kloubert et al. 2015; Ollig et al. 2016) Figure 2 shows the zinc distribution within the human body. Intracellularly about 30-40% of the total cellular zinc is in the nucleus, about 50% is in the cytoplasm and its organelles, and the rest is associated with membranes. (Vallee et al. 1993)

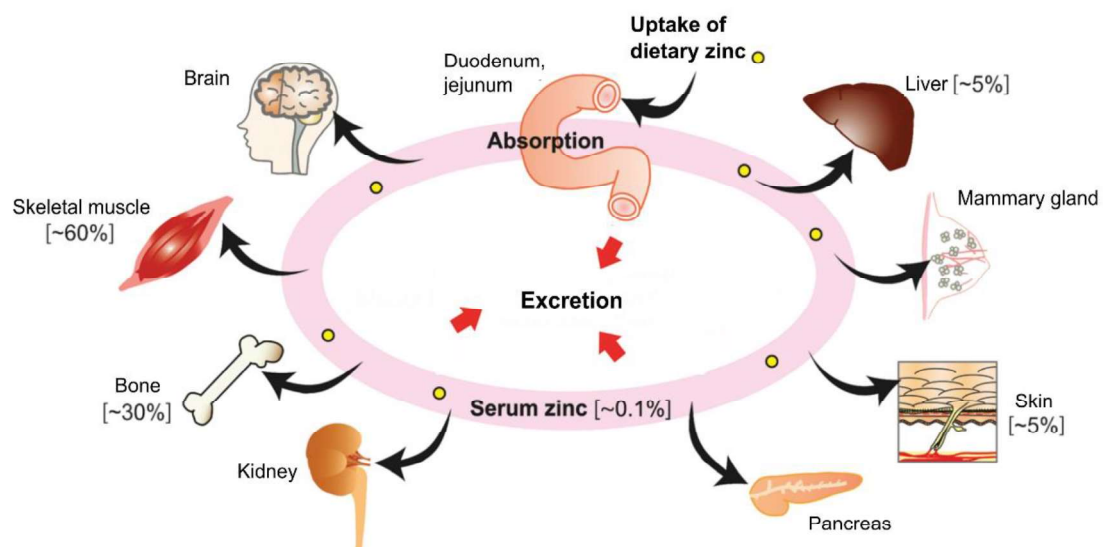


Figure 2: Zinc distribution in the human body

Dietary zinc is primarily absorbed in the duodenum and the jejunum and then distributed to peripheral tissues such as skeletal muscle (~60%), bone (~30%), liver (~5%), skin (~5%), and other tissues and organs, including the brain, kidney, and pancreas. When in excess, zinc is excreted from the body through gastrointestinal secretion, sloughing of mucosal cells and integument, and renal excretion. Modified according to (Golan et al. 2017).

5.1.2 Zinc proteins

Zinc plays a very important role for many vital bodily functions, such as cell proliferation, differentiation, and metabolic activity. We can see this from the fact that up to 3'000 proteins potentially bind to zinc. It is estimated that zinc is a cofactor for the function of approximately 4–10% of all proteins encoded in the genome of organisms ranging from prokaryotic to eukaryotic. Zinc is essential for the function of 200 human enzymes of all enzyme classes. (Sandstead 1994; Andreini et al. 2006a, 2006b; Osredkar 2011; Kloubert et al. 2015; Prashanth et al. 2015)

Many zinc proteins are only present in minor concentrations in the human body, or they are restricted to certain tissues. This hindered the discovery of the diversity of zinc protein chemistry until more elaborate analytical methods came up. As the first zinc protein, carbonic anhydrase was discovered in 1939. Carbonic anhydrase is responsible for the conversion of carbon dioxide into bicarbonate, and vice versa, in the blood. Its structure is shown in Figure 3.

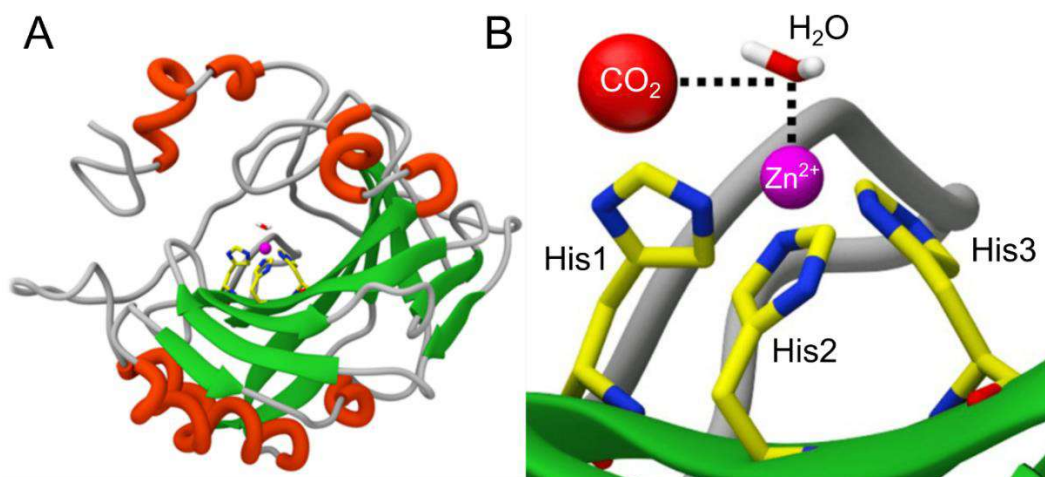


Figure 3: Carbonic anhydrase as a zinc protein

(A) shows the ribbon representation of carbonic anhydrase with its active centre containing a zinc ion. The active site (B) is composed of a zinc ion which is coordinated by three histidine (His1-3) and one water molecule. Modified according to (Fu et al. 2018).

It took fifteen more years to discover that another important protein is zinc dependent—the carboxypeptidase—which cleaves the peptide linkage during digestion of proteins. Finally, the zinc-finger proteins were discovered from about the 1980s onward, which dramatically increased the number of known zinc dependent proteins. Zinc-finger proteins mostly bind nucleic acids. They are characterized by a repetitive sequence most often consisting of cysteine and histidine residues, interrupted by spacer sequences. The cysteine and histidine residues are coordinated by zinc ions to

stabilize the finger-like structure of these proteins which conveys their nucleic acid binding capacity, as shown in Figure 4. (Osredkar 2011; Maret 2013) The zinc-finger domain is one of the most frequently used DNA-binding motifs in eukaryotic transcription factors and the zinc-finger proteins are one of the most abundant groups of proteins. They are involved in transcriptional regulation, protein degradation, signal transduction, DNA repair, migration, and numerous other cellular processes. (Cassandri et al. 2017) Besides zinc-finger proteins, also other transcription factors such as the prominent transcription factor p53 require zinc ions for proper structure and folding. (Loh 2010)

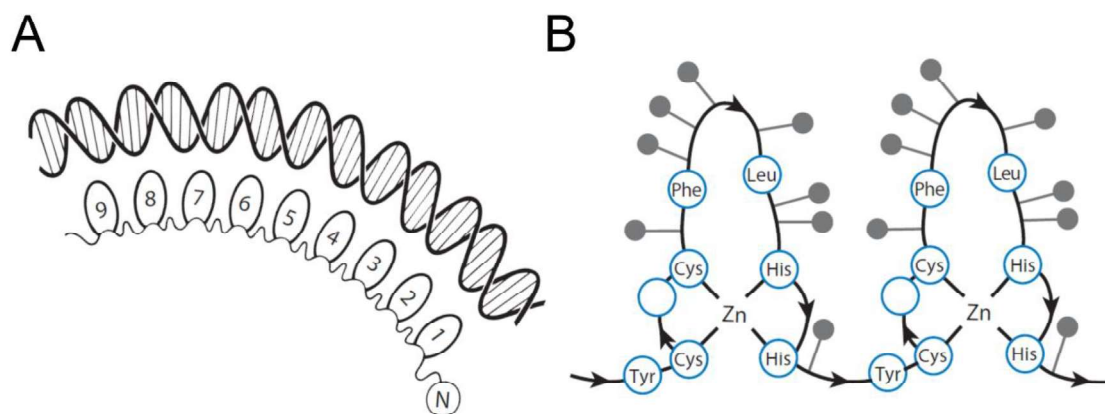


Figure 4: Structural features of zinc-finger proteins

(A) shows the modular design of transcription factor IIIA (TFIIIA) as archetype of zinc-finger proteins. Each of the 9 “zinc fingers” of the protein neatly fits into the major groove of the DNA, which enables sequence specific binding. The zinc ion in each “zinc finger” is coordinated tetrahedrally by two histidine and two cysteine residues. Thereby the alpha helices are stabilized that recognize the DNA in a sequence specific manner (B). Modified according to (Klug 2010).

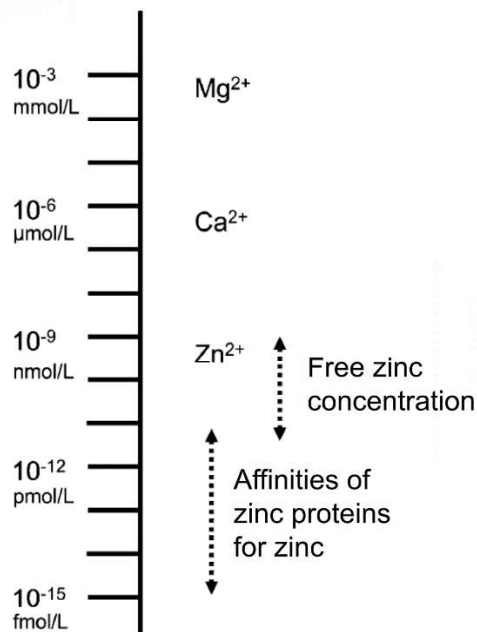
Zinc can perform catalytic, regulatory, and structural roles in proteins, and it has a very flexible coordination geometry with coordination numbers varying from two to eight. The kinetic lability of zinc complexes allows zinc proteins to rapidly shift conformation to perform different biological reactions. This also involves changes in the coordination geometry. (Vallee et al. 1993; McCall et al. 2000; Osredkar 2011; Krężel et al. 2016)

Zinc ions are mainly coordinated by the side chains of four different amino acids: aspartic acid, glutamic acid (at the carbonyl oxygen of the carboxyl group), cysteine (at the sulphur atom), and histidine (at the nitrogen atom in the imidazole ring). (Osredkar 2011; Laitaoja et al. 2013) Coordination by histidine is most common, followed by cysteine. (McCall et al. 2000)

5.1.3 Intracellular zinc homeostasis

The total intracellular zinc concentration in human cells ranges from 200 to 300 μM , and even into the mM range in specialised vesicles. Cells maintain the amount of zinc that is not bound to any binding partners—known as “free zinc”—strictly at extremely low levels in the picomolar range. This is at least six or seven magnitudes lower than the total intracellular zinc amount. (Maret 2013) This is related to the Irving-Williams series, shown in Figure 5. It states that zinc, besides copper, has the highest affinity for ligands among the transition metal ions. Cells keep free zinc levels low because zinc has such a high affinity for forming complexes. (Maret 2015) Regulation of the free zinc level is achieved not only by binding of zinc to specific metal binding proteins and low molecular weight ligands—known as buffering—but also by sequestration in intracellular vesicles or transport out of the cell—the so-called muffling. Having to compartmentalize the ion so extensively is characteristic for zinc. (Maret 2013, 2015; Prashanth et al. 2015)

(A) Cellular concentration of divalent redox-inert metal ions



(B) Irving-Williams series

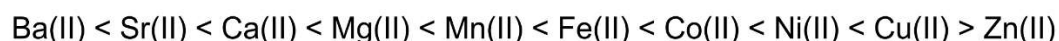


Figure 5: Intracellular concentration of unbound divalent metal ions and Irving-Williams series

Magnesium, calcium, and zinc are the three major redox-inert metal ions, which are involved in cellular regulation. They cover many orders of magnitude with respect to intracellular concentration (A) and affinities, which are described by the Irving-Williams series (B). Modified according to (Maret 2013).

As small as the free zinc concentration may be, it is not negligible and it is safeguarded by a notable intracellular zinc-buffering capacity in the micromolar range. ((Krężel et al. 2006) and personal communication with Artur Krężel). In these cellular conditions cells react extremely sensitive to changes in the free zinc concentration once the buffering capacity is exhausted. (Bozym et al. 2010)

5.1.3.1 Zinc transport

The enormously elaborate system of tight intracellular zinc control necessitates a high amount of zinc transporters. Zinc as a charged divalent cation is not able to cross the cellular membrane by passive diffusion. Thus, to maintain cellular zinc homeostasis, zinc transporters are needed. (Kloubert et al. 2015)

Human cells contain at least 10 zinc transporters of the ZnT family and 14 of the ZIP family. Zinc transporters of the ZnT family decrease the cytoplasmic zinc level by promoting the efflux of zinc out of the cell or into intracellular vesicles and organelles. ZIP transporters on the other hand increase the cytoplasmic zinc level by promoting the uptake of zinc from the extracellular space and the release of zinc from vesicles and organelles. The putative structure of both transporter families is shown in Figure 6.

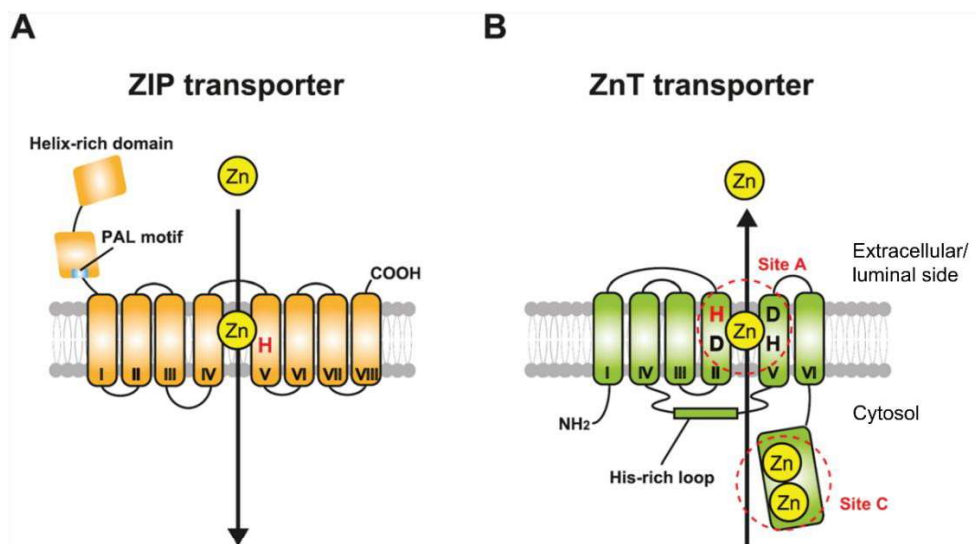


Figure 6: Putative structure of ZIP and ZnT zinc transporters

(A) ZIP transporters are thought to have eight transmembrane helices. The histidine residue (H) in the transmembrane helix V is believed to be part of an intramembranous zinc-binding site. This motif may be involved in determining the metal cation specificity. Members of the LIV-1 subfamily—the largest ZIP transporter family—have a proline-alanine-leucine-containing (PAL) domain and a helix-rich domain in the large extracellular domain (ECD). (Zhang et al. 2016) (B) Most ZnT transporters are thought to harbour six transmembrane helices. Two histidine (H) and two aspartate (D) residues in the transmembrane helices II and V form the intramembranous zinc-binding site (site A). The cytosolic histidine-rich loop has been implicated in sensing zinc levels and modulating metal substrate specificity. The cytosolic carboxyl-terminal portion exhibits another zinc-coordination site (site C). Modified according to (Golan et al. 2017).

Both transporter families exhibit unique tissue-specific expression and are subjected to complex regulation by different physiological stimuli such as hormones, cytokines, and the zinc supply situation. (Cousins et al. 2006; Roohani et al. 2013)

To perceive the amount of zinc that is present, cells express the metal regulatory transcription factor 1 (MTF 1), the only known eukaryotic zinc ion sensor, which itself is a zinc-finger protein. It is involved in the cellular response to various stress conditions, primarily exposure to metals such as cadmium, mercury, lead, zinc, and copper, but also to hypoxia or oxidative stress. By binding to the metal response element (MRE) in the promoter region MTF 1 controls the expression of zinc-dependent genes, in particular the expression of metallothioneins (MTs). (Maret et al. 2007; Günther et al. 2012; Maret 2013)

5.1.3.2 Metallothionein and redox signalling

Humans have at least a dozen different metallothioneins. These are comprised of 60 to 68 amino acids, of which are 20 or 21 cysteines. MTs can bind up to seven zinc ions. Each zinc ion is being complexed by four sulphurs of the surrounding cysteines, as shown in Figure 7.

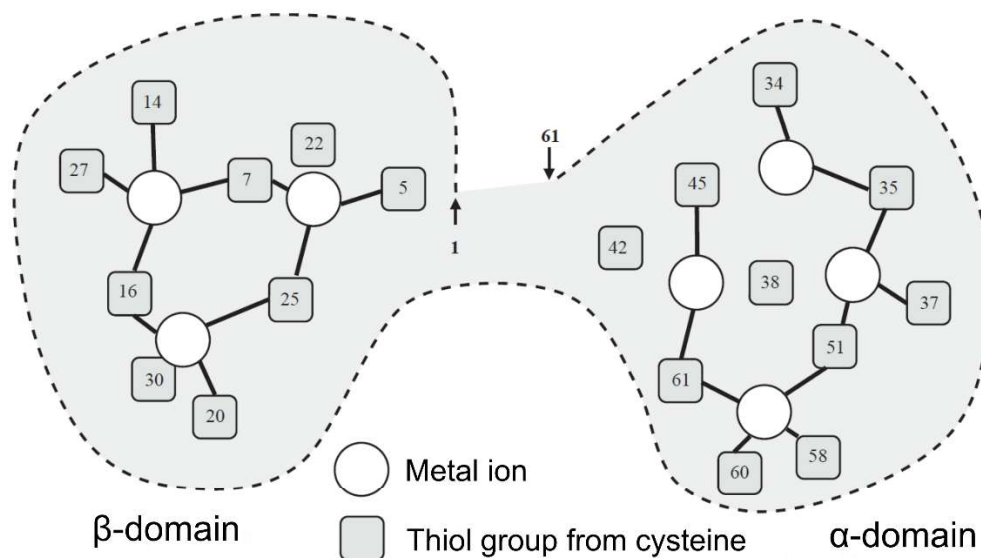


Figure 7: Structure of metallothionein

Modified according to (Gumulec et al. 2012).

Two remarkable properties of MTs confer special importance to these proteins. One is that even though all seven zinc ions are in tetrathiolate coordination environments, they are bound with different affinities. As a result, MTs do not simply bind any metal

ion they come across but can rather serve both as dynamic zinc acceptors and zinc donors.

Even though zinc is a transition metal, zinc ions in biological systems only occur at the oxidation state +2, meaning zinc is redox-inert. (Ollig et al. 2016). At first glance it appears paradoxical that zinc which is not redox-active in contrast to copper and iron, has profound impact on the redox metabolism and the cellular management of oxidative stress. (Hao et al. 2005) Part of this special property of zinc in biological systems is attributable to the second remarkable characteristic of MTs: MTs are redox proteins which are influenced by the redox environment. Oxidation of the sulphur donors leads to zinc release. Reduction of the oxidized sulphurs leads to restoration of the zinc binding capacity. Thus, the structure of MTs *in vivo* is dynamic depending on the metal ion availability and the redox state. It was shown that the thiols in MT exist in three states: free, metal-bound, and disulphide. This means that the protein exists as fully reduced apoprotein (thionein), and fully oxidized apoprotein (thionin), as well as mixtures of these states. Thionein and thionin form a redox pair and their ratio depends on the cellular redox state. This state is directly linked to zinc homeostasis as reactive oxygen species can release zinc from MTs. Thus, redox signals can be converted to zinc signals and vice versa. (Krężel et al. 2007; Maret 2013; Krężel et al. 2017) This regulatory mechanism is called “redox-switch”, which is depicted in Figure 8. (Pace et al. 2014)

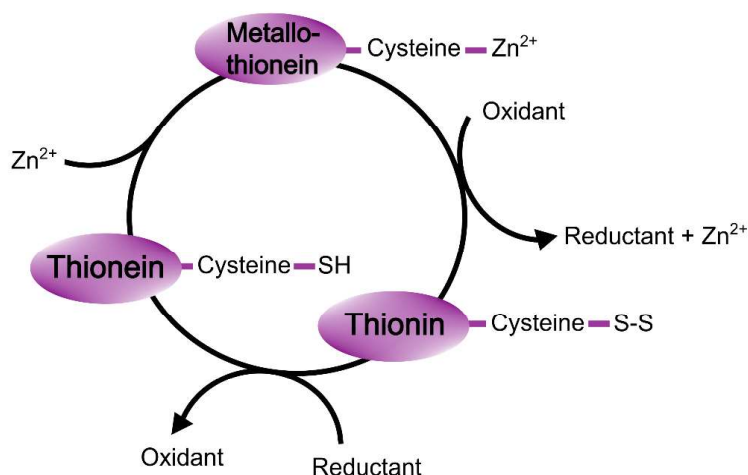


Figure 8: Cellular zinc and redox buffering capacity of metallothionein

Modified according to (Krężel et al. 2007; Maret 2009).

Moreover, zinc is involved in the reaction to oxidative stress as a structural component of the copper/zinc superoxide dismutase (SOD). It promotes the conversion of two

superoxide radicals to hydrogen peroxide and molecular oxygen, which is an important step to limit toxic effects of oxidative stress. Additionally, zinc affects the expression of the glutamate-cysteine ligase, which is the rate-limiting enzyme of glutathione *de novo* synthesis. Furthermore, zinc can compete with redox-active metal ions such as iron and copper for binding sites at proteins and nucleotides. The replacement of these ions prevents the site-specific formation of highly reactive radicals through Fenton chemistry in case of oxidative stress since zinc is not redox-active and cannot participate in these reactions.

As stated above, zinc influences the reaction to oxidative stress via multiple indirect mechanisms. Deficiency in zinc favours the manifestation of oxidative stress and resulting degenerative diseases. Nevertheless, referring to zinc as an antioxidant without further qualification does not tell the whole truth, as lack of zinc as well as excess zinc have pro-oxidant effects. Zinc can have anti- and pro-apoptotic, anti- and pro-inflammatory and cytoprotective as well as cytotoxic effects depending on the concentration. Zinc was quite aptly described as “essential toxin”. (Powell 2000; Plum et al. 2010; Kloubert et al. 2015; Jarosz et al. 2017; Marreiro et al. 2017; Maret 2019)

5.1.3.3 Zinc as a signalling ion

Recently it became apparent that zinc ions themselves can perform regulatory tasks akin to calcium ions. (Maret 2013) On top of the normal capacity to export an excess of zinc, several cells—including neurons with specific glutamatergic synaptic vesicles—have the capacity to secrete zinc ions through calcium-dependent exocytosis. Zinc can serve special tasks within vesicles in cells of the pancreas, the prostate and mammary epithelium, the intestine, and the immune system. Additionally, intracellular signalling cascades are influenced by zinc waves. (Maret 2017)

5.1.4 Pathological dyshomeostasis of zinc

Dysregulation of the zinc homeostasis can also be involved in pathobiology, as one prominent example I want to discuss diabetes mellitus. The β cells of the pancreas are known to contain very high zinc concentrations, which are needed for the appropriate synthesis of insulin, its storage, and its structural stability. The three-dimensional structure of insulin is shown in Figure 9.

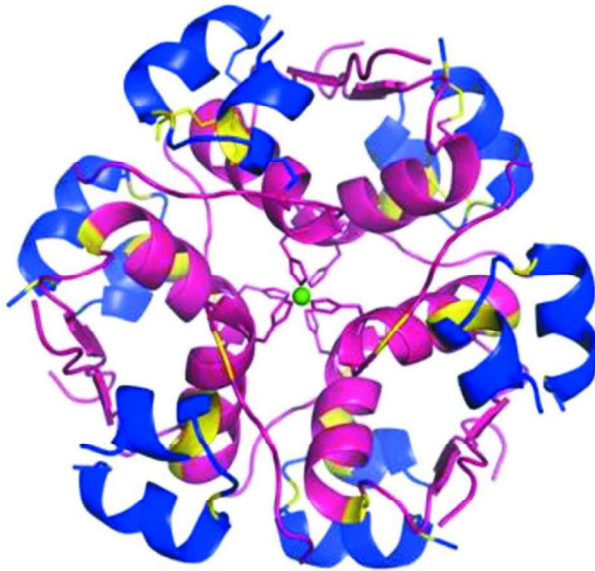


Figure 9: Insulin hexamer with central zinc atoms

Insulin in its storage form is stabilized as a hexamer by two central zinc atoms (green), which are coordinated by three histidine residues (purple). This figure shows the T₆ bovine insulin hexamer, one of the three known 3D structures of insulin. The A chain (21 amino acids) is coloured in blue and the B chain (30 amino acids) is coloured in purple. Both chains are held together by disulphide bonds, coloured in yellow. Both zinc atoms lie on one axis, thus only one is visible in the figure. Modified according to (Margiolaki et al. 2013).

Since pancreatic cells produce large amounts of ATP, they are especially prone to oxidative stress and as zinc is involved in many mechanisms to detoxify ROS, pancreatic cells can easily sustain damage in case of zinc deficiency. Additionally, a polymorphism in the zinc transporter ZnT8 may increase the susceptibility to type 2 diabetes. Thus, proper zinc supply and signalling influence endocrine functions on multiple levels. This demonstrates the far-reaching functions that zinc performs in our body. (Fukunaka et al. 2018)

Furthermore, zinc has also been implicated in the pathogenesis of other diseases such as multiple sclerosis (Choi et al. 2017a), epilepsy (Doboszewska et al. 2018), and Alzheimer's disease (Watt et al. 2010). It is becoming increasingly clear, that the maintenance of zinc homeostasis is important on multiple levels for the health of the human body.

Even though the importance of zinc on the human body's health is far from being completely elucidated it can be assumed that its impact is at least as far-reaching as that of iron. (Maret 2013)

5.1.4.1 Zinc intoxication and zinc deficiency

Compared to several other metal ions, zinc is relatively harmless and non-toxic, as the body has very efficient strategies to safeguard zinc homeostasis on cellular and systemic levels.

Severe impact on human health by intoxication with zinc is a rather rare event which is limited to some anecdotal reports. Oral uptake of large amounts of zinc is highly improbable as vomiting is induced at amounts of approximately 200–400 mg zinc. (Plum et al. 2010) Acute oral toxicity in rats exposed to zinc salts was found to give LD₅₀ (median lethal dose) in the range of approximately 200–600 mg/kg body weight depending on the zinc salt administered. LD₅₀ for intraperitoneal injection ranged from approximately 30 to 70 mg/kg. (Maret et al. 2006) Uptake of large dose of zinc over extended periods of time is frequently associated with copper deficiency. (Plum et al. 2010)

Exposure to large amounts of zinc by inhalation can occur via zinc-containing smoke (300 mg zinc/m³ and higher) which causes the so-called metal fume fever. Symptoms of this reversible syndrome include fever, muscle soreness, nausea, fatigue, and respiratory effects.

Dermal absorption of zinc is fathomable; however creams, lotions, and other products for external application contain concentrations that are not considered a noteworthy toxicological risk. (Plum et al. 2010)

Systemic zinc toxicity is not a major health problem. Instead estimates suggest frequency of zinc deficiency worldwide to be higher than 20%. Adequate supply with zinc is particularly important for the immune system as zinc is involved in several immunological functions. In severe cases of zinc deficiencies patients present additional clinical manifestations. Figure 10 sums up the most important clinically known symptoms of both zinc excess and zinc deficiency.

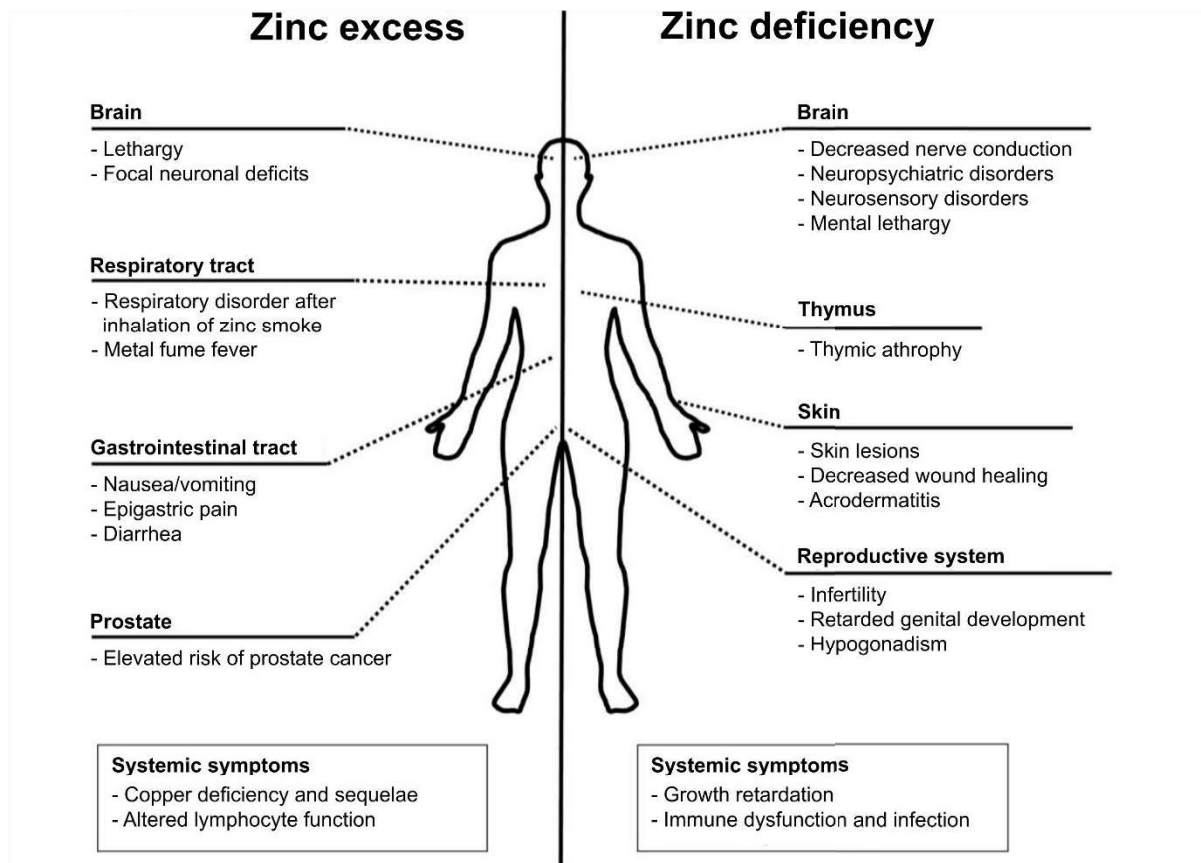


Figure 10: Clinical symptoms of zinc excess and zinc deficiency

Modified according to (Plum et al. 2010).

5.1.4.2 Zinc in tumorigenesis and tumor progression

As zinc is a critical component of numerous proteins and signalling pathways it is not surprising that it also plays a role in tumorigenesis and tumor progression. Zinc levels in blood serum are typically decreased in tumor patients. (Gumulec et al. 2014) Different studies within the last years were able to demonstrate that in some cancer entities there is an association between a marked increase or decrease in the intracellular zinc level and malignant transformation of formerly healthy tissue. In many cases the disturbance of the zinc homeostasis was linked to the deregulation of one of the zinc transporters as depicted in Table 1.

Table 1: Association between deregulated zinc transporters and tumorigenesis

Modified according to (Mudipalli et al. 2017; Takatani-Nakase 2018).

Transporter	Cancer type	Zinc level	Reference
ZIP1	Prostate	Reduced	(Milon et al. 2010; Costello et al. 2011a; Zou et al. 2011; Costello et al. 2015)
ZIP2	Prostate	Reduced	(Desouki et al. 2007)
ZIP3	Prostate, pancreatic	Reduced	(Desouki et al. 2007; Costello et al. 2011b; Costello et al. 2012; Franklin et al. 2014)
ZIP14	Hepatocellular	Reduced	(Franklin et al. 2012)
ZIP6	Breast	Increased	(Grattan et al. 2012; Matsui et al. 2017)
ZIP7	Breast	Increased	(Taylor et al. 2008)
ZIP10	Breast	Increased	(Kagara et al. 2007)
ZnT2	Breast	Increased	(Lopez et al. 2011; Bostanci et al. 2014)

The human prostate gland is characterized by a high zinc level compared to other soft tissues. The zinc concentration in prostatic fluid is about 500-fold higher than the plasma zinc concentration. (Bafaro et al. 2017; Mudipalli et al. 2017) In contrast, malignant prostate tissue was shown to display markedly lower zinc levels. This decline in the zinc level seems to be an early event in the malignant transformation. Healthy prostate cells can be described as “citrate-producing”, “zinc-accumulating”, and “low-respiring” cells. (Costello et al. 2004; Costello et al. 2016) During malignant progression these conditions must be reversed, since they represent a brake to uncontrolled proliferation. This reduction of the zinc level is achieved by reduction of the ZIP1 expression which is discussed to have the function of a tumor suppressor in prostate tissue. (Costello et al. 2006; Bafaro et al. 2017) Additionally, ZIP2, ZIP3, and ZIP4 exhibit reduced expression in prostate cancer. (Bafaro et al. 2017) While the risk of prostate cancer appears to be lower in men with a moderate to higher zinc intake, long-term supplemental zinc intake of more than 100 mg/day caused a higher prostate cancer risk. (Leitzmann, et al. 2003; Jarrard 2005; Gutiérrez-González et al. 2018) However, the underlying mechanisms are currently unknown.

Similar relations have been found in pancreatic tumors, where zinc levels are reduced early during malignant transformation. (Costello et al. 2011b) However, in tumor cells of the pancreas the expression of zinc transporters is more complicated with downregulation of the mRNA of all ZIP proteins except ZIP4, which is upregulated. (Yang et al. 2013; Bafaro et al. 2017)

The expression of ZIP14 seems to be relevant for the progression of hepatocellular carcinoma (HCC), as the protein is consistently decreased in malignant tissue which is accompanied by reduced zinc levels. (Costello et al. 2014). Additionally, it was shown that treatment of cancerous cells with physiological amounts of zinc was able to dampen cellular proliferation. (Franklin et al. 2012) In their review Costello and colleagues lament that “up to now too little attention was devoted to the connection between alternations of the zinc homeostasis and tumorigenesis”.(Costello et al. 2014)

In contrast to most solid tumors, the zinc level in cancerous breast tissue was found to be increased, which is attributed to the elevated expression of ZIP6, ZIP7, and ZIP10 zinc transporters. Additionally, the downregulation of ZnT2 may facilitate sequestration of zinc in vesicles. Depending on the subtype of the tumor other zinc transporters may possibly be involved in breast cancer progression. (Taylor et al. 2008; Lopez et al. 2011; Alam et al. 2012; Bafaro et al. 2017; Mudipalli et al. 2017)

Besides these relatively well studied relations, aberrant zinc levels and zinc transporter quantities were also found in other cancer entities. Practically all zinc transporters are discussed to be involved in tumor progression. Furthermore, zinc is suspected to be involved in the regulation of other ion channels which are themselves involved in tumor progression. Zinc might also act via the numerous different zinc proteins and the signalling cascades regulated by them. More and more evidence shows, that dysregulated zinc homeostasis might not only be of “passenger nature” in tumorigenesis but rather be a driver in at least some cancer entities. (Mudipalli et al. 2017; Pan 2017)

5.2 Nanomedicine

The prefix “nano” is derived from the Greek word “*νάνος*” which means “dwarf”. One nanometer (nm) is a billionth of a meter (m). Ten hydrogen atoms laid side by side would be a single nanometer. Red blood cells are approximately 7'000 nm in length. This can give us at least a vague idea of how small a nanometer is. (Idrees 2015) To grasp the size of nanomaterials their scale is depicted in Figure 11 in relation to different objects.

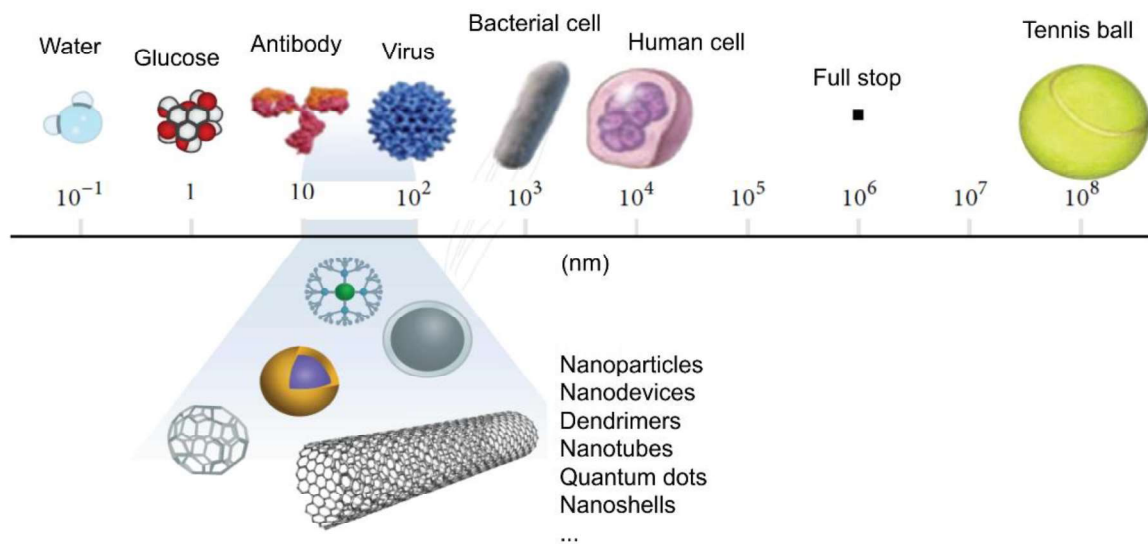


Figure 11: Scale of nanomaterials

Modified according to (Amin et al. 2014)

The International Organization for Standardization (ISO) has defined “nanoparticle” as a “nano-object with all three external dimensions in the nanoscale” where nanoscale is defined as the size ranging from approximately 1 to 100 nm. (Boverhof et al. 2015) “Nanotechnology is the design, characterization, production, and application of structures, devices and systems by controlling shape and size at nanometer scale”, according to the definition of The Royal Society & The Royal Academy of Engineering in 2004. (Whatmore 2006) Nanomedicine is the application of nanotechnological advancements in medicine. This involves the areas of diagnosis as well as therapeutic intervention to improve human health and wellbeing. (Satalkar et al. 2016)

Over the last decades research on the biomedical application of nanomaterials has advanced with great strides. From 1995 until 2017, 50 nanopharmaceuticals received FDA approval. (Ventola 2017)

Nanomedical applications provide a huge opportunity to exploit therapeutic potential that was hitherto unattainable due to chemical, physical or biological restrictions. Nanomaterials hold the promise to improve the solubility and pharmacokinetics of currently available drugs, reduce their off-target effects, and increase their specificity. Hence the dose that is needed to achieve the desired effect can be reduced. In addition to nanocarriers for drug delivery, nanomaterials are being investigated that are able to mediate specific effects on their own. (Rasmussen et al. 2010; Ventola 2017) Different families of nanotherapeutics are shown in Figure 12.

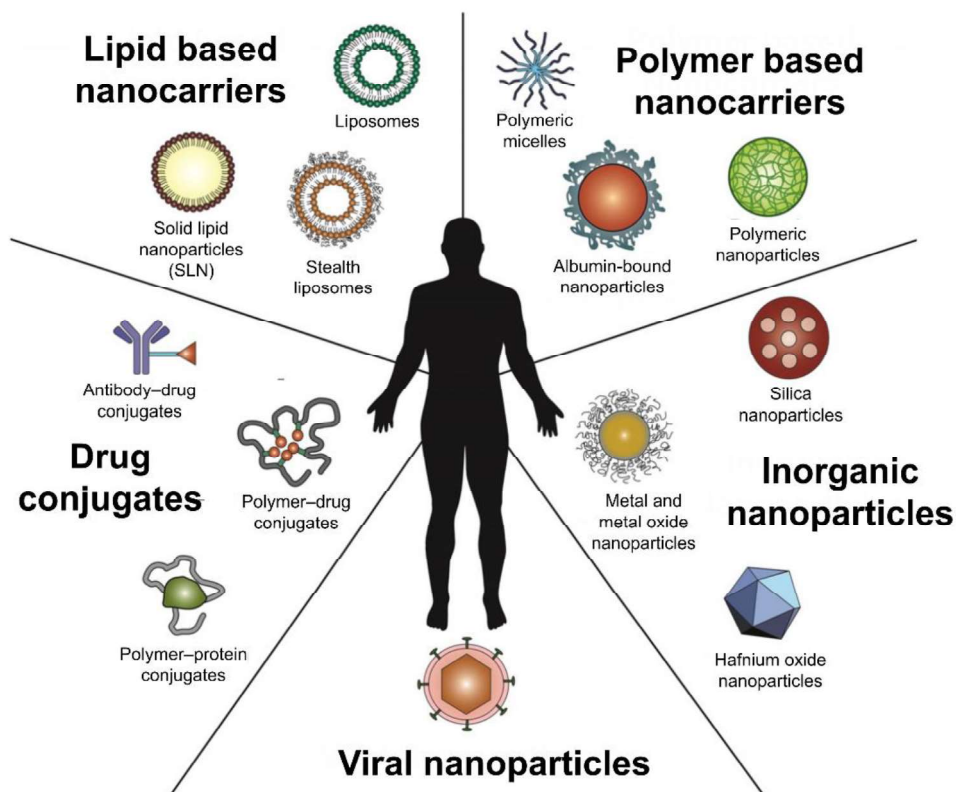


Figure 12: Different nanotherapeutic platforms

Modified according to (Wicki et al. 2015).

Materials –interact differently with their environment when they are sized on the nano scale. In bulk materials—meaning material that is not nanosized—most atoms are located inside the volume of the material rather than on the surface. In contrast, the relative number of atoms on the surface is greatly increased in nanomaterials. Their surface-to-volume ratio is much larger, which is associated with an increase in surface reactivity. (Grassian 2008; Idrees 2015) Thus, reducing the size of particles from bulk material to nano scale is accompanied by a modification of the chemical, physical, and biological properties. (Goesmann et al. 2010; Schladt et al. 2011; Bai et al. 2013)

Nanomaterials match the typical size of naturally occurring functional units and biomolecules of living organisms. These special characteristics allow nanoparticles (NP) to interact in a unique manner with cellular biomolecules such as proteins and nucleic acids. In this way the transfer of NP into inner cellular structures is facilitated, which allows the manipulation of intracellular processes to hitherto an extent that was previously unthinkable. (Rasmussen et al. 2010; Idrees 2015)

Despite recent advancements in nanomedicine, research is still far away from achieving a profound understanding of the dynamic behavior of nanomaterials in the human body. (Nel et al. 2009; Sun et al. 2014) Multiple challenges include the profound characterization of the new materials, the solving of possible toxicity issues and safety concerns, the clearing of regulatory hurdles, and the solving of manufacturing and storage issues. (Wicki et al. 2015; Ventola 2017) Settling these issues is especially important in medicine, which requires cooperation between the fields of physics, chemistry, biology and medicine. (Kunz-Schughart et al. 2017)

5.2.1 Nanotechnology in tumor therapy

Tumor therapy has undergone profound developments within the last decades. Nevertheless, cancer continues to be one of the most serious healthcare problems worldwide, due to the development of resistances and the recidivation of tumors. According to estimates from the World Health Organization (WHO), cancer is the first or second leading cause of death before age 70 in 91 out of 172 countries in 2015, with 18.1 million new cases worldwide in 2018. (Bray et al. 2018)

The major challenge of tumor therapy is to achieve death of tumor cells as selectively and precisely as possible while sparing the healthy tissue of the patient. To meet this challenge great hopes rest on innovative nanotherapeutics to overcome biological barriers that hinder therapy. The goal is to reduce limitation of the therapy due to low specificity, rapid drug clearance and low bioavailability, as well as high levels of adverse effects. (Wicki et al. 2015; Tran et al. 2017)

5.2.2 Nanoparticles as radiosensitizer

Radiotherapy—besides surgery and chemotherapy—is a very important part of the treatment regimen for different types of cancer. It is non-invasive and not accompanied by an intense systemic toxicity as is typical in chemotherapy. (Deorukhkar et al. 2010) Approximately 50–60% of all cancer patients receive radiotherapy as stand-alone treatment or in combination with other options. (Kunz-Schughart et al. 2017) Unfortunately, the curative potential of radiotherapy is impeded by mechanisms of tumor radiation resistance, which enable tumor cells to survive and repopulate. Thus, clinicians are in desperate need of new strategies to overcome these resistances or even better to improve the outcome of radiotherapy in the first place to prevent the establishment of resistances.

Since water is the main component of cells, ionizing radiation used in radiotherapy primarily results in radiation mediated lysis of water. The process generates radicals such as hydrogen radicals ($H\bullet$), hydroxyl radicals ($OH\bullet$), and superoxide radicals ($O_2^{\bullet-}$) all of which are reactive oxygen species (ROS). (Kwatra et al. 2013) The main target of radiotherapy in tumor cells is the DNA. Directly or indirectly via ROS, bases of the DNA can be damaged, the sugar-phosphate backbone interrupted—resulting in single strand breaks (SSB) or double strand breaks (DSB)—, or DNA crosslinks produced. (Maier et al. 2016) DSB are considered to have the most devastating effect on tumor cell viability. (McMillan et al. 2001) Apart from DNA damage among other effects lipid peroxidation plays an important role in radiation mediated cellular damage. (Azzam et al. 2012)

In principle there are three major approaches to enhance the efficacy of radiotherapy: radioresistance of healthy tissue may be enhanced, radiation resistance mechanisms specifically in tumor cells may be blocked, or radiosensitivity of the tumor tissue may be enhanced by radiosensitizers. The most promising nanoparticulate drug support strategies that go beyond the improvement of existing therapeutic strategies aim at achieving the last approach. (Kwatra et al. 2013)

Radiosensitizers are usually mainly metal-based nanoparticles made from high- z metals (metals with a high atomic number; e.g. gold). Those metals have the property that incoming radiation energy ejects one electron of the atom from an orbital. The ejected electron is replaced with electrons dropping from higher orbits and energy is released. This creates a photoelectric effect which increases the therapeutic efficacy of radiotherapy. (Kwatra et al. 2013)

Additionally, quantum dots—nanocrystals that display quantum mechanical properties made from semiconductors—can be used as radiosensitizers. Their mechanism of action is based on the generation of radicals upon absorption of visible light. Major drawback of this technique is that visible and UV light do not penetrate far into the human body.

Superparamagnetic substances such as iron oxide nanoparticles are also investigated as radiosensitizer. They can be targeted to the tumor tissue by an external magnetic force. Within the tumor tissue they generate ROS which enhances the radiation induced DNA damage. (Rasmussen et al. 2010; Kwatra et al. 2013) Additionally they can be used to convey local hyperthermic effects. (Rasmussen et al. 2010; Sharma et al. 2015)

5.3 Zinc oxide nanoparticles (ZnO NP)

Zinc oxide (ZnO) is one of the most important manufactured compounds of zinc, with a wide variety of applications in various branches of industry, such as rubber, pharmaceutical, cosmetics, textile, electronic and electrotechnology, and photocatalysis. ZnO has a hexagonal wurtzite crystal structure at ambient pressure and temperature. Zinc oxide nanoparticles occur in a great variety of structures and offer a wide range of properties, as shown in Figure 13. This probably makes them one of the most versatile families of nanostructures among all materials. (Wang 2004; Kołodziejczak-Radzimska et al. 2014)

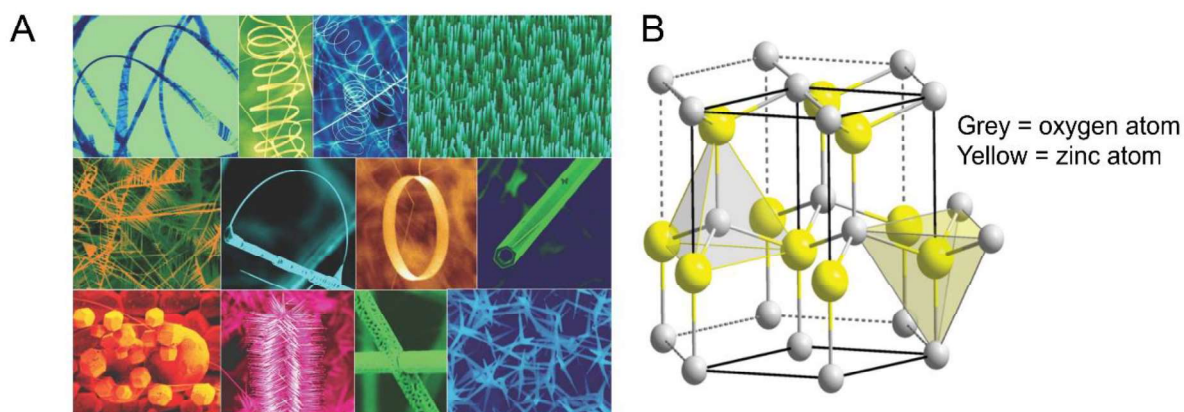


Figure 13: Zinc oxide nanostructures

Zinc oxide can occur in varied forms and shapes. (A) shows a collection of nanostructures of ZnO synthesized under controlled conditions by thermal evaporation of solid powders. (B) shows the typical wurtzite crystal structure of ZnO. Modified according to (Wang 2004; Samanta 2017).

5.3.1 Biomedical application of ZnO NP

Chemically, ZnO NP possess several characteristics that are favourable for their biomedical application. For one, the synthesis of ZnO NP is relatively inexpensive and it can be easily tuned to achieve different sizes and geometries. Additionally, the surface of ZnO NP enables its modification by different coatings.

The FDA recognizes zinc oxide as a so-called GRAS (= **G**enerally **R**ecognized **A**s **S**afe) substance (database of the Select Committee on GRAS Substances (SCOGS), <https://www.accessdata.fda.gov/scripts/fdcc/?set=SCOGS&sort=Sortsubstance&order=ASC&startrow=1&type=basic&search=zinc%20oxide>, accessed 24.01.2019). This enables its application in healthcare and drugstore products. Zinc oxide is found in numerous medical formulations as well as in creams and lotions, for example in sun cream and in wound healing preparations. (Racca et al. 2018) Compared to other metal oxides zinc oxide is relatively non-toxic and biocompatible.

ZnO NP are said to exhibit an inherent anti-cancer and antibacterial activity which is attributed to their ability to induce the generation of reactive oxygen species. (Padmavathy et al. 2008) Furthermore ZnO NP possess antifungal properties. ZnO NP are also discussed as drug carriers and immunomodulatory agents. (Mishra et al. 2017) On the one hand, the number of applications for which the use of ZnO NP is suggested is long. Unfortunately, on the other hand many characteristics of ZnO NP are not fully understood. We are still far from completely understanding their behaviour in interaction with cells and living organisms which is substantial for their safe biomedical application.

In the following chapter I want to shed light on the most important characteristics of ZnO NP which are known to contribute to their *in vitro* toxicity. This will then lay the basis for understanding why ZnO NP are very attractive as innovative anti-tumor agent.

5.3.2 Characteristics and *in vitro* cytotoxicity mechanism of ZnO NP

First of all, I want to introduce you into the interactions between ZnO NP and cells at the outer surface of the cell (5.3.2.1). This involves the extracellular release of zinc ions as well as the influence of coatings and the adsorption of proteins onto the nanoparticle surface. Then we will continue with the uptake of ZnO NP into cells and the damage they are able to cause to cellular membranes and to the cytoskeleton (5.3.2.2). Next, I will discuss the generation of reactive oxygen species by ZnO NP, their best-known mechanism of toxicity (5.3.2.3). After that I want to illustrate what is known about ZnO NP's ability to induce genotoxicity and epigenetic changes (5.3.2.4). Finally, I will discuss the cellular reaction that follows cytotoxic damage conveyed by ZnO NP (5.3.2.5).

The content of the chapter on the characteristics of ZnO NP which can convey cytotoxicity (1–5) is shown graphically in Figure 14.

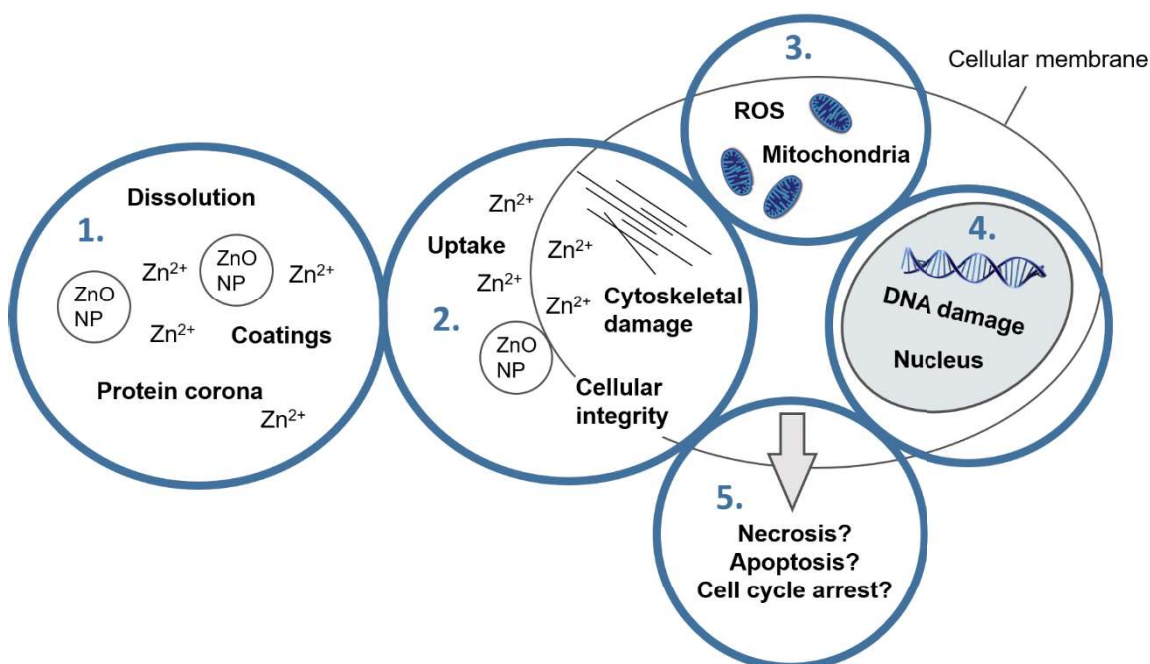


Figure 14: Overview over the most important characteristics which contribute to the cytotoxicity of ZnO NP

5.3.2.1 Coatings, stability against dissolution, and protein corona

The characteristic electrostatic properties of ZnO NP are quite favourable for their biomedical application. Typically, they have neutral hydroxyl groups attached to their surface. In aqueous medium with a pH value larger than 9 (the isoelectric point) chemisorbed protons (H^+) detach from the surface, leaving behind a negatively charged surface with partially bonded oxygen atoms (ZnO^-). In contrast at lower pH values (neutral or acidic), protons from the environment are transferred onto the particles' surface. This leads to a positively charged surface due to $ZnOH_2^+$ groups. (Rasmussen et al. 2010; Punnoose et al. 2014) This also holds true for physiological conditions and provides good conditions for the interaction of ZnO NP with tumor cells, which are known to frequently carry a negative charge at their surface. (Chen et al. 2016; Shi 2017)

ZnO NP are prone to dissolution, while extracellular release of zinc ions is known to contribute to the cytotoxicity of ZnO NP. (Song et al. 2010) Release of zinc ions from ZnO NP is also higher at low pH values which is especially relevant for ZnO NP taken up via the endo-lysosomal system. (Avramescu et al. 2017; Odzak et al. 2017) Additionally, dissolution is affected by the ionic strength of the surrounding medium. (Odzak et al. 2017) Zinc ions released from ZnO NP are readily bound by different components of the cell culture medium, such as phosphate, carbonate, amino acids, as well as serum proteins. Thus, a considerable amount of zinc ions is buffered by the cell culture medium until the buffer capacity is exhausted. Zinc phosphate and zinc carbonate together with retained proteins can precipitate in crystalline or amorphous form. They constitute another (nano-sized) species that can take influence on the system. (Turney et al. 2012; Shen et al. 2013; Mu et al. 2014; Eixenberger et al. 2017) Furthermore metal oxide nanoparticles are prone to agglomeration and aggregation which are followed by sedimentation. (David et al. 2012; Mu et al. 2014; Pradhan et al. 2016)

Up to now there is no consensus whether extracellularly released zinc ions are responsible for all of the cytotoxicity of ZnO NP. Direct cell–nanoparticle contact and/or uptake of NP might be required additionally. (Shen et al. 2013) It is well known that typically ZnO NP are not dissolved completely which contributes to the idea that zinc ions are not solely responsible for the cytotoxicity of ZnO NP. (Xia et al. 2008; Moos et al. 2010; Song et al. 2010)

It is always important to bear in mind that the moment that nanoparticles are released into biological medium their chemical properties can change quickly. The biological identity of the nanoparticles is not necessarily the same as the synthetic identity as shown in Figure 15. This also holds true for ZnO NP. The surface properties of the nanoparticles can change due to different buffer conditions and the adsorption of biological molecules. Consequently the colloidal stability, hydrodynamic diameter, and nanoparticle agglomeration are affected. (De Angelis et al. 2013)

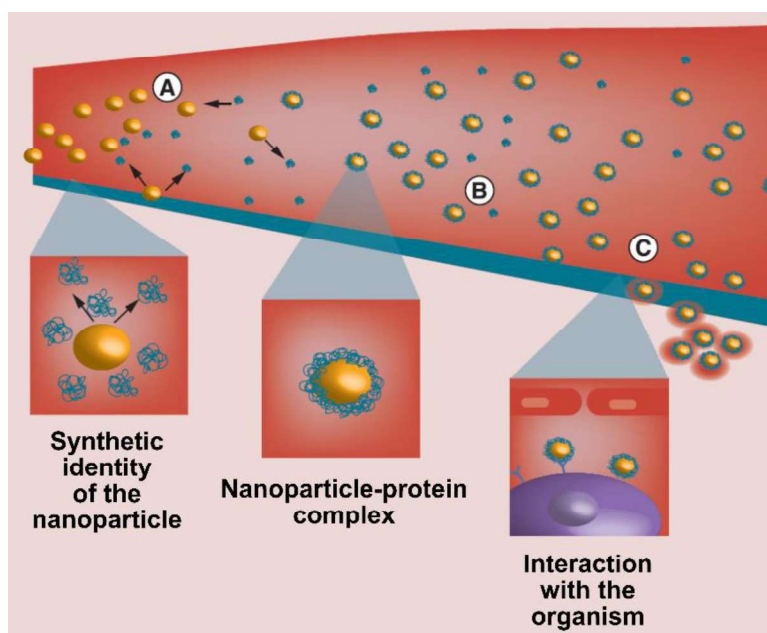


Figure 15: Transition of NP from their synthetic to the biological identity

When nanoparticles are introduced into biological medium they are modified in various ways. Their synthetic identity is changed to a biological identity and they are covered by a hard and a soft protein corona, which ultimately determines the physiological response they evoke in the bloodstream. The adsorbed proteins on their surface determine how the nanoparticles interact with both the immune system and biological barriers, as well as their deposition in the body and their excretion. Modified according to (Corbo et al. 2016).

Furthermore, an important topic in this context is the stability against dissolution. On one hand it can be influenced by coatings intentionally applied during the synthetic procedures. On the other hand, it is influenced unintentionally by the protein corona that is deposited on the nanoparticles.

ZnO NP possess a strong ability to absorb proteins from serum in the cell culture medium. Consequently, serum proteins are depleted from the cell culture medium. Potential toxicity that is observed might not only stem from the nanoparticles but also from protein–nanoparticle complexes which differ in reactivity, cellular uptake, and surface chemistry from the pristine uncoated nanoparticles. (Horie et al. 2009)

Several reports find that proteins and coatings deposited on the surface of ZnO NP reduce their cytotoxicity in adherent cell cultures. This is possibly due to reduced dissolution, reduced ROS generation, or hampered direct surface contact between NP and cells. (De Angelis et al. 2013; Mu et al. 2014; Ramasamy et al. 2014; Anders et al. 2015; Yin et al. 2015; Žūkienė et al. 2015) However cytotoxicity in suspension cell models can be increased by protein adsorption and coatings. This is possibly attributable to the increase in dispersion stability, and the decrease in agglomeration and sedimentation, which enhances the bioavailability in suspension cell cultures. (Anders et al. 2015) Furthermore the modification of the membrane activity of ZnO NP by protein adsorption is discussed. NP uptake may differ depending on the nature of the coating and the corresponding cell type. (Churchman et al. 2013; Mu et al. 2014) Figure 16 graphically summarises the most important aspects of the interaction between ZnO NP and the cellular surface as well as potential mechanisms of uptake.

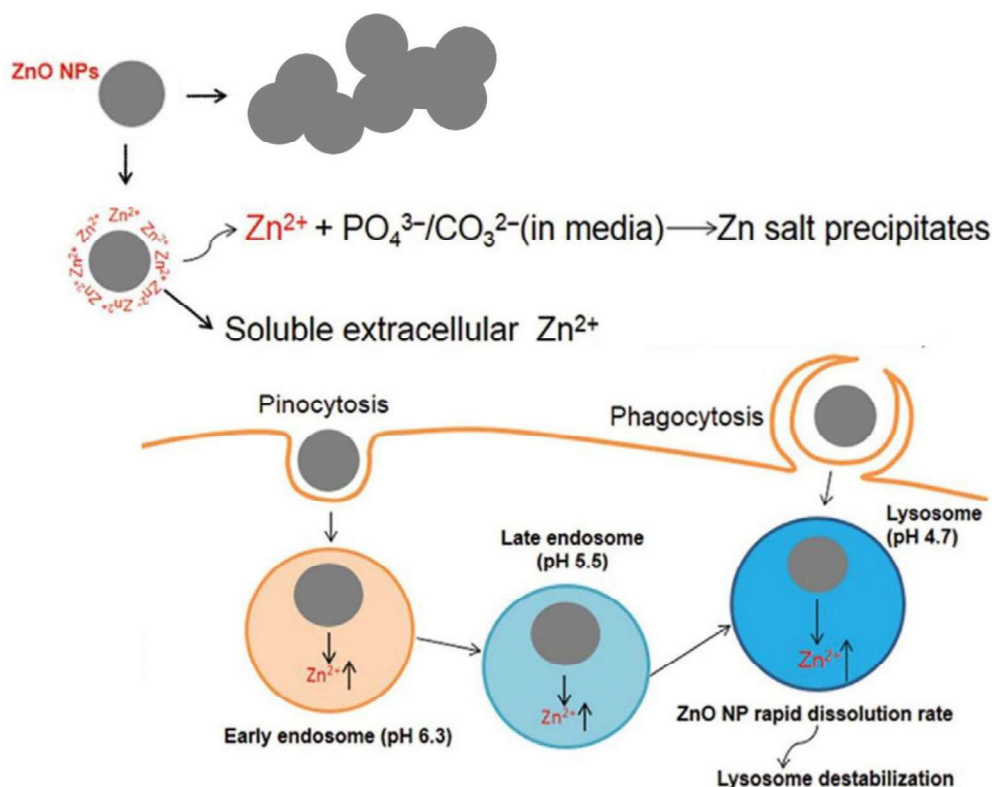


Figure 16: Cell-nanoparticle interactions

In the cell culture medium ZnO NP form agglomerates and they also release zinc ions. Extracellularly released zinc ions can form precipitates with components of the cell culture medium. ZnO NP can interact with cells in various ways. They can interact with the cellular membrane and they can be taken up into the cells via the endo-lysosomal system by pinocytosis and phagocytosis. Within lysosomes ZnO NP are dissolved rapidly due to the low pH value and further zinc ions are released intracellularly. Modified according to (Shen et al. 2013; Bisht et al. 2016; Racca et al. 2018).

5.3.2.2 Cytoskeletal damage, cellular integrity, and cellular uptake

Several different studies report that ZnO NP take influence on the cytoskeleton. Rounding of the cells, cell retraction, and collapse of cells were observed. This was accompanied by detachment from the cell culture plate, depolymerisation of actin, and reorganisation of the microtubules (Condello et al. 2016; Garcia-Hevia et al. 2016; Pati et al. 2016; Choudhury et al. 2017; Liu et al. 2017). The reorganization of the cytoskeleton was connected to the loosening of the continuous cell layer on the cell culture plate and the loss of intercellular contact. (Paszek et al. 2012; Reshma et al. 2017) Interestingly zinc ions are involved in the regulation of cell migration by attenuating focal adhesion density and size, just like calcium ions. (Li et al. 2016) Additionally, they were shown to be able to induce epithelial to mesenchymal transition (Ninsontia et al. 2016); possibly via binding to N-cadherin. (Heiliger et al. 2015).

Disruption of the cellular membrane has been frequently observed after treatment with ZnO NP (Huang et al. 2010; Song et al. 2010; Paszek et al. 2012). Usually the membrane integrity is measured with a lactate dehydrogenase release assay (LDH release assay) which measures the spillage of the cytosolic protein into the extracellular space. It is important to bear in mind that this kind of assay without further information does not prove that the disruption of the cellular membrane is the cause for the cytotoxicity since membrane leakage can also be the consequence of necrotic cell death. However, it is fathomable that ZnO NP interfere with the cellular integrity. In antimicrobial studies the abrasiveness of ZnO NP was linked to bacterial death (Padmavathy et al. 2008). Up until now, further studies on this topic in mammalian cells are missing.

ZnO NP convey toxicity by increasing the intracellular zinc level but it is still subject of debate whether zinc is internalized as a particle. Some studies see uptake of ZnO NP by cells (Sharma et al. 2011; Gilbert et al. 2012; Condello et al. 2016; Garcia-Hevia et al. 2016; Choudhury et al. 2017); possibly via the lysosomal pathway (Ancona et al. 2018). In contrast, others state that the only convincing proofs of entry of ZnO NP in nanoparticulate form exist solely for macrophages which are the champions in rapidly engulfing everything they come across. (Chevallet et al. 2016) The dissolution kinetics of ZnO NP and their surface coating most probably have a great impact on whether cells take them up or whether zinc ions released from the NP enter the cells.

5.3.2.3 Generation of reactive oxygen species (ROS)

It is well established that generation of reactive oxygen species (ROS) is an important part of the mechanism of nanotoxicity. (Fu et al. 2014) A certain level of ROS is always present in cells as by-product of the cellular oxidative metabolism. In the mitochondria ATP is synthesized by reduction of molecular oxygen to water through a sequence of coupled proton and electron transfer reactions. During this process, a small percentage of oxygen is not reduced completely, which can result in the formation of superoxide radicals, and subsequently other ROS. (Fu et al. 2014) Mitochondrial respiration is the main endogenous source of ROS, but there are others, such as inflammatory responses and peroxisomes. (Babusikova et al. 2012; Manke et al. 2013) Cells have evolved efficient mechanisms to deal with a certain level of ROS by using enzymes like the superoxide dismutases, peroxidases, and catalases. They all promote the reaction of highly reactive radicals to more harmless substances to protect the cell. Problems begin to occur when the generation of ROS exceeds the physiologically normal level and the antioxidative capacity is exhausted. This process culminates in oxidative stress which can harm cells on various levels (Babusikova et al. 2012; Fu et al. 2014) Figure 17 depicts the most important aspects of how ROS generation can damage cells.

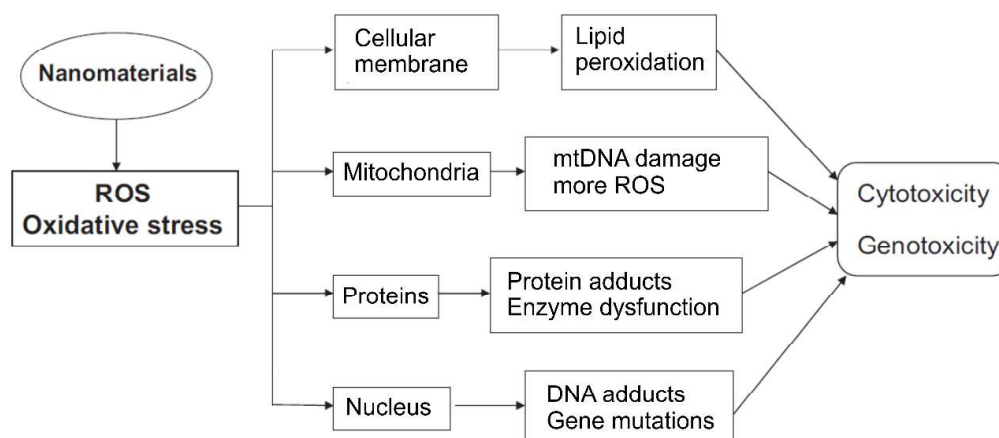


Figure 17: Nanotoxicity conveyed by the generation of ROS

Modified according to (Fu et al. 2014).

Due to their small size and their high reactivity many nanomaterials possess the ability to generate ROS. Many metal oxide nanoparticles do so by participating in Fenton and Haber-Weiss reactions. (Fu et al. 2014) However, since zinc is redox inert in biological systems this can be ruled out for them. Nevertheless, they are also potent producers of ROS by different mechanism which will be discussed in the following.

5.3.2.3.1 Photocatalytic activity of zinc oxide nanoparticles

Zinc oxide is a semiconductor with a wide band gap of 3.37 eV and a large exciton binding energy of 60 meV at room temperature. It absorbs a wide range of the solar spectrum. Photocatalysis can be defined as the “acceleration of a photoreaction in the presence of a catalyst”. In this case the photocatalytic reactions are initiated when ZnO NP absorb photons with energies greater than the energy of their band gap. This can occur by illumination with visible or UV light. As a consequence, one electron is excited from the valence band (VB) to the conduction band (CB). This leads to the formation of a positively charged hole (h^+_{VB}) and a negatively charged electron (e^-_{CB}), a so-called electron–hole pair on the surface of the ZnO NP. This is depicted schematically in Figure 18.

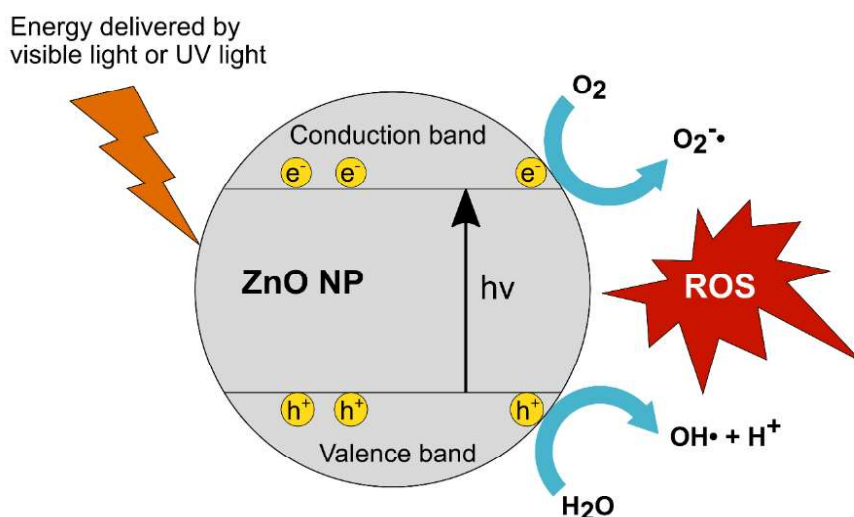


Figure 18: Photocatalytic activity of zinc oxide nanoparticles

Modified according to (Sivakumar et al. 2018).

Electrons and holes often recombine quickly, but they can also migrate to the surface of the nanoparticle and react with surrounding molecules. The conduction band electrons e^-_{CB} are good reductants and can reduce oxygen from the surrounding environment to form superoxide radicals ($O_2^{\bullet-}$). The valence band holes h^+_{VB} are strong oxidants that can react with water to hydroxyl radicals (OH^{\bullet}), hydrogen peroxide (H_2O_2), or protonated superoxide radicals (HO_2^{\bullet}). Both processes pave the way for further reactions which involve different reactive oxygen species. (Padmavathy et al. 2008; Rasmussen et al. 2010; Punnoose et al. 2014; Lee et al. 2016; Podporska-Carroll et al. 2017; Ancona et al. 2018)

Compared to ZnO bulk material in which the electron–hole pairs recombine quickly and hinder catalytic activity, the presence of oxygen vacancies and other surface defects in the nanoparticulate matter help to keep the electron–hole pairs separated. They can reach the surface more efficiently where they can participate in redox reactions. (Punnoose et al. 2014; Wang et al. 2017; Ancona et al. 2018) It has been shown that ZnO NP are also capable of generating ROS under abiotic conditions, which means without the presence of cells. (Xia et al. 2008; Song et al. 2010; Zijno et al. 2015)

The photocatalytic activity of ZnO NP was found to greatly enhance the cytotoxicity of ZnO NP *in vitro*. This was shown in studies using UV irradiation or visible light in combination with the nanoparticles. (Hackenberg et al. 2010a; Yang et al. 2014; Ancona et al. 2018) Additionally, generation of ROS at the surface of ZnO NP is also possible in the dark fostered by surface defects of the crystalline structure. (Prasanna et al. 2015)

On top of that, ZnO NP can also induce intracellular increase in ROS. This has been shown in numerous studies. (Xia et al. 2008; Sharma et al. 2012; Toduka et al. 2012; De Angelis et al. 2013; Kang et al. 2013; Wahab et al. 2013; Gao et al. 2016; Pati et al. 2016; Choudhury et al. 2017; Ng et al. 2017) In principle, ROS could be generated directly by the interaction of ZnO NP with the biological surroundings or by released zinc ions. Which mechanism really underlies the intracellular elevation of ROS is extremely difficult to decipher since the visualization of ZnO NP, zinc ions, and ROS in time and place intracellularly in a living system is very challenging. Another question still to be resolved is where exactly within the cell ROS are generated. Mostly, intracellular increase in ROS is related to mitochondrial damage, but it is unclear whether mitochondrial damage is cause or effect of the increase in ROS.

5.3.2.3.2 ROS and mitochondrial damage—cause or effect?

Somewhat surprisingly, zinc ions seem to play a role in the regulation of mitochondrial activity under normal physiological conditions and as a part of cellular stress response. It has been shown that zinc ions are a very potent inhibitor of cellular respiration and terminal oxidation. Zinc seems to inhibit the succinate-stimulated reduction of oxidized cytochrome c, thereby likely inhibiting complex III, the cytochrome c reductase. Zinc also likely inhibits the α -ketoglutarate dehydrogenase

complex upstream in the tricarboxylic acid (TCA) cycle. (Skulachev et al. 1967; Kleiner et al. 1972; Brown et al. 2000; Costello et al. 2004; Costello et al. 2016)

The mitochondrial tricarboxylic acid (TCA) cycle and electron transport chain (ETC) are depicted in Figure 19 to show where zinc can intervene.

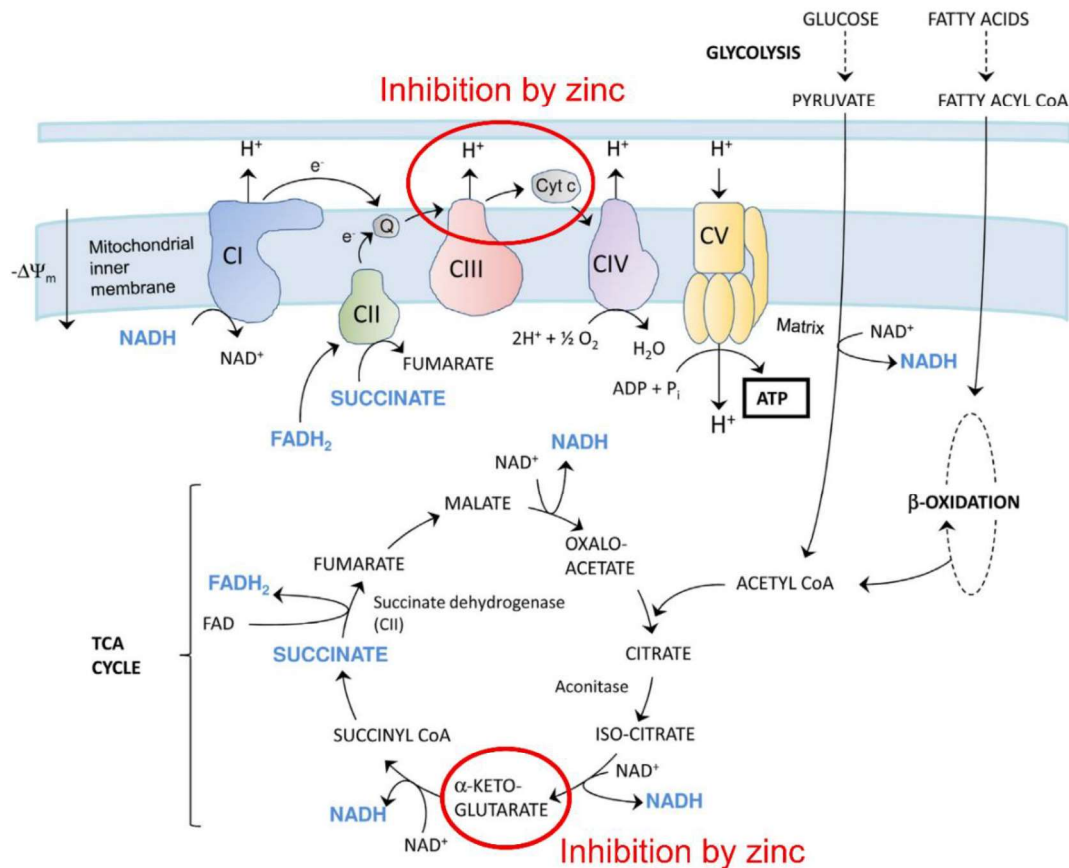


Figure 19: Mitochondrial tricarboxylic acid cycle and electron transport chain

Complexes CI, CII, CIII, CIV, and CV comprise the electron transport chain (ETC). The ETC uses NADH and FADH₂ to make ATP. These reducing equivalents for ETC are generated during glycolysis, fatty acid breakdown, and in the tricarboxylic acid cycle, the latter also being known as Krebs cycle. The electron flow starts with the binding of NADH to complex I or with succinate and FADH₂ binding to complex II. Ultimately, ATP is produced at complex V, the ATPase. If these pathways malfunction, ATP production is reduced, placing stress on the cell. In the ETC at complex III and in the TCA cycle at the α-ketoglutarate dehydrogenase zinc ions can intervene and inhibit respiration. Modified according to (Polyzos et al. 2017).

The interrelations between mitochondria and zinc ions have been discussed especially in neural and endothelial cells, where zinc levels were found to be elevated in a variety of pathological conditions, such as ischemia-reperfusion injury and Alzheimer's disease. (Brown et al. 2000) Studies suggest biphasic effects of zinc ions on the mitochondrial function. On one hand high levels of zinc ions were found to decrease O₂ consumption, lower the mitochondrial membrane potential, and increase ROS production. This is in line with the above-mentioned findings suggesting that zinc

ions inhibit components of both the TCA cycle and the ETC. Low levels of zinc on the other hand increased O₂ consumption and decreased ROS generation. (Sensi et al. 2003) Several different working groups found crosstalk between zinc ions, mitochondria, and ROS. (Slepchenko et al. 2017; Lien et al. 2018) It was shown that ZnO NP can affect the cellular respiration of cancer cells. (Prasanth et al. 2013) In response to oxidative stress, endothelial cells were shown to exhibit increased levels of free zinc ions, concomitant loss of the mitochondrial function, and induction of cellular death. (Wiseman et al. 2007) When the cellular ability to maintain zinc homeostasis is overwhelmed, it seems as if a vicious circle of cellular damage is initiated that finally leads to cell death. This demonstrates the important role of intracellular zinc flows. They connect the oxidative stress response to the mitochondria, and thereby cellular signalling cascades, which finally can induce cellular (apoptotic) death. Signal transduction can possibly be achieved by the import of metallothionein loaded with zinc ions into mitochondria, where zinc ions are subsequently set free to modulate respiration. (Ye et al. 2001) Instead of being bound to metallothionein, zinc ions might enter the mitochondria on their own via a calcium uniporter (Lien et al. 2018) or yet unknown mechanisms (Malaiyandi et al. 2005). Mitochondrial dysfunction has been frequently observed following treatment with ZnO NP. (Berardis et al. 2010; Zhang et al. 2011; Choudhury et al. 2017) In principle, mitochondrial dysfunction can be the consequence of the generation of ROS in the cytosol and subsequent damage to the mitochondria. It is however also possible that zinc ions or ZnO NP directly interact with mitochondria. Additionally, it was suggested that treatment with ZnO NP may result in the inhibition of the superoxide dismutase and catalase activity. (Pati et al. 2016; Kononenko et al. 2017) This would suggest that failure of mitochondria may not be directly related to the interaction with ZnO NP or zinc ions but rather is a consequence of the exhaustion of the antioxidative capacity of the cells.

The generation of ROS could in part also be a result of the cytotoxicity of ZnO NP rather than its cause. During the induction of cell death ROS can be released and membrane leakage can occur. We have to bear in mind that a complex series of events occurs upon treatment with ZnO NP and a mechanistic link is not necessarily a causality. (Shen et al. 2013)

5.3.2.4 Genotoxicity and epigenetic changes

This chapter will start with a description of possibly naturally occurring interactions between nucleic acids and zinc ions.

The affinity of positively charged metal ions for the DNA is predictable considering that its structure includes a negatively charged phosphate backbone, a deoxyribose sugar with oxygen atoms, and purine and pyrimidine bases that contain oxygen and nitrogen atoms. One might consider the stabilization of the DNA by binding of Mg^{2+} ions a well-known example. Similarly, redox-active metals are known to intercalate into the DNA and induce metal-mediated DNA damage. (Morris 2014)

In 1993 it was proposed for the first time that zinc ions can form a DNA-metal ion complex—the so-called M-DNA—in which the zinc ions are located in-between the base pairs. (Lee et al. 1993) This is shown in Figure 20. First it was unclear whether zinc intercalation into the DNA was only an *in vitro* phenomenon, but since then it was shown that M-DNA can be created under physiological conditions. (Nejdl et al. 2014) The melting temperature of DNA is influenced by the binding of zinc (Nejdl et al. 2014) and it is fathomable that zinc ions bound to dsDNA and ssDNA have regulatory functions *in vivo*. (Martínez-Balbás et al. 1995; Lu 2014) Additionally, zinc ions can also bind to the phosphate backbone. (Langlais et al. 1990)

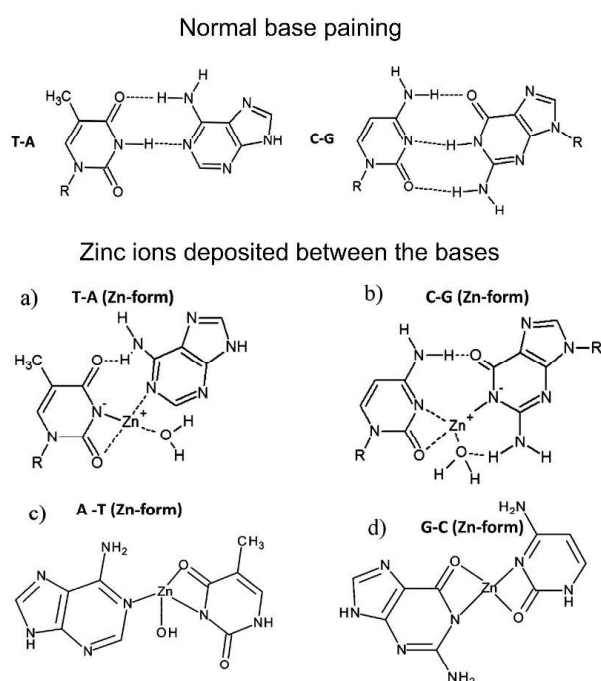


Figure 20: Interaction of zinc ions with the nucleobases in the DNA

Modified according to (Nejdl et al. 2014).

It was also shown that ZnO NP as a whole can interact with DNA strands under abiotic conditions. (Wahab et al. 2009; Saha et al. 2014; Preedia Babu et al. 2015; Ma et al. 2016) In a therapeutic setting ZnO NP are discussed to stabilize RNA and RNA-based medication. (McCall et al. 2017; Ramani et al. 2017) In experiments with calf thymus DNA under abiotic conditions it was furthermore shown that ZnO NP can intercalate into the DNA, where they can potentiate the generation of ROS in response to gamma-irradiation and subsequent DNA damage. (Preedia Babu et al. 2015) Up until now it is not known whether whole particles could possibly directly interact with nucleic acids in cells under biotic conditions.

It is well established that ZnO NP can induce DNA damage (Dufour et al. 2006; Sharma et al. 2009; Osman et al. 2010; Sharma et al. 2012; Toduka et al. 2012; Alarifi et al. 2013; Valdiglesias et al. 2013; Roy et al. 2014; Zijno et al. 2015; Condello et al. 2016; Pati et al. 2016; El Yamani et al. 2017; Kononenko et al. 2017; Ng et al. 2017; Thongkam et al. 2017), but the exact mechanisms of genotoxicity are largely unknown. DNA damage that was detected after treatment with ZnO NP ranged from single and double strand breaks evaluated in comet assays or via γ H2AX staining over nucleobase derivatives like 8-oxo-2'-deoxyguanosine (8-oxo-dG) to chromosomal breaks and the formation of micronuclei. (Hackenberg et al. 2017)

In the context of DNA damage, it is especially interesting whether ZnO NP can induce DNA damage directly or via ROS. This question remained largely unanswered up until now because ROS generation and DNA damage arise simultaneously, and it is difficult to disentangle both processes. Unfortunately, ROS scavenger N-acetylcysteine (NAC) cannot be used to assess the effect of ZnO NP on the DNA without ROS being present since NAC has a high affinity to zinc ions. (Pace et al. 2014; Xueju et al. 2015) In general it is important to evaluate the genotoxic effects of ZnO NP at sub-cytotoxic timepoints—and equivalently sub-cytotoxic concentrations—since the induction of cell death is also accompanied by DNA fragmentation.

On top of the known ability of ZnO NP to evoke genotoxic effects they have also been implicated in epigenetic changes. (Gao et al. 2016; Choudhury et al. 2017)

5.3.2.5 Cellular fate after treatment with ZnO NP

One common question concerning nanotoxicity is the one about the cell death mechanism. In the narrow sense this means whether cells die via apoptosis, necrosis, or autophagy-associated cell death. The most important features of these cell death mechanisms are summarised in Figure 21.

After treatment with ZnO NP mostly apoptosis (Ahamed et al. 2011; Zhang et al. 2011; Wahab et al. 2014; Gao et al. 2016; Bai et al. 2017; Moghaddam et al. 2017) or necrosis in conjunction with apoptosis (Wilhelmi et al. 2013; Garcia-Hevia et al. 2016) has been reported. Growing evidence suggests that apoptosis after treatment with ZnO NP is induced via the intrinsic, i.e. mitochondrial, pathway (Sharma et al. 2012; Gao et al. 2016; Ng et al. 2017). In some cases autophagy (Roy et al. 2014; Bai et al. 2017; Reshma et al. 2017) and mitophagy (Wang et al. 2018) were also shown.

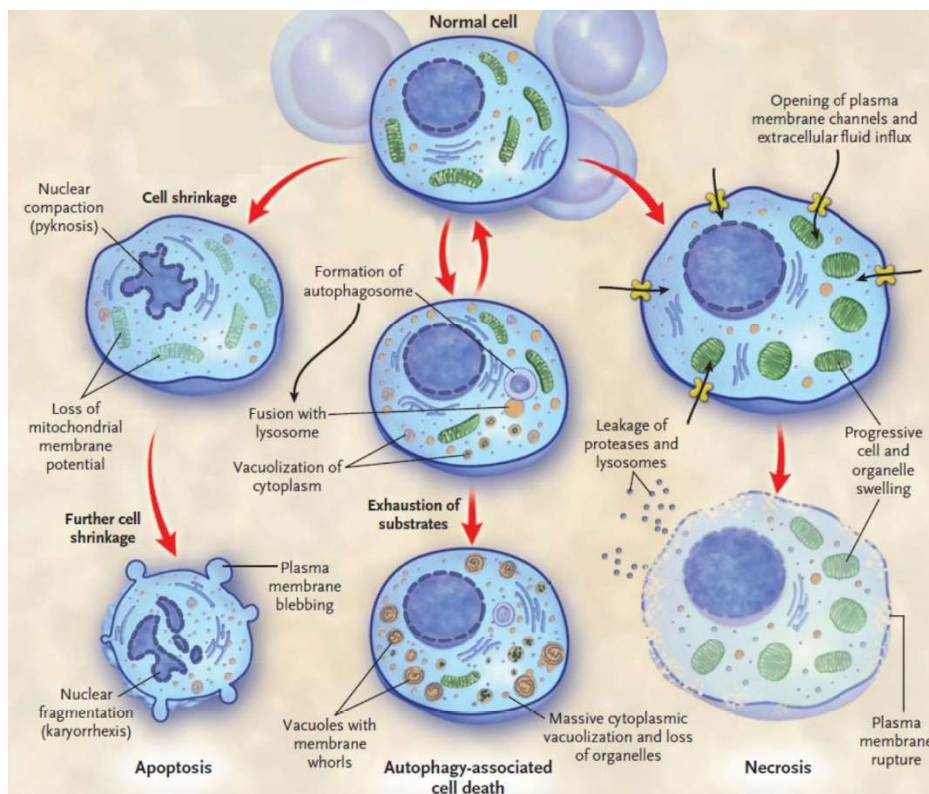


Figure 21: Cell death mechanisms

Apoptosis is a controlled mechanism of cell death which occurs within normal developmental processes and due to sustained damage, that cannot be repaired. It serves to eliminate a single cell from the organism without evoking an immune response. Necrosis is not a controlled cell death; it occurs when cells are hit by traumatic damage that cannot be handled in any other way. In contrast to apoptosis, necrosis involves uncontrolled rupture of the cellular membrane which induces an immune response. Autophagy occurs when cells suffer from starvation. It involves the digestion of intracellular components. Autophagy can be reversed, and cells can re-enter into proliferation, or it can lead to autophagy-associated cell death. The predominant mode of cell death depends on the type of cell and injury. Among the different types of cell death, cross-talk exists on multiple levels, which is not shown here. Modified according to (Hotchkiss et al. 2009).

Mitochondria seem to play a decisive role in determining the cellular fate after treatment with ZnO NP. Most likely they are either involved in the ROS generation following treatment with ZnO NP or they are one of the first targets of ROS that are generated elsewhere in the cell. Aside from mitochondria, the nucleus may also sustain lasting damage following treatment with ZnO NP. Intracellular signalling cascades determine the fate of cells in the end. This can lead to controlled apoptosis most likely induced via the mitochondrial pathway or it can lead to the attempt to repair sustained damage. In the case of uncontrolled increase in ROS and membrane leakage necrosis is possible too.

5.3.3 Zinc oxide nanoparticles as innovative anti-tumor agents

During the last years evidence accumulated that ZnO NP represent a promising candidate as an innovative anti-tumor agent. Numerous studies have been published that show toxicity of ZnO NP against tumor cells involving mechanisms mentioned in the previous chapters.

One central question which always arises when an innovative agent is proposed for the treatment of tumors is the question of the selectivity of the new drug. Several studies show that ZnO NP seem to possess selective anti-cancer characteristics *in vitro* that could help to spare healthy tissue and target the cancer cells selectively. In the following table the current state of research concerning the selective cytotoxicity of ZnO NP against tumor cells is depicted.

Table 2: Selective anti-cancer activity of zinc, zinc compounds, and ZnO NP

In the first and second column the malignant and non-malignant cell types that were used in the corresponding study are named. The third column presents the parameters that were analysed set in *italics* and thereafter the main findings of the study concerning the selective anti-cancer activity. The last column gives the corresponding publication for reference. Unless stated otherwise, the cells used in the publications were of human origin and the ZnO NP were uncoated. Compounds others than ZnO NP or coatings that were added to pristine ZnO NP are both set in **bold**.

Malignant cell type	Non-malignant cell type	Key points	Reference
T cells (Jurkat, Hut78)	Resting T cells, activated T cells	<i>Viability in co-culture, ROS, apoptosis/necrosis</i> → cancerous T cells were 28–35 times more susceptible → toxicity was correlated with proliferative potential	(Hanley et al. 2008)
-	Peripheral blood mononuclear cells (PBMC)	<i>Viability, ROS, cytokine production</i> → T and B lymphocytes were more resistant compared to monocytes and NK cells, memory T cells were more sensitive than naïve T cells → toxicity was cell-type specific dependent on membrane association, phagocytic ability, capacity for ROS production	(Hanley et al. 2009)
Glioma cells (A172, U87, LN2308, LN18, LN229), breast cancer cells (MCF-7)	Astrocytes, breast cells (MCF-10A), prostate cells (RWPE-1)	<i>Viability, apoptosis/necrosis, ROS</i> → selective cytotoxic effects on cancerous cells, increased ROS production compared to normal cells	(Ostrovsky et al. 2009)
Myelogenous leukemia cells (K562)	Lymphocytes from peripheral blood	<i>Viability, DNA damage</i> → more pronounced cyto- and genotoxicity of ZnSO₄ to cancer cells than to normal cells	(Sliwinski et al. 2009)
T cells (Jurkat)	CD4 ⁺ T cells from PBMC	<i>Viability, uptake</i> → preferential killing of cancerous cells by ZnO@SiO₂ NP	(Wang et al. 2009)
HNSCC cells (HLaC 78, UD-SCC 7A)	Primary oral mucosa cells (pOMC)	<i>Treatment with ZnO NP and UVA-1, viability, apoptosis/necrosis</i> → 0.2 or 2 µg/mL ZnO NP + 15 min UVA induced preferred killing of cancerous cells	(Hackenberg et al. 2010b)

Malignant cell type	Non-malignant cell type	Key points	Reference
Myelogenous leukemia cells (HL60)	Peripheral blood mononuclear cells (PBMC)	<i>Viability, apoptosis (DNA fragmentation, annexin V staining), lipid peroxidation</i> → preferential killing of cancerous cells	(Premanathan et al. 2011)
Breast adenocarcinoma cells (MCF-7, MDA-MB-231), nasopharyngeal carcinoma cells (KB)	HUVECs, lymphocytes from PBMC, breast epithelial cells, normal human dermal fibroblasts (NHDF)	<i>Viability, morphology, cytoskeleton, intracellular + mitochondrial ROS, mitochondrial membrane potential, apoptosis/necrosis, cell cycle progression; coating with starch, silica, and PEG</i> → more pronounced effects on cancerous cells in the above-mentioned variables, measurement of extracellular pH value suggested association with preferred dissolution in acidic tumor-microenvironment	(Sasidharan et al. 2011)
Neuroblastoma cells (SH-SY5Y)	Rat mesenchymal stem cells	<i>Viability, ROS</i> → proliferating pluripotent mesenchymal stem cells were more sensitive than osteogenically differentiated mesenchymal cells	(Taccola et al. 2011)
Hepatocellular carcinoma cells (HepG2), lung adenocarcinoma cells (A549)	Immortalized bronchial epithelial cells (BEAS-2B) [non-cancerous origin see (Reddel et al. 1989)], primary rat hepatocytes and astrocytes	<i>Viability, signalling (qPCR and western blot p53, bax, bcl-2; caspase-3 activity), ROS, lipid peroxidation, antioxidant enzyme activity level</i> → immortalized cell lines were more sensitive than primary cells	(Akhtar et al. 2012)
-	Immortalized murine myoblast cells (C2C12) [non-cancerous origin see (McMahon et al. 1994)], mouse embryonic fibroblast cells (3T3-L1)	<i>Viability, lipid peroxidation, ROS, signalling (qPCR and western blot p53, bax, bcl-2; caspase-3 activity)</i> → C2C12 were more sensitive than 3T3-L1	(Chandrasekaran et al. 2015)

Malignant cell type	Non-malignant cell type	Key points	Reference
Cervical cancer cells (HeLa), breast cancer cells (MCF-7)	Murine fibroblasts (L929)	<i>Viability, uptake, ROS, apoptosis/necrosis, cell cycle progression, morphology, mitochondrial membrane potential</i> → preferential killing of cancer cells over normal cells by FITC-ZnO nanocomposites	(Gupta et al. 2015)
Breast cancer cells (MCF-7, MDA-MB-231, MB-468, T47D)	Peripheral blood mononuclear cells (PBMC)	<i>Viability, apoptosis, cell cycle progression, ROS, lipid peroxidation, signalling</i> (various proteins, please refer to publication) → doses of PEG-functionalized ZnO NP that were effective against tumor cells proved to be safe for PBMC	(Chakraborti et al. 2016)
Breast cancer cells (MDA-MB-231)	Murine fibroblasts (NIH-3T3)	<i>Viability, apoptosis (DNA fragmentation)</i> → unmodified ZnO NP and Triton-X-100 modified ZnO NP had larger cytotoxic effect on cancer cells than on normal cells	(KC et al. 2016)
Cervical cancer cells (HeLa)	Murine fibroblasts (L929)	<i>ROS, apoptosis/necrosis (annexin V staining, DNA fragmentation), uptake</i> → ZnO nanoflowers exhibited a higher cytotoxic effect against cancerous cells than against non-cancerous cells	(Paino et al. 2016)
Cervical cancer cells (HeLa)	Madin-Darby canine kidney (MDCK) cells	<i>Viability, morphology, signalling (qPCR p53, caspase-3), ROS, lipid peroxidation</i> → higher cytotoxic effect on cancerous cells than on non-cancerous cells	(Pandurangan et al. 2016)
Glioblastoma cells (T98G), lung carcinoma cells (H460), thyroid cancer cells (SNU-80)	Embryonic kidney cells (HEK293), lung fibroblasts (MRC-5)	<i>Viability, ROS, caspase activity, micronuclei formation, migration, signalling (various proteins, please refer to publication), immunocytochemistry</i> → different ZnO nanostructures displayed lower IC ₅₀ in three cancerous cell types compared to two non-cancerous cell types	(Wahab et al. 2016)

Malignant cell type	Non-malignant cell type	Key points	Reference
T cells (Jurkat), cutaneous T lymphocytes with cancerous Sézary disease (Hut-78T)	CD4 ⁺ T cells from PBMC	<i>Viability, uptake, dissolution, mitochondrial ROS, GSH activity</i> → selective cytotoxicity against cancer cells which was influenced by coating with polyacrylic acid (PAA) associated with decrease in zeta potential	(Wingett et al. 2016)
Breast cancer cells (MCF-7, MDA-MB-231)	Embryonic kidney cells (HEK293)	<i>Viability, apoptosis (DNA fragmentation, TUNEL assay), cell cycle progression, CFA, migration, expression of bax, bcl-2</i> → ZnO NP quantum dots displayed preferential killing of cancerous cells	(Arivazhagan et al. 2017)
Different oesophageal squamous cell carcinoma cell lines (ESCC)	-	<i>Cell proliferation, cell cycle</i> → zinc supplementation inhibited cell proliferation, mechanism might be associated with Orai1-mediated intracellular calcium oscillations	(Choi et al. 2017b)
Hypopharyngeal squamous cell carcinoma cells (FaDu)	Bone marrow derived mesenchymal stem cells (BMSC)	<i>Viability, morphology, apoptosis/necrosis, cell cycle progression, zinc ion release, qPCR caspase-3, DNA damage (comet assay)</i> → enhanced cyto- and genotoxicity towards cancerous cells compared to non-cancerous cells	(Moratin et al. 2017)

As the table shows up until now there is no consensus on the mechanism of cytotoxicity that conveys the preferential killing of tumor cells, but there are different mechanisms that are proposed to play an important role.

One theory is that preferential killing of tumor cells is based on the high metabolic activity of the usually fast dividing tumor cells. (Hanley et al. 2008; Hanley et al. 2009; Taccola et al. 2011) Nevertheless, it has also been shown that the doubling time alone is not sufficient to explain the sensitivity towards treatment with ZnO NP. (Wingett et al. 2016) The cell-specific vulnerability to suffer from oxidative stress and the phagocytic activity were also brought up as possible factors of influence. (Wang et al. 2009; Wingett et al. 2016)

Another theory is that ZnO NP are more easily dissolved in the acidic tumor microenvironment that stems from the Warburg effect. (Gatenby et al. 2004; Sasidharan et al. 2011; Liberti et al. 2016; Arivazhagan et al. 2017) Additionally, the usually positive charge of ZnO NP at the surface can favour the interaction with the negatively charged membrane of cancer cells. (Wingett et al. 2016; Shi 2017).

Besides the possibility to use ZnO NP as a stand-alone therapeutic agent, there is also the possibility to combine NP with the well-established standard therapies: chemotherapy and radiotherapy. It has been envisioned that anti-cancer drugs could be loaded into ZnO NP to combine both therapies and achieve additive or synergistic effects of both treatments. Preliminary studies show very promising results concerning the combination of ZnO NP with doxorubicin, daunorubicin, paclitaxel, or cisplatin. (Guo et al. 2008; Hackenberg et al. 2012; Deng et al. 2013; Sharma et al. 2016; Aswathanarayan et al. 2018)

Considering the photocatalytic activity of ZnO NP, it could be especially promising to combine the nanoparticles with irradiation. This might be visible light as used in photodynamic therapy (PDT), gamma-irradiation as used in radiotherapy or UV-light. Promising findings were made in *in vitro* experiments. (Guo et al. 2008; Zhang et al. 2008; Li et al. 2010; Hackenberg et al. 2012; Deng et al. 2013; Wang et al. 2013; Generalov et al. 2015; Sharma et al. 2016; Aswathanarayan et al. 2018) Cytotoxic effects of ZnO NP increase due to the radiation's energy, which likely generates ROS. It was already shown that gamma-irradiation can enhance the antimicrobial activity of ZnO NP (Swaroop et al. 2015; Hosny et al. 2017) , which is another indication that anti-cancer effects of ZnO NP may also be potentiated by the combination with irradiation. Currently the detailed evaluation of ZnO NP as a radiosensitizer for the treatment of cancer is still missing.

If the administration of ZnO NP is considered in therapeutic settings, the risk-assessment must go beyond experimental tests *in vitro*. Several recent reviews on the anti-cancer activity of ZnO NP (Rasmussen et al. 2010; Bedi et al. 2015; Mishra et al. 2017; Racca et al. 2018) show their huge potential in biomedical applications. Simultaneously they show that we are still far away from completely understanding the interactions between cells and ZnO NP; not to mention ZnO NP's behaviour in the human body. In order to pave the way for the translation of ZnO NP into clinics the hemocompatibility of the nanoparticles must be ensured. This includes the compatibility with erythrocytes, coagulation system, and an escape from the

immune system—which enables sufficiently long circulation times to reach the tumor site. (Racca et al. 2018) To allow for hemocompatibility, coating of ZnO NP with an appropriate shell may be considered. The protein corona may influence active or passive targeting—via specific targeting moieties or the EPR effect (enhanced permeability and retention effect (Nakamura et al. 2016)), respectively—to the tumor site. (Mishra et al. 2017)

After intraperitoneal administration of ZnO NP in mice the nanoparticles were found to have a very broad tissue distribution and accumulate in liver, spleen, lung, heart, and kidney. Zinc serum levels peaked 6 h after injection and remained high until 72 h after treatment. No elevation of the zinc level in the brain was seen which suggests that the blood brain barrier successfully blocks the entry of ZnO NP. (Li et al. 2012) Intravenously injected ZnO NP showed a similar biodistribution in mice. ZnO NP were rapidly removed from the bloodstream and accumulated in lung, spleen, kidney, and liver. As indicative of oxidative stress, the 8-oxo-2'-deoxyguanosine (8-oxo-dG) level in urine was found to be elevated after ZnO NP treatment and pathological changes were observed in lung and liver. (Fujihara et al. 2015) Another study detected changes in the blood values and confirmed the occurrence of oxidative stress and additionally noticed genotoxic effects. (Aula et al. 2018)

To my knowledge there is only one preliminary study that deals with the *in vivo* evaluation of ZnO NP as an anti-tumor agent. (Hassan et al. 2017) Further analyses must follow to unveil the behaviour of ZnO NP in a living organism and to assess their potential to be specifically targeted to a solid tumor to set free their toxic load at the tumor site.

6 Aim of the work

As illustrated in the introduction of this doctoral thesis zinc oxide nanoparticles (ZnO NP) hold great promise as innovative anti-tumor agent. They can be easily and cheaply synthesized in different forms and shapes and their toxicity can be tuned in different ways. Additionally, the human body can easily excrete an excess of zinc ions and it possesses many buffering mechanisms to protect non-malignant cells from sustaining damage by treatment with ZnO NP.

At the same time, zinc ions participate in a bunch of different vital bodily functions. Our knowledge of the exact role of zinc in all the signalling pathways is far away from being complete. There might be the danger that introducing ZnO NP into the human body will open a Pandora's Box of uncontrollable health hazards.

Many studies on the toxicity of ZnO NP lack meticulous description of the exact experimental conditions under which the nanoparticles were brought into contact with living cells. To work with ZnO NP and zinc ions being released by them is particularly challenging. Metal ions intervene with many signalling pathways and they can elicit toxicities via a multitude of mechanisms. Thus, to analyse the mechanisms of ZnO NP's toxicity, we need an in-depth understanding of the chemical and biological properties of the experimental system.

This doctoral thesis strives to broaden the knowledge on the interaction between ZnO NP and human cells—tumor cells and non-malignant cells—and their potential as innovative anti-tumor agent. To achieve that, a broad set of experiments was conducted under exactly uniform experimental conditions. This systematic approach aims at unveiling the concepts underlying the toxicity of ZnO NP in order to be able to precisely control their behaviour in an *in vivo* setting in the future.

In particular, the aim of this study was to investigate the chemical properties that convey the NP's toxicity (8.2), which also included ZnO@SiO₂ NP, zinc oxide nanoparticles covered by a silica shell (8.3). Furthermore, the intracellular consequences of treatment with ZnO NP were studied (8.4) with particular focus on genotoxicity (8.5) and the role of mitochondria and ROS (8.6). Finally, the selectivity of ZnO NP (8.7) and their performance as radiosensitizer (8.8) were evaluated.

7 Materials and methods

7.1 Materials

7.1.1 Chemicals

Unless stated otherwise, all standard chemicals were obtained from Carl Roth GmbH (Karlsruhe, Germany), Merck KGaA (Darmstadt, Germany), AppliChem GmbH (Darmstadt), Sigma-Aldrich Corporation (St. Louis, MO, USA), and Serva Feinbiochemica GmbH & Co. (Heidelberg, Germany).

7.1.2 Equipment

Table 3: Equipment

Equipment	Manufacturer
Atomic adsorption spectrometer	PerkinElmer Inc., Waltham, MA, USA
Autoclave 5050 ELV	Tuttnauer Europe B.V., Breda, Netherlands
Blotter Biorad criterion tank blotter	Bio-Rad Laboratories GmbH, Munich, Germany
Blotter Eco-mini tank blotter	Biometra GmbH, Göttingen, Germany
CASY® Cell Counter, model TT	Roche Diagnostics International AG, Basel, Switzerland
Centrifuge Biofuge fresco	Heraeus, Kendro Laboratory Products GmbH, Hanau, Germany
Centrifuge model 100 VAC Fisherbrand®	Thermo Fisher Scientific Inc., Waltham, MA, USA
Centrifuge Multifuge 1L-R	Heraeus, Kendro Laboratory Products GmbH, Hanau, Germany
ChemiDoc™MP imaging system	Bio-Rad Laboratories GmbH, Munich, Germany
CLSM Leica TCS SP5	Leica Microsystems GmbH, Wetzlar, Germany
COLCOUNT system	Oxford Optronix Ltd., Abingdon, UK
Electrophoresis chamber and corresponding gel plates with fixed spacers 1.0 mm and silicone seal 1.0 mm	Biometra GmbH, Göttingen, Germany
Flow Cytometer BD FACS Calibur	Becton, Dickinson and Company, Franklin Lakes, NJ, USA
Flow Cytometer BD FACS Canto	Becton, Dickinson and Company, Franklin Lakes, NJ, USA
Fluorometer Fluoroskan Ascent Microplate Reader	Thermo Fisher Scientific Inc., Waltham, MA, USA
Freezer	Robert Bosch GmbH, Stuttgart, Germany; Thermo Fisher Scientific Inc., Waltham, MA, USA; Heraeus, Kendro Laboratory Products GmbH, Hanau, Germany
Incubator HeraCell 150i CO ₂ Incubator	Heraeus, Kendro Laboratory Products GmbH, Hanau, Germany

Irradiation facility Gammacell 2000, gamma-source (Cs137)	Mølgaard Medical, Risø, Denmark
Laminar flow hood Flow Hera safe	Heraeus, Kendro Laboratory Products GmbH, Hanau, Germany
Magnetic stirrer Starlab Smart Instruments	Starlab International GmbH, Hamburg, Germany
Microscope AxioVert 200M	Carl Zeiss Jena GmbH, Jena, Germany
Microscope Nikon Eclipse TE2000-U	Nikon GmbH, Düsseldorf, Germany
Microscope Nikon TMS Inverted Phase Contrast Microscope	Nikon GmbH, Düsseldorf, Germany
Neubauer counting chamber	Brand GmbH + Co. KG, Wertheim, Germany
Nitrogen tank CRYO-4000	Chart Industries, Burnsville, MN, USA
Photometer Multiskan Ascent	Thermo Fisher Scientific Inc., Waltham, MA, USA
Pipettes	Eppendorf AG, Hamburg, Germany; Greiner bio-one International GmbH, Kremismünster, Austria; Brand GmbH + Co. KG, Wertheim, Germany
Pipetting aid pipetus®	Hirschmann Laborgeräte GmbH & Co. KG, Eberstadt, Germany
Plate reader Infinite 200 Pro	Tecan, Männedorf, Switzerland
Power supply 1000/500	Bio-Rad Laboratories GmbH, Munich, Germany
Power supply Standard Power Pack P25	Biometra GmbH, Göttingen, Germany
Refrigerator profi line	Liebherr-International Deutschland GmbH, Biberach an der Riß, Germany
Scale Kern PCB	Kern und Sohn GmbH, Balingen, Germany
Scale Precision Advanced DHAUS	As-Wägetechnik GmbH, Garching, Germany
Shaker IKA® KS 260 basic	IKA®-Werke GmbH & CO. KG, Staufen, Germany
Spectrometer 5100 ZL AA	PerkinElmer Inc., Waltham, MA, USA
Swivel table Rocky® 3D	Labortechnik Fröbel GmbH, Lindau, Germany
Swivel table WS-10	Edmund Bühler GmbH, Hechingen, Germany
Thermomixer comfort	Eppendorf AG, Hamburg, Germany
Transmission electron microscope FEI Tecnai G2 12 BioTwin	FEI Company, Hillsboro, OR, USA
Ultrasonic bath Emag Emmi 40HC	emag AG, Mörfelden-Waldof, Germany
Ultrasonic homogeniser Sonoplus mini20	BANDELIN electronic GmbH & Co. KG, Berlin, Germany
Vortex IR Starlab Smart Instruments	Starlab International GmbH, Hamburg, Germany
Vortex Top-Mix 11118 Fisherbrand®	Thermo Fisher Scientific Inc., Waltham, MA, USA
Vortex VWR VV3	VWR International GmbH, Darmstadt, Germany
Water bath GFL Shaking Water Bath 1083	GFL Gesellschaft für Labortechnik mbH, Burgwedel, Germany
X-ray diffractometer AXS D8 Advance	Bruker Corporation, Billerica, MA, USA
Zetasizer Nano ZS	Malvern Instruments Ltd., Malvern, UK

7.1.3 Consumables

Table 4: Consumables

Product	Manufacturer
Cell culture dishes Advanced TC Dish, Sterile, 60x15 mm	Greiner bio-one International GmbH, Kremsmünster, Austria
Cell culture dishes ibiTreat, sterile, μ -Dish 35 mm, high	ibidi GmbH, Munich, Germany
Cell culture flasks 175 cm ² , 75 cm ² , 25 cm ²	Greiner bio-one International GmbH, Kremsmünster, Austria
Cell culture plate μ CLEAR 96 well plate, black	Greiner bio-one International GmbH, Kremsmünster, Austria
Cell culture plate 6 well cellstar®	Greiner bio-one International GmbH, Kremsmünster, Austria
Cell scraper BD Falcon TM	Becton, Dickinson and Company, Franklin Lakes, NJ, USA
Centrifuge Tubes cellstar® 10 mL, 50 mL	Greiner bio-one International GmbH, Kremsmünster, Austria
Cover glasses	IDL GmbH & Co. KG, Nidderau, Germany
Cryo tubes Cryo.S™	Greiner bio-one International GmbH, Kremsmünster, Austria
Immobilon®-P-Transfer-Membran (PVDF; 0.45 μ m)	Millipore Corporation, Billerica, MA, USA
Parafilm „M“™ Laboratory Film	Pechiney Plastic Packaging, Inc., Chicago, IL, USA
Pasteur pipettes (glass, disposable)	Carl Roth GmbH, Karlsruhe, Germany
Pipette tips 0,5-20 μ L, 10-200 μ L, 100 μ L-1'000 μ L	Kisker Biotech GmbH & Co. KG, Steinfurt, Germany Sarstedt AG & Co. KG, Nümbrecht, Germany
Serological pipettes 5 mL, 10 mL, 25 mL	Greiner bio-one International GmbH, Kremsmünster, Austria
TEM Grids, carbon film, coated, 5-6 nm, 300 Mesh, Cu	EMS Electron Microscopy Sciences, Hatfield, PA, USA
Tubes Round-Bottom Polystyrene Tube 12x75 mm style	Corning Incorporated, Corning, NY, USA
Tubes safe-lock 0,5 mL, 1,5 mL, 2 mL, 5 mL	Eppendorf AG, Hamburg, Germany

7.1.4 Buffers, solutions, and cell culture medium

Cell culture medium

- DMEM/ F-12 Ham with L-glutamine and phenol red without HEPES (Dulbecco's Modified Eagle Medium)
- + 10% (v/v) fetal calf serum (FCS)
- + 2% (v/v) penicillin and streptomycin (Pen-Strep)

Wet blot transfer buffer

- 6.06 g Tris
- 29.3 g glycine
- 400 mL methanol
- 7.4 mL 10% (w/v) sodium dodecyl sulphate (SDS) solution
- filled up to 2'000 mL with deionized water

Cell lysis buffer

- 0.8 g SDS
- 1 mL 2 M Tris/ HCl pH 6.8-7.5
- 4.6 mL glycerine
- 2 mL deionized water
- 2 tablets cOmplete™ Protease Inhibitor Cocktail (Roche, Grenzach-Wyhlen, Germany)
- 1 tablet PhosSTOP EASYpack phosphatase inhibitor cocktail (Roche, Grenzach-Wyhlen, Germany)

10x TBS-washing buffer (Tris buffered saline)

- 24.2 g Tris
- 80 g NaCl
- 1'000 mL deionized water
- pH value adjusted to 7.6 with HCl

1x TBST₂₀-washing buffer

- 200 mL 10x TBS-Washing buffer
- 1'800 mL deionized water
- 2 mL Tween₂₀

5x Electrophoresis buffer

- 30 g Tris
- 144 g glycine
- 1'000 mL deionized water

1x Electrophoresis buffer

- 100 mL 5x Electrophoresis buffer
- 5 mL SDS
- filled up to 500 mL with deionized water

Stripping buffer

- 1.) 1.876 g glycine in 1 L deionized water, pH value adjusted to 2.0 with HCl
- 2.) 1% (w/v) SDS

BSA-T-PBS washing buffer

- 0.2% (v/v) Triton X-100
- 1% (w/v) BSA
- in PBS

PI (propidium iodide) staining solution

- 0.1% (w/v) RNase A (ribonuclease A from bovine pancreas, Sigma-Aldrich Corporation, St. Louis, MO, USA)
- 5 µg/mL PI (Abcam, Cambridge, UK)
- in PBS

7.2 Methods

7.2.1 Synthesis of zinc oxide nanoparticle (ZnO and ZnO@SiO₂ NP)

The solvothermal synthesis of the unmodified ZnO NP was adapted from (Cheng et al. 2006) with some modifications. 5 mmol of Zn(ac)₂·2 H₂O was dissolved in 10 mL methanol and gently shaken. 20 mL of tetramethylammonium hydroxide 25% (w/w) in methanol were slowly added and the mixture was stirred for 20 min. The reaction mixture was transferred to a 50 mL teflon-lined stainless-steel autoclave and heated at 50°C for 24 h. The colourless precipitate was separated by centrifugation and washed twice with deionized water. Finally, the product was dispersed in ethanol and stored at RT for long term storage or dried in air for short term storage.

The APTES FITC conjugate synthesis for dye functionalization of ZnO@SiO₂ NP was carried out by dissolving 0.003 mmol of FITC in 0.5 mL of dry DMSO (solution 1). 0.009 mmol of APTES were dissolved in 0.5 mL of dry DMSO (solution 2). Afterwards, solution 1 was added to solution 2 and the mixture was stirred overnight at RT under exclusion of light. The APTES FITC conjugate can be stored at 8°C for up to 2 d.

The synthesis of “heat up” ZnO (HU) NP was adapted from (Tahir et al. 2013) with some modifications. 0.5 mmol Zn(ac)₂·2 H₂O (pre-annealed at 110°C for 10 min) were dispersed in 4 mL of benzyl alcohol, 3 mL of oleyl amine, and 2 mL of 1-octadecene under inert gas conditions and stirred for 5 min. The mixture was heated to 120°C for 20 min and then heated to 230°C for 30 min. Afterwards, the mixture was slowly cooled to RT. The colourless product was precipitated, separated by centrifugation, dispersed in cyclohexane, and washed twice by adding ethanol (cyclohexane:ethanol = 1:2). Finally, the product was dispersed in cyclohexane and stored at RT.

The synthesis of ZnO@SiO₂ NP with HU ZnO NP was carried out using a reverse microemulsion technique. 2 g of Igepal CO-520 and 100 µL of oleyl amine were dispersed in 40 mL of cyclohexane. The mixture was ultrasonicated for 15 min. 10 mg of HU ZnO NP were added and the mixture was ultrasonicated for additional 15 min. 150 µL of ammonium hydroxide solution of pH 11.5 were added and the mixture was stirred for additional 10 min. The stirring speed was increased to maximum and 120 µL of TEOS were injected rapidly. After 20 min 5 µL of the preformed APTES-FITC conjugate was added. The mixture was stirred overnight at maximum stirring speed. In the morning and evening of the next day 15 µL of TEOS each were added, and the mixture was again stirred overnight. 100 µL of PEGTES were subsequently added and the mixture was stirred for additional 4 h. The precipitate

was separated by centrifugation, dispersed in ethanol, and washed twice by adding cyclohexane (ethanol:cyclohexane = 1:2). Finally, the product was dispersed in ethanol and stored at 8°C.

For description of the synthesis in greater detail please refer to the doctoral thesis of Martin Klünker. From 2015 until January 2017 all NP were synthesized and characterized by Martin Klünker. Then Melanie Viel took over synthesis and characterization. Both were members of the working group of Prof. Dr. Wolfgang Tremel, Inorganic and Analytical Chemistry, Mainz.

7.2.1.1 Characterization of the nanoparticles

The NP were characterized by transmission electron microscopy (TEM), X-ray diffraction, and zeta potential measurements. Samples for TEM were prepared by placing a drop of NP dispersion in cyclohexane on a carbon coated copper grid. TEM images for the characterization of size and morphology were obtained using a FEI Tecnai 12 equipped with LaB6 source at 120 kV and a twin-objective together with a Gatan US1000 CCD-camera (2kx2k pixels). X-ray diffraction patterns were recorded on a Bruker AXS D8 Advance diffractometer equipped with a SolX energy dispersive detector in reflection mode using unfiltered MoK α radiation. Crystalline phases were identified according to the PDF-2 database using Bruker AXS EVA 10.0 software. Measurements of the zeta potential of the NP were performed using a Zetasizer Nano ZS (Malvern Instruments Ltd., Malvern, UK) and a disposable capillary cell. Typically, 1 mL aliquots of each sample were injected into the capillary cell and 5–10 measurements per sample were performed at 25°C.

7.2.1.1.1 Atomic absorption spectroscopy

Atomic absorption spectroscopy (AAS) measurements were conducted using a Perkin Elmer 5100 ZL AA spectrometer (PerkinElmer Inc., Waltham, MA, USA) with a Zeeman Furnace Module and a Zn hollow cathode lamp at 213.9 nm and air/acetylene mixture. For zinc ion detection the sample was treated with aqua regia overnight to dissolve any ZnO and denature any proteins. Afterwards the sample was diluted with deionized water. Samples were analysed using the whole flame width to ensure maximum ionization and reduced matrix effects. A 3-point calibration was carried out with 9 measurements for each concentration. Between sample measurements the instrument was rinsed with aqua regia and deionized water.

7.2.1.1.2 Measurement of reactive oxygen species (ROS) at the NP

We tested ZnO NP for the formation of reactive oxygen species (ROS) at the surface in two *in vitro* assays without cells being present.

The formation of superoxide radicals was assessed with the help of a solution of iodinitrotetrazolium chloride (INT, 1.23 mg/mL). For this purpose, 300 μ L 1 mg/mL ZnO NP were mixed with 2'100 μ L deionized water or cell culture medium, respectively, and 600 μ L INT solution. Upon reaction with superoxide radicals INT is transformed into a red dye with an absorption maximum at 505 nm. The reaction mixture was incubated in the plate reader (Infinite 200 Pro plate reader, Tecan Trading AG, Männedorf, Switzerland) which measured in the range from 400–700 nm every 15 min.

To detect hydroxyl radicals 3,3',5,5'-tetramethylbenzidine (TMB) was used. 270 μ L 1 mg/mL ZnO NP were mixed with 1'872 μ L deionized water or cell culture medium, respectively, 108 μ L 1 mg/mL horseradish peroxidase (HRP), and 450 μ L 0.48 mg/mL TMB. The reaction mixture was incubated in the plate reader (Infinite 200 Pro plate reader, Tecan Trading AG, Männedorf, Switzerland). It was measured in the range from 300 to 800 nm every 10 min which covered the expected absorbance after reaction at 652 nm.

7.2.2 Cells, cell culture, and nanoparticle treatment

7.2.2.1 Cells

For the study immortalized tumor cell lines of different origin we chosen. Those were the following: A549 (non-small cell lung cancer (NSCLC)), HeLa (cervix carcinoma), HNSCCUM-02T (squamous cell carcinoma (SCC) of the tongue), T24 (urothelial carcinoma), RPMI 2650 (SCC of the nasal septum) and FaDu (SCC of the pharynx). The head and neck squamous cell carcinoma (HNSCC) cell line HNSCCUM-02T was previously established and characterized in our laboratory (Welkoborsky et al. 2003). The other cell lines were purchased from DSMZ (German Collection of Microorganisms and Cell Cultures, Braunschweig, Germany). Their identity was verified by STR analysis. As representatives of healthy, non-malignant tissue, human fibroblasts isolated from oral mucosa and human umbilical vein endothelial cells (HUVECs) isolated from umbilical cord were chosen. Fibroblasts were isolated from material obtained from patients who underwent surgery at the University Medical

Center, Mainz, Germany as previously described. (Heller et al. 2016) The isolation of HUVECs was described in (Heller et al. 2015).

7.2.2.2 Cell culture

For cell culture PBS (Dulbecco's Phosphate Buffered Saline), cell culture medium (DMEM = Dulbecco's Modified Eagle Medium / Nutrient Mixture F-12 Ham), penicillin and streptomycin (Pen-Strep), Accutase[®] solution, and trypsin-EDTA were obtained from Sigma-Aldrich Corporation (St. Louis, MO, USA).

Cells were maintained in DMEM/Ham's F12 supplemented with 10% (v/v) FCS (fetal calf serum) and antibiotics (100 U/mL penicillin and 100 mg/mL streptomycin) at 37°C in 5% (v/v) CO₂. HUVECs were cultivated in special cell culture medium for endothelial cells (Endopan 3, Pan Biotech, Aidenbach, Germany).

From 2015 until 2017 fetal calf serum (FCS) from Sigma-Aldrich (Newborn Calf Serum, product number: N4637, Sigma-Aldrich Corporation, St. Louis, MO, USA) was used. Beginning on January 2018 a new batch FCS was used which was obtained from Seradigm (Bovine calf serum iron supplemented, product number: 2100, VWR Life Science Seradigm, Radnor, PA, USA). With the new batch of FCS, the cells exhibited an increased proliferation but for consistency reasons the level of 10% (v/v) FCS in the cell culture medium was maintained. The following experiments were conducted with the new FCS: MitoSOX[™] Red assay, cytochrome c release assay, western blots, and the colony formation assay.

All cell culture work was carried out within a laminar flow hood to avoid any contamination from outside and cells were subjected regularly to a PCR-based test to ensure absence of mycoplasma.

To harvest cells, culture medium was discarded, cells were washed with PBS, and detached from the cell culture plate by trypsin-EDTA or Accutase[®] solution. The latter was used when flow cytometry experiments were planned. If necessary, cell numbers were determined microscopically by staining with 0.4% (w/v) trypan blue solution and counting of the cells in the Neubauer counting chamber. For the colony formation assay the CASY[®] cell counter was used to determine cell numbers. Cells were only used until passage 50 and were then discarded.

7.2.2.3 Nanoparticle treatment conditions

ZnO NP were stored airtightly sealed at 8°C and 10 mg/mL ZnO NP dispersions were freshly prepared immediately before each experiment with high-purity water

(Ampuwa®, Fresenius Kabi GmbH, Bad Homburg, Germany). To disperse the NP, they were ultrasonicated 5 min with 220–240 V and 37 kHz in an Elmasonic S 40 bath sonicator (Elma Schmidbauer GmbH, Singen, Germany). Before and after the ultrasonication NP were thoroughly vortexed for ten seconds. To prevent sedimentation the NP dispersion was pipetted up and down immediately before the NP were added to the cells. This step was repeated for every cell culture dish that was treated with NP. Cells in 25 cm² cell culture flasks, small cell culture dishes, and in 6 well plates were directly treated with the 10 mg/mL stock solution of ZnO NP, cells in 96 well plates were treated with an intermediate dilution of 1 mg/mL.

ZnCl₂ solution (0.1 M solution, Sigma-Aldrich Corporation, St. Louis, MO, USA) was diluted to the proper concentration with high-purity water.

ZnO@SiO₂ NP were stored in ethanol and transferred to water immediately before usage by centrifugation, redispersion by short ultrasonication, and two washing steps to eliminate remnants of ethanol.

Cells were incubated with the indicated amount of ZnCl₂ / ZnO NP / ZnO@SiO₂ NP for 4 h, followed by an exchange of the cell culture medium. To remove the cell culture medium with excessive NP completely a vacuum pump was used. At that timepoint cells were still attached to the cell culture plate. If cells were harvested for any analysis later than 4 h after beginning treatment with NP, the cells, that were detached from the cell culture plate, were included in the analysis by pooling the cells in the cell culture medium and the cells harvested from the cell culture plate.

7.2.3 Viability measurement

For the analysis of the cellular viability the cellular metabolic activity (CMA) of the cells was assessed with the alamar Blue® reagent (BIOZOL Diagnostica Vertrieb GmbH, Eching, Germany and Thermo Fisher Scientific Inc., Waltham, MA, USA). 10'000 cells per well were seeded in a 96 well plate and cultivated overnight for adherence. The next day, cells received fresh cell culture medium (200 µl) and were treated with the indicated amount of ZnO NP, ZnO@SiO₂ NP, ZnCl₂, MgCl₂ or supernatant of ZnO NP depending on the aim of the experiment. The required amount of ZnO@SiO₂ NP was calculated based on the estimated zinc oxide amount that was enclosed in the silica shell measured by AAS. Treatment with the equivalent amount of water served as negative control (= untreated) and treatment with 70% (v/v) ethanol in water as positive control. Unless stated otherwise in the results section, medium was exchanged for fresh medium after 4 h with the help of a vacuum pump. To the cell

culture medium of all wells 10% alamar Blue® was added at the indicated time points and the samples were incubated for additional 3 h at 37°C. The results were obtained using a plate reader (Fluoroskan Ascent Microplate reader, Thermo Fisher Scientific Inc., Waltham, MA, USA; excitation: 540 nm, emission: 600 nm) and normalized to control cells (=100% viability).

7.2.4 *In vitro* DNA damage analysis

To test *in vitro* the influence of ZnO NP, ZnCl₂, ROS and combinations on the integrity of plasmid DNA we diluted 200 ng plasmid DNA (pGlow TOPO™ with CMV insert, Thermo Fisher Scientific Inc., Waltham, MA, USA) in 20 µL nuclease-free water (water, bioscience grade, nuclease free, autoclaved DEPC-treated water, Carl Roth GmbH, Karlsruhe, Germany) and incubated it with 100 µg/mL ZnO NP or equivalent amounts of ZnCl₂, respectively, at 37°C for 1 h. Some samples were additionally treated with 1 mM hydrogen peroxide (H₂O₂). To assess potential pH dependence of the reaction the pH-value of the H₂O (Ampuwa®, Fresenius Kabi Deutschland GmbH, Bad Homburg, Germany) used to dilute the ZnO NP or ZnCl₂, respectively, was adjusted to pH 5, 7 or 8. As a positive control for double strand breaks plasmid DNA was linearized by enzymatic digestion using KpnI, resulting in a single 5988 bp fragment. After incubation, 10 µL of the samples were loaded onto an agarose gel, stained with ethidium bromide, and run according to standard conditions.

7.2.5 Microscopy

7.2.5.1 Light Microscopy

For light microscopical imaging of cellular morphology after ZnO NP treatment, cells were seeded in 25 cm² cell culture flasks and treated with NP according to the standard procedure. Pictures were taken prior to the treatment and after 2 h, 4 h, 8 h, and 24 h with a fluorescence microscope AxioVert 200M (Carl Zeiss Jena GmbH, Jena, Germany). Cells treated with an equivalent amount of water served as control.

7.2.5.2 Confocal laser scanning microscopy (CLSM)

For confocal laser scanning microscopy 250'000 cells were seeded in cell culture dishes (ibiTreat, ibidi GmbH, Munich, Germany) and cultivated overnight for adherence. Cells were then treated with ZnO@SiO₂ NP according to the standard procedure on the basis of the estimated zinc oxide amount that was enclosed in the

silica shell measured by AAS. After 4 h cells excessive NP were removed with the cell culture medium using a vacuum pump and cells were washed twice with PBS. Then the cells were maintained in cell culture medium without phenol red and transported to the Max Planck Institute for Polymer Research for CLSM imaging in the working group of Prof. Dr. Volker Mailaender. CellMask™ Orange Plasma membrane stain (Thermo Fisher Scientific Inc., Waltham, MA, USA) was used to visualize the cell contours. Confocal images were acquired on a Leica TCS SP5 (Leica Microsystems GmbH, Wetzlar, Germany).

7.2.5.3 Immunofluorescence

For immunofluorescence staining 250'000 cells were seeded on cover glasses in 6 well plates and treated with ZnO@SiO₂ NP according to the standard procedure based on the estimated zinc oxide amount that was enclosed in the silica shell measured by AAS. After 4 h excessive NP were removed with the cell culture medium using a vacuum pump and cells were washed three times with PBS (3x5 min). Cells were fixed with 4% (w/v) paraformaldehyde in PBS (15 min), washed again three times with PBS, and stored at 4°C in the dark until staining. Prior to staining cells were incubated in blocking buffer (5% (w/v) BSA and 0.3% (v/v) Triton-x-100 in PBS) for 1 h. Then they were incubated with the primary antibody (Anti-Lamin A + C antibody [EPR4100], nuclear envelope marker (ab108595) 1:500 in PBS with 0.3% (v/v) Triton-x-100) for 1 h at RT, washed twice with PBS, incubated 2 min in TBS with 400 mmol NaCl, and washed again with PBS. Afterwards cells were incubated with the secondary antibody (goat anti-rabbit 1:500 in PBS with 0.5% (w/v) BSA and 0.3% (v/v) Triton-x-100) for 1 h at RT. Finally, cells were washed again twice with PBS, incubated 2 min in TBS with 400 mmol NaCl and washed with PBS. Then the cover glasses with the cells were removed from the 6 well plates and transferred to microscope slides using Fluorescence Mounting Medium (Dako Omnis, Agilent, Santa Clara, CA, USA). Immunofluorescent staining was conducted by Karin Benz. Images were taken at the fluorescence microscope AxioVert 200M (Carl Zeiss Jena GmbH, Jena, Germany).

7.2.6 Flow cytometry

Flow cytometry is a very powerful tool to analyse the optical and fluorescent characteristics of single cells in a fluid stream in a fast and quantitative manner. While fluorescence microscopy can be biased by the image section that is chosen for

analysis flow cytometry allows the accurate and simple analysis of high numbers of cells. In flow cytometry refracted or emitted light is used to identify certain cellular characteristics. Two types of light scatter occur when cells are hit by the laser beam, the forward scatter (FSC) that is proportional to the cell size and the side scatter (SSC) that is proportional to the granularity of the cell. Those values provide first information about the cells which can be supplemented with a huge amount of different dyes. (Adan et al. 2017) The principle of flow cytometry is depicted in Figure 22.

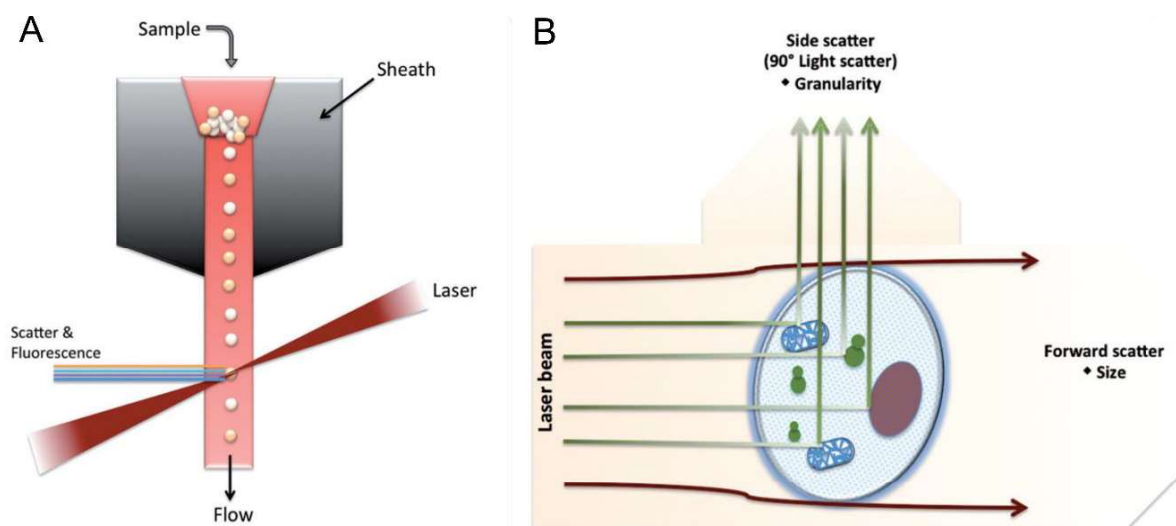


Figure 22: Principle of flow cytometry

Flow cytometry is a technology that is used to analyse the physical and chemical characteristics of cells in a fluid as it passes through a couple of lasers (A). Cell components are fluorescently labelled and then excited by the lasers to emit light at varying wavelengths. Additionally, light scattering provides insights into cellular size (forward scatter = FSC) and cellular granularity (side scatter = SSC) (B). [image modified according to (Adan et al. 2017)]

7.2.6.1 Apoptosis assay

Apoptosis and necrosis were assessed via parallel staining with propidium iodide (PI) and annexin V-FITC, followed by flow cytometric analysis. Positive staining with PI marks loss of cellular integrity. Positive staining with annexin V-FITC labels cells that are undergoing apoptosis while necrotic cells are not stained.

For the apoptosis assay 600'000 cells were seeded in 25 cm² cell culture flasks, the next day they were treated with the indicated amount of ZnO NP or ZnCl₂ for 4 h according to the standard procedure, then cell culture medium was changed, and cells were harvested 4 h, 12 h, 16 h, 18 h, 20 h, 24 h, 48 h, 72 h, and 96 h after the beginning of the treatment. Please note that the indicated time points in all figures and analyses refer to the beginning of the NP treatment, that means "8 h" = eight hours after beginning of the NP treatment and four hours after the removal of

excessive particles, as NP treatment lasted four hours. Cells treated with an equivalent amount of water served as control. Cells that additionally were irradiated received 4 Gray gamma irradiation 3 h after beginning NP treatment using the irradiation facility Gammacell 2000.

Afterwards cells were stained with PI (Thermo Fisher Scientific Inc., Waltham, MA, USA) and annexin V-FITC (BioLegend™, San Diego, CA, USA) according to manufacturers' specifications. All cells were included in the analysis, those that were still attached to the cell culture plate and those that were detached and were found in the cell culture medium. Cell samples were then analysed with a FACS Canto II flow cytometer (Becton, Dickinson and Company, Franklin Lakes, NJ, USA) and data was analysed via the cytobank platform (<https://www.cytobank.org/>, Cytobank, Inc., Santa Clara, CA, USA). Cells without staining, were considered to be alive, cells which were single stained by PI to be necrotic and single stained by annexin V-FITC to be apoptotic and those which were stained by PI and annexin V-FITC to be dead.

7.2.6.2 Cell cycle analysis

To analyse the cell cycle distribution of non-synchronized cells, staining with DNA binding dyes and subsequent flow cytometric analysis can be used. DNA binding dyes such as propidium iodide (PI) are stoichiometric, this means that they bind in proportion to the amount of DNA present in the cell. Thus, the amount of staining of every cell indicates the amount of DNA in the cell and thus the cell cycle phase it is currently in.

For the cell cycle analysis 600'000 cells were seeded in 25 cm² cell culture flasks, the next day they were treated with the indicated amount of nanoparticles according to the standard procedure. At the indicated time points cells were then harvested for flow cytometric analysis. Firstly, cells were washed with PBS and after centrifugation the supernatant was discarded. Cells were then taken up into 500 µL PBS and 4.5 mL of ice-cold ethanol was added. Both liquids were carefully mixed, and the cells were incubated for at least two hours at -20°C. This step ensures fixation and permeabilization of the cells to allow PI to enter the cells in the following step. Cells were washed two times with BSA-T-PBS washing buffer (suspending of the cells + 5 min incubation at RT + centrifugation + discarding of the supernatant). Then cells were suspended in PI staining buffer, transferred to round button tubes for flow cytometry and after 5 min 400 µL PBS was added to each sample. Cells were analysed with the FACSCanto™ flow cytometer and the collected data was evaluated

with the corresponding software. The measurements were corrected for doublets using the PI-A (area) vs. the PI-W (width) values. The analysis with the ModFit LT software was not possible because the huge increase in debris after NP treatment interfered with the automated cell cycle phase detection.

7.2.6.3 MitoSOX™ Red mitochondrial superoxide indicator assay

MitoSOX™ Red is a novel fluorescent dye which selectively labels superoxide in the mitochondria of living cells. MitoSOX™ Red reagent is live-cell permeant and is rapidly and selectively targeted to the mitochondria. Once in the mitochondria, MitoSOX™ Red is oxidized by superoxide it exhibits red fluorescence. Two different aspects complicate the data acquisition with MitoSOX™ Red: MitoSOX™ Red is a non-ratiometric probe that exhibits substantial cell-to-cell variability and every cell contains little amounts of superoxide in the mitochondria, thus the expected staining pattern is not of clear on-off fashion. To cope with these hurdles and obtain meaningful quantitative information, suitably big numbers of cells were analysed, every experiment was accompanied by positive and negative controls which served as reference values and the assay required some fine-tuning regarding the handling of the cells as proposed in (Polster et al. 2014). As positive control I used cells which were treated with 50 µM antimycin A for 2 h (antimycin A from *Streptomyces* sp., Sigma-Aldrich Corporation, St. Louis, MO, USA, dissolved in ethanol to a 10 mM stock solution, and stored at 4°C. Please note that this reagent is only stable for 3 to 4 months.) Untreated cells served as negative control. As treatment with ZnO NP also induced a huge amount of unspecific autofluorescence an unstained probe for compensation was carried along for each stained cell sample. Additionally, a live-dead staining was carried out, to be able to exclude the dead cells from the evaluation. It was refrained from using N-acetylcysteine (NAC) as ROS scavenger as negative control as cysteines have a high affinity to zinc and thus distort the treatment with ZnO NP (Pace et al. 2014; Xueju et al. 2015).

The staining procedure that provided best results concerning cellular viability, reproducibility, and consistence was based on (Puleston 2015). For the assay 600'000 cells were seeded in 25 cm² cell culture flasks and the next day they were treated with the indicated amount of nanoparticles according to standard procedure. At the indicated time points cells were then harvested for flow cytometric analysis. Please note that the indicated time points in all figures and analyses refer to the beginning of the NP treatment, that means "8 h" = eight hours after beginning of the

NP treatment and four hours after the removal of excessive particles as NP treatment lasted four hours. Cells were harvested using Accutase[®] cell detachment solution and all cells were included in the measurement, also those that did already detach from the cell culture plate upon treatment with ZnO NP. After centrifugation cells were washed with Hank's Balanced Salt Solution with calcium and magnesium (HBSS, Thermo Fisher Scientific Inc., Waltham, MA, USA). Afterwards cells were suspended in 1 mL of PBS with 1% (w/v) glucose, and each sample was divided into three samples of 333 μ L volume. One sample remained unstained, one was stained for cellular integrity with 7-Aminoactinomycin D (2 μ L / 333 μ L cell suspension, Thermo Fisher Scientific Inc., Waltham, MA, USA), and one for cellular integrity and ROS production. For MitoSOX[™] Red staining 1 μ L / 333 μ L cell suspension of freshly prepared MitoSOX[™] Red staining solution in DMSO was used which was prepared according to manufacturers' specifications. Cells were incubated with the MitoSOX[™] Red staining solution for 30 min in the incubator, whereby cells were carefully moved every 10 min by tapping against the tubes. At the flow cytometer cells were further diluted by adding 200 μ L PBS with 1% (w/v) glucose. Cells were analysed with the FACSCanto[™] flow cytometer and the collected data was evaluated with the corresponding software. Each sample was corrected for autofluorescence, dead cells were excluded, and the relative mitochondrial superoxide level was calculated by setting the staining of the untreated cells to 100% and expressing the other values in relation to that. The experiment was repeated independently several times such that every time point was covered at least three times.

7.2.6.4 Cytochrome c release assay

For the cell cytochrome c release assay 600'000 cells were seeded in 25 cm² cell culture flasks and the next day they were treated with the indicated amount of nanoparticles according to the standard procedure. At the indicated time points cells were then harvested for flow cytometric analysis using Accutase[®] cell detachment solution. All cells were included in the measurement, also those that did already detach from the cell culture plate upon treatment with ZnO NP. Please note that the indicated time points in all figures and analyses refer to the beginning of the NP treatment, that means "8 h" = eight hours after beginning of the NP treatment and four hours after the removal of excessive particles as NP treatment lasted four hours. After harvesting and washing cells with PBS (suspension, centrifugation, discarding of the supernatant), each cell sample was suspended in 1 mL PBS and subjected to

a live-dead-staining with 7-Aminoactinomycin D (1 μ L /1 mL cell suspension, 20 min, Thermo Fisher Scientific Inc., Waltham, MA, USA). Cells were again washed with PBS (suspension, centrifugation, discarding of the supernatant). Then the cytochrome c release assay was conducted with the FlowCelect™ Cytochrome c Kit (Millipore Corporation, Billerica, AM, USA) according to manufacturers' specifications. Cells treated with ZnO NP exhibited a high level of autofluorescence. Therefore, to correct for that, for every stained cell sample an unstained control sample was processed in parallel. Additionally, a staining with the isotype control included in the kit was carried along for all samples, which ensured that unspecific binding of the antibody was ruled out. Cells were analysed with the FACSCalibur™ flow cytometer and the collected data was evaluated with the corresponding software. Each sample was corrected for autofluorescence and dead cells were excluded from the analysis.

7.2.7 Colony formation assay (CFA)

For the colony formation assay (CFA) 600'000 cells were seeded in 25 cm² cell culture flasks and the next day they were treated with 100 μ g/mL ZnO NP and/or 4 Gray gamma-irradiation according to the following scheme in Table 5.

Table 5: Treatment groups for the colony formation assay

1	Untreated	Untreated control cells
2	4 Gray	Treated with 4 Gray irradiation
3	NP	Treated with 100 μ g/mL ZnO NP for 4 h
4	NP + 4 Gray	Treated with 100 μ g/mL ZnO NP for 4 h, at 3 h 4 Gray irradiation was applied
5	4 Gray -> NP	Irradiated first with 4 Gray, then treated with 100 μ g/mL for 4 h
6	NP -> 4 Gray	Treated with 100 μ g/mL for 4 h, then irradiated with 4 Gray

Immediately after treatment all cells were harvested with Accutase® cell detachment solution and the number of viable cells was determined with the CASY® cell counter. In order to reach representative yet not too high colony numbers between 5'000 and 35'000 cells were seeded in new 25 cm² cell culture flasks depending on the experimental group. After ten days cultivation time in the incubator, cells were washed with deionized water and fixed with cold ethanol and acetone (1:1). The cell culture flasks were dried at RT overnight. After 24 h the colonies were stained with Giemsa staining solution (10% (v/v) Giemsa's azur eosin methylene blue solution in deionized water, Merck KGaA, Darmstadt, Germany), washed again with deionized water, and dried at RT overnight. Colony numbers were assessed with the COLCOUNT system

(Oxford Optronix Ltd., Abingdon, UK). Each experiment was performed in duplicates and repeated at least three times. The relative surviving fraction and the relative colony size were calculated.

7.2.8 Expression analysis by SDS-PAGE and western blotting

To assess the expression profile of different proteins that are relevant for apoptosis sodium dodecyl sulphate polyacrylamide gel electrophoresis (SDS-PAGE) and western blotting were performed. According to the standard procedure 600'000 cells were seeded in 25 cm² cell culture flasks, the next day they were treated with the indicated amount of ZnO NP for 4 h and harvested at the indicated time points. Please note that the indicated time points refer to the beginning of the NP treatment, that means "8 h" = eight hours after beginning of the NP treatment and four hours after the removal of excessive particles as NP treatment lasted four hours. The whole time series analysis was performed independently in triplicate for all cell lines. The corresponding negative control of cells, that were not treated with ZnO NP, was harvested together with the "4 h ZnO NP" sample.

7.2.8.1 Harvesting of the cells

All cells treated with ZnO NP were included in the lysates. To that, the cell culture medium containing detached cells was collected in a centrifuge tube. Then the cell culture flask was washed with PBS, which was carefully removed completely and also collected. While the detached cells in the supernatant were collected via a centrifugation step, the remaining cells on the cell culture plate were lysed with 300 µL lysis buffer, collected with a cell scraper, and transferred to a micro tube. The supernatant of the cells in the cell culture medium was discarded after centrifugation, cells were lysed in 100 µL lysis buffer, and both lysates were pooled. To ensure complete lysis of the cells, lysates were homogenized ultrasonically (2 x 30 s with pulses of 0.5 s with pauses of 1 s in between at 88% amplitude). Then they were stored frozen until further processing for the SDS-PAGE. All steps of the harvesting procedure were performed on ice to avoid any protein degradation.

7.2.8.2 Preparation of the lysates for the SDS-PAGE

The protein concentration of the lysates was assessed in triplicate with the DC Protein Assay (Bio-Rad Laboratories GmbH, Munich, Germany) using bovine serum albumin (BSA) as protein standard. In short, 5 µL of the lysate were mixed with 25 µL reagent

A' (A' = 1 mL reagent A + 20 μ L reagent S) in a 96 well plate. Then 200 μ L reagent B was added. After 10 min extinction at 750 nm was measured using the photometer Multiskan Ascent (Thermo Fisher Scientific Inc., Waltham, MA, USA). Lysates were diluted to the same protein concentration (60 μ g per gel) using lysis buffer. Bromophenol blue (1 μ L 5% (w/v) BPB / 100 μ L lysis buffer) was added for visualization and dithiothreitol (5 μ L 2 M DTT / 100 μ L lysis buffer) for reduction of all disulphide bridges.

7.2.8.3 Running of the SDS-PAGE

The SDS-PAGE performed here was a one-dimensional separation of reduced and denatured proteins according to their size in an electric field in a polyacrylamide gel. For the SDS-PAGE the TGX Stain-Free™ FastCast™ Acrylamide Solutions, 12% (Bio-Rad Laboratories GmbH, Munich, Germany) were used according to manufacturers' specifications. The TGX Stain-Free chemistry enables rapid fluorescent detection of proteins directly within gels and blots with the ChemiDoc™ MP imaging system. As molecular weight marker 5 μ L of PageRuler™ Protein Ladder (Fermentas Life Sciences, Thermo Fisher Scientific Inc., Waltham, MA, USA) were used. Shortly before loading the samples onto the gel, they were boiled at 95°C for 10 min. The gels were run at 10 mA per gel until the migration front reached the bottom of the gel.

7.2.8.4 Western blotting by wet-tank method

After the electrophoresis the proteins in gel were visualized using the Bio-Rad stain free system and then immediately transferred to a polyvinylidene fluoride membrane (PVDF membrane, Millipore Corporation, Billerica, MA, USA) using a wet blot according to the transfer apparatus manufacturer's instructions. The transfer was run at 4°C at 19 mA for 21 h under continuous stirring of the transfer buffer. After the transfer the membrane was activated, and the transferred proteins were visualized via the Bio-Rad stain free system.

The following washing and incubations steps were all performed on a swivel table. After the transfer the membrane was washed 5 min with 1xTBST₂₀ washing buffer. Next the membrane was blocked for 1 h with milk powder in 1xTBST₂₀ washing buffer, followed by another washing step of 3x5 min with 1xTBST₂₀ washing buffer. Then the membrane was incubated overnight with the primary antibody. The next day the membrane was washed 3x5 min with 1xTBST₂₀ washing buffer and then incubated

with the secondary antibody for 1 h and washed again 3x5 min with 1xTBST₂₀ washing buffer.

For imaging the membrane was incubated 1-2 min with enhanced chemiluminescent substrate (Western Lightning ECL Plus, Waltham, MA, USA) and pictures were taken with the ChemiDoc™MP imaging system. The densitometric analysis was performed with the ImageLab Software (Bio-Rad Laboratories GmbH, Munich, Germany) using the stain free images as loading control. If the membrane was used once again for another antibody it was stripped with stripping buffer 1 (glycine) for 30 min and stripping buffer 2 (SDS) for 30 min followed by washing with 1xTBST₂₀ washing buffer (10 min).

Table 6: Antibodies and corresponding incubation strategies

MP = milk powder; BSA = bovine serum albumin

Specificity	Product name	Manufacturer	Blocking	1 st antibody incubation	2 nd antibody incubation
P53	Anti-p53 antibody, Mouse monoclonal, P6874	Sigma-Aldrich Corporation (St. Louis, MO, USA)	5% (w/v) MP	1:10'000 in 5% (w/v) BSA	Anti-mouse 1:4'000 in 4% (w/v) MP
Bcl-xL	Bcl-xL (54H6) Rabbit mAb #2764	Cell Signaling Technology, Inc. (CST) (Danvers, MA, USA)	5% (w/v) MP	1:1'000 in 5% (w/v) MP	Anti-rabbit 1:4'000 in 4% (w/v) MP
Bax	Bax (D2E11) Rabbit mAb #5023	Cell Signaling Technology, Inc. (CST) (Danvers, MA, USA)	5% (w/v) MP	1:1'000 in 4% (w/v) BSA	Anti-rabbit 1:4'000 in 4% (w/v) MP
Caspase-9	Caspase-9 (C9) Mouse mAb #9508	Cell Signaling Technology, Inc. (CST) (Danvers, MA, USA)	5% (w/v) MP	1:750 in 4% (w/v) BSA	Anti-mouse 1:4'000 in 4% (w/v) MP

7.2.9 Statistical evaluation

All collected data was shown together with a statement of the amount of independent experiments (N) that underlies. For this study only explorative-descriptive statistical methods were used. If possible, all values were shown as the arithmetic mean \pm standard deviation (SD). All exceptions were stated in the corresponding caption.

As standard, data was analysed with a one-way ANOVA comparing all sample groups with the corresponding control group including a correction for multiple testing with the Dunnett's test. The sample sizes were too small to test for normal distribution.

Nevertheless, ANOVA in contrast to the Kruskal-Wallis was the method of choice, since ANOVA proved to yield better results when analysing data with small sample sizes. (Khan et al. 2003)

Special statistical evaluations that were performed on top of what is described here were depicted in detail in the corresponding section of the results.

All statistical analyses were conducted with the GraphPad Prism Software (Prism 6 for Windows, version 6.01, GraphPad Software, San Diego, CA, USA), IBM SPSS Statistics (version 22.0.0.0 for Windows, International Business Machines Corporation, Armonk, NY, USA) or with the statistical programming language R (R version 3.3.3 (2017-03-06)), using RStudio as integrated development environment (version 1.0.136, RStudio Inc. Boston, MA, USA)

8 Results

The results section is subdivided into eight main chapters to structure the key topics of this doctoral thesis.

Chapter 8.1 deals with the characterization of ZnO NP. This involves transmission electron microscopy, x-ray diffraction, and zeta potential measurements, as well as analysis of the generation of reactive oxygen species (ROS) at the NP's surface.

Chapter 8.2 discusses the question of what exactly causes the cytotoxicity of ZnO NP. Subjects of this chapter are the release of zinc ions from the NP and their toxicity, the relevance of changes in the ionic strength and the pH value for the toxicity, as well as the contribution of ZnO NP as nanoparticulate matter to toxicity.

Chapter 8.3 is dedicated to ZnO@SiO₂ NP, zinc oxide nanoparticles that are coated by a silica shell. In this chapter their characterization, toxicity, and cellular uptake are illustrated.

Chapter 8.4 deals with the cellular reaction to ZnO NP treatment. This includes the description of morphological characteristics after ZnO NP treatment, the assessment of apoptotic and necrotic cell death, and the analysis of the cell cycle distribution.

Chapter 8.5 analyses genotoxic effects of ZnO NP in combination with ROS in a cell-free DNA damage analysis.

Chapter 8.6 takes a closer look at the significance of mitochondria and ROS generation for the toxicity of ZnO NP. For this purpose, the generation of superoxide in the mitochondria as well as the cytochrome c release from the mitochondria were evaluated. Finally, signalling pathways were examined by western blots.

Chapter 8.7 deals with the comparative analysis of the toxicity of ZnO NP towards both tumor cells and healthy cells of the human body.

Chapter 8.8 finally evaluates the suitability of ZnO NP as radiosensitizing anti-tumor agent with the help of a colony formation assay (CFA).

In the Figure 23 the main topics of this doctoral thesis are depicted in a graphical abstract, which sums up the key areas of interaction between human cells and ZnO NP or ZnO@SiO₂ NP, respectively.

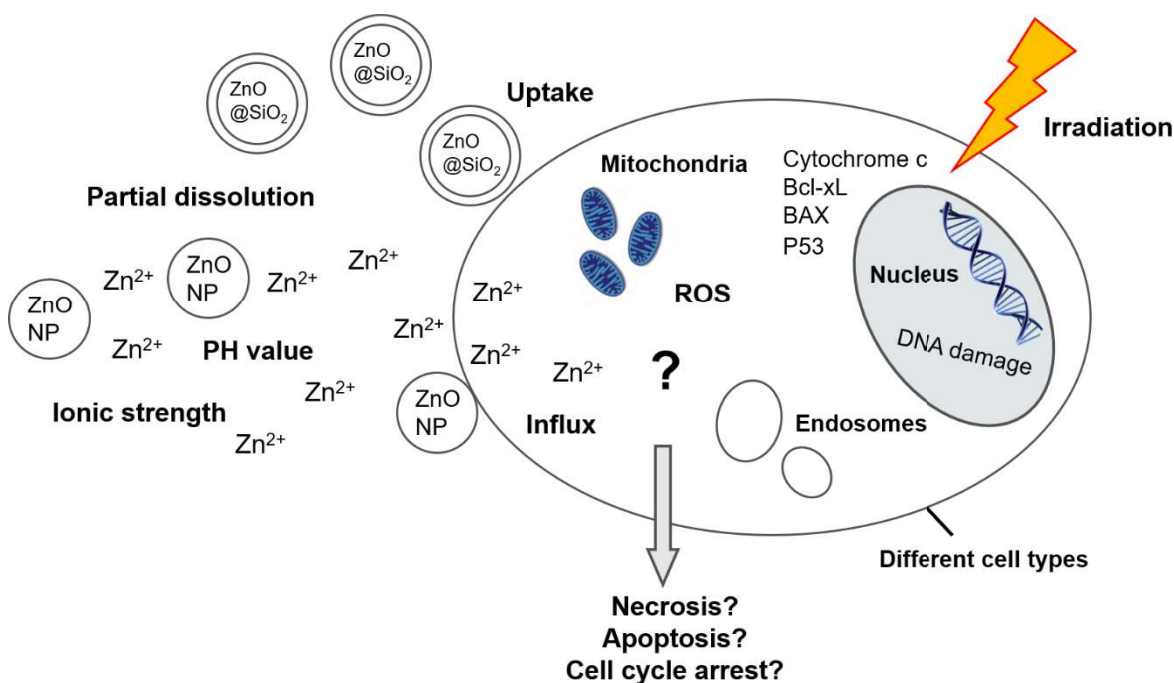


Figure 23: Graphical representation of the different aspects of the cell–nanoparticle interaction

8.1 Characterization of ZnO NP

Transmission electron microscopy (TEM) showed that the solvothermally synthesized ZnO NP were of spherical shape. Their size ranged from 5 to 22 nm in diameter (Figure 24A). For the experiments, different batches of ZnO NP were used which showed minor variations in size. X-ray diffraction (XRD) patterns of ZnO NP were obtained and all reflection could be assigned to the hexagonal wurtzite-type ZnO structure with lattice parameters $a = 3.24 \text{ \AA}$ and $c = 5.20 \text{ \AA}$ and space group (SG) P63mc (No. 186) (Figure 24B).

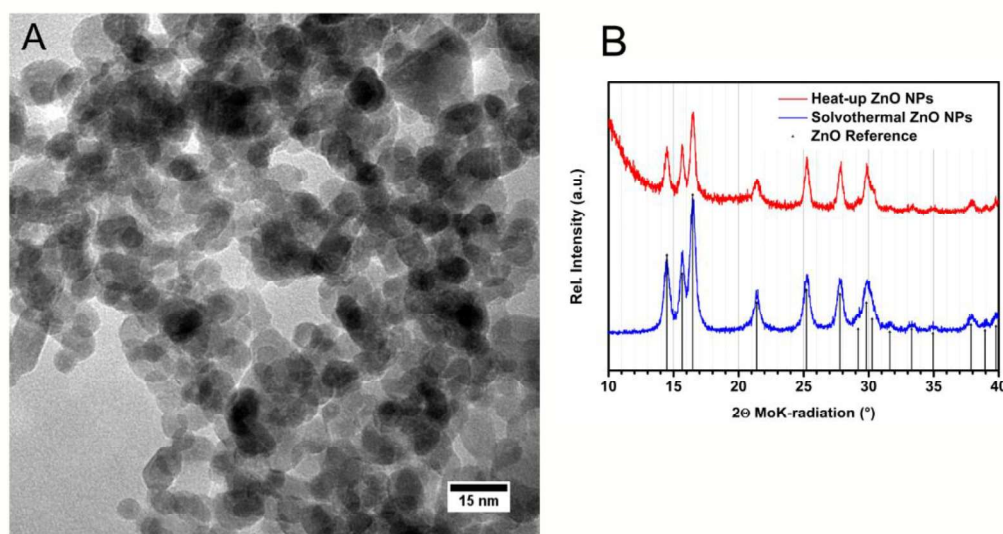


Figure 24: Characterization of ZnO NP by TEM and x-ray diffraction

(A) shows a representative transmission electron microscopy image (TEM) of ZnO NP and (B) a representative x-ray diffraction (XRD) pattern. Those analyses were performed for every batch of ZnO NP with similar results.

To further characterize the NP, their zeta potential was determined. In water the ZnO NP revealed a zeta potential of +20 to +30 mV. In cell culture medium the measurement of the zeta potential was not possible, most likely due to the presence of other charged species that hindered a reliable measurement.

Additionally, we analysed the generation of reactive oxygen species (ROS) at the surface of ZnO NP since in literature there are described zinc oxide nanoparticles that generate ROS without the presence of any biological medium or cells. (Prasanna et al. 2015) The ZnO NP described here were neither able to generate superoxide nor hydroxyl radicals at the surface without being in contact with a biological system.

8.2 What causes the toxicity of ZnO NP?

Concerning the toxicity of metal oxide NP, there are different possibilities which part of the NP exactly induces cytotoxicity. Apart from the NP themselves being the toxic agents, also released zinc ions can have toxic effects. Furthermore, released ions can be directly toxic or they can act via manipulation of the pH value or the ionic strength of the surrounding medium. This chapter strives to answer the question which chemical components or characteristics contribute to the toxicity of ZnO NP.

8.2.1 Zinc ion release from ZnO NP

One important property of all metal oxide NP is their stability against dissolution. During treatment with these NP they can set free metal ions which can contribute to the cellular reaction upon NP treatment. With atomic absorption spectroscopy (AAS) measurements we assessed the amount of zinc ions that was released by ZnO NP within 4 h and 24 h in different media. These were water, Tris-NaCl buffer, pure cell culture medium, and cell culture medium supplemented with 10% (v/v) FCS (Figure 25). In total, 100 $\mu\text{g}/\text{mL}$ ZnO NP could theoretically correspond to up to 1.23 mM zinc ions. However, only at most 250–300 μM zinc ions were actually released. In cell culture medium the equilibrium was already established after 4 h and the amount of additional zinc ions that was released within further 20 h was small. In contrast, the equilibrium in water was not yet established after 4 h and additional zinc ions were liberated until the time of measurement after 24 h. In total, in cell culture medium with FCS more zinc ions were released than in pure cell culture medium.

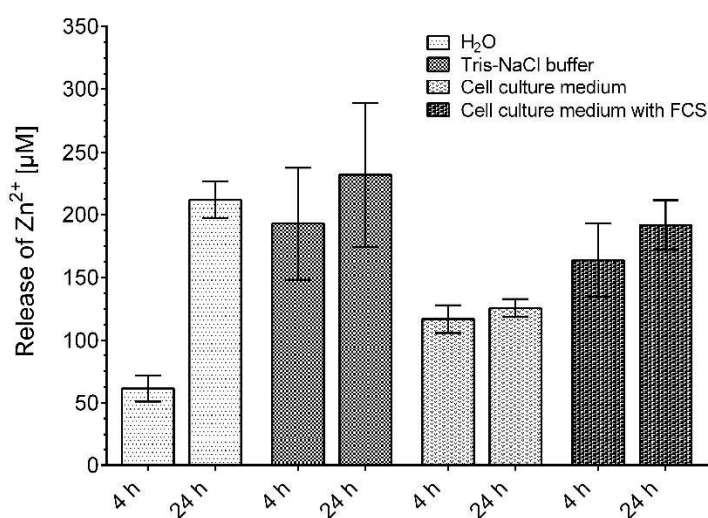


Figure 25: Zinc ions released from ZnO NP

The amount of zinc ions released from ZnO NP within 4 h and 24 h in different media was measured repeatedly ($N \geq 3$) by atomic absorption spectroscopy (AAS).

8.2.2 Toxicity of released zinc ions

To assess the cellular reaction to released zinc ions ZnCl_2 was used because it completely dissolves in aqueous medium. A549 tumor cells were treated with different amounts of ZnCl_2 ranging from 20 $\mu\text{g/mL}$ to 100 $\mu\text{g/mL}$ for 4 h. Then cell culture medium was exchanged for fresh medium and the cells were analysed microscopically and by flow cytometry. Flow cytometric analysis showed that starting from an amount of 40–50 $\mu\text{g/mL}$ ZnCl_2 there was a toxic effect resulting in a decrease of the percentage of viable cells and an increase in dead, apoptotic, and necrotic cells (Figure 26). There was not seen a continuous increase in cell death but rather 40 $\mu\text{g/mL}$ ZnCl_2 seemed to represent a threshold level which marked the onset of toxic effects. From day one (1d) after treatment till day two (2d) the level of dying cells was increasing in those cell samples that received a high dose of ZnCl_2 . On day three (3d) some cells were able to recover from the treatment depending on the dose they received. In these samples the number of viable cells began to increase again.

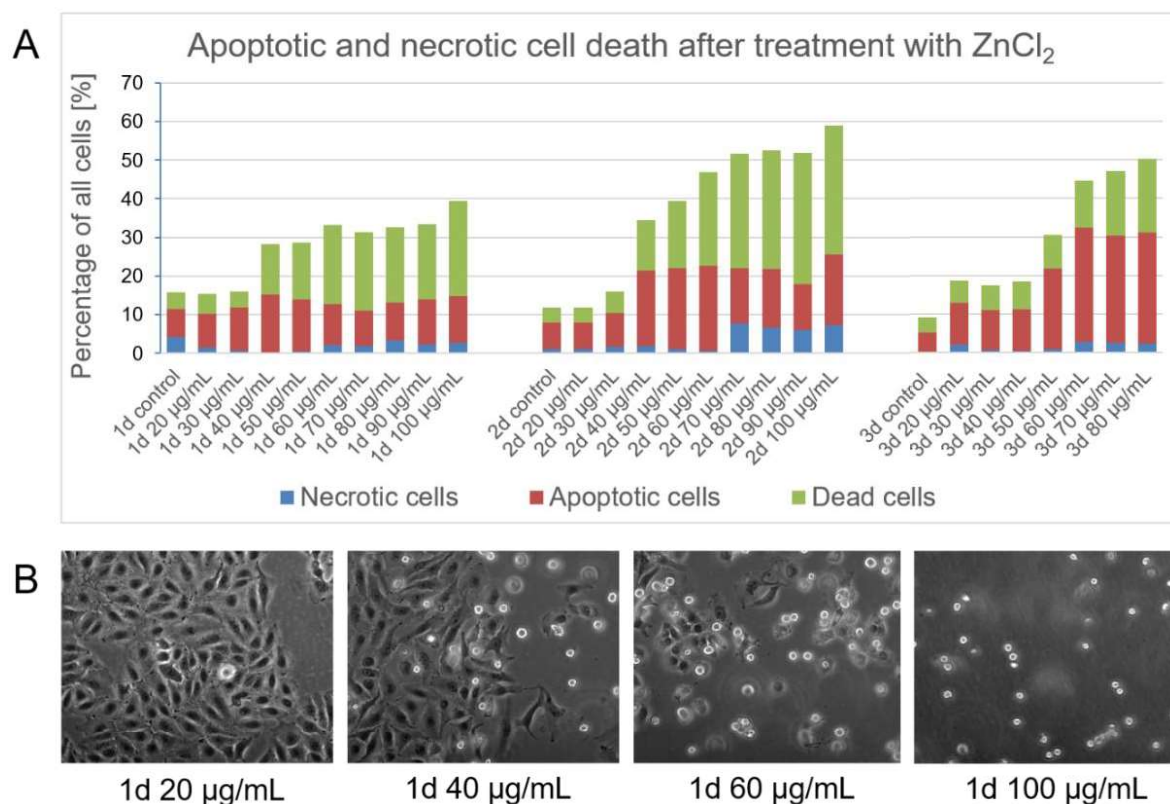


Figure 26: Toxicity of released zinc ions

The toxicity of ZnCl_2 as representative of released zinc ions was assessed by flow cytometric analysis (A) of the amount of necrotic, apoptotic, and dead cells one, two, and three days after treatment with 20–100 $\mu\text{g/mL}$ ZnCl_2 (N=1). In parallel the morphology of cells treated with ZnCl_2 was observed by light microscopy (B).

Microscopical analysis of the cells treated with ZnCl_2 (Figure 26B) showed that high doses induced rounding of the cells and detachment from the cell culture plate.

8.2.3 Influence of changes in pH value and ionic strength

To further investigate which characteristics of ZnO NP account for their cytotoxicity we evaluated potential origins of cytotoxicity from a chemical perspective. We analysed whether the toxicity of ZnO NP was attributable to changes in the pH value, or the ionic strength of the surrounding medium.

ZnO is an amphoteric oxide that can react both as an acid and as a base. ZnO NP slightly rose the pH value in pure water from 6 to 6.67. Nevertheless, the pH value of the cell culture medium under cell culture conditions ($37^\circ\text{C} / 5\% \text{ (v/v) CO}_2$) was unaffected by ZnO NP.

To evaluate whether changes of the ionic strength contribute to cytotoxicity, we compared the toxicity of MgCl_2 , ZnO NP, and ZnCl_2 by treating cells with equimolar amounts of zinc or magnesium ions, respectively (Figure 27). Thus, the probe “100 $\mu\text{g/mL}$ ” contained an amount of ions that was equivalent to the amount of zinc contained in 100 $\mu\text{g/mL}$ ZnO NP.

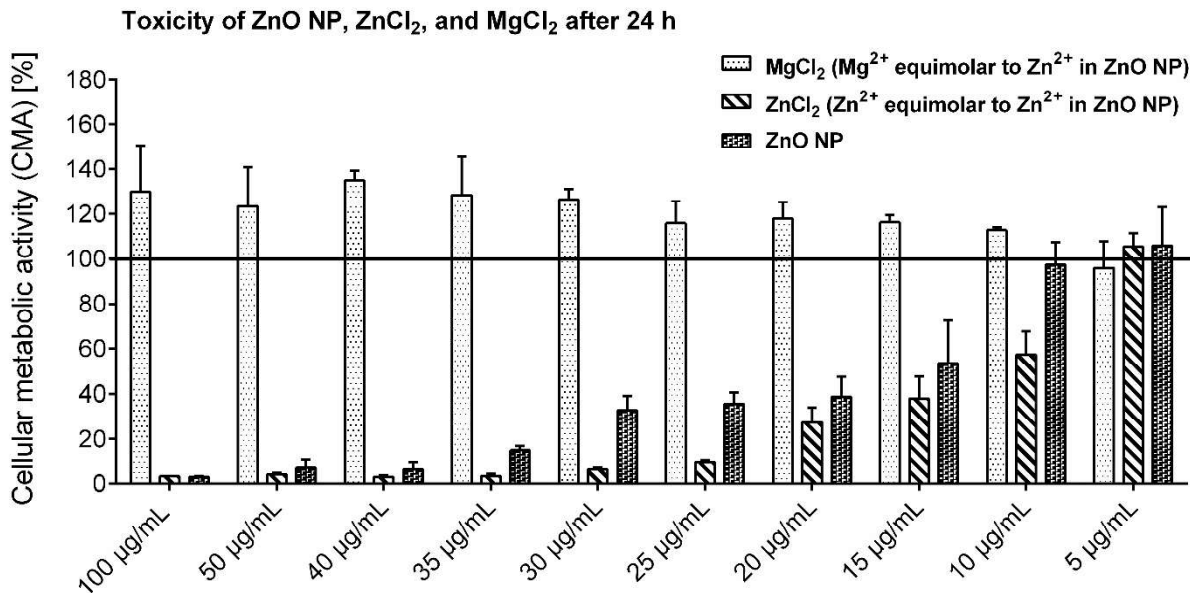


Figure 27: Comparative analysis of the toxicity of MgCl_2 , ZnCl_2 , and ZnO NP

To comparatively assess the toxicity of MgCl_2 , ZnCl_2 , and ZnO NP the cellular metabolic activity (CMA) of A549 cells treated with 5–100 $\mu\text{g/mL}$ ZnO NP or equimolar amounts of magnesium ions (MgCl_2) or zinc ions (ZnCl_2) was measured with an alamar Blue® assay. CMA was assessed 3 h, 6 h, and 24 h after beginning treatment with the different substances. Representatively the CMA after 24 h is shown here. In the bar chart are depicted means \pm SD of three independent experiments (N=3).

MgCl₂ induced no cytotoxicity in all tested concentrations. In contrast, it seemed to somehow stimulate the cellular metabolic activity (CMA) of A549 cells. After 24 h ZnCl₂ decreased the CMA significantly beginning at zinc ion concentrations that were equivalent to 10 µg/mL ZnO NP. The onset of toxicity of ZnO NP was slightly shifted beginning at 15 µg/mL ZnO NP. The data obtained by the measurement of the CMA 24 h after treatment with ZnO NP or ZnCl₂, respectively, was modelled with a non-linear regression for a dose-response curve in response to an inhibitor. The half maximal inhibitory concentrations were calculated to be IC₅₀ = 211.4 µM Zn²⁺ (R² = 0.9307) for ZnO NP and IC₅₀ = 141.4 µM Zn²⁺ (R² = 0.97187) for ZnCl₂ (Figure 28).

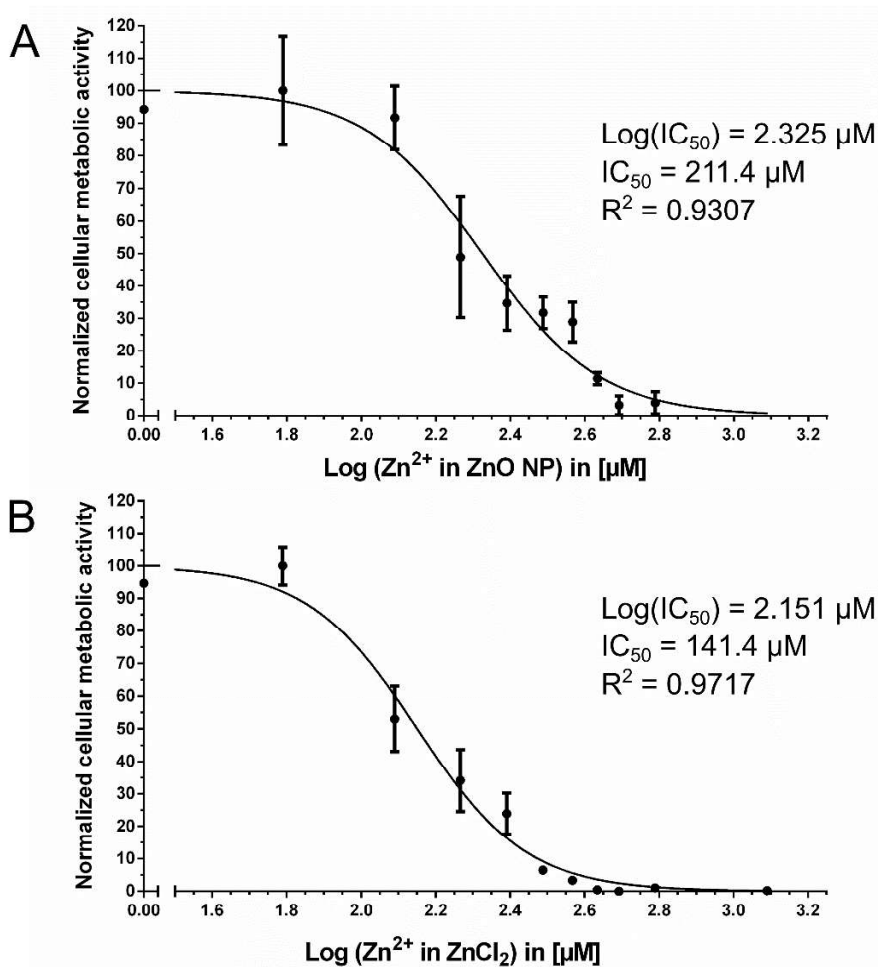


Figure 28: Dose-response curves for the inhibition of the cellular metabolic activity (CMA) by treatment with ZnO NP (A) or ZnCl₂ (B), respectively

To determine the IC₅₀ (half maximal inhibitory concentration) of ZnO NP and ZnCl₂ treatment with respect to their zinc content, the CMA of A549 cells 24 h after treatment with different concentrations was used. Zinc concentrations were transformed by taking their logarithm, the CMA was normalized, and the data was modelled by a non-linear regression for a dose-response curve in response to an inhibitor (log(inhibitor) vs normalized response, variable slope, least-square fit).

8.2.4 Particles vs. ions—how do the NP contribute to the toxicity?

Next, we addressed the question, whether toxicity of ZnO NP was solely attributable to extracellularly released zinc ions or whether toxicity in parts could also be traced back to the NP themselves. To quantify the effect attributed to extracellular release of zinc ions a dispersion of 100 µg/mL ZnO NP was incubated for 4 h under cell culture conditions to allow for zinc ion release. Thereupon remaining NP were separated by centrifugation. Then cells were either incubated directly with ZnO NP for 4 h or with the supernatant of the NP (Figure 29). Both treatments resulted in a reduction of cellular viability of A549 cells within 4 h. After 4 h, the cells were washed, and the cell culture medium was replaced with fresh medium. After 4-7 h and after 21-24 h cells treated with the supernatant were able to recover from the treatment while cells treated with the NP exhibited further reduced cellular viability.

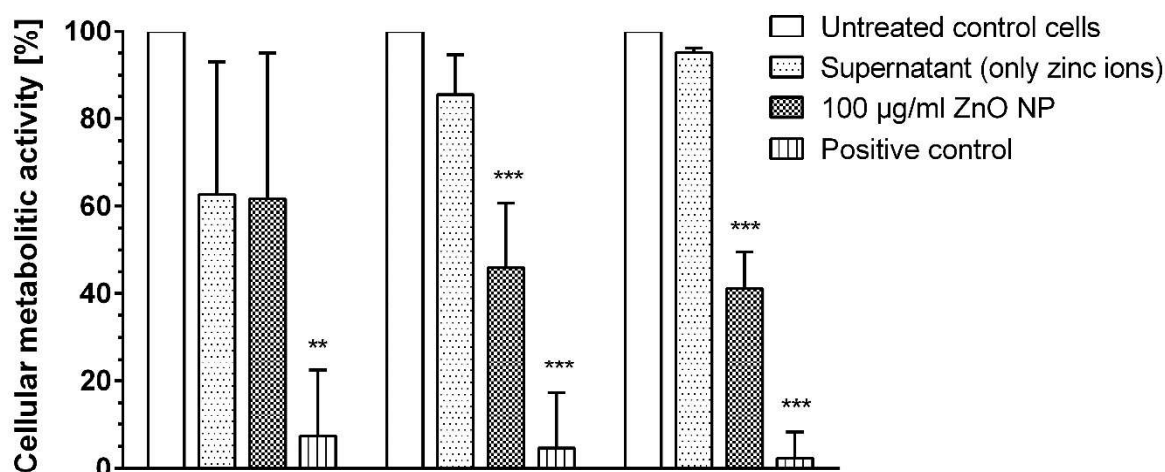


Figure 29: Cellular viability after treatment with ZnO NP or released zinc ions

To assess the cellular viability after treatment with ZnO NP directly or with zinc ions set free by ZnO NP (supernatant) the cellular metabolic activity was determined with an alamar Blue® assay after 4 h, 7 h, and 24 h. The bar chart shows means ± SD of three independent experiments (N=3). For statistical analysis a one-way ANOVA was used comparing every treatment group with the untreated control cells, * p < 0.05, ** p < 0.01, *** p < 0.001, correction with Dunnett's test for multiple testing.

8.3 ZnO@SiO₂ NP—ZnO NP covered by a silica coating

The synthesis of ZnO@SiO₂ NP served three different purposes: the inclusion of a fluorescent dye into the silica shell of the particles to enable tracking of the NP by fluorescent microscopy (1), the possibility to tag moieties to the outer surface of the NP to enable active targeting (2), and the wrapping of the potential toxic ZnO loading into a coating that enables safe transport within the bloodstream to avoid off-target effects due to premature dissolution (3).

Unfortunately, we were not able to set up a reproducible synthesis of ZnO@SiO₂ NP which met all those requirements. Thus, the following experiments should be classified as a proof of concept, which shows that NP with these favourable properties are technically possible but in order to achieve batch-to-batch control the system requires further fine-tuning.

8.3.1 Transmission electron microscopy

The ZnO@SiO₂ NP were coated by a silica shell of about 21 nm thickness. In the TEM images the dark ZnO core was seen within the light silica shell (Figure 30) due to their different scattering contrast.

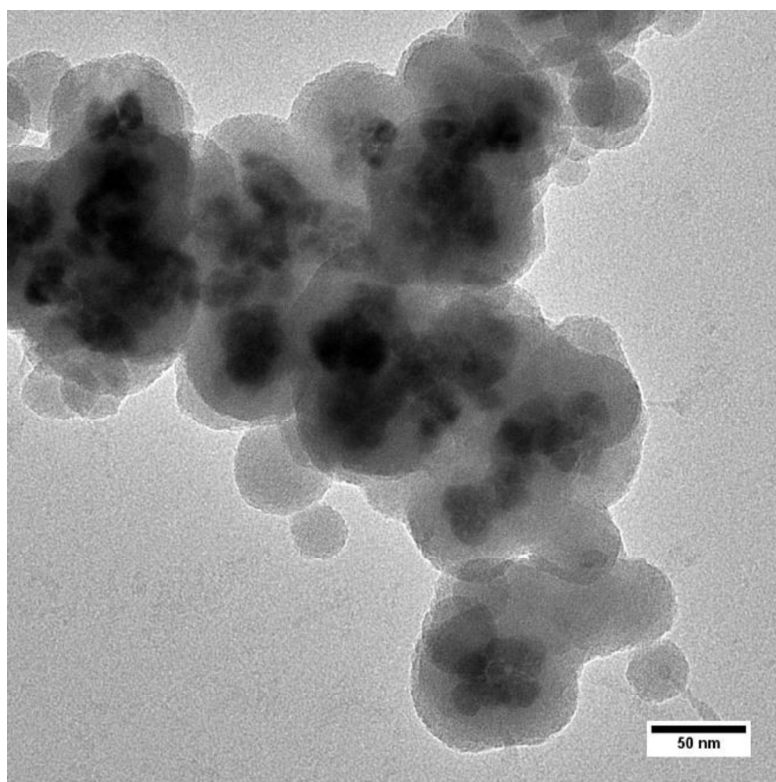


Figure 30: TEM imaging of ZnO@SiO₂ NP

Transmission electron microscopy imaging of ZnO@SiO₂ showed spherical ZnO cores that were surrounded by an irregularly shaped silica shell. The NP were partly fused together.

8.3.2 Comparative toxicity analysis of ZnO@SiO₂ NP and ZnO NP

Comparison of the cytotoxicity of ZnO NP and ZnO@SiO₂ NP showed that both types of NP induced approximately the same toxicity after 24 h but compared to ZnO NP the onset of cytotoxicity of ZnO@SiO₂ NP was delayed (Figure 31). After 4 h, treatment with ZnO NP was able to significantly decrease cellular viability but treatment with ZnO@SiO₂ NP was not. After 6 h the toxicity of ZnO@SiO₂ NP started. After 24 h both types of NP induced approximately the same extent of toxicity.

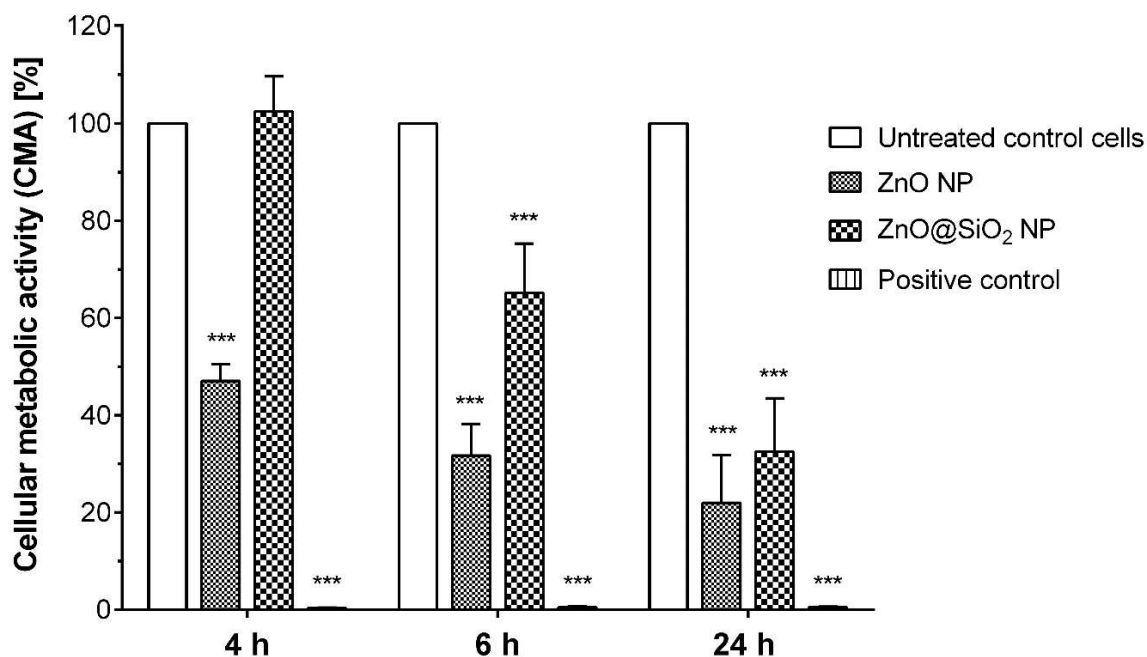


Figure 31: Comparison of the toxicity of ZnO NP and ZnO@SiO₂ NP

To comparatively analyse the toxicity of pristine ZnO NP and ZnO@SiO₂ NP the cellular metabolic activity (CMA) of A549 cells treated with 100 µg/mL ZnO NP or an equivalent amount of ZnO@SiO₂ NP was assessed with an alamar Blue® assay 4 h, 6 h, and 24 h after beginning treatment. The bar chart shows means ± SD of three independent experiments (N=3). For statistical analysis a one-way ANOVA was used, comparing every treatment group with the untreated control cells, * p < 0.05, ** p < 0.01, *** p < 0.001, correction with Dunnett's test for multiple testing. Comparison between ZnO NP and ZnO@SiO₂ NP did not reach statistical significance.

8.3.3 Cellular uptake

To track ZnO NP we designed ZnO@SiO₂ NP that were covered by a silica coating in which FITC was incorporated. Fluorescent imaging revealed that after incubation for 4 h with an amount of ZnO@SiO₂ NP that was equivalent to the amount of zinc that is contained in 100 µg/mL ZnO NP, many NP were attached to the cellular membrane. In Figure 32 one can see in green the NP and in red a staining of the nuclear membrane with an antibody against lamins.

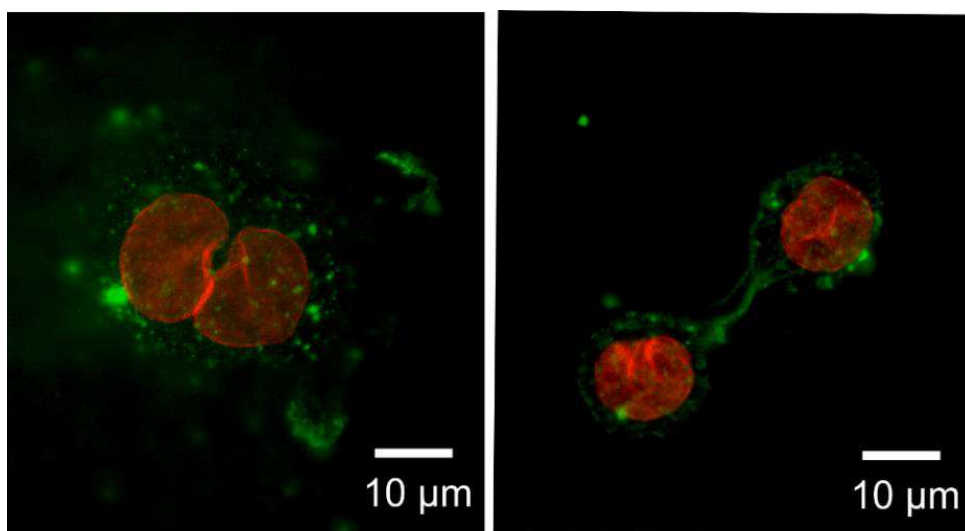


Figure 32: Fluorescent imaging of ZnO@SiO₂ NP

Fluorescent imaging of ZnO@SiO₂ NP after incubation with human cells revealed that after 4 h incubation time, multiple particles and most likely also agglomerates were deposited on the cellular membrane.

With the help of confocal laser scanning microscopy (CLSM), we were able to show that ZnO@SiO₂ NP were internalized by different tumor cell lines within 4 h (Figure 33, I: A549; II: HNSCCUM 02T; III: FaDu; IV: RPMI-2650).

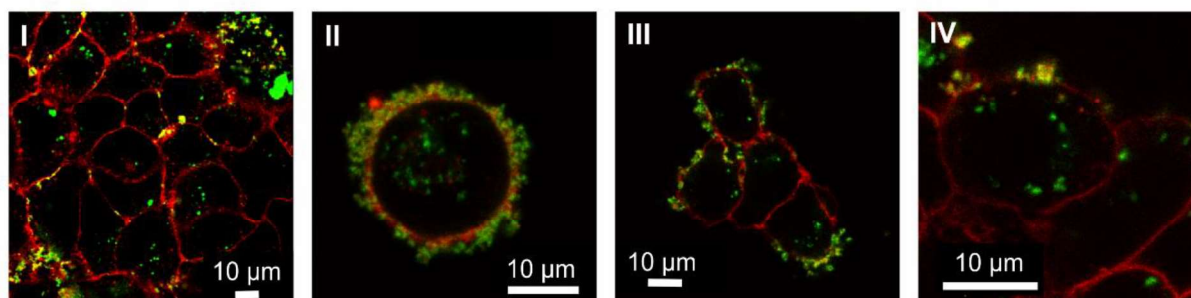


Figure 33: CLSM imaging of cells treated with ZnO@SiO₂ NP

Confocal laser scanning microscopy revealed deposition of ZnO@SiO₂ NP on the cellular membrane of human tumor cells (I: A549; II: HNSCCUM 02T; III: FaDu; IV: RPMI-2650) as well as uptake of NP into the cells.

Many NP were attached to the outer cellular membrane stained by CellMask™ Orange Plasma membrane stain and others were already internalized, which was verified by taking pictures along a z-stack at different focal planes.

8.4 Cellular reaction to treatment with ZnO NP

8.4.1 Morphology

To analyse the cellular reaction to treatment with ZnO NP four different cancer cell lines (A549, HeLa, HNSCCUM-02T, T24) were treated with 100 $\mu\text{g}/\text{mL}$ ZnO NP for 4 h and their morphology was studied under the light microscope. It was observed that ZnO NP treatment in all cell lines resulted in a pronounced rounding of the cells which was accompanied by an increase in granularity. Finally, cells detached from the cell culture plate (Figure 34A). Until 4 h after beginning treatment, when cell culture medium was changed and excessive particles were washed away, cells were still attached to the cell culture plate (second row). Within the next 4 h cells began to detach from the cell culture plate and nearly all cells showed a rounded shape (third row). 24 h after beginning treatment most cells were detached and exhibited a granular morphology (last row).

This observation was also verified by flow cytometry, where a shift of the cell population to higher SSC (side-scatter) and lower FSC (forward-scatter) values was seen (representative pictures in Figure 34B). This indicated a decrease in cell size and an increase in granularity.

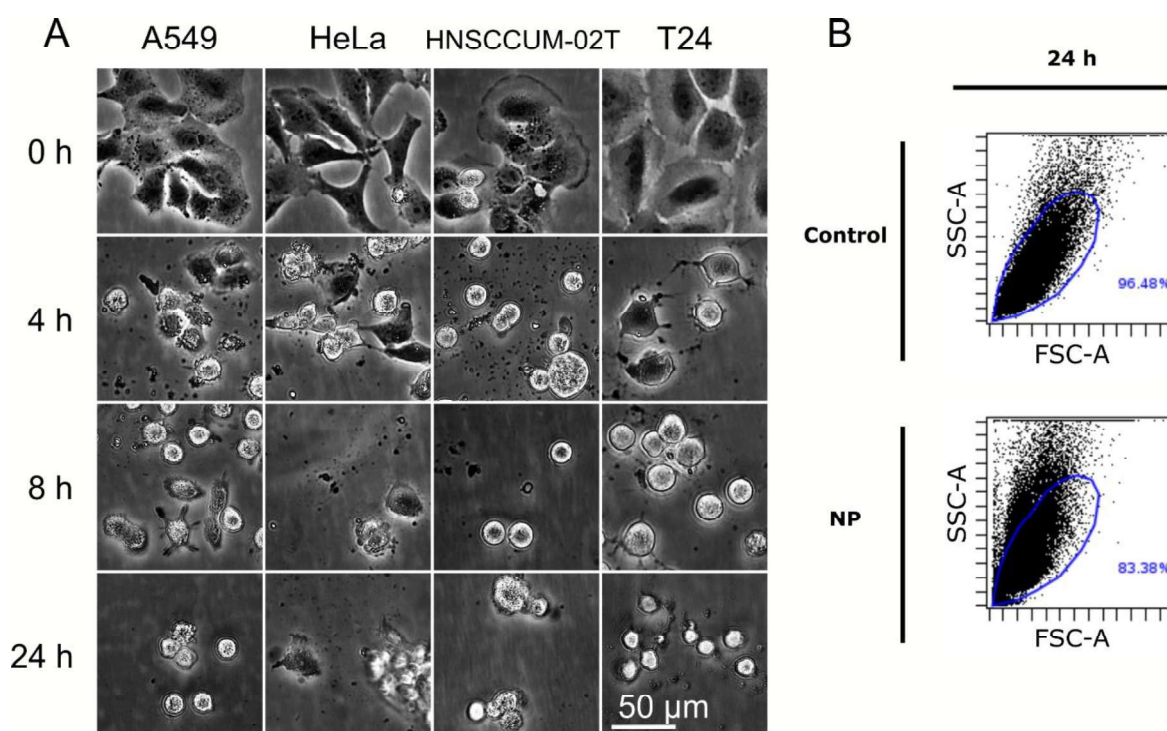


Figure 34: Morphology of different tumor cell lines after treatment with ZnO NP

The morphology of four different tumor cell lines (A549, HeLa, HNSCCUM-02T, T24) was analysed following treatment with 100 $\mu\text{g}/\text{mL}$ ZnO NP for four hours (A). Morphological changes were confirmed by flow cytometric analysis (B). Shown are representative images of both analyses.

8.4.2 Apoptosis and necrosis

Since we saw pronounced cellular toxicity induced by ZnO NP we finally posed the question, whether apoptosis was induced or whether unspecific toxicity resulted in necrotic processes leading to cell death. We performed a flow cytometric assay using propidium iodide (PI) as a marker for the intactness of the outer cellular membrane and annexin V-FITC as apoptotic marker.

Figure 35A shows a representative panel of stained A549 cells analysed 4 h, 12 h, 18 h, 24 h, and 48 h after beginning treatment with ZnO NP or ZnCl₂.

The analyses after 72 h, and 96 h were not included in the picture because at these timepoints the amount of debris was increased. Probably many cells were destroyed during the preparation process for the analysis which may have distorted the ratios between the different cell populations.

In Figure 35A the intact, living cells are in the lower left quadrant, the (early) apoptotic cells are located in the upper left quadrant, dead cells (either late apoptotic or necrotic) lie in the upper right quadrant and necrotic cells in the lower right quadrant of each panel.

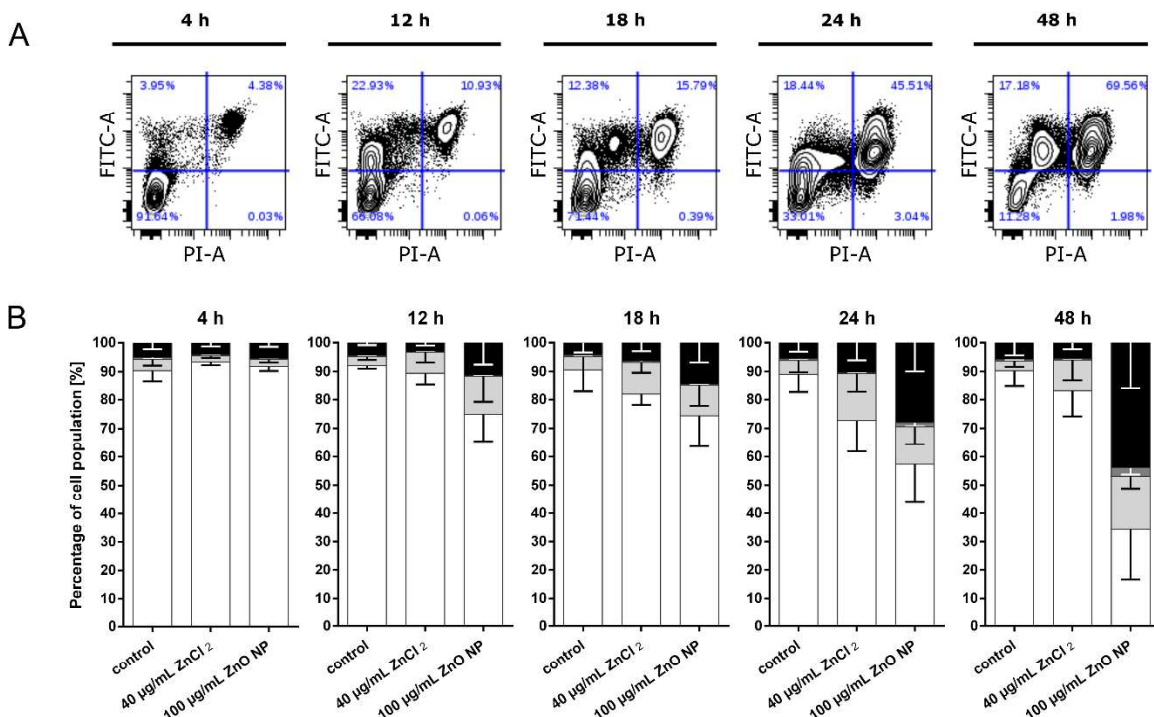


Figure 35: Analysis of necrotic and apoptotic cell death in A549 cells

The relative proportion of viable, necrotic, apoptotic, and dead cells in the cell population after treatment with 100 µg/mL ZnO NP or 40 µg/mL ZnCl₂, respectively, was assessed by flow cytometry. 40 µg/mL ZnCl₂ approximated the amount of zinc ions that were set free extracellularly by the NP. (A) shows representative images of the analysis. In the bar charts in (B) are shown means ± SD of at least three independent experiments (N ≥ 3). The data was statistically analysed with a 2-way ANOVA which compared all experimental groups with the control group and corrected for multiple comparisons with Dunnett.

In Figure 35B the bar charts show the percentages of viable cells (white bar), apoptotic cells (light grey bar), necrotic cells (dark grey bar), and dead cells (black bar) in the total A549 cell population at the indicated timepoints.

The number of dead cells and apoptotic cells rapidly increased after ZnO NP treatment while the percentage of healthy/intact cells decreased. After 48 h the number of living cells was significantly decreased ($p < 0.001$) after treatment with 100 $\mu\text{g}/\text{mL}$ ZnO NP compared to control cells and the number of apoptotic ($p < 0.01$) and dead cells ($p < 0.001$) was significantly increased.

The relative number of necrotic cells in all samples was small and did not rise significantly at any timepoint.

ZnCl₂ is completely dissolved in aqueous media, thus it is a suitable control to assess the effect of extracellularly released zinc ions, excluding the effects of the NP themselves. If we consider that the amount of zinc ions that was set free by 100 $\mu\text{g}/\text{mL}$ ZnO NP within the incubation time did not exceed 300 μM , 40 $\mu\text{g}/\text{mL}$ ZnCl₂ roughly approximates this amount of zinc ions. Thus, treatment of tumor cells with 40 $\mu\text{g}/\text{mL}$ ZnCl₂ represents an upper border for the effect of ZnO NP if only extracellularly released zinc ions were relevant. The flow cytometric assay showed that 40 $\mu\text{g}/\text{mL}$ ZnCl₂ were not able to induce pronounced cell death. The number of living cells was only slightly reduced after 4 h ($p < 0.01$), and the number of apoptotic cells was slightly increased after 24 h ($p < 0.05$) but cells were able to recover from the damage.

Given the fact that over 50% of human cancers carry loss of function mutations in the p53 gene and the fact that the protein influences apoptosis on multiple levels (Ozaki et al. 2011), this assay was repeated with three other cell lines with different p53 states: HNSCCUM-02T, HeLa and T24 (Figure 36). A549 as well as HeLa cells bear wild-type p53, while HNSCCUM-02T cells bear a p53 mutation which results in unusually high p53 expression. (Wiesmann et al. 2017) HeLa cells represent a special case with regard to their p53 level since they are affected by a mutation-independent reduction in p53 protein level due to the expression of the viral E6 protein. (Leroy et al. 2014) T24 cells also bear a mutation in the p53 gene which results in unusually low p53 expression. (Hinata et al. 2003) Thus, we covered a wide range of different p53 states.

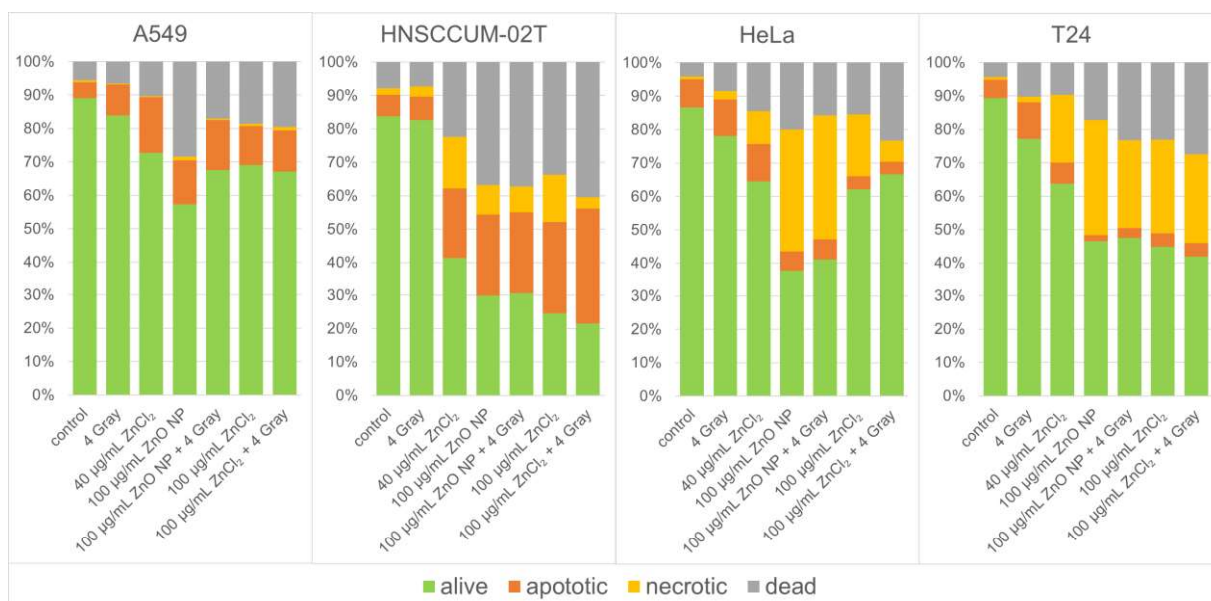


Figure 36: Analysis of the mechanism of cell death in A549, HNSCCUM-02T, HeLa, and T24 cells

The relative amount of viable, necrotic, apoptotic, and dead cells in the cell population of A549, HNSCCUM-02T, HeLa, and T24 cells 24 h after treatment with 4 Gray gamma-irradiation, 40 µg/mL ZnCl₂, 100 µg/mL ZnO NP, 100 µg/mL ZnO NP + 4 Gray, 100 µg/mL ZnCl₂, or 100 µg/mL ZnCl₂ + 4 Gray, respectively, compared to untreated control cells was assessed by flow cytometry. In the bar charts are shown means of at least three independent experiments ($N \geq 3$). To provide an overview, SD are omitted.

While in A549 cells nearly no necrosis was detectable, and all cells died via apoptosis the level of necrosis was much higher in T24 and HeLa cells. In HNSCCUM-02T cells we detected apoptosis and some necrosis.

Gamma-irradiation with 4 Gray did not have a major influence on cellular viability of all four tumor cell lines. Treatment with 40 µg/mL did slightly increase the amount of dead and necrotic or apoptotic cells depending on the cell line, even though the effect remained behind the effect of the NP. The treatment with 100 µg/mL ZnO NP or 100 µg/mL ZnCl₂ clearly increased the amount of apoptosis and / or necrosis in the cell population depending on the cell line. The additional treatment with 4 Gray combined with zinc treatment did not result in additional increase in cell death.

8.4.3 Cell cycle distribution

To get another hint concerning the cellular events that take place after treatment with ZnO NP we evaluated whether a cell cycle arrest is induced in A549 cells. A flow cytometric assay (Figure 37) was used to determine the distribution of the cell population between G1, synthesis (S), G2, and sub-G1 phase (debris). This revealed that there was a pronounced increase in debris, this means cell fragments, while the distribution between the cell cycle phases remained within normal range. The loss of cells in G1 phase could be attributed to the increase in fragmented cells. This means that most likely there is no induction of a cell cycle arrest after ZnO NP treatment.

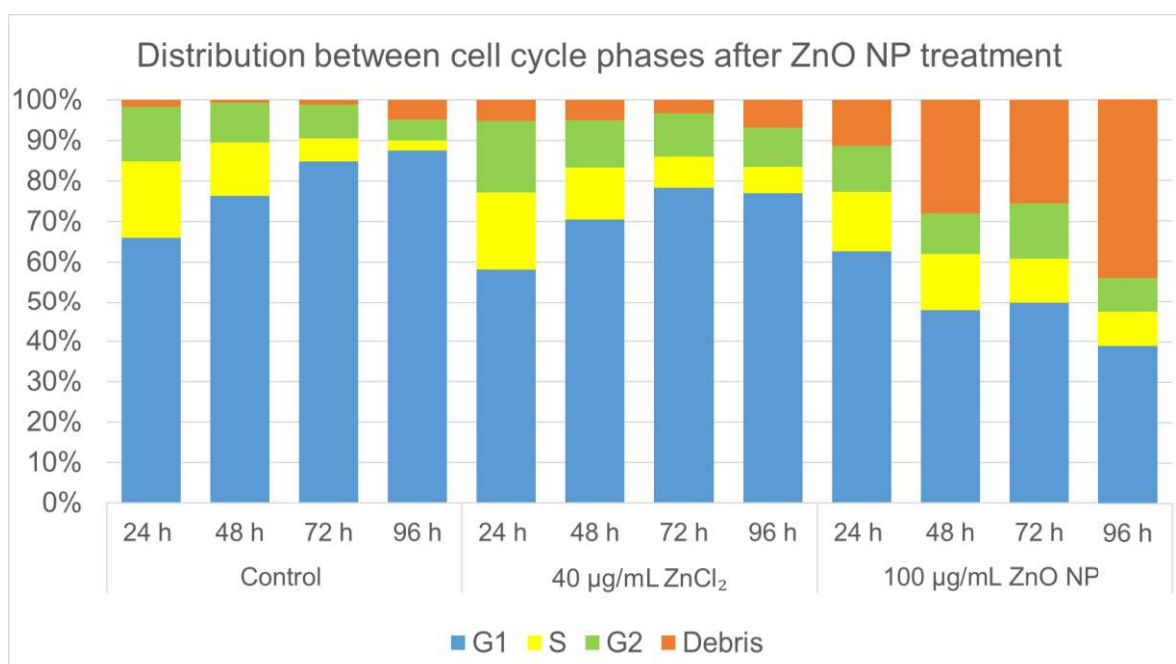


Figure 37: Distribution between the cell cycle phases after ZnO NP treatment

The cell cycle distribution of A549 cells 24 h, 48 h, 72 h, and 96 h after treatment with 40 µg/mL, or 100 µg/mL ZnO NP, respectively, compared to untreated control cells was assessed by flow cytometry. In the bar chart there are only depicted the mean values of three independent experiments (N=3) without standard deviations (SD) for reasons of clarity. The relative amounts of cells in the G1 phase (blue), the synthesis phase (yellow), the G2 phase (green), and the debris (orange) are depicted as percentage of the whole cell population.

8.5 Genotoxic effects of ZnO NP

8.5.1 *In vitro* DNA damage analysis

To decipher the DNA damaging potential of ZnO NP, zinc ions and/or ROS we performed a cell-free *in vitro* experiment using plasmids as a DNA model (Figure 38). H₂O₂ (=ROS) treatment induced single strand breaks (SSB). The treatment with ZnCl₂ which represented the treatment with zinc ions (=Zn²⁺) also induced SSB. ZnO NP induced SSB and some double strand breaks (DSB). Combinations of ZnO NP or Zn²⁺ with ROS increased the level of DNA damage substantially. Especially combined treatment with ZnO NP and ROS was highly destructive. The effects were independent of the pH in the surrounding water (data not shown).

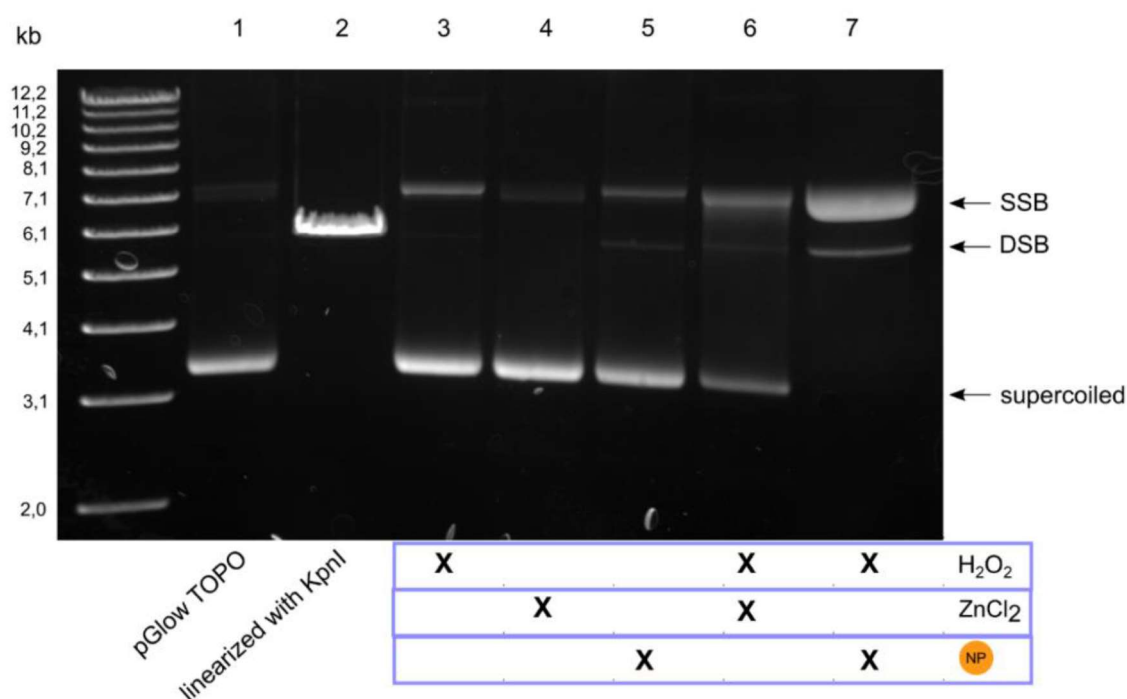


Figure 38: DNA damage analysis in cell-free environment using plasmids

In this experiment plasmids were used as a DNA model. The figure shows a representative DNA gel. The first lane contained a molecular weight marker to identify the different fragments of the plasmid. In the next seven lanes different samples were placed namely (1) the plasmid alone, and (2) the plasmid linearized with KpnI as control, and different combinations of zinc ions, ZnO NP, and H₂O₂ (3–7) as indicated in the table below. The intact plasmid existed in supercoiled form, plasmid DNA that sustained DSB, or SSB lost their supercoiled form. The position of the different forms of the plasmid in the gel is indicated at the righthand side.

8.6 The role of mitochondria and reactive oxygen species (ROS)

It is generally recognized that the generation ROS is involved in the toxicity of ZnO NP (Bisht et al. 2016) but the exact location where ROS are generated and the mechanisms of generation are still under debate. In order to decipher the role of ROS and the mitochondria in the mechanism of toxicity of ZnO NP the following analyses were performed.

8.6.1 MitoSOX™ Red assay

As previous experiments showed breakdown of the mitochondrial membrane potential after ZnO NP treatment (see doctoral thesis of Julia Heim), we tested for the generation of superoxide in the mitochondria with a MitoSOX™ Red assay (Figure 39).

The assay clearly demonstrated that beginning at 12 h after the first contact of the cells with ZnO NP, increasing numbers of superoxide radicals were generated at the mitochondria. Up to 24 h the superoxide level further increased, then there was a plateau phase and at day four there was another gain in mitochondrial superoxide.

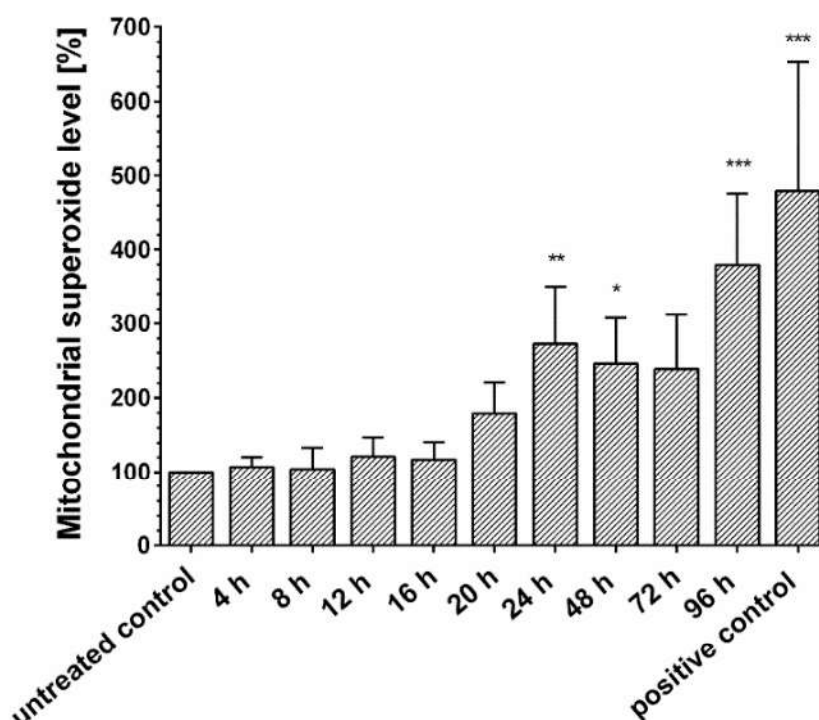


Figure 39: Assessment of the mitochondrial superoxide level

The bar chart shows means \pm SD of three independent experiments (N=3). For statistical analysis a one-way ANOVA was used comparing every treatment group with untreated control cells, * p < 0.05, ** p < 0.01, *** p < 0.001, correction with Dunnett's test for multiple testing.

8.6.2 Cytochrome c release assay

The analysis of the relative amount of cytochrome c release compared to untreated control cells showed that beginning at 12 h after treatment with 100 µg/mL ZnO NP for 4 h the release of cytochrome c from the mitochondria increased (Figure 40).

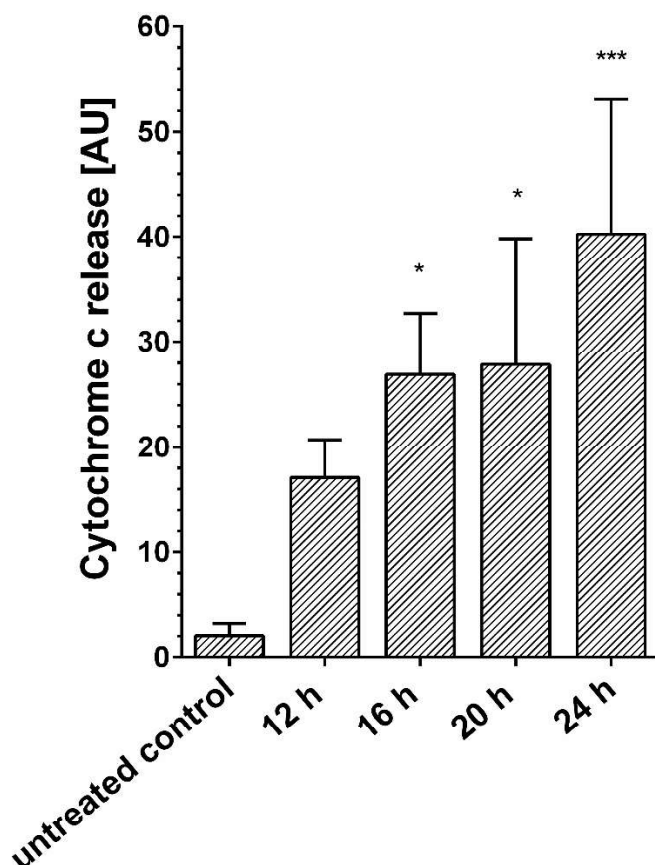


Figure 40: Cytochrome c release assay

The bar chart shows means \pm SD of three independent experiments (N=3). For statistical analysis a one-way ANOVA was used comparing every treatment group with untreated control cells, * $p < 0.05$, ** $p < 0.01$, *** $p < 0.001$, correction with Dunnett's test for multiple testing, AU = arbitrary units.

8.6.3 Western blot analysis of p53, bax, bcl-xL, and caspase-9

To further examine the cellular reaction to the treatment with ZnO NP the expression of the signalling proteins bax, bcl-xL, p53, and caspase-9 was analysed in HNSCCUM-02T, HeLa, T24, and A549 cells. Those cell lines were chosen accordingly due to differences in their p53 state (Hinata et al. 2003; Leroy et al. 2014; Wiesmann et al. 2017).

As expected, the cell lines differed in their baseline expression of the four different proteins (Figure 41).

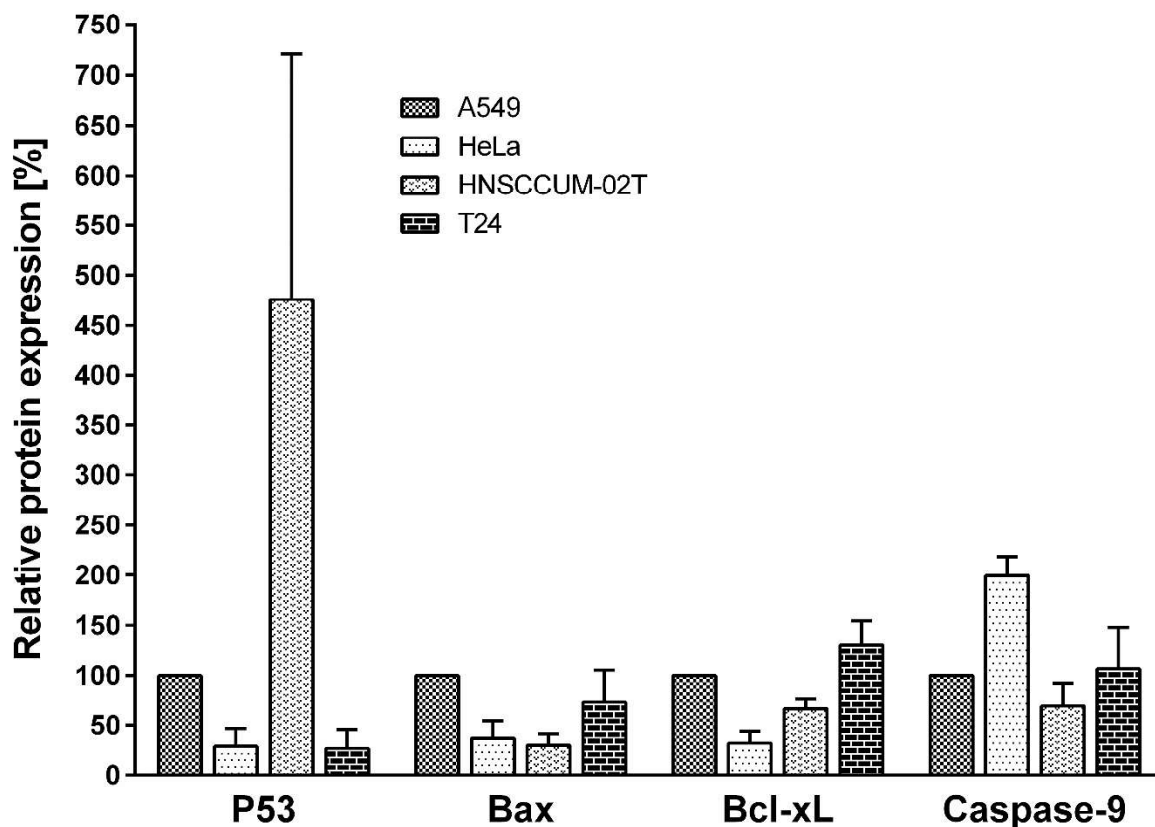


Figure 41: Relative expression levels of p53, bax, bcl-xL, and caspase-9 in untreated A549, HeLa, HNSCCUM-02T, and T24 cells

The expression level of each protein was normalized to the expression in A549 cells (= 100%) and means \pm SD of three independent experiments (N=3) are shown in the bar chart.

Cells were treated with 100 μ g/mL ZnO NP for 4 h. Then lysates were harvested after 4 h, 8 h, 12 h, 16 h, 20 h, 24 h, 48 h, 72 h, and 96 h. In this time course “4 h” again refers to cells harvested directly after the treatment and all other time points were named accordingly. As reference, lysates of untreated cells were chosen.

After getting a general idea of the cellular processes, the time points 4 h and 20 h turned out to be the most interesting ones. Therefore, lysates from untreated control cells and lysates harvested 4 h and 20 h after beginning NP treatment of all four different cell lines were loaded onto one gel and were compared to each other (Figure 42).

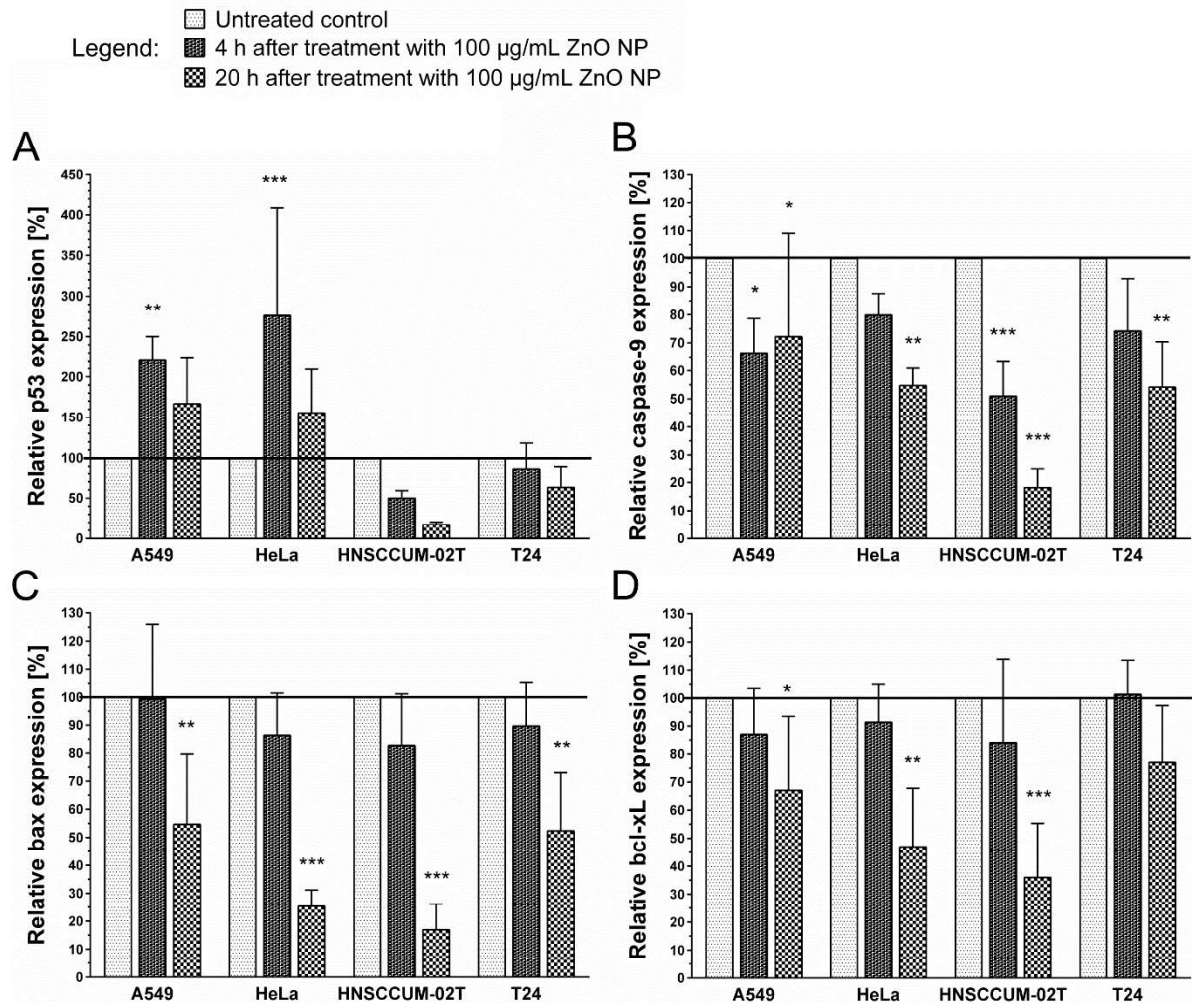


Figure 42: Expression of p53, caspase-9, bax, and bcl-xL 4 h and 20 h after treatment with ZnO NP

The bar charts A–D show the relative expression [%] of p53 (A), caspase-9 (B), bax (C), and bcl-xL (D) after treatment with 100 µg/mL ZnO NP compared to untreated control cells in the four cell lines A549, HeLa, HNSCCUM-02T, and T24. Shown are means \pm SD of three independent experiments (N=3). The data was statistically analysed with a 2-way ANOVA which compared all experimental groups with the control group and corrected for multiple comparisons with Dunnett.

In A549 and in HeLa cells the amount of p53 was increased 4 h and 20 h after treatment with ZnO NP compared to untreated control cells. The increase in p53 in the cells came in several waves: first after 4 h, then after 16 h to 24 h and again at a late time point (data not shown). As the waves did not have exactly the same chronological evolution in every independent experiment, they did not reach statistical significance. In HNSCCUM-02T and in T24 cells the amount of p53 was reduced after treatment with ZnO NP.

The amount of full-length caspase-9 was decreased in all four cell lines after treatment with ZnO NP.

The amount of bax did not show a clear trend 4 h after treatment with ZnO NP. In some runs of the experiment a slight increase in bax was seen, in others the amount of the protein was decreased. After 20 h the level of bax was decreased in all cell lines to different extent. It was further decreased in the following time course (data not shown).

The amount of bcl-xL was decreased in all four cell lines 20 h after beginning treatment with ZnO NP compared to untreated control cells.

8.7 Toxicity of ZnO NP against malignant and non-malignant cells

To evaluate the cellular toxicity of ZnO NP to tumor cells on the one hand and to healthy tissue on the other hand we compared toxicity in A549 tumor cells, to toxic effects in fibroblasts and endothelial cells (HUVECs) of healthy donors. The cellular viability of the different cell types after treatment with 100 µg/mL, 50 µg/mL or 10 µg/mL ZnO NP was assessed with an alamar Blue® assay after 4 h, 8 h, 12 h, and 24 h. The viability of untreated control cells was set to 100% and all test samples were normalized to this value.

Treatment with 100 µg/mL ZnO NP reduced cellular viability of A549 tumor cells, fibroblasts, and endothelial cells within 4 h below 25% of the untreated control cells. A549 cells and fibroblasts were able to slightly recover from the treatment after 8 h but viability was further reduced after 12 h and 24 h (Figure 43).

For the intermediate dose of 50 µg/mL ZnO NP we saw a reduction of tumor cell viability to 70% within 12 h compared to untreated control cells. Fibroblasts remained largely unaffected by that dose. Cellular viability of endothelial cells was clearly reduced at this concentration.

All three cell types were able to cope with 10 µg/mL ZnO NP without sustaining lasting damage.

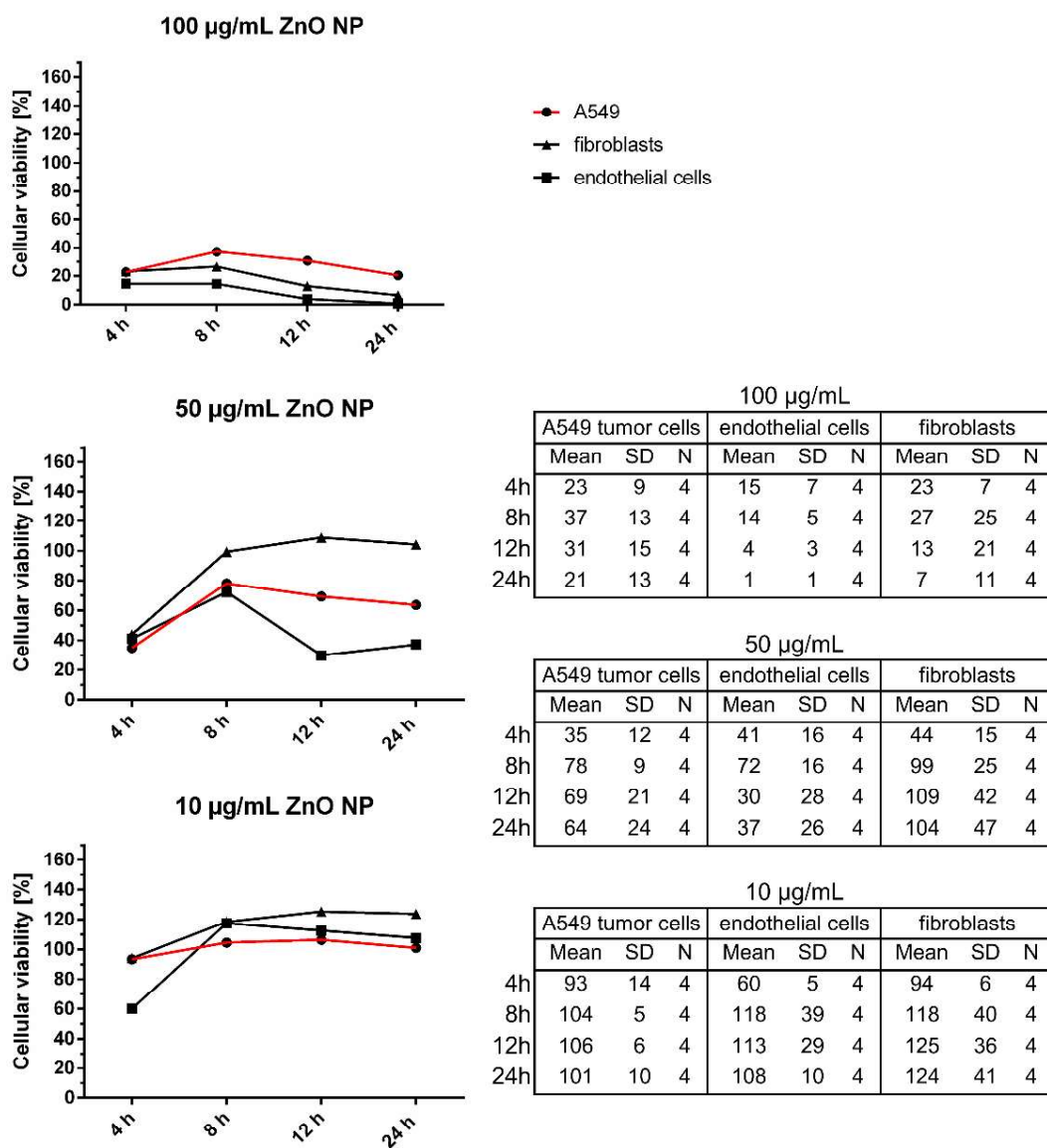


Figure 43: Toxicity of ZnO NP towards malignant and non-malignant cells

The cellular viability of A549 cells, endothelial cells, and fibroblasts was assessed in four different independent experiments (N=4), 4 h, 8 h, 12 h, and 24 h after treatment with the indicated amount of ZnO NP. Depicted in the diagrams are only the mean values without SD values for clarity reasons. The table at the righthand side lists means and SDs.

8.8 ZnO NP as a radiosensitizer

One of the standard experiments to assess the performance of a substance as a radiosensitizer is a colony formation assay (CFA). Such an assay was performed with six different treatment groups (Table 7) to assess tumor cells survival after combined treatment with irradiation and ZnO NP as well as the optimal treatment order (Figure 44).

Table 7: Treatment groups for the colony formation assay

1	Untreated	Untreated control cells
2	4 Gray	Treated with 4 Gray irradiation
3	NP	Treated with 100 µg/mL ZnO NP for 4 h
4	NP + 4 Gray	Treated with 100 µg/mL ZnO NP for 4 h, at 3 h 4 Gray irradiation was applied
5	4 Gray -> NP	Irradiated first with 4 Gray, then treated with 100 µg/mL for 4 h
6	NP -> 4 Gray	Treated with 100 µg/mL for 4 h, then irradiated with 4 Gray

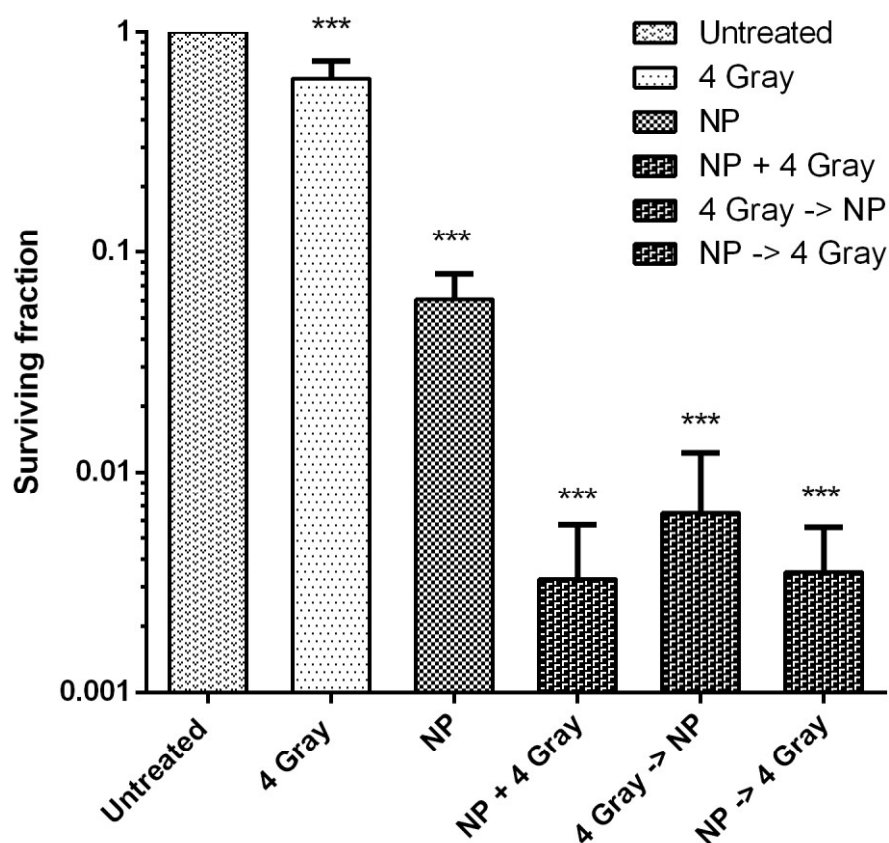


Figure 44: Colony formation assay (CFA) after ZnO NP treatment

The bar chart shows means \pm SD of three independent experiments (N=3). For statistical analysis a one-way ANOVA was used comparing every treatment group with the untreated control cells, * $p < 0.05$, ** $p < 0.01$, *** $p < 0.001$, correction with Dunnett's test for multiple testing. Comparison between the different treatment orders did not reach statistical significance.

The colony formation assay clearly showed that the combined treatment of A549 cells with ZnO NP and irradiation was able to further reduce tumor cell survival compared to irradiation as stand-alone treatment.

Concerning the treatment order, we did not detect a significant difference in the surviving fraction depending on whether irradiation was applied before the treatment with ZnO NP, in parallel to the incubation with ZnO NP or after the treatment with the ZnO NP. Nevertheless, one can see that the surviving fraction in those groups which received irradiation together with or after incubation with the NP exhibited slightly reduced surviving fractions compared to application of the NP after irradiation.

To estimate the influence of the treatment with ZnO NP, irradiation, and the combination of both on the surviving fraction (SF) the data was modelled with a beta regression model using the package “betareg” in R. Beta regression models are used to model outcome-variables with values in the standard unit interval between zero and one. (Cribari-Neto et al. 2010)

The regression equation can be written as:

$$\frac{SF_i}{(1 - SF_i)} = \exp(\beta_0 + \beta_1 \cdot X_{i,1} + \beta_2 \cdot X_{i,2} + \beta_3 \cdot X_{i,3})$$

where SF_i is beta-distributed with:

- β_0 intercept
- β_1 variable describing the influence of irradiation
- β_2 variable describing the influence of the treatment with ZnO NP
- β_3 variable describing the influence of the interaction of both treatments

To perform the analysis, the surviving fraction of the control group was set to 0.999.

The fitting of the model to the data provided the following coefficients:

		significance	$\exp(beta)$
β_0	= 5.0636	***	158.16
β_1	= -4.5572	***	0.01
β_2	= -7.7036	***	0.00045
β_3	= 2.4482	***	11.57

with * $p < 0.05$, ** $p < 0.01$, *** $p < 0.001$.

The exponential coefficients $\exp(\beta_1)$, $\exp(\beta_2)$, and $\exp(\beta_3)$ describe the odds which are defined as the probability that an event will occur divided by the probability that the event will not occur. This means that $\exp(\text{coefficient})$ describes the relative change in the odds of the tumor cells for surviving the treatment with the corresponding therapeutic intervention compared to the control group.

- The odds to survive under treatment with 4 Gray gamma-irradiation are 0.01 times as high as the odds to survive under non-treatment.
- The odds to survive under treatment with 100 $\mu\text{g/mL}$ ZnO NP are 0.00045 times as high as the odds to survive under non-treatment.
- Finally, the odds to survive under treatment with 4 Gray and ZnO NP are $0.01 \cdot 0.00045 \cdot 11.57 = 0.000052$ times as high as the odds to survive under non-treatment.

To sum up we see that treatment with ZnO NP alone has a bigger influence on the surviving fraction of A549 cells than treatment with 4 Gray gamma-irradiation as stand-alone treatment. Both treatments together have lesser influence on the surviving fraction than the addition of both effects, since $\beta_3 > 0$. A β_3 value smaller than zero would indicate a synergistic effect of both treatments.

9 Discussion

Within this chapter I will go through the results in the order of the eight sections 8.1-8.8 and discuss the main findings of this doctoral thesis and what we can learn from them.

9.1 The nature of ZnO NP used in this study

This work was performed with ZnO NP of spherical shape. They were medium sized compared to the zinc oxide nanoparticles described in literature. With 5–22 nm in diameter they were bigger than quantum dots but still relatively small compared to nanoparticles of several tens of nanometres. One important property of nanoparticles is the zeta potential, their surface charge. The zeta potential provides an idea of how the nanoparticles interact with each other and with the medium they will be introduced into. As the zeta potential in aqueous solutions increases, the repulsive interactions between the nanoparticles also increase, which leads to the formation of more stable particles with a more uniform size distribution. This stability is important to prevent agglomeration and subsequent precipitation leading to a stable colloidal dispersion of the nanoparticles. Nanoparticles with a zeta potential between -10 mV and $+10$ mV are considered approximately neutral, while nanoparticles with zeta potentials of greater than $+30$ mV or less than -30 mV are considered strongly cationic and strongly anionic, respectively. The greater the deviation of the zeta potential from zero is, the larger is the colloidal stability of the particles. (Clogston et al. 2011; Gutierrez et al. 2017) The ZnO NP used in this work exhibited a zeta potential of $+20$ mV to $+30$ mV, which suggested agglomeration to some extent when being introduced into aqueous medium. ZnO NP were dispersed in an ultrasonic bath and began to precipitate shortly afterwards. This indeed suggested agglomeration. To ensure reproducible and uniform treatment of cells with ZnO NP, the nanoparticles were freshly prepared and carefully held in dispersion before being added to the cells. Four hours after beginning treatment with ZnO NP, large agglomerates were visible to the naked eye in the cell culture plate. These precipitates likely did not only contain ZnO NP, but also both serum proteins—which were deposited on the nanoparticles' surface—, and precipitates of zinc ions with components of the cell culture medium. All of these were previously described in literature. (Horie et al. 2009; Turney et al. 2012; Mu et al. 2014).

In summary, we are talking about small cationic ZnO NP which readily form agglomerates. Since most cellular membranes are negatively charged, zeta potential

suggests that they have a tendency to interact with and possibly permeate membranes (Clogston et al. 2011).

9.2 Toxicity of ZnO NP is not solely based on release of zinc ions

ZnO NP are described to be prone to dissolution. This means that zinc ions are released from the nanoparticles and contribute to their cytotoxicity. (Song et al. 2010) This fact also holds true for the ZnO NP we used in this study. We quantified the amount of zinc ions that the nanoparticles released within 4 h and 24 h in several buffers (Figure 25). In water the release of zinc ions from ZnO NP was relatively slow, with a release of approximately 50 μM zinc after 4 h. After 24 h around 200 μM zinc release was reached. In contrast, the dissolution equilibrium in cell culture medium was nearly established after 4 h; and the amount of additional zinc ions that was set free within the subsequent 20 h was low. In total, 100 $\mu\text{g}/\text{mL}$ ZnO NP could theoretically correspond to up to 1.23 mM zinc ions. However, only at most 250 to 300 μM zinc ions were released, which is only one fourth that amount. Clearly, particles are not completely disintegrated in tested media. The amount of released zinc ions was higher in cell culture medium with FCS than in cell culture medium without. This effect might result from the higher number of biomolecules in the media with FCS, which might be able to bind zinc ions and thus remove them from the equilibrium, which in turn might lead to additional release of zinc ions.

One repeatedly emerging controversial issue is the question of whether the toxic effect of ZnO NP is exerted only by zinc ions that are rapidly liberated from the nanoparticles outside the cells or whether ZnO NP also take effect as nanoparticulate material. To address this question, we tested whether free zinc ions can have toxic effects at all (Figure 26) and whether the toxicity of ZnO NP is solely based on the release of zinc ions or whether nanoparticulate matter is somehow involved (Figure 29). (Moos et al. 2010)

As a representative of free zinc ions ZnCl_2 was chosen because it completely dissolves in aqueous media. A549 tumor cells were incubated with different concentrations of ZnCl_2 for 4 h and the amount of apoptotic, necrotic, and dead cells was measured after one, two, and three days. This experiment showed that ZnCl_2 indeed did exert cytotoxic effects on tumor cells, starting from a concentration of 40 $\mu\text{g}/\text{mL}$. This data shows that there is seemingly a threshold concentration which marks the onset of cytotoxicity. When this threshold was exceeded the concentration of free zinc ions reached a level that could not be tolerated by the cells any more. This

threshold may depend on the buffer capacity of the cell culture medium. At the start, the zinc ions that are set free by the nanoparticles are mainly adsorbed by proteins, amino acids, and phosphates and carbonates in the cell culture medium and do not enter the cells. When this buffer capacity is exhausted, zinc ions also enter the cells and exert corresponding cytotoxicity.

Summarising the above, it can be said that zinc ions released extracellularly definitely can exert cytotoxic effects.

We wanted to know whether the toxicity of zinc ions is based on alternation of the pH value or the ionic strength of the cell culture medium (Figure 27). Changes in the pH value under cell culture conditions were excluded. To test for changes in the ionic strength we chose another divalent metal ion—magnesium—with the same counter ion—chloride—to compare its toxicity to the toxicity of $ZnCl_2$. We used equimolar amounts of magnesium and zinc ions. This experiment showed that the toxic effect of $ZnCl_2$ is based on the zinc ions and not simply on a change in the ionic strength as $MgCl_2$ proved to be non-toxic and even slightly increased the cellular metabolic activity.

To address the question whether extracellularly released zinc ions are responsible for all of the cytotoxicity of ZnO NP, we incubated cells either directly with ZnO NP or with their supernatant, which contained only zinc ions (Figure 29).

Both zinc ions and ZnO NP reduced the cellular viability within 4 h to the same extent. After 4 h, the cells were washed, and the cell culture medium replaced with fresh medium. The cells that had been treated only with zinc ions recovered from the treatment within 24 h. In contrast, cells which were treated with nanoparticles exhibited significantly reduced cellular viability after 24 h. This finally proves that the cytotoxicity of ZnO NP cannot be traced back exclusively to the release of zinc ions outside the cells. Thus, it must be considered that the particles directly interact with the tumor cells. It is conceivable that ZnO NP stick to the cellular membrane and exert further cytotoxicity by interacting with it; or by the release of zinc ions beyond the time scale of 4 h. Furthermore, ZnO NP might be taken up by the cells which then may induce further intracellular damage fostered by the particles themselves or by intracellularly released zinc ions.

We used both $ZnCl_2$ and ZnO NP with equimolar amounts of zinc ions to treat A549 tumor cells in order to directly compare the toxicity of both substances. IC_{50} values (half maximal inhibitory concentration) were determined by measuring the cellular

metabolic activity (Figure 28). The IC_{50} of $ZnCl_2$ turned out to be at 141.4 μM zinc ($R^2 = 0.9717$) and the IC_{50} of ZnO NP at 211.4 μM zinc ($R^2 = 0.9307$), which corresponds to 19.3 $\mu g/mL$ $ZnCl_2$ and 17.2 $\mu g/mL$ ZnO NP, respectively. This shows that both substances have similar toxicity levels with respect to the amount of zinc ions that they contain. The IC_{50} of $ZnCl_2$ was lower; thus its cytotoxicity was higher compared to ZnO NP. Interpreting this, we must bear in mind that $ZnCl_2$ is dissolved completely. On the contrary, ZnO NP only release approximately one fourth of their zinc load within 4 h. This, in turn, again points to the idea that ZnO NP do not exclusively act via extracellularly released zinc ions but rather via additional effects mediated by the nanoparticulate matter.

9.3 Zinc oxide nanoparticles covered by a silica shell

Uncoated ZnO NP have several major disadvantages if we envision using them as a therapeutic agent in an *in vivo* setting. Firstly, ZnO NP cannot be made visible easily in a living system, which would be important to track their way within cells and within the human body. Secondly, ZnO NP show uncontrollable dissolution and release of zinc ions which we proved to exert toxic effects on cells. If we intend to introduce ZnO NP into an organism, their stability must be ensured to protect healthy cells and to guarantee that the NP reach their target while keeping their zinc load. This also involves an important third point: in order to be able to target tumor cells directly in the body using ZnO NP, it would be favourable to have a surface which enables the attachment of targeting moieties.

All those three problems were addressed by the incorporation of zinc oxide nanoparticles into a silica coating: the silica coating should enable tracking of the nanoparticles within the cells by embedded FITC dye in the shell, it should prevent premature dissolution, and it should enable the attachment of targeting moieties (8.3). For one batch of $ZnO@SiO_2$ NP, we showed a delayed onset of toxicity compared to the uncoated ZnO NP. This points to a delayed release of zinc ions (Figure 31). For the same batch of $ZnO@SiO_2$ NP, we saw uptake of the nanoparticles into different tumor cells within 4 h (Figure 33). Furthermore, we saw additional particles deposited on the cellular membrane. As a proof of concept, the experiments show that these kinds of nanoparticles are technically possible. Unfortunately, we were not able to reliably synthesize $ZnO@SiO_2$ NP which met all these favourable requirements. The system demands further fine-tuning. Reaction conditions must be found under which both the zinc oxide core is stable, and a silica coating of defined thickness can be

applied on the particles. Applying the coating is further complicated by the reduced Pearson compatibility of the rather “soft” Zn^{2+} and the rather “hard” Si^{4+} . (Pearson 1963)

9.4 ZnO NP can convey apoptotic and necrotic cell death

To optimally be able to control the toxicity of ZnO NP on human cells—malignant and non-malignant—it is of great benefit to understand the cellular reaction to the treatment with ZnO NP. The question which mechanism of cytotoxicity underlies cell death after treatment with ZnO NP is addressed in the next chapter.

Morphological analysis of cells after ZnO NP treatment showed rounding and shrinkage of the cells, detachment from the cell culture plate, and an increasingly granular cell structure (Figure 34). These morphological characteristics pointed to a cellular death by apoptosis. (Elmore 2007) Flow cytometric analysis of A549 tumor cells after treatment with ZnO NP confirmed that the nanoparticles can convey apoptotic cell death (Figure 35). The percentage of apoptotic and dead cells of the total cell population was significantly increased within 48 h after treatment while the percentage of living cells was decreased to 30–50% compared to untreated control cells. The percentage of necrotic cells was low and did not significantly increase, thus necrosis can be regarded to be less frequent in A549 cells. $40 \mu\text{g/mL ZnCl}_2$ roughly approximate the amount of zinc ions that is set free by $100 \mu\text{g/mL ZnO NP}$. Hence this number can serve as a control to estimate the effect of zinc ions extracellularly released from the NP. $40 \mu\text{g/mL ZnCl}_2$ were not able to significantly reduce the proportion of living cells 48 h after treatment. Thus, the flow cytometric assay confirmed that the cytotoxicity of ZnO NP cannot only be attributed to zinc ions that were released extracellularly. This confirmed the findings of chapter 8.2.

Since central importance in the cellular response to a wide range of stress stimuli is attributed to the protein p53, we chose three more cell lines besides A549 with different p53 background to analyse the cell death mechanism after treatment with ZnO NP (Figure 36). (Meek 2015) A549 as well as HeLa cells bear wild-type p53, but HeLa cells represent a special case with regard to their p53 level. They are affected by a mutation-independent reduction in p53 protein level due to the expression of the viral E6 protein. (Leroy et al. 2014) T24 and HNSCCUM-02T cells bear mutations of p53. The mutation of p53 in HNSCCUM-02T cells results in unusually high p53 expression. This heightened expression is unaffected by treatment with irradiation, which normally would increase the p53 level. (Wiesmann et al. 2017) This indicates

that the mutation is probably a so-called gain-of-function (GOF) mutation. GOF mutations of p53 are typically characterized by overexpression of the mutant protein. These mutations are thought to endow the mutant protein with additional activities which in contrast to the normal role of p53 contribute to tumor progression. (Oren et al. 2010; Meek 2015) T24 cells also bear a mutation in the p53 gene, which in contrast to HNSCCUM-02T cells results in unusually low p53 expression. (Hinata et al. 2003)

Analysis of the cell death mechanism after treatment with ZnO NP in the four cell lines showed that A549 and HNSCCUM-02T cells predominantly died via apoptosis, with some necrosis occurring in the latter. In contrast, HeLa cells and T24 cells predominantly passed away via necrosis. This might indicate that the level of p53 in T24 and HeLa cells does not suffice to perform apoptosis whereas the p53 of HNSCCUM-02T cells might retain some normal functionality which allows the cells to initiate apoptosis. Without detailed analysis of the underlying signalling cascades, these are only presumptions. The assay furthermore showed that HNSCCUM-02T, HeLa, and T24 cells were more sensitive to the treatment with ZnO NP than A549 cells, with HNSCCUM-02T cells being the most sensitive cell line among the tested. While analysing the cell death mechanism, cells either received 4 Gray of gamma-irradiation or a combined treatment with ZnO NP and irradiation. For this purpose, cells were incubated with 100 µg/mL ZnO NP for 3 h and then irradiated. After 4 h of incubation in total, the cell culture medium was exchanged, and any remaining particles were washed away. We hoped to see an additive effect of treatment with the nanoparticles and irradiation, but this was not the case. Our first idea was that the irradiation somehow altered the surface of the particles and rendered them more inert. We compared the treatment with 100 µg/mL ZnCl₂ alone with a combination of ZnCl₂ and irradiation and we did not see an additive effect with this treatment combination either. This means that the absence of additive effects is not directly linked to the particles. Instead pre-incubation with zinc ions—in the form of ZnCl₂ or ZnO NP—might initiate the upregulation of metallothionein. This may enhance the antioxidative capacity of the cells, which in turn may result in an improved ability to cope with the ROS that were generated upon irradiation. Additionally, at 4 Gray the irradiation dose chosen was not very high. Possibly, higher doses would yield different results. The flow cytometric analysis of apoptotic and necrotic cell death is only suitable for assessing the mechanism of cell death. It does not show the clonogenic survival of

the tumor cells after treatment in the long run. One of the limitations of the assay is the fact that in cell culture apoptotic cells suffer from permeabilization of the cellular membrane at some point, because in contrast to the human body there are no immune cells present to clear them up. Thus, cells in late apoptosis are indistinguishable from cells which died by necrotic cell death. Additionally, cells may be lost during the preparation steps for the assay if they died early and were getting fragile. In this way, the number of dead cells may be underestimated when measuring 72 and 96 h after treatment. The “gold standard” experimental setting to determine the capacity of an agent as radiosensitizer is a colony formation assay (CFA) which was performed in the course of this work. The CFA allows determining reproductive cell death after treatment with irradiation alone or in combination with other treatment options. (Franken et al. 2006; Nuryadi et al. 2018)

In order to characterize the cellular reaction to treatment with ZnO NP more closely, the cell cycle distribution of A549 cells was determined after treatment (Figure 37). Short periods of time of up to 24 h were tested (data not shown), as well as long periods of time of up to 96 h after treatment. At no time point was there cell cycle arrest detectable. A reduction was seen in the percentage of cells in the G1 phase at the late time points, but this reduction was not attributable to a cell cycle arrest and instead occurred simultaneously with an increase in severely injured cells in the form of debris. The fact that we did not see a cell cycle arrest indicates either that the cells are not able to take measures to repair the sustained damage by treatment with ZnO NP, or the kind of damage that is sustained is not answered by cell cycle arrest at all.

9.5 ZnO NP induce DNA damage

It is well established that ZnO NP can induce generation of ROS and DNA damage, but unfortunately the underlying fundamental mechanisms mostly lie in the dark. To decipher whether the generation of ROS and DNA damage could be interconnected I performed an experiment with plasmid DNA under cell-free conditions in the dark (Figure 38). This experiment showed that H₂O₂ was able to induce single strand breaks (SSB) in the DNA. ZnO NP were able to induce SSB as well, but also a tiny amount of double strand breaks (DSB). Both together induced high amounts of SSB and some DSB, leaving nearly no plasmid DNA intact. This clearly shows that there seems to be some enhancing effect of the ZnO NP on the effect H₂O₂ has on the

plasmid DNA. The effect was independent of different physiological pH values that were tested (data not shown).

It is known that zinc can intercalate between the DNA base pairs (Lee et al. 1993) and due to the negative charge the phosphate backbone is likely to interact with zinc ions (Langlais et al. 1990), but it is not known whether zinc ions can have a damaging effect on DNA strands. Zinc ions are redox-inert under physiological conditions; thus, any kind of Fenton-like reaction can be excluded. Photocatalytic activity of ZnO NP (5.3.2.3.1) is also unlikely as it requires energy input in the form of light and the experiment was conducted in the dark. We tested whether ZnO NP can directly generate ROS at their surface in a cell-free environment since such an activity has been previously described (Xia et al. 2008; Song et al. 2010; Zijno et al. 2015) but for our ZnO NP we could not show generation of superoxide radicals or hydroxyl radicals at the nanoparticle surface. Thus, the mechanism of action remains elusive. It is likely that generation of ROS and of DNA damage go hand in hand and reinforce each other.

9.6 Mitochondria are central for the toxicity of ZnO NP

Since mitochondria are the main endogenous source of ROS and zinc ions are known to interfere with the respiration as well as the fact that Julia Heim showed breakdown of the mitochondrial membrane potential after treatment with ZnO NP in her doctoral thesis, it was plausible to test whether ROS are generated in the mitochondria upon treatment of A549 cells with ZnO NP (Figure 39).

Staining with MitoSOX™ Red showed that 20 h after beginning treatment with ZnO NP the mitochondrial superoxide level began to increase and exceed the level in untreated control cells. Until 72 h after beginning treatment the relative mitochondrial superoxide level remained at an elevated level, if only to further rise after 96 h. Furthermore, beginning at 12 h after treatment we detected cytochrome c release from the mitochondria which further increased after 16 h, 20 h, and 24 h. Altogether, this shows that mitochondria are involved in the cellular reaction upon treatment with ZnO NP.

Mitochondrial cytochrome c release and initiation of apoptosis appeared approximately at the same time. This shows that initiation of apoptosis via the intrinsic pathway is fathomable. In order to shed light on intracellular signalling we performed an expression analysis to assess protein level differences in some of the key players in mitochondrial apoptosis. In order to also include differences in the p53 state in the

analysis, these experiments were not only conducted with A549 cells, which bear wild-type p53, but also with HeLa, T24, and HNSCCUM-02T cells. Figure 45 describes in short, the part of the mitochondrial apoptosis that was analysed in the following.

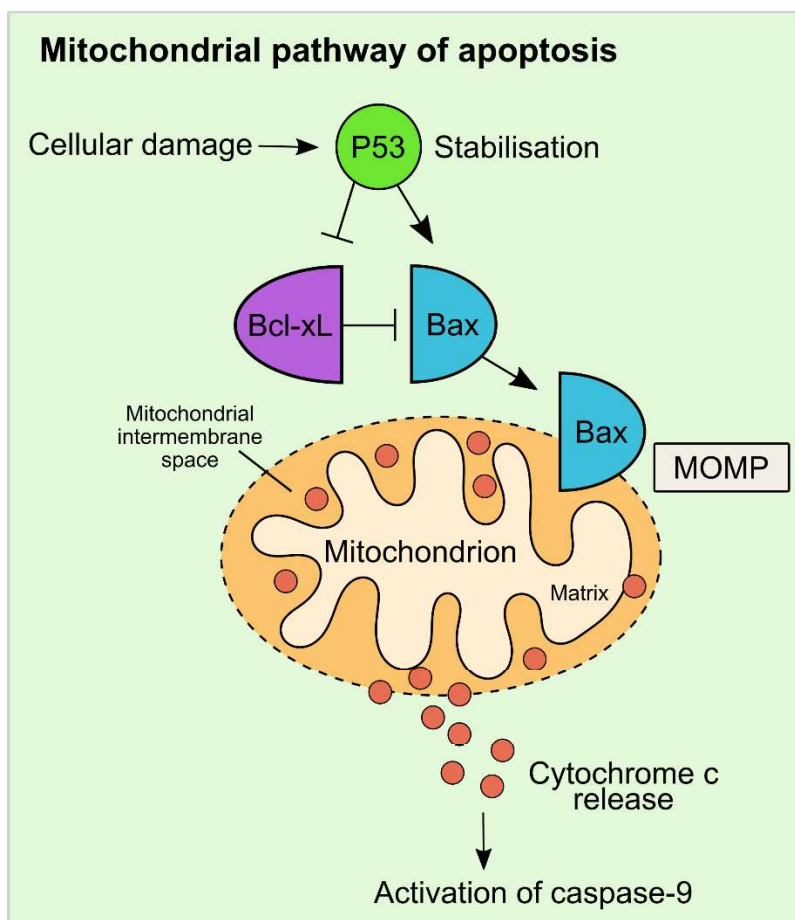


Figure 45: Part of the intrinsic / mitochondrial pathway of apoptosis

Upon cellular damage the tumor suppressor p53 which is normally subjected to rapid turnover is stabilized. Among multiple other functions, it inhibits the pro-survival protein bcl-xL and enhances the pro-apoptotic protein bax. This concentration shift releases bax from inhibition by bcl-xL (for exact mechanism please refer to (Edlich et al. 2011)). Bax can then translocate to the mitochondrial membrane and convey the permeabilization of the mitochondrial outer membrane (MOMP). As a result, cytochrome c is released which mediates the activation of caspase-9 by cleavage followed by induction of apoptosis. This diagram shows only the small part of the whole cascade which was analysed in this doctoral thesis. There exist multiple alternative signalling cascades, intermediate steps, and bypaths. Modified according to (Amaral et al. 2010; Tait et al. 2010).

To correct for differences between the baseline expression of the four proteins p53, caspase-9, bax, and bcl-xL, the expression in untreated control cells was set to 100% in the corresponding cell line and the expression level 4 h and 20 h after treatment with 100 µg/mL ZnO NP was expressed in relation to that value (Figure 42).

In A549 and HeLa cells the level of p53 increased 4 h and 20 h after treatment with ZnO NP. This indicates that these cells perform some kind of stress response via the p53 protein. These exact cell lines also bear wild-type p53 although HeLa cells

contain only very low levels of the protein. In contrast, the level of p53 in HNSCCUM-02T cells and in T24 cells which bear mutant p53 was decreased upon treatment with ZnO NP. This indicates that in those cell lines the p53 protein was not able to conduct its normal tasks. As expected HNSCCUM-02T cells exhibited a very high level of p53 (Figure 41) compared to the other cell lines which may point to a gain-of-function (GOF) mutation of the protein. In contrast, the p53 level in T24 cells was very low and was even reduced upon treatment with ZnO NP instead of elevated as one might expect as a reaction to a stress stimulus.

If cells initiate mitochondrial apoptosis upon treatment with ZnO NP, we would expect the level of full-length caspase-9 to decrease since the protein is cleaved to induce apoptosis. We did indeed detect reduction of caspase-9, except for the fact that we saw it in all cell lines under investigation—those bearing wild-type p53 and those bearing mutant p53. The decrease in caspase-9 occurred irrespective of apoptosis. It was detectable in cell lines which exhibited apoptotic and necrotic cell death upon treatment with ZnO NP.

The pro-apoptotic protein bax and the anti-apoptotic protein bcl-xL were also subjected to a decrease in their expression level after treatment with ZnO NP in all cell lines within 4 h and 20 h. The decrease was more prominent or less prominent depending on the cell line. With these proteins we were not able to link the expression level to the state of p53 or to the amount of apoptosis that had been seen in the corresponding cell line upon treatment with ZnO NP.

In summary, with reference to the elevation of wild-type p53 we can conclude that in A549 and HeLa cells some kind of stress response seems to be initiated after treatment with ZnO NP. The expression levels of caspase-9, bax, and bcl-xL were inconclusive since we did not find a link between the information about the cell death mechanism typical to the cell line and the expression levels of the proteins. This might be due to alternative pathways apart from those analysed here.

To sum up the whole experimental series on the cellular reaction to treatment with ZnO NP we can say that dependent on the tumor cell line the particles can induce apoptotic as well as necrotic cell death. Mitochondria seem to play a central role in the cell death mechanism. The mitochondrial membrane potential was decreased (doctoral thesis of Julia Heim), ROS were elevated in the mitochondria, and cytochrome c was released. In A549 and HeLa cells which bear wild-type p53, the expression of the protein was elevated in response to treatment with ZnO NP. The

exact series of events is not yet decipherable, but mitochondria and the generation of ROS seem to play a pivotal role; and generation of ROS seems to be involved in the genotoxic effects of ZnO NP as well.

9.7 ZnO NP can damage malignant and non-malignant cells

Besides the toxicity mechanism itself, it is important to know whether an agent, that is intended to be used as tumor therapy, is selectively toxic only to tumor cells. In this case that means to test the sensitivity of tumor cells to treatment with ZnO NP compared to non-malignant cells of the human body. As model tumor cells we chose A549 cells; and as representative non-malignant cells we chose primary fibroblasts and HUVECs (Figure 43). At an intermediate concentration of 50 $\mu\text{g}/\text{mL}$ ZnO NP we saw that fibroblasts were less sensitive to treatment with ZnO NP than A549 cells. Unfortunately, endothelial cells showed high sensitivity towards treatment. This shows that treatment of tumors with ZnO NP is a double-edged sword. Although several studies showed that ZnO NP were more toxic to tumor cells than to non-malignant cells (Table 2) our experiments show that damage to the more sensitive cell types of the human body cannot be completely excluded. This demands for a targeting strategy which ensures that ZnO NP which are injected into the bloodstream primarily target the tumor and release their toxic load only at the tumor site. Additionally, ZnO NP must be protected by a coating to safely travel through the bloodstream and to protect the sensitive endothelial layer.

9.8 ZnO NP can reduce survival of tumor cells after irradiation

The potential of ZnO NP as a radiosensitizer was assessed with a colony formation assay. The first goal of this experiment was to analyse whether ZnO NP can improve the effect of radiotherapy. The second goal was to assess how to schedule application of both therapeutic means to yield the highest amount of tumor cell death. Concerning the second question, it can be said that there were no significant differences in the surviving fraction of tumor cells depending on the sequence of the treatments. We found that treatment with ZnO NP significantly reduced the surviving fraction of tumor cells compared to untreated control cells and their effect on the tumor cell survival was bigger than the effect of 4 Gray of gamma-irradiation as a stand-alone treatment. Concerning the combination of both treatments, we did not see synergistic or additive effects. This means the treatment with irradiation and ZnO NP in combination was less effective than the addition of both single-treatment effects. Nevertheless, ZnO NP

may become attractive as adjuvant therapeutic agent, to complement radiotherapy. The nanoparticles may help to reduce the irradiation dose while yielding the same level of tumor cell death. This can help to reduce radiation damage to the healthy tissue surrounding the tumor, especially in very delicate regions, for example in the head and neck region.

10 Conclusions

The aim of this study was to broaden the knowledge on the interaction between ZnO NP and human cells—tumor cells and non-malignant cells—and the NP's potential as innovative anti-tumor agent. To achieve this, a broad set of experiments was conducted and herein described in detail to document precisely the experimental conditions that were used.

We were able to show the importance of the direct interaction of ZnO NP with tumor cells to exert their cytotoxicity, while also describing the toxic effects of extracellularly released zinc ions. We documented the uptake of ZnO@SiO₂ NP into tumor cells as well as their silica coating delaying onset of cytotoxicity.

ZnO NP were shown to initiate apoptotic and necrotic cell death. We observed DNA as well as mitochondrial damage upon treatment with the particles. Reactive oxygen species seemed to play a central role in the intracellular effects of ZnO NP, being involved both in mitochondrial and DNA damage.

Besides usage as stand-alone treatment ZnO NP could also be combined with radiotherapy as adjuvant treatment.

Many questions concerning the cytotoxicity mechanism were answered; however further problems emerged from the new findings. Hitherto unknown is how ZnO NP can convey genotoxic damage, the sequence of events following treatment with ZnO NP is still not fully elucidated, and *in vivo* data concerning the toxic effects on whole organisms is still sparse. A coating strategy is needed to safely transport ZnO NP through the bloodstream. Active targeting may help to enrich the nanoparticles at the tumor site. These are the next challenges which must be met to pave the way for the translation of ZnO NP into clinical practice.

11 References

Adan, A.; Alizada, G.; Kiraz, Y.; Baran, Y.; Nalbant, A. (2017): Flow cytometry: basic principles and applications. In: *Critical Reviews in Biotechnology* 37 (2), pp. 163-176.

Ahamed, M.; Akhtar, M.J.; Raja, M.; Ahmad, I.; Siddiqui, M.K.; AlSalhi, M.S.; Alrokayan, S.A. (2011): ZnO nanorod-induced apoptosis in human alveolar adenocarcinoma cells via p53, survivin and bax/bcl-2 pathways. Role of oxidative stress. In: *Nanomedicine: Nanotechnology, Biology and Medicine* 7 (6), pp. 904-913.

Akhtar, M.J.; Ahamed, M.; Kumar, S.; Khan, M.M.; Ahmad, J.; Alrokayan, S.A. (2012): Zinc oxide nanoparticles selectively induce apoptosis in human cancer cells through reactive oxygen species. In: *International Journal of Nanomedicine* 7, pp. 845-857.

Alam, S.; Kelleher, S.L. (2012): Cellular mechanisms of zinc dysregulation: a perspective on zinc homeostasis as an etiological factor in the development and progression of breast cancer. In: *Nutrients* 4 (8), pp. 875-903.

Alarifi, S.; Ali, D.; Alkahtani, S.; Verma, A.; Ahamed, M.; Ahmed, M.; Alhadlaq, H.A. (2013): Induction of oxidative stress, DNA damage, and apoptosis in a malignant human skin melanoma cell line after exposure to zinc oxide nanoparticles. In: *International Journal of Nanomedicine* 8, pp. 983-993.

Al-Fartusie, F.S.; Mohssan, S.N. (2017): Essential Trace Elements and Their Vital Roles in Human Body. In: *Indian Journal of Advances in Chemical Science* 5 (3), pp. 127-136.

Amaral, J.D.; Xavier, J.M.; Steer, C.J.; Rodrigues, C.M.P. (2010): The Role of p53 in Apoptosis. In: *Discovery Medicine* 9 (45), pp. 145-152.

Ancona, A.; Dumontel, B.; Garino, N.; Demarco, B.; Chatzitheodoridou, D.; Fazzini, W.; Engelke, H.; Cauda, V. (2018): Lipid-Coated Zinc Oxide Nanoparticles as Innovative ROS-Generators for Photodynamic Therapy in Cancer Cells. In: *Nanomaterials* 8 (3), pp. 1-15.

- Anders, C.B.; Chess, J.J.; Wingett, D.G.; Punnoose, A. (2015): Serum Proteins Enhance Dispersion Stability and Influence the Cytotoxicity and Dosimetry of ZnO Nanoparticles in Suspension and Adherent Cancer Cell Models. In: *Nanoscale Research Letters* 10 (1), pp. 1-22.
- Andreini, C.; Banci, L.; Bertini, I.; Rosato, A. (2006a): Counting the zinc-proteins encoded in the human genome. In: *Journal of Proteome Research* 5 (1), pp. 196-201.
- Andreini, C.; Banci, L.; Bertini, I.; Rosato, A. (2006b): Zinc through the three domains of life. In: *Journal of Proteome Research* 5 (11), pp. 3173-3178.
- Arivazhagan, R.; Jagadeesan, S.; Cho, Y.-J.; Lim, J.-H.; Choi, K.H. (2017): Synthesis and evaluation of the cytotoxic and anti-proliferative properties of ZnO quantum dots against MCF-7 and MDA-MB-231 human breast cancer cells. In: *Materials Science & Engineering: C, Materials for Biological Applications* 81, pp. 551-560.
- Aswathanarayan, J.B.; Vittal, R.R.; Muddegowda, U. (2018): Anticancer activity of metal nanoparticles and their peptide conjugates against human colon adenorectal carcinoma cells. In: *Artificial Cells, Nanomedicine, and Biotechnology* 46 (7), pp. 1444-1451.
- Aula, S.; Lakkireddy, S.; Kapley, A.; Adimadhyam, V.N.; Sharma, R.K.; Uppin, S.G.; Jamil, K. (2018): Route of administration induced in vivo effects and toxicity responses of Zinc Oxide nanorods at molecular and genetic levels. In: *International Journal of Nano Dimension* 9 (2), pp. 158-169.
- Avramescu, M.-L.; Rasmussen, P.E.; Chenier, M.; Gardner, H.D. (2017): Influence of pH, particle size and crystal form on dissolution behaviour of engineered nanomaterials. In: *Environmental Science and Pollution Research International* 24 (2), pp. 1553-1564.
- Azzam, E.I.; Jay-Gerin, J.-P.; Pain, D. (2012): Ionizing radiation-induced metabolic oxidative stress and prolonged cell injury. In: *Cancer Letters* 327 (1-2), pp. 48-60.
- Babusikova, E.; Jurecekova, J.; Evinova, A.; Jesenak, M.; Dobrot, D. (2012): Oxidative Damage and Bronchial Asthma. In: Chen, W., Huang, X., Rong, Y. and Liu, Y. (Hg.): *Respiratory Diseases Among Dust Exposed Workers*: INTECH Open Access Publisher, pp. 151-176.

- Bafaro, E.; Liu, Y.; Xu, Y.; Dempski, R.E. (2017): The emerging role of zinc transporters in cellular homeostasis and cancer. In: *Signal Transduction and Targeted Therapy* 2, pii: 17029.
- Bai, C.; Liu, M. (2013): From Chemistry to Nanoscience: Not Just a Matter of Size. In: *Angewandte Chemie (International Ed.)* 52 (10), pp. 2678-2683.
- Bai, D.-P.; Zhang, X.-F.; Zhang, G.-L.; Huang, Y.-F.; Gurunathan, S. (2017): Zinc oxide nanoparticles induce apoptosis and autophagy in human ovarian cancer cells. In: *International Journal of Nanomedicine* 12, pp. 6521-6535.
- Bedi, P.S.; Kaur, A. (2015): An overview on uses of zinc oxide nanoparticles. In: *World Journal of Pharmacy and Pharmaceutical Sciences* 4 (12), pp. 1177-1196.
- Berardis, B. de; Civitelli, G.; Condello, M.; Lista, P.; Pozzi, R.; Arancia, G.; Meschini, S. (2010): Exposure to ZnO nanoparticles induces oxidative stress and cytotoxicity in human colon carcinoma cells. In: *Toxicology and Applied Pharmacology* 246 (3), pp. 116-127.
- Bisht, G.; Rayamajhi, S. (2016): ZnO Nanoparticles. A Promising Anticancer Agent. In: *Nanobiomedicine* 3 (9), pp. 1-11.
- Bostanci, Z.; Alam, S.; Soybel, D.I.; Kelleher, S.L. (2014): Prolactin receptor attenuation induces zinc pool redistribution through ZnT2 and decreases invasion in MDA-MB-453 breast cancer cells. In: *Experimental Cell Research* 321 (2), pp. 190-200.
- Boverhof, D.R.; Bramante, C.M.; Butala, J.H.; Clancy, S.F.; Lafranconi, M.; West, J.; Gordon, S.C. (2015): Comparative assessment of nanomaterial definitions and safety evaluation considerations. In: *Regulatory toxicology and pharmacology : RTP* 73 (1), pp. 137-150.
- Bozym, R.A.; Chimienti, F.; Giblin, L.J.; Gross, G.W.; Korichneva, I.; Li, Y.; Libert, S.; Maret, W.; Parviz, M.; Frederickson, C.J.; Thompson, R.B. (2010): Free zinc ions outside a narrow concentration range are toxic to a variety of cells in vitro. In: *Experimental Biology and Medicine* 235 (6), pp. 741-750.
- Bray, F.; Ferlay, J.; Soerjomataram, I.; Siegel, R.L.; Torre, L.A.; Jemal, A. (2018): Global cancer statistics 2018: GLOBOCAN estimates of incidence and mortality worldwide for 36 cancers in 185 countries. In: *CA: A Cancer Journal for Clinicians* 68 (6), pp. 394-424.

- Brown, A.M.; Kristal, B.S.; Efron, M.S.; Shestopalov, A.I.; Ullucci, P.A.; Sheu, K.-F.R.; Blass, J.P.; Cooper, A.J. (2000): Zn²⁺ Inhibits α -Ketoglutarate-stimulated Mitochondrial Respiration and the Isolated α -Ketoglutarate Dehydrogenase Complex. In: *Journal of Biological Chemistry* 275 (18), pp. 13441-13447.
- Cassandri, M.; Smirnov, A.; Novelli, F.; Pitolli, C.; Agostini, M.; Malewicz, M.; Melino, G.; Raschellà, G. (2017): Zinc-finger proteins in health and disease. In: *Cell Death Discovery* 3, pp. 17071.
- Chakraborti, S.; Chakraborty, S.; Saha, S.; Manna, A.; Banerjee, S.; Adhikary, A.; Sarwar, S.; Hazra, T.K.; Das, T.; Chakraborti, P. (2016): PEG-functionalized zinc oxide nanoparticles induce apoptosis in breast cancer cells through reactive oxygen species-dependent impairment of DNA damage repair enzyme NEIL2. In: *Free Radical Biology & Medicine* 103, pp. 35-47.
- Chandrasekaran, M.; Pandurangan, M. (2015): In Vitro Selective Anti-Proliferative Effect of Zinc Oxide Nanoparticles Against Co-Cultured C2C12 Myoblastoma Cancer and 3T3-L1 Normal Cells. In: *Biological Trace Element Research* 172 (1), pp. 148-154.
- Chen, B.; Le, W.; Wang, Y.; Li, Z.; Wang, D.; Ren, L.; Lin, L.; Cui, S.; Hu, J.J.; Hu, Y.; Yang, P.; Ewing, R.C. et al. (2016): Targeting Negative Surface Charges of Cancer Cells by Multifunctional Nanoproboscopes. In: *Theranostics* 6 (11), pp. 1887-1898.
- Cheng, B.; Shi, W.; Russell-Tanner, J.M.; Zhang, L.; Samulski, E.T. (2006): Synthesis of variable-aspect-ratio, single-crystalline ZnO nanostructures. In: *Inorganic Chemistry* 45 (3), pp. 1208-1214.
- Chevallet, M.; Veronesi, G.; Fuchs, A.; Mintz, E.; Michaud-Soret, I.; Deniaud, A. (2016): Impact of labile metal nanoparticles on cellular homeostasis. Current developments in imaging, synthesis and applications. In: *Biochimica et Biophysica Acta* 1861 (6), pp. 1566-1577.
- Choi, B.Y.; Jung, J.W.; Suh, S.W. (2017a): The Emerging Role of Zinc in the Pathogenesis of Multiple Sclerosis. In: *International Journal of Molecular Sciences* 18 (10), pp. 1-11.

- Choi, S.; Cui, C.; Luo, Y.; Kim, S.-H.; Ko, J.-K.; Huo, X.; Ma, J.; Fu, L.-W.; Souza, R.F.; Korichneva, I.; Pan, Z. (2017b): Selective inhibitory effects of zinc on cell proliferation in esophageal squamous cell carcinoma through Orai1. In: *FASEB journal : official publication of the Federation of American Societies for Experimental Biology* 32 (1), pp. 404-416.
- Choudhury, S.R.; Ordaz, J.; Lo, C.-L.; Damayanti, N.P.; Zhou, F.; Irudayaraj, J. (2017): Zinc oxide Nanoparticles-Induced Reactive Oxygen Species Promotes Multimodal Cyto- and Epigenetic Toxicity. In: *Toxicological Sciences* 156 (1), pp. 261-274.
- Churchman, A.H.; Wallace, R.; Milne, S.J.; Brown, A.P.; Brydson, R.; Beales, P.A. (2013): Serum albumin enhances the membrane activity of ZnO nanoparticles. In: *Chemical Communications* 49 (39), pp. 4172-4174.
- Clogston, J.D.; Patri, A.K. (2011): Zeta Potential Measurement. In: McNeil, S. (Hg.): *Characterization of Nanoparticles Intended for Drug Delivery: Humana Press (Methods in Molecular Biology, Methods and Protocols, 697)*, pp. 63-70.
- Condello, M.; Berardis, B. de; Ammendolia, M.G.; Barone, F.; Condello, G.; Degan, P.; Meschini, S. (2016): ZnO nanoparticle tracking from uptake to genotoxic damage in human colon carcinoma cells. In: *Toxicology In Vitro* 35, pp. 169-179.
- Corbo, C.; Molinaro, R.; Parodi, A.; Toledano Furman, N.E.; Salvatore, F.; Tasciotti, E. (2016): The impact of nanoparticle protein corona on cytotoxicity, immunotoxicity and target drug delivery. In: *Nanomedicine* 11 (1), pp. 81-100.
- Costello, L.C.; Franklin, R.B. (2006): The clinical relevance of the metabolism of prostate cancer; zinc and tumor suppression: connecting the dots. In: *Molecular Cancer* 5, pp. 17.
- Costello, L.C.; Franklin, R.B. (2014): The status of zinc in the development of hepatocellular cancer. An important, but neglected, clinically established relationship. In: *Cancer Biology & Therapy* 15 (4), pp. 353-360.
- Costello, L.C.; Franklin, R.B. (2016): A comprehensive review of the role of zinc in normal prostate function and metabolism; and its implications in prostate cancer. In: *Archives of Biochemistry and Biophysics* 611, pp. 100-112.

- Costello, L.C.; Franklin, R.B.; Zou, J.; Feng, P.; Bok, R.; Swanson, M.G.; Kurhanewicz, J. (2011a): Human prostate cancer ZIP1/zinc/citrate genetic/metabolic relationship in the TRAMP prostate cancer animal model. In: *Cancer Biology & Therapy* 12 (12), pp. 1078-1084.
- Costello, L.C.; Franklin, R.B.; Zou, J.; Naslund, M.J. (2015): Evidence that Human Prostate Cancer is a ZIP1-Deficient Malignancy that could be Effectively Treated with a Zinc Ionophore (Clioquinol) Approach. In: *Chemotherapy* 4 (2).
- Costello, L.C.; Guan, Z.; Kukoyi, B.; Feng, P.; Franklin, R.B. (2004): Terminal oxidation and the effects of zinc in prostate versus liver mitochondria. In: *Mitochondrion* 4 (4), pp. 331-338.
- Costello, L.C.; Levy, B.A.; Desouki, M.M.; Zou, J.; Bagasra, O.; Johnson, L.A.; Hanna, N.; Franklin, R.B. (2011b): Decreased zinc and downregulation of ZIP3 zinc uptake transporter in the development of pancreatic adenocarcinoma. In: *Cancer Biology & Therapy* 12 (4), pp. 297-303.
- Costello, L.C.; Zou, J.; Desouki, M.M.; Franklin, R.B. (2012): Evidence for changes in RREB-1, ZIP3, and Zinc in the early development of pancreatic adenocarcinoma. In: *Journal of Gastrointestinal Cancer* 43 (4), pp. 570-578.
- Cousins, R.J.; Liuzzi, J.P.; Lichten, L.A. (2006): Mammalian Zinc Transport, Trafficking, and Signals. In: *Journal of Biological Chemistry* 281 (34), pp. 24085-24089.
- Cribari-Neto, F.; Zeileis, A. (2010): Beta Regression in R. In: *Journal of Statistical Software* 34 (2), pp. 1-24.
- David, C.A.; Galceran, J.; Rey-Castro, C.; Puy, J.; Companys, E.; Salvador, J.; Monné, J.; Wallace, R.; Vakourov, A. (2012): Dissolution Kinetics and Solubility of ZnO Nanoparticles Followed by AGNES. In: *The Journal of Physical Chemistry C* 116 (21), pp. 11758-11767.
- De Angelis, I. de; Barone, F.; Zijno, A.; Bizzarri, L.; Russo, M.T.; Pozzi, R.; Franchini, F.; Giudetti, G.; Uboldi, C.; Ponti, J.; Rossi, F.; Berardis, B. de (2013): Comparative study of ZnO and TiO₂ nanoparticles. Physicochemical characterisation and toxicological effects on human colon carcinoma cells. In: *Nanotoxicology* 7 (8), pp. 1361-1372.

- Deng, Y.; Zhang, H. (2013): The synergistic effect and mechanism of doxorubicin-ZnO nanocomplexes as a multimodal agent integrating diverse anticancer therapeutics. In: *International Journal of Nanomedicine* 8, pp. 1835-1841.
- Deorukhkar, A.; Krishnan, S. (2010): Targeting inflammatory pathways for tumor radiosensitization. In: *Biochemical Pharmacology* 80 (12), pp. 1904-1914.
- Desouki, M.M.; Geradts, J.; Milon, B.; Franklin, R.B.; Costello, L.C. (2007): hZip2 and hZip3 zinc transporters are down regulated in human prostate adenocarcinomatous glands. In: *Molecular Cancer* 6, pp. 37.
- Doboszewska, U.; Młyniec, K.; Właż, A.; Poleszak, E.; Nowak, G.; Właż, P. (2018): Zinc signaling and epilepsy. In: *Pharmacology & Therapeutics* 193, pp. 156-177.
- Dufour, E.K.; Kumaravel, T.; Nohynek, G.J.; Kirkland, D.; Toutain, H. (2006): Clastogenicity, photo-clastogenicity or pseudo-photo-clastogenicity: Genotoxic effects of zinc oxide in the dark, in pre-irradiated or simultaneously irradiated Chinese hamster ovary cells. In: *Mutation Research* 607 (2), pp. 215-224.
- Edlich, F.; Banerjee, S.; Suzuki, M.; Cleland, M.M.; Arnoult, D.; Wang, C.; Neutzner, A.; Tjandra, N.; Youle, R.J. (2011): Bcl-x(L) retrotranslocates Bax from the mitochondria into the cytosol. In: *Cell* 145 (1), pp. 104-116.
- Eixenberger, J.E.; Anders, C.B.; Hermann, R.J.; Brown, R.J.; Reddy, K.M.; Punnoose, A.; Wingett, D.G. (2017): Rapid Dissolution of ZnO Nanoparticles Induced by Biological Buffers Significantly Impacts Cytotoxicity. In: *Chemical Research in Toxicology* 30 (8), pp. 1641-1651.
- El Yamani, N.; Collins, A.R.; Rundén-Pran, E.; Fjellsbø, L.M.; Shaposhnikov, S.; Zienolddiny, S.; Dusinska, M. (2017): In vitro genotoxicity testing of four reference metal nanomaterials, titanium dioxide, zinc oxide, cerium oxide and silver. Towards reliable hazard assessment. In: *Mutagenesis* 32 (1), pp. 117-126.
- Elmore, S. (2007): Apoptosis: A Review of Programmed Cell Death. In: *Toxicologic Pathology* 35 (4), pp. 495-516.
- Franken, N.A.; Rodermond, H.M.; Stap, J.; Haveman, J.; van Bree, C. (2006): Clonogenic assay of cells *in vitro*. In: *Nature Protocols* 1 (5), pp. 2315-2319.

- Franklin, R.B.; Levy, B.A.; Zou, J.; Hanna, N.; Desouki, M.M.; Bagasra, O.; Johnson, L.A.; Costello, L.C. (2012): ZIP14 zinc transporter downregulation and zinc depletion in the development and progression of hepatocellular cancer. In: *Journal of Gastrointestinal Cancer* 43 (2), pp. 249-257.
- Franklin, R.B.; Zou, J.; Costello, L.C. (2014): The cytotoxic role of RREB1, ZIP3 zinc transporter, and zinc in human pancreatic adenocarcinoma. In: *Cancer Biology & Therapy* 15 (10), pp. 1431-1437.
- Fu, P.P.; Xia, Q.; Hwang, H.-M.; Ray, P.C.; Yu, H. (2014): Mechanisms of nanotoxicity. Generation of reactive oxygen species. In: *Journal of Food and Drug Analysis* 22 (1), pp. 64-75.
- Fu, Y.; Jiang, Y.-B.; Dunphy, D.; Xiong, H.; Coker, E.; Chou, S.S.; Zhang, H.; Vanegas, J.M.; Croissant, J.G.; Cecchi, J.L.; Rempe, S.B.; Brinker, C.J. (2018): Ultra-thin enzymatic liquid membrane for CO₂ separation and capture. In: *Nature Communications* 9 (1), pp. 1-12.
- Fujihara, J.; Tongu, M.; Hashimoto, H.; Yamada, T.; Kimura-Kataoka, K.; Yasuda, T.; Fujita, Y.; Takeshita, H. (2015): Distribution and toxicity evaluation of ZnO dispersion nanoparticles in single intravenously exposed mice. In: *Journal of Medical Investigation* 62 (1-2), pp. 45-50.
- Fukunaka, A.; Fujitani, Y. (2018): Role of Zinc Homeostasis in the Pathogenesis of Diabetes and Obesity. In: *International Journal of Molecular Sciences* 19 (2), pp. 1-14.
- Gao, F.; Ma, N.; Zhou, H.; Wang, Q.; Zhang, H.; Wang, P.; Hou, H.; Wen, H.; Li, L. (2016): Zinc oxide nanoparticles-induced epigenetic change and G2/M arrest are associated with apoptosis in human epidermal keratinocytes. In: *International Journal of Nanomedicine* 11, pp. 3859-3874.
- Garcia-Hevia, L.; Valiente, R.; Martin-Rodriguez, R.; Renero-Lecuna, C.; Gonzalez, J.; Rodriguez-Fernandez, L.; Aguado, F.; Villegas, J.C.; Fanarraga, M.L. (2016): Nano-ZnO leads to tubulin microtubule assembly and actin bundling, triggering cytoskeletal catastrophe and cell necrosis. In: *Nanoscale* 8 (21), pp. 10963-10973.
- Gatenby, R.A.; Gillies, R.J. (2004): Why do cancers have high aerobic glycolysis? In: *Nature Reviews. Cancer* 4 (11), pp. 891-899.

- Generalov, R.; Kuan, W.B.; Chen, W.; Kristensen, S.; Juzenas, P. (2015): Radiosensitizing effect of zinc oxide and silica nanocomposites on cancer cells. In: *Colloids and Surfaces B: Biointerfaces* 129, pp. 79-86.
- Gilbert, B.; Fakra, S.C.; Xia, T.; Pokhrel, S.; Mädler, L.; Nel, A.E. (2012): The fate of ZnO nanoparticles administered to human bronchial epithelial cells. In: *ACS Nano* 6 (6), pp. 4921-4930.
- Goesmann, H.; Feldmann, C. (2010): Nanoparticulate functional materials. In: *Angewandte Chemie (International Ed.)* 49 (8), pp. 1362-1395.
- Golan, Y.; Kambe, T.; Assaraf, Y.G. (2017): The role of the zinc transporter SLC30A2/ZnT2 in transient neonatal zinc deficiency. In: *Metallomics* 9 (10), pp. 1352-1366.
- Grassian, V.H. (2008): When Size Really Matters. Size-Dependent Properties and Surface Chemistry of Metal and Metal Oxide Nanoparticles in Gas and Liquid Phase Environments †. In: *The Journal of Physical Chemistry C* 112 (47), pp. 18303-18313.
- Grattan, B.J.; Freake, H.C. (2012): Zinc and cancer: implications for LIV-1 in breast cancer. In: *Nutrients* 4 (7), pp. 648-675.
- Gumulec, J.; Masarik, M.; Adam, V.; Eckschlager, T.; Provaznik, I.; Kizek, R. (2014): Serum and tissue zinc in epithelial malignancies: a meta-analysis. In: *PLOS ONE* 9 (6), e99790.
- Gumulec, J.; Masarik, M.; Krizkova, S.; Hlavna, M.; Babula, P.; Hrabec, R.; Rovny, A.; Masarikova, M.; Sochor, J.; Adam, V.; Eckschlager, T.; Kizek, R. (2012): Evaluation of alpha-methylacyl-CoA racemase, metallothionein and prostate specific antigen as prostate cancer prognostic markers. In: *Neoplasma* 59 (02), pp. 191-201.
- Günther, V.; Lindert, U.; Schaffner, W. (2012): The taste of heavy metals: gene regulation by MTF-1. In: *Biochimica et Biophysica Acta* 1823 (9), pp. 1416-1425.
- Guo, D.; Wu, C.; Jiang, H.; Li, Q.; Wang, X.; Chen, B. (2008): Synergistic cytotoxic effect of different sized ZnO nanoparticles and daunorubicin against leukemia cancer cells under UV irradiation. In: *Journal of Photochemistry and Photobiology B: Biology* 93 (3), pp. 119-126.

- Gupta, J.; Bhargava, P.; Bahadur, D. (2015): Fluorescent ZnO for imaging and induction of DNA fragmentation and ROS-mediated apoptosis in cancer cells. In: *Journal of Materials Chemistry B* 3 (9), pp. 1968-1978.
- Gutierrez, R.M.; Mendez, J.V.; Vazquez, I.A. (2017): Chapter 2 - A novel approach to the oral delivery of bionanostructures for systemic disease. In: Andronescu, E. and Grumezescu, A. (Hg.): *Nanostructures for oral medicine: Elsevier (Nanostructures in therapeutic medicine series)*, pp. 27-59.
- Gutiérrez-González, E.; Castelló, A.; Fernández-Navarro, P.; Castaño-Vinyals, G.; Llorca, J.; Salas, D.; Salcedo-Bellido, I.; Aragonés, N.; Fernández-Tardón, G.; Alguacil, J.; Gracia-Lavedan, E.; García-Esquinas, E. et al. (2018): Dietary Zinc and Risk of Prostate Cancer in Spain: MCC-Spain Study. In: *Nutrients* 11 (1), pii: E18.
- Hackenberg, S.; Scherzed, A.; Ginzkey, C.; Koehler, C.; Froelich, K.; Burghartz, M.; Kessler, M.; Hagen, R.; Kleinsasser, N. (2010a): Zinc oxide nanoparticles induce photocatalytic cell death in human head and neck squamous cell carcinoma cell lines in vitro. In: *International Journal of Oncology* 37 (6), pp. 1583-1590.
- Hackenberg, S.; Scherzed, A.; Harnisch, W.; Froelich, K.; Ginzkey, C.; Koehler, C.; Hagen, R.; Kleinsasser, N. (2012): Antitumor activity of photo-stimulated zinc oxide nanoparticles combined with paclitaxel or cisplatin in HNSCC cell lines. In: *Journal of Photochemistry and Photobiology B: Biology* 114, pp. 87-93.
- Hackenberg, S.; Scherzed, A.; Kessler, M.; Froelich, K.; Ginzkey, C.; Koehler, C.; Burghartz, M.; Hagen, R.; Kleinsasser, N. (2010b): Zinc oxide nanoparticles induce photocatalytic cell death in human head and neck squamous cell carcinoma cell lines in vitro. In: *International Journal of Oncology* 37 (6), pp. 1583-1590.
- Hackenberg, S.; Scherzed, A.; Zapp, A.; Radeloff, K.; Ginzkey, C.; Gehrke, T.; Ickrath, P.; Kleinsasser, N. (2017): Genotoxic effects of zinc oxide nanoparticles in nasal mucosa cells are antagonized by titanium dioxide nanoparticles. In: *Mutation Research* 816-817, pp. 32-37.
- Hanley, C.; Layne, J.; Punnoose, A.; Reddy, K.M.; Coombs, I.; Coombs, A.; Feris, K.; Wingett, D. (2008): Preferential killing of cancer cells and activated human T cells using ZnO nanoparticles. In: *Nanotechnology* 19 (29), pp. 295103.

- Hanley, C.; Thurber, A.; Hanna, C.; Punnoose, A.; Zhang, J.; Wingett, D.G. (2009): The Influences of Cell Type and ZnO Nanoparticle Size on Immune Cell Cytotoxicity and Cytokine Induction. In: *Nanoscale Research Letters* 4 (12), pp. 1409-1420.
- Hao, Q.; Maret, W. (2005): Imbalance between pro-oxidant and pro-antioxidant functions of zinc in disease. In: *Journal of Alzheimer's Disease* 8 (2), pp. 161-170.
- Hassan, H.F.; Mansour, A.M.; Abo-Youssef, A.M.; Elsadek, B.E.; Messiha, B.A. (2017): Zinc oxide nanoparticles as a novel anticancer approach; in vitro and in vivo evidence. In: *Clinical and Experimental Pharmacology & Physiology* 44 (2), pp. 235-243.
- Heiliger, E.; Osmanagic, A.; Haase, H.; Golenhofen, N.; Grabrucker, A.M.; Weth, A.; Baumgartner, W. (2015): N-Cadherin-mediated cell adhesion is regulated by extracellular Zn²⁺. In: *Metallomics* 7 (2), pp. 355-362.
- Heller, M.; Frerick-Ochs, E.V.; Bauer, H.-K.; Schiegnitz, E.; Flesch, D.; Brieger, J.; Stein, R.; Al-Nawas, B.; Brochhausen, C.; Thüroff, J.W.; Unger, R.E.; Brenner, W. (2016): Tissue engineered pre-vascularized buccal mucosa equivalents utilizing a primary triculture of epithelial cells, endothelial cells and fibroblasts. In: *Biomaterials* 77, pp. 207-215.
- Heller, M.; Kämmerer, P.W.; Al-Nawas, B.; Luszpinski, M.-A.; Förch, R.; Brieger, J. (2015): The effect of extracellular matrix proteins on the cellular response of HUVECS and HOBS after covalent immobilization onto titanium. In: *Journal of Biomedical Materials Research: Part A* 103 (6), pp. 2035-2044.
- Hinata, N.; Shirakawa, T.; Zhang, Z.; Matsumoto, A.; Fujisawa, M.; Okada, H.; Kamidono, S.; Gotoh, A. (2003): Radiation induces p53-dependent cell apoptosis in bladder cancer cells with wild-type- p53 but not in p53-mutated bladder cancer cells. In: *Urological Research* 31 (6), pp. 387-396.
- Horie, M.; Nishio, K.; Fujita, K.; Endoh, S.; Miyauchi, A.; Saito, Y.; Iwahashi, H.; Yamamoto, K.; Murayama, H.; Nakano, H.; Nanashima, N.; Niki, E. et al. (2009): Protein adsorption of ultrafine metal oxide and its influence on cytotoxicity toward cultured cells. In: *Chemical Research in Toxicology* 22 (3), pp. 543-553.
- Hosny, A.E.-D.; Kashef, M.T.; Taher, H.A.; El-Bazza, Z.E. (2017): The use of unirradiated and γ -irradiated zinc oxide nanoparticles as a preservative in cosmetic preparations. In: *International Journal of Nanomedicine* 12, pp. 6799-6811.

- Hotchkiss, R.S.; Strasser, A.; McDunn, J.E.; Swanson, P.E. (2009): Cell Death. In: *New England Journal of Medicine* 361 (16), pp. 1570-1583.
- Huang, C.-C.; Aronstam, R.S.; Chen, D.-R.; Huang, Y.-W. (2010): Oxidative stress, calcium homeostasis, and altered gene expression in human lung epithelial cells exposed to ZnO nanoparticles. In: *Toxicology In Vitro* 24 (1), pp. 45-55.
- Huat, T.J.; Camats-Perna, J.; Newcombe, E.A.; Valmas, N.; Kitazawa, M.; Medeiros, R. (2019): Metal Toxicity Links to Alzheimer's Disease and Neuroinflammation. In: *Journal of Molecular Biology*, pii: S0022-2836(19)30027-0.
- Idrees, M. (2015): Role of Nanotechnology in Medical Sciences: a Review. In: *International Journal of Innovative Drug Discovery* 5 (1), pp. 14-24.
- Jarosz, M.; Olbert, M.; Wyszogrodzka, G.; Młyniec, K.; Librowski, T. (2017): Antioxidant and anti-inflammatory effects of zinc. Zinc-dependent NF- κ B signaling. In: *Inflammopharmacology* 25 (1), pp. 11-24.
- Jarrard, D.F. (2005): Does zinc supplementation increase the risk of prostate cancer? In: *Archives of ophthalmology (Chicago, Ill. : 1960)* 123 (1), pp. 102-103.
- Kagara, N.; Tanaka, N.; Noguchi, S.; Hirano, T. (2007): Zinc and its transporter ZIP10 are involved in invasive behavior of breast cancer cells. In: *Cancer Science* 98 (5), pp. 692-697.
- Kang, T.; Guan, R.; Chen, X.; Song, Y.; Jiang, H.; Zhao, J. (2013): In vitro toxicity of different-sized ZnO nanoparticles in Caco-2 cells. In: *Nanoscale Research Letters* 8 (1), pp. 496.
- KC, B.; Paudel, S.N.; Rayamajhi, S.; Karna, D.; Adhikari, S.; Shrestha, B.G.; Bisht, G. (2016): Enhanced preferential cytotoxicity through surface modification. Synthesis, characterization and comparative in vitro evaluation of TritonX-100 modified and unmodified zinc oxide nanoparticles in human breast cancer cell (MDA-MB-231). In: *Chemistry Central Journal* 10, pp. 16.
- Khan, A.; Rayner, G.D. (2003): Robustness to Non-Normality of Common Tests for the Many-Sample Location Problem. In: *Journal of Applied Mathematics and Decision Sciences* 7 (4), pp. 187-206.
- Kleiner, D.; van Jagow, G. (1972): On the inhibition of mitochondrial electron transport by Zn²⁺ ions. In: *FEBS Letters* 20 (2), pp. 229-232.

- Kloubert, V.; Rink, L. (2015): Zinc as a micronutrient and its preventive role of oxidative damage in cells. In: *Food & Function* 6 (10), pp. 3195-3204.
- Klug, A. (2010): The discovery of zinc fingers and their applications in gene regulation and genome manipulation. In: *Annual Review of Biochemistry* 79, pp. 213-231.
- Kołodziejczak-Radzimska, A.; Jesionowski, T. (2014): Zinc Oxide-From Synthesis to Application: A Review. In: *Materials* 7 (4), pp. 2833-2881.
- Kononenko, V.; Repar, N.; Marusic, N.; Drasler, B.; Romih, T.; Hocevar, S.; Drobne, D. (2017): Comparative in vitro genotoxicity study of ZnO nanoparticles, ZnO macroparticles and ZnCl₂ to MDCK kidney cells: Size matters. In: *Toxicology In Vitro* 40, pp. 256-263.
- Kreżel, A.; Maret, W. (2006): Zinc-buffering capacity of a eukaryotic cell at physiological pZn. In: *Journal of Biological Inorganic Chemistry* 11 (8), pp. 1049-1062.
- Kreżel, A.; Maret, W. (2007): Different redox states of metallothionein/thionein in biological tissue. In: *Biochemical Journal* 402 (3), pp. 551-558.
- Kreżel, A.; Maret, W. (2016): The biological inorganic chemistry of zinc ions. In: *Archives of Biochemistry and Biophysics* 611, pp. 3-19.
- Kreżel, A.; Maret, W. (2017): The Functions of Metamorphic Metallothioneins in Zinc and Copper Metabolism. In: *International Journal of Molecular Sciences* 18 (6), pii: E1237.
- Kunz-Schughart, L.A.; Dubrovskaja, A.; Peitzsch, C.; Ewe, A.; Aigner, A.; Schellenburg, S.; Muders, M.H.; Hampel, S.; Cirillo, G.; Iemma, F.; Tietze, R.; Alexiou, C. et al. (2017): Nanoparticles for radiooncology: Mission, vision, challenges. In: *Biomaterials* 120, pp. 155-184.
- Kwatra, D.; Venugopal, A.; Anant, S. (2013): Nanoparticles in radiation therapy: a summary of various approaches to enhance radiosensitization in cancer. In: *Translational Cancer Research* 2 (4), pp. 330-342.
- Laitaoja, M.; Valjakka, J.; Jänis, J. (2013): Zinc coordination spheres in protein structures. In: *Inorganic Chemistry* 52 (19), pp. 10983-10991.

Langlais, M.; Tajmir-Riahi, H.A.; Savoie, R. (1990): Raman spectroscopic study of the effects of Ca^{2+} , Mg^{2+} , Zn^{2+} , and Cd^{2+} ions on calf thymus DNA: Binding sites and conformational changes. In: *Biopolymers* 30 (7-8), pp. 743-752.

Lee, J.S.; Latimer, L.J.P.; Reid, R.S. (1993): A cooperative conformational change in duplex DNA induced by Zn^{2+} and other divalent metal ions. In: *Biochemistry and Cell Biology* 71 (3-4), pp. 162-168.

Lee, K.M.; Lai, C.W.; Ngai, K.S.; Juan, J.C. (2016): Recent developments of zinc oxide based photocatalyst in water treatment technology: A review. In: *Water Research* 88, pp. 428-448.

Leitzmann, M.F.; Stampfer, M.J.; Wu, K.; Colditz, G.A.; Willett, W.C.; Giovannucci, E.L. (2003): Zinc Supplement Use and Risk of Prostate Cancer. In: *JNCI Journal of the National Cancer Institute* 95 (20), pp. 1556.

Leroy, B.; Girard, L.; Hollestelle, A.; Minna, J.D.; Gazdar, A.F.; Soussi, T. (2014): Analysis of TP53 mutation status in human cancer cell lines. A reassessment. In: *Human Mutation* 35 (6), pp. 756-765.

Li, C.-H.; Shen, C.-C.; Cheng, Y.-W.; Huang, S.-H.; Wu, C.-C.; Kao, C.-C.; Liao, J.-W.; Kang, J.-J. (2012): Organ biodistribution, clearance, and genotoxicity of orally administered zinc oxide nanoparticles in mice. In: *Nanotoxicology* 6 (7), pp. 746-756.

Li, F.; Abuarab, N.; Sivaprasadarao, A. (2016): Reciprocal regulation of actin cytoskeleton remodelling and cell migration by Ca^{2+} and Zn^{2+} . Role of TRPM2 channels. In: *Journal of Cell Science* 129 (10), pp. 2016-2029.

Li, J.; Guo, D.; Wang, X.; Wang, H.; Jiang, H.; Chen, B. (2010): The Photodynamic Effect of Different Size ZnO Nanoparticles on Cancer Cell Proliferation In Vitro. In: *Nanoscale Research Letters* 5 (6), pp. 1063-1071.

Liberti, M.V.; Locasale, J.W. (2016): The Warburg Effect: How Does it Benefit Cancer Cells? In: *Trends in Biochemical Sciences* 41 (3), pp. 211-218.

Lien, C.-F.; Lee, W.-S.; Wang, I.-C.; Chen, T.-I.; Chen, T.-L.; Yang, K.-T. (2018): Intermittent hypoxia-generated ROS contributes to intracellular zinc regulation that limits ischemia/reperfusion injury in adult rat cardiomyocyte. In: *Journal of Molecular and Cellular Cardiology* 118, pp. 122-132.

- Liu, J.; Kang, Y.; Yin, S.; Song, B.; Wei, L.; Chen, L.; Shao, L. (2017): Zinc oxide nanoparticles induce toxic responses in human neuroblastoma SHSY5Y cells in a size-dependent manner. In: *International Journal of Nanomedicine* 12, pp. 8085-8099.
- Loh, S.N. (2010): The missing zinc: p53 misfolding and cancer. In: *Metallomics* 2 (7), pp. 442-449.
- Lopez, V.; Foolad, F.; Kelleher, S.L. (2011): ZnT2-overexpression represses the cytotoxic effects of zinc hyper-accumulation in malignant metallothionein-null T47D breast tumor cells. In: *Cancer Letters* 304 (1), pp. 41-51.
- Lu, S. (2014): Zn²⁺ Blocks Annealing of Complementary Single-Stranded DNA in a Sequence-Selective Manner. In: *Scientific Reports* 4, pp. 5464.
- Ma, L.; Liu, B.; Huang, P.-J.J.; Zhang, X.; Liu, J. (2016): DNA Adsorption by ZnO Nanoparticles near Its Solubility Limit. Implications for DNA Fluorescence Quenching and DNazyme Activity Assays. In: *Langmuir : the ACS journal of Surfaces and Colloids* 32 (22), pp. 5672-5680.
- Maier, P.; Hartmann, L.; Wenz, F.; Herskind, C. (2016): Cellular Pathways in Response to Ionizing Radiation and Their Targetability for Tumor Radiosensitization. In: *International Journal of Molecular Sciences* 17 (1), pii: E102.
- Malaiyandi, L.M.; Vergun, O.; Dineley, K.E.; Reynolds, I.J. (2005): Direct visualization of mitochondrial zinc accumulation reveals uniporter-dependent and -independent transport mechanisms. In: *Journal of Neurochemistry* 93 (5), pp. 1242-1250.
- Manke, A.; Wang, L.; Rojanasakul, Y. (2013): Mechanisms of nanoparticle-induced oxidative stress and toxicity. In: *BioMed Research International* 2013, pp. 942916.
- Maret, W. (2009): Molecular aspects of human cellular zinc homeostasis. Redox control of zinc potentials and zinc signals. In: *BioMetals* 22 (1), pp. 149-157.
- Maret, W. (2013): Zinc biochemistry: from a single zinc enzyme to a key element of life. In: *Advances in Nutrition* 4 (1), pp. 82-91.
- Maret, W. (2015): Analyzing free zinc(II) ion concentrations in cell biology with fluorescent chelating molecules. In: *Metallomics* 7 (2), pp. 202-211.

- Maret, W. (2017): Zinc in Cellular Regulation. The Nature and Significance of "Zinc Signals". In: *International Journal of Molecular Sciences* 18 (11), pii: E2285.
- Maret, W. (2019): The redox biology of redox-inert zinc ions. In: *Free Radical Biology & Medicine* 134, pp. 311-326.
- Maret, W.; Krężel, A. (2007): Cellular Zinc and Redox Buffering Capacity of Metallothionein/Thionein in Health and Disease. In: *Molecular Medicine* 13 (7-8), pp. 371-375.
- Maret, W.; Sandstead, H.H. (2006): Zinc requirements and the risks and benefits of zinc supplementation. In: *Journal of Trace Elements in Medicine and Biology* 20 (1), pp. 3-18.
- Margiolaki, I.; Giannopoulou, A.E.; Wright, J.P.; Knight, L.; Norrman, M.; Schluckebier, G.; Fitch, A.N.; Dreele, R.B. von (2013): High-resolution powder X-ray data reveal the T(6) hexameric form of bovine insulin. In: *Acta crystallographica. Section D, Biological crystallography* 69 (Pt 6), pp. 978-990.
- Marreiro, D.d.; Cruz, K.J.; Morais, J.B.; Beserra, J.B.; Severo, J.S.; Oliveira, A.R. de (2017): Zinc and Oxidative Stress. Current Mechanisms. In: *Antioxidants* 6 (2), pii: E24.
- Martínez-Balbás, M.A.; Jiménez-García, E.; Azorín, F. (1995): Zinc(II) ions selectively Interact with DNA sequences present at the TFIIIA binding site of the *Xenopus* 5S-RNA gene. In: *Nucleic Acids Research* 23 (13), pp. 2464-2471.
- Matsui, C.; Takatani-Nakase, T.; Hatano, Y.; Kawahara, S.; Nakase, I.; Takahashi, K. (2017): Zinc and its transporter ZIP6 are key mediators of breast cancer cell survival under high glucose conditions. In: *FEBS Letters* 591 (20), pp. 3348-3359.
- McCall, J.; Smith, J.J.; Marquardt, K.N.; Knight, K.R.; Bane, H.; Barber, A.; DeLong, R.K. (2017): ZnO Nanoparticles Protect RNA from Degradation Better than DNA. In: *Nanomaterials* 7 (11), pii: E378.
- McCall, K.A.; Huang, C.-c.; Fierke, C.A. (2000): Function and Mechanism of Zinc Metalloenzymes. In: *Journal of Nutrition* 130 (5S Suppl), 1437S-46S.

- McMahon, D.K.; Anderson, P.A.; Nassar, R.; Bunting, J.B.; Saba, Z.; Oakeley, A.E.; Malouf, N.N. (1994): C2C12 cells: biophysical, biochemical, and immunocytochemical properties. In: *American Journal of Physiology* 266 (6 Pt 1), C1795-802.
- McMillan, T.J.; Tobi, S.; Mateos, S.; Lemon, C. (2001): The use of DNA double-strand break quantification in radiotherapy. In: *International Journal of Radiation Oncology*Biography*Physics* 49 (2), pp. 373-377.
- Meek, D.W. (2015): Regulation of the p53 response and its relationship to cancer. In: *The Biochemical journal* 469 (3), pp. 325-346.
- Milon, B.C.; Agyapong, A.; Bautista, R.; Costello, L.C.; Franklin, R.B. (2010): Ras responsive element binding protein-1 (RREB-1) down-regulates hZIP1 expression in prostate cancer cells. In: *The Prostate* 70 (3), pp. 288-296.
- Mishra, P.K.; Mishra, H.; Ekielski, A.; Talegaonkar, S.; Vaidya, B. (2017): Zinc oxide nanoparticles. A promising nanomaterial for biomedical applications. In: *Drug Discovery Today* 22 (12), pp. 1825-1834.
- Moghaddam, A.B.; Moniri, M.; Azizi, S.; Abdul Rahim, R.; Bin Ariff, A.; Navaderi, M.; Mohamad, R. (2017): Eco-Friendly Formulated Zinc Oxide Nanoparticles. Induction of Cell Cycle Arrest and Apoptosis in the MCF-7 Cancer Cell Line. In: *Genes* 8 (10), pp. 1-15.
- Moos, P.J.; Chung, K.; Woessner, D.; Honegger, M.; Cutler, N.S.; Veranth, J.M. (2010): ZnO particulate matter requires cell contact for toxicity in human colon cancer cells. In: *Chemical Research in Toxicology* 23 (4), pp. 733-739.
- Moratin, H.; Scherzad, A.; Gehrke, T.; Ickrath, P.; Radloff, K.; Kleinsasser, N.; Hackenberg, S. (2017): Toxicological characterization of ZnO nanoparticles in malignant and non-malignant cells. In: *Environmental and Molecular Mutagenesis* 59 (3), pp. 247-259.
- Morris, D.L. (2014): DNA-bound metal ions. Recent developments. In: *Biomolecular Concepts* 5 (5), pp. 397-407.

- Mu, Q.; David, C.A.; Galceran, J.; Rey-Castro, C.; Krzemiński, L.; Wallace, R.; Bamiduro, F.; Milne, S.J.; Hondow, N.S.; Brydson, R.; Vizcay-Barrena, G.; Routledge, M.N. et al. (2014): Systematic investigation of the physicochemical factors that contribute to the toxicity of ZnO nanoparticles. In: *Chemical Research in Toxicology* 27 (4), pp. 558-567.
- Mudipalli, Anuradha; Zelikoff, Judith T. (2017): Essential and Non-essential Metals. Carcinogenesis, Prevention and Cancer Therapeutics: Springer International Publishing.
- Nakamura, Y.; Mochida, A.; Choyke, P.L.; Kobayashi, H. (2016): Nanodrug Delivery. Is the Enhanced Permeability and Retention Effect Sufficient for Curing Cancer? In: *Bioinorganic Chemistry and Applications* 27 (10), pp. 2225-2238.
- Nejdl, L.; Ruttkay-Nedecky, B.; Kudr, J.; Krizkova, S.; Smerkova, K.; Dostalova, S.; Vaculovicova, M.; Kopel, P.; Zehnalek, J.; Trnkova, L.; Babula, P.; Adam, V. et al. (2014): DNA interaction with zinc(II) ions. In: *International Journal of Biological Macromolecules* 64, pp. 281-287.
- Nel, A.E.; Madler, L.; Velegol, D.; Xia, T.; Hoek, E.M.; Somasundaran, P.; Klaessig, F.; Castranova, V.; Thompson, M. (2009): Understanding biophysicochemical interactions at the nano-bio interface. In: *Nature Materials* 8 (7), pp. 543-557.
- Ng, C.T.; Yong, L.Q.; Hande, M.P.; Ong, C.N.; Yu, L.E.; Bay, B.H.; Baeg, G.H. (2017): Zinc oxide nanoparticles exhibit cytotoxicity and genotoxicity through oxidative stress responses in human lung fibroblasts and *Drosophila melanogaster*. In: *International Journal of Nanomedicine* 12, pp. 1621-1637.
- Ninsontia, C.; Phiboonchaiyanan, P.P.; Chanvorachote, P. (2016): Zinc induces epithelial to mesenchymal transition in human lung cancer H460 cells via superoxide anion-dependent mechanism. In: *Cancer Cell International* 16, pp. 48.
- Nuryadi, E.; Permata, T.B.; Komatsu, S.; Oike, T.; Nakano, T. (2018): Inter-assay precision of clonogenic assays for radiosensitivity in cancer cell line A549. In: *Oncotarget* 9 (17), pp. 13706-13712.
- Odzak, N.; Kistler, D.; Sigg, L. (2017): Influence of daylight on the fate of silver and zinc oxide nanoparticles in natural aquatic environments. In: *Environmental Pollution* 226, pp. 1-11.

Ollig, J.; Kloubert, V.; Weßels, I.; Haase, H.; Rink, L. (2016): Parameters Influencing Zinc in Experimental Systems in Vivo and in Vitro. In: *Metals* 6 (12), pp. 1-16.

Oren, M.; Rotter, V. (2010): Mutant p53 gain-of-function in cancer. In: *Cold Spring Harbor perspectives in biology* 2 (2), pp. a001107.

Osman, I.F.; Baumgartner, A.; Cemeli, E.; Fletcher, J.N.; Anderson, D. (2010): Genotoxicity and cytotoxicity of zinc oxide and titanium dioxide in HEp-2 cells. In: *Nanomedicine* 5 (8), pp. 1193-1203.

Osredkar, J. (2011): Copper and Zinc, Biological Role and Significance of Copper/Zinc Imbalance. In: *Journal of Clinical Toxicology* s3, pp. 1.

Ostrovsky, S.; Kazimirsky, G.; Gedanken, A.; Brodie, C. (2009): Selective cytotoxic effect of ZnO nanoparticles on glioma cells. In: *Nano Research* 2 (11), pp. 882-890.

Ozaki, T.; Nakagawara, A. (2011): Role of p53 in Cell Death and Human Cancers. In: *Cancers* 3 (1), pp. 994-1013.

Pace, N.J.; Weerapana, E. (2014): Zinc-binding cysteines. Diverse functions and structural motifs. In: *Biomolecules* 4 (2), pp. 419-434.

Padmavathy, N.; Vijayaraghavan, R. (2008): Enhanced bioactivity of ZnO nanoparticles-an antimicrobial study. In: *Science and Technology of Advanced Materials* 9 (3), pp. 35004.

Paino, I.M.; J Goncalves, F.; Souza, F.L.; Zucolotto, V. (2016): Zinc Oxide Flower-Like Nanostructures That Exhibit Enhanced Toxicology Effects in Cancer Cells. In: *ACS Applied Materials & Interfaces* 8 (48), pp. 32699-32705.

Pan, Z. (2017): Zinc transporters and dysregulated channels in cancers. In: *Frontiers in Bioscience* 22 (4), pp. 623-643.

Pandurangan, M.; Enkhtaivan, G.; Kim, D.H. (2016): Anticancer studies of synthesized ZnO nanoparticles against human cervical carcinoma cells. In: *Journal of Photochemistry and Photobiology B: Biology* 158, pp. 206-211.

Paszek, E.; Czyz, J.; Woźnicka, O.; Jakubiak, D.; Wojnarowicz, J.; Łojkowski, W.; Stępień, E. (2012): Zinc Oxide Nanoparticles Impair the Integrity of Human Umbilical Vein Endothelial Cell Monolayer *In Vitro*. In: *Journal of Biomedical Nanotechnology* 8 (6), pp. 957-967.

- Pati, R.; Das, I.; Mehta, R.K.; Sahu, R.; Sonawane, A. (2016): Zinc-Oxide Nanoparticles Exhibit Genotoxic, Clastogenic, Cytotoxic and Actin Depolymerization Effects by Inducing Oxidative Stress Responses in Macrophages and Adult Mice. In: *Toxicological Sciences* 150 (2), pp. 454-472.
- Pearson, R.G. (1963): Hard and Soft Acids and Bases. In: *Journal of the American Chemical Society* 85 (22), pp. 3533-3539.
- Plum, L.M.; Rink, L.; Haase, H. (2010): The essential toxin: impact of zinc on human health. In: *International Journal of Environmental Research and Public Health* 7 (4), pp. 1342-1365.
- Podporska-Carroll, J.; Myles, A.; Quilty, B.; McCormack, D.E.; Fagan, R.; Hinder, S.J.; Dionysiou, D.D.; Pillai, S.C. (2017): Antibacterial properties of F-doped ZnO visible light photocatalyst. In: *Journal of Hazardous Materials* 324 (Pt A), pp. 39-47.
- Polster, B.M.; Nicholls, D.G.; Ge, S.X.; Roelofs, B.A. (2014): Use of potentiometric fluorophores in the measurement of mitochondrial reactive oxygen species. In: *Methods in Enzymology* 547, pp. 225-250.
- Polyzos, A.A.; McMurray, C.T. (2017): The chicken or the egg: mitochondrial dysfunction as a cause or consequence of toxicity in Huntington's disease. In: *Mechanisms of ageing and development* 161 (Pt A), pp. 181-197.
- Powell, S.R. (2000): The Antioxidant Properties of Zinc. In: *Journal of Nutrition* 130 (5S Suppl), 1447S-54S.
- Pradhan, S.; Hedberg, J.; Blomberg, E.; Wold, S.; Odnevall Wallinder, I. (2016): Effect of sonication on particle dispersion, administered dose and metal release of non-functionalized, non-inert metal nanoparticles. In: *Journal of Nanoparticle Research* 18 (9), pp. 285.
- Prasad, A.S. (2013): Discovery of human zinc deficiency: its impact on human health and disease. In: *Advances in nutrition (Bethesda, Md.)* 4 (2), pp. 176-190.
- Prasanna, V.L.; Vijayaraghavan, R. (2015): Insight into the Mechanism of Antibacterial Activity of ZnO. Surface Defects Mediated Reactive Oxygen Species Even in the Dark. In: *Langmuir : the ACS journal of Surfaces and Colloids* 31 (33), pp. 9155-9162.

- Prasanth, R.; Gopinath, D. (2013): Effect of ZnO nanoparticles on nasopharyngeal cancer cells viability and respiration. In: *Applied Physics Letters* 102 (11), pp. 113702.
- Prashanth, L.; Kattapagari, K.K.; Chitturi, R.T.; Baddam, V.R.; Prasad, L.K. (2015): A review on role of essential trace elements in health and disease. In: *Journal of Dr. NTR University of Health Sciences* 4 (2), pp. 75-85.
- Preedia Babu, E.; Subastri, A.; Suyavaran, A.; Lokeshwara Rao, P.; Suresh Kumar, M.; Jeevaratnam, K.; Thirunavukkarasu, C. (2015): Extracellularly synthesized ZnO nanoparticles interact with DNA and augment gamma radiation induced DNA damage through reactive oxygen species. In: *RSC Advances* 5 (76), pp. 62067-62077.
- Premanathan, M.; Karthikeyan, K.; Jeyasubramanian, K.; Manivannan, G. (2011): Selective toxicity of ZnO nanoparticles toward Gram-positive bacteria and cancer cells by apoptosis through lipid peroxidation. In: *Nanomedicine: Nanotechnology, Biology and Medicine* 7 (2), pp. 184-192.
- Puleston, D. (2015): Detection of Mitochondrial Mass, Damage, and Reactive Oxygen Species by Flow Cytometry. In: *Cold Spring Harbor Protocols* 2015 (9), pdb.prot086298.
- Punnoose, A.; Dodge, K.; Rasmussen, J.W.; Chess, J.; Wingett, D.; Anders, C. (2014): Cytotoxicity of ZnO Nanoparticles Can Be Tailored by Modifying Their Surface Structure. A Green Chemistry Approach for Safer Nanomaterials. In: *ACS Sustainable Chemistry & Engineering* 2 (7), pp. 1666-1673.
- Racca, L.; Canta, M.; Dumontel, B.; Ancona, A.; Limongi, T.; Garino, N.; Laurenti, M.; Canavese, G.; Cauda, V. (2018): Zinc Oxide Nanostructures in Biomedicine. In: Ciofani, G. (Hg.): *Smart nanoparticles for biomedicine: Elsevier (Micro & nano technologies series)*, pp. 171-187.
- Ramani, M.; Nguyen, T.D.; Aryal, S.; Ghosh, K.C.; DeLong, R.K. (2017): Elucidating the RNA Nano–Bio Interface. Mechanisms of Anticancer Poly I:C RNA and Zinc Oxide Nanoparticle Interaction. In: *The Journal of Physical Chemistry C* 121 (29), pp. 15702-15710.

- Ramasamy, M.; Das, M.; An, S.S.; Yi, D.K. (2014): Role of surface modification in zinc oxide nanoparticles and its toxicity assessment toward human dermal fibroblast cells. In: *International Journal of Nanomedicine* 9, pp. 3707-3718.
- Rasmussen, J.W.; Martinez, E.; Louka, P.; Wingett, D.G. (2010): Zinc oxide nanoparticles for selective destruction of tumor cells and potential for drug delivery applications. In: *Expert Opinion on Drug Delivery* 7 (9), pp. 1063-1077.
- Reddel, R.R.; Yang, K.; Rhim, J.S.; Brash, D.; Su, R.T.; Lechner, J.F.; Gerwin, B.I.; Harris, C.C.; Amstad, P. (1989): IMMORTALIZED HUMAN BRONCHIAL EPITHELIAL MESOTHELIAL CELL LINES. Patent number: 4,885,238.
- Reshma, V.G.; Mohanan, P.V. (2017): Cellular interactions of zinc oxide nanoparticles with human embryonic kidney (HEK 293) cells. In: *Colloids and Surfaces B: Biointerfaces* 157, pp. 182-190.
- Robert J. P. Williams (1991): The Chemical Elements of Life. In: *Journal of the Chemical Society, Dalton Transactions*, pp. 539-546.
- Roohani, N.; Hurrell, R.; Kelishadi, R.; Schulin, R. (2013): Zinc and its importance for human health: An integrative review. In: *Journal of Research in Medical Sciences* 18 (2), pp. 144-157.
- Roy, R.; Singh, S.K.; Chauhan, L.K.; Das, M.; Tripathi, A.; Dwivedi, P.D. (2014): Zinc oxide nanoparticles induce apoptosis by enhancement of autophagy via PI3K/Akt/mTOR inhibition. In: *Toxicology Letters* 227 (1), pp. 29-40.
- Saha, S.; Sarkar, P. (2014): Understanding the interaction of DNA-RNA nucleobases with different ZnO nanomaterials. In: *Physical Chemistry Chemical Physics : PCCP* 16 (29), pp. 15355-15366.
- Samanta, P.K. (2017): Review on Wet Chemical Growth and Anti-bacterial Activity of Zinc Oxide Nanostructures. In: *Journal of Tissue Science & Engineering* 08 (01), pp. 1-4.
- Sandstead, H.H. (1994): Understanding zinc: recent observations and interpretations. In: *Journal of Laboratory and Clinical Medicine* 124 (3), pp. 322-327.
- Sasidharan, A.; Chandran, P.; Menon, D.; Raman, S.; Nair, S.; Koyakutty, M. (2011): Rapid dissolution of ZnO nanocrystals in acidic cancer microenvironment leading to preferential apoptosis. In: *Nanoscale* 3 (9), pp. 3657-3669.

- Satakar, P.; Elger, B.S.; Shaw, D.M. (2016): Defining Nano, Nanotechnology and Nanomedicine: Why Should It Matter? In: *Science and Engineering Ethics* 22 (5), pp. 1255-1276.
- Schladt, T.D.; Schneider, K.; Schild, H.; Tremel, W. (2011): Synthesis and bio-functionalization of magnetic nanoparticles for medical diagnosis and treatment. In: *Dalton Transactions* 40 (24), pp. 6315-6343.
- Sensi, S.L.; Ton-That, D.; Sullivan, P.G.; Jonas, E.A.; Gee, K.R.; Kaczmarek, L.K.; Weiss, J.H. (2003): Modulation of mitochondrial function by endogenous Zn²⁺ pools. In: *Proceedings of the National Academy of Sciences* 100 (10), pp. 6157-6162.
- Sharma, H.; Kumar, K.; Choudhary, C.; Mishra, P.K.; Vaidya, B. (2016): Development and characterization of metal oxide nanoparticles for the delivery of anticancer drug. In: *Artificial Cells, Nanomedicine, and Biotechnology* 44 (2), pp. 672-679.
- Sharma, H.; Mishra, P.K.; Talegaonkar, S.; Vaidya, B. (2015): Metal nanoparticles: A theranostic nanotool against cancer. In: *Drug Discovery Today* 20 (9), pp. 1143-1151.
- Sharma, V.; Anderson, D.; Dhawan, A. (2012): Zinc oxide nanoparticles induce oxidative DNA damage and ROS-triggered mitochondria mediated apoptosis in human liver cells (HepG2). In: *Apoptosis : an international journal on programmed cell death* 17 (8), pp. 852-870.
- Sharma, V.; Shukla, R.K.; Saxena, N.; Parmar, D.; Das, M.; Dhawan, A. (2009): DNA damaging potential of zinc oxide nanoparticles in human epidermal cells. In: *Toxicology Letters* 185 (3), pp. 211-218.
- Sharma, V.; Singh, S.K.; Anderson, D.; Tobin, D.J.; Dhawan, A. (2011): Zinc Oxide Nanoparticle Induced Genotoxicity in Primary Human Epidermal Keratinocytes. In: *Journal of Nanoscience and Nanotechnology* 11 (5), pp. 3782-3788.
- Shen, C.; James, S.A.; Jonge, M.D. de; Turney, T.W.; Wright, P.F.; Feltis, B.N. (2013): Relating cytotoxicity, zinc ions, and reactive oxygen in ZnO nanoparticle-exposed human immune cells. In: *Toxicological Sciences* 136 (1), pp. 120-130.
- Shi, D. (2017): Cancer Cell Surface Negative Charges: A Bio-Physical Manifestation of the Warburg Effect. In: *Nano LIFE* 07 (03n04), pp. 1771001.

- Sivakumar, P.; Lee, M.; Kim, Y.-S.; Shim, M.S. (2018): Photo-triggered antibacterial and anticancer activities of zinc oxide nanoparticles. In: *Journal of Materials Chemistry B* 6 (30), pp. 4852-4871.
- Skulachev, V.P.; Chistyakov, V.V.; Jasaitis, A.A.; Smirnova, E.G. (1967): Inhibition of the respiratory chain by zinc ions. In: *Biochemical and Biophysical Research Communications* 26 (1), pp. 1-6.
- Slepchenko, K.G.; Lu, Q.; Li, Y.V. (2017): Cross talk between increased intracellular zinc (Zn^{2+}) and accumulation of reactive oxygen species in chemical ischemia. In: *American Journal of Physiology. Cell Physiology* 313 (4), C448-C459.
- Sliwinski, T.; Czechowska, A.; Kolodziejczak, M.; Jajte, J.; Wisniewska-Jarosinska, M.; Blasiak, J. (2009): Zinc salts differentially modulate DNA damage in normal and cancer cells. In: *Cell Biology International* 33 (4), pp. 542-547.
- Song, W.; Zhang, J.; Guo, J.; Zhang, J.; Ding, F.; Li, L.; Sun, Z. (2010): Role of the dissolved zinc ion and reactive oxygen species in cytotoxicity of ZnO nanoparticles. In: *Toxicology Letters* 199 (3), pp. 389-397.
- Sun, T.; Zhang, Y.S.; Pang, B.; Hyun, D.C.; Yang, M.; Xia, Y. (2014): Engineered nanoparticles for drug delivery in cancer therapy. In: *Angewandte Chemie (International Ed.)* 53 (46), pp. 12320-12364.
- Swaroop, K.; Sana, S.; Chandrashekar, K.R.; Somashekarappa, h.M. (2015): A Study of NanoParticles of Gamma Irradiated Zinc Oxide and Its Antibacterial effect on *Klebsiella pneumonia* and *Pseudomonas aeruginosa*. In: *IOSR Journal of Applied Physics* 7 (4), pp. 58-63.
- Taccola, L.; Raffa, V.; Riggio, C.; Vittorio, O.; Iorio, M.C.; Vanacore, R.; Pietrabissa, A.; Cuschieri, A. (2011): Zinc oxide nanoparticles as selective killers of proliferating cells. In: *International Journal of Nanomedicine* 6, pp. 1129-1140.
- Tahir, M.N.; Natalio, F.; Cambaz, M.A.; Panthöfer, M.; Branscheid, R.; Kolb, U.; Tremel, W. (2013): Controlled synthesis of linear and branched Au@ZnO hybrid nanocrystals and their photocatalytic properties. In: *Nanoscale* 5 (20), pp. 9944-9949.
- Tait, S.W.; Green, D.R. (2010): Mitochondria and cell death: outer membrane permeabilization and beyond. In: *Nature Reviews. Molecular Cell Biology* 11 (9), pp. 621-632.

- Takatani-Nakase, T. (2018): Zinc Transporters and the Progression of Breast Cancers. In: *Biological & Pharmaceutical Bulletin* 41 (10), pp. 1517-1522.
- Taylor, K.M.; Vichova, P.; Jordan, N.; Hiscox, S.; Hendley, R.; Nicholson, R.I. (2008): ZIP7-mediated intracellular zinc transport contributes to aberrant growth factor signaling in antihormone-resistant breast cancer Cells. In: *Endocrinology* 149 (10), pp. 4912-4920.
- Thongkam, W.; Gerloff, K.; van Berlo, D.; Albrecht, C.; Schins, R.P. (2017): Oxidant generation, DNA damage and cytotoxicity by a panel of engineered nanomaterials in three different human epithelial cell lines. In: *Mutagenesis* 32 (1), pp. 105-115.
- Toduka, Y.; Toyooka, T.; Ibuki, Y. (2012): Flow cytometric evaluation of nanoparticles using side-scattered light and reactive oxygen species-mediated fluorescence-correlation with genotoxicity. In: *Environmental Science & Technology* 46 (14), pp. 7629-7636.
- Tran, S.; DeGiovanni, P.-J.; Piel, B.; Rai, P. (2017): Cancer nanomedicine: a review of recent success in drug delivery. In: *Clinical and Translational Medicine* 6 (1), pp. 44.
- Turney, T.W.; Duriska, M.B.; Jayaratne, V.; Elbaz, A.; O'Keefe, S.J.; Hastings, A.S.; Piva, T.J.; Wright, P.F.; Feltis, B.N. (2012): Formation of zinc-containing nanoparticles from Zn²⁺ ions in cell culture media: implications for the nanotoxicology of ZnO. In: *Chemical Research in Toxicology* 25 (10), pp. 2057-2066.
- Valdiglesias, V.; Costa, C.; Kiliç, G.; Costa, S.; Pásaro, E.; Laffon, B.; Teixeira, J.P. (2013): Neuronal cytotoxicity and genotoxicity induced by zinc oxide nanoparticles. In: *Environment International* 55, pp. 92-100.
- Vallee, B.L.; Falchuk, K.H. (1993): The biochemical basis of zinc physiology. In: *Physiological Reviews* 73 (1), pp. 79-118.
- Ventola, C.L. (2017): Progress in Nanomedicine: Approved and Investigational Nanodrugs. In: *Pharmacology & Therapeutics* 42 (12), pp. 742-755.
- Wahab, R.; Dwivedi, S.; Umar, A.; Singh, S.; Hwang, I.H.; Shin, H.-S.; Musarrat, J.; Al-Khedhairi, A.A.; Kim, Y.-S. (2013): ZnO Nanoparticles Induce Oxidative Stress in Cloudman S91 Melanoma Cancer Cells. In: *Journal of Biomedical Nanotechnology* 9 (3), pp. 441-449.

- Wahab, R.; Kaushik, N.; Khan, F.; Kaushik, N.K.; Choi, E.H.; Musarrat, J.; Al-Khedhairi, A.A. (2016): Self-Styled ZnO Nanostructures Promotes the Cancer Cell Damage and Supresses the Epithelial Phenotype of Glioblastoma. In: *Scientific Reports* 6, pp. 19950.
- Wahab, R.; Kim, Y.-S.; Hwang, I.H.; Shin, H.-S. (2009): A non-aqueous synthesis, characterization of zinc oxide nanoparticles and their interaction with DNA. In: *Synthetic Metals* 159 (23-24), pp. 2443-2452.
- Wahab, R.; Siddiqui, M.A.; Saquib, Q.; Dwivedi, S.; Ahmad, J.; Musarrat, J.; Al-Khedhairi, A.A.; Shin, H.-S. (2014): ZnO nanoparticles induced oxidative stress and apoptosis in HepG2 and MCF-7 cancer cells and their antibacterial activity. In: *Colloids and Surfaces B: Biointerfaces* 117, pp. 267-276.
- Wang, C.-C.; Wang, S.; Xia, Q.; He, W.; Yin, J.-J.; Fu, P.P.; Li, J.-H. (2013): Phototoxicity of Zinc Oxide Nanoparticles in HaCaT Keratinocytes-Generation of Oxidative DNA Damage During UVA and Visible Light Irradiation. In: *Journal of Nanoscience and Nanotechnology* 13 (6), pp. 3880-3888.
- Wang, D.; Zhao, L.; Ma, H.; Zhang, H.; Guo, L.-H. (2017): Quantitative Analysis of Reactive Oxygen Species Photogenerated on Metal Oxide Nanoparticles and Their Bacteria Toxicity. The Role of Superoxide Radicals. In: *Environmental Science & Technology* 51 (17), pp. 10137-10145.
- Wang, H.; Wingett, D.; Engelhard, M.H.; Feris, K.; Reddy, K.M.; Turner, P.; Layne, J.; Hanley, C.; Bell, J.; Tenne, D.; Wang, C.; Punnoose, A. (2009): Fluorescent dye encapsulated ZnO particles with cell-specific toxicity for potential use in biomedical applications. In: *Journal of Materials Science. Materials in Medicine* 20 (1), pp. 11-22.
- Wang, J.; Gao, S.; Wang, S.; Xu, Z.; Wei, L. (2018): Zinc oxide nanoparticles induce toxicity in CAL 27 oral cancer cell lines by activating PINK1/Parkin-mediated mitophagy. In: *International Journal of Nanomedicine* 13, pp. 3441-3450.
- Wang, Z.L. (2004): Nanostructures of zinc oxide. In: *Materials Today* 7 (6), pp. 26-33.
- Watt, N.T.; Whitehouse, I.J.; Hooper, N.M. (2010): The role of zinc in Alzheimer's disease. In: *International Journal of Alzheimer's Disease* 2011, pp. 971021.

- Welkoborsky, H.-J.; Jacob, R.; Riazimand, S.H.; Bernauer, H.S.; Mann, W.J. (2003): Molecular Biologic Characteristics of Seven New Cell Lines of Squamous Cell Carcinomas of the Head and Neck and Comparison to Fresh Tumor Tissue. In: *Oncology* 65 (1), pp. 60-71.
- Whatmore, R.W. (2006): Nanotechnology--what is it? Should we be worried? In: *Occupational Medicine* 56 (5), pp. 295-299.
- Wicki, A.; Witzigmann, D.; Balasubramanian, V.; Huwyler, J. (2015): Nanomedicine in cancer therapy. Challenges, opportunities, and clinical applications. In: *Journal of Controlled Release* 200, pp. 138-157.
- Wiesmann, N.; Strozynski, J.; Beck, C.; Zimmermann, N.; Mendler, S.; Gieringer, R.; Schmidtman, I.; Brieger, J. (2017): Knockdown of hnRNPK leads to increased DNA damage after irradiation and reduces survival of tumor cells. In: *Carcinogenesis* 38 (3), pp. 321-328.
- Wilhelmi, V.; Fischer, U.; Weighardt, H.; Schulze-Osthoff, K.; Nickel, C.; Stahlmecke, B.; Kuhlbusch, T.A.; Scherbart, A.M.; Esser, C.; Schins, R.P.; Albrecht, C. (2013): Zinc oxide nanoparticles induce necrosis and apoptosis in macrophages in a p47phox- and Nrf2-independent manner. In: *PLOS ONE* 8 (6), e65704.
- Wingett, D.; Louka, P.; Anders, C.B.; Zhang, J.; Punnoose, A. (2016): A role of ZnO nanoparticle electrostatic properties in cancer cell cytotoxicity. In: *Nanotechnology, Science and Applications* 9, pp. 29-45.
- Wiseman, D.A.; Wells, S.M.; Hubbard, M.; Welker, J.E.; Black, S.M. (2007): Alterations in zinc homeostasis underlie endothelial cell death induced by oxidative stress from acute exposure to hydrogen peroxide. In: *American Journal of Physiology. Lung Cellular and Molecular Physiology* 292 (1), L165-77.
- Xia, T.; Kovoichich, M.; Liong, M.; Madler, L.; Gilbert, B.; Shi, H.; Yeh, J.I.; Zink, J.I.; Nel, A.E. (2008): Comparison of the mechanism of toxicity of zinc oxide and cerium oxide nanoparticles based on dissolution and oxidative stress properties. In: *ACS Nano* 2 (10), pp. 2121-2134.
- Xueju, X.; Daniels, R.S.; Myers, F.; Gahan, P.; Springs, B. (2015): N-ACETYL L-CYSTEINE CHELATES AND METHODS FOR MAKING AND USING THE SAME. Patent number: US 2015/0038577 A1.

- Yang, J.; Zhang, Y.; Cui, X.; Yao, W.; Yu, X.; Cen, P.; E. Hodges, S.; E. Fisher, W.; C. Brunicardi, F.; Chen, C.; Yao, Q.; Li, M. (2013): Gene Profile Identifies Zinc Transporters Differentially Expressed in Normal Human Organs and Human Pancreatic Cancer. In: *Current Molecular Medicine* 13 (3), pp. 401-409.
- Yang, Q.; Ma, Y. (2014): Irradiation-Enhanced Cytotoxicity of Zinc Oxide Nanoparticles. In: *International Journal of Toxicology* 33 (3), pp. 187-203.
- Ye, B.; Maret, W.; Vallee, B.L. (2001): Zinc metallothionein imported into liver mitochondria modulates respiration. In: *Proceedings of the National Academy of Sciences* 98 (5), pp. 2317-2322.
- Yin, H.; Chen, R.; Casey, P.S.; Ke, P.C.; Davis, T.P.; Chen, C. (2015): Reducing the cytotoxicity of ZnO nanoparticles by a pre-formed protein corona in a supplemented cell culture medium. In: *RSC Advances* 5 (90), pp. 73963-73973.
- Zhang, T.; Sui, D.; Hu, J. (2016): Structural insights of ZIP4 extracellular domain critical for optimal zinc transport. In: *Nature Communications* 7, pp. 11979.
- Zhang, X.Q.; Yin, L.H.; Tang, M.; Pu, Y.P. (2011): ZnO, TiO₂, SiO₂ and Al₂O₃ nanoparticles-induced toxic effects on human fetal lung fibroblasts. In: *Biomedical and Environmental Sciences* 24 (6), pp. 661-669.
- Zhang, Y.; Chen, W.; Wang, S.; Liu, Y.; Pope, C. (2008): Phototoxicity of Zinc Oxide Nanoparticle Conjugates in Human Ovarian Cancer NIH: OVCAR-3 Cells. In: *Journal of Biomedical Nanotechnology* 4 (4), pp. 432-438.
- Zijno, A.; Angelis, I. de; Berardis, B. de; Andreoli, C.; Russo, M.T.; Pietraforte, D.; Scorza, G.; Degan, P.; Ponti, J.; Rossi, F.; Barone, F. (2015): Different mechanisms are involved in oxidative DNA damage and genotoxicity induction by ZnO and TiO₂ nanoparticles in human colon carcinoma cells. In: *Toxicology In Vitro* 29 (7), pp. 1503-1512.
- Zou, J.; Milon, B.C.; Desouki, M.M.; Costello, L.C.; Franklin, R.B. (2011): hZIP1 zinc transporter down-regulation in prostate cancer involves the overexpression of ras responsive element binding protein-1 (RREB-1). In: *The Prostate* 71 (14), pp. 1518-1524.
- Žūkienė, R.; Snitka, V. (2015): Zinc oxide nanoparticle and bovine serum albumin interaction and nanoparticles influence on cytotoxicity in vitro. In: *Colloids and Surfaces B: Biointerfaces* 135, pp. 316-323.

12 Appendix

In the appendix all raw values are shown according to the order of the experiments in the results section. To every table the corresponding figure in the results section is linked to be able to assign the figures to the raw values unambiguously. Numbering in bold indicates the different independent runs of the experiment.

Table 8 corresponding to Figure 25

To measure the amount of zinc ions released from ZnO NP, nanoparticles were prepared according to the standard procedure and incubated in the different media in centrifuge tubes under cell culture conditions. Remaining particles were separated by centrifugation and the amount of zinc ions in the supernatant was measured by atomic absorption spectroscopy.

	H ₂ O			Tris-NaCl buffer			
	1	2	3	1	2	3	
4 h	49.3	67.9	66.2	157.5	177.9	243.5	
24 h	228.4	203.8	202.4	169.2	282.3	243.2	
	Cell culture medium			Cell culture medium with FCS			
	1	2	3	1	2	3	4
4 h	104.5	125.7	120.3	128.1	198.5	170.9	156.9
24 h	119.9	133.5	123.4	208.2	208.9	177.4	171.8

Table 9 corresponding to Figure 26

To evaluate the toxicity of ZnCl₂ as a representative zinc salt that is fully dissolved under cell culture conditions, staining with propidium iodide and annexin V-FITC was performed and measured by flow cytometry. As a proof of concept this experiment was only performed once. Alive = PI negative and annexin V negative, apoptotic = PI negative, annexin V positive, dead = PI positive and annexin V positive, necrotic = PI positive and annexin V negative.

	Viable cells	Necrotic cells	Apoptotic cells	Dead cells
0d control	74.4	0.56	11.89	9.94
0d 20 µg/mL	64.57	4.58	16	9.25
0d 30 µg/mL	63.15	1.51	23.39	6.83
0d 40 µg/mL	65.66	1.05	8.66	4.68
0d 50 µg/mL	60.84	1.87	7.38	3.51
0d 60 µg/mL	58.35	1.43	12.47	5.82
0d 70 µg/mL	58.9	2.96	11.56	8.08
0d 80 µg/mL	62.75	0.46	13.89	4.55
0d 90 µg/mL	56.44	0.9	15.7	8.64
0d 100 µg/mL	60.45	1.22	9.24	8.5
1d control	79.52	4.32	7.14	4.4
1d 20 µg/mL	77.79	1.57	8.76	5.05
1d 30 µg/mL	80.37	0.73	11.12	4.21
1d 40 µg/mL	65.07	0.29	15.01	12.88
1d 50 µg/mL	63.57	0.57	13.34	14.81
1d 60 µg/mL	55.77	2.11	10.72	20.34
1d 70 µg/mL	57.4	2.02	9.11	20.23
1d 80 µg/mL	53.02	3.36	9.68	19.64
1d 90 µg/mL	57.5	2.4	11.58	19.38

	Viable cells	Necrotic cells	Apoptotic cells	Dead cells
1d 100 µg/mL	52.15	2.76	12.14	24.64
1d control	79.52	4.32	7.14	4.4
2d control	75.3	1.2	6.69	4.05
2d 20 µg/mL	75.3	1.2	6.69	4.05
2d 30 µg/mL	77.98	1.67	8.87	5.53
2d 40 µg/mL	58.19	1.99	19.52	12.89
2d 50 µg/mL	52.36	1.15	20.92	17.33
2d 60 µg/mL	47.39	0.79	21.81	24.32
2d 70 µg/mL	40.4	7.81	14.32	29.47
2d 80 µg/mL	39.48	6.81	14.96	30.69
2d 90 µg/mL	38.69	6	12	34
2d 100 µg/mL	34.85	7.35	18.17	33.53
3d control	77.54	0.28	4.91	3.96
3d 20 µg/mL	72.07	2.11	10.8	5.82
3d 30 µg/mL	73.28	0.73	10.27	6.49
3d 40 µg/mL	72.63	0.4	10.98	7.22
3d 50 µg/mL	59.55	1	20.86	8.71
3d 60 µg/mL	47.83	2.7	29.75	12.27
3d 70 µg/mL	46.64	2.67	27.76	16.69
3d 80 µg/mL	28.01	2.28	28.83	19.08
3d control	77.54	0.28	4.91	3.96
3d 20 µg/mL	72.07	2.11	10.8	5.82
3d 30 µg/mL	73.28	0.73	10.27	6.49

Table 10 corresponding to Figure 27

To evaluate the toxicity of different divalent metal ions in contrast to ZnO NP equimolar amounts of magnesium and zinc ions were used in the form of ZnO NP, MgCl₂ and ZnCl₂. The viability of A549 cells was measured via the cellular metabolic activity, after 3 h, after 6 h and after 24 h after beginning treatment. “0–3 h” refers to the timespan the alamar Blue[®] reagent was incubated with the cells in relation to the start point of the treatment. All values are stated in reference to untreated control cells (=100%) to correct for differences between the runs of the experiment.

0–3 h	ZnO NP			MgCl ₂			ZnCl ₂		
	1	2	3	1	2	3	1	2	3
100 µg/mL	112.8	51.1	115.4	134.1	157.1	138.4	78.8	26.5	83.2
50 µg/mL	97.7	30.6	72.9	122.5	150.5	120.1	46.5	23.9	65.1
40 µg/mL	57.1	26.0	56.4	150.9	151.2	152.9	59.1	18.6	62.0
35 µg/mL	56.5	24.4	46.8	117.7	125.2	145.7	53.6	19.1	58.4
30 µg/mL	81.1	33.8	77.2	150.6	158.4	161.4	74.7	28.0	89.7
25 µg/mL	97.9	36.4	97.7	128.6	153.8	141.5	74.3	27.9	96.7
20 µg/mL	87.4	43.7	87.6	120.8	140.7	127.0	71.2	33.3	92.5
15 µg/mL	86.0	52.0	76.3	127.1	143.6	124.5	86.2	43.8	137.0
10 µg/mL	103.7	81.6	87.6	116.3	129.3	106.8	89.8	90.6	150.8
5 µg/mL	115.5	103.4	103.8	106.4	131.6	92.1	95.1	121.6	144.9
4–6 h	ZnO NP			MgCl ₂			ZnCl ₂		
	1	2	3	1	2	3	1	2	3
100 µg/mL	4.7	17.5	4.8	118.7	155.2	118.9	8.4	32.4	7.5
50 µg/mL	3.0	12.6	4.8	101.6	148.9	111.4	35.2	19.2	34.6
40 µg/mL	2.6	12.6	2.7	134.4	148.9	129.4	2.5	17.4	1.9
35 µg/mL	2.4	13.3	2.9	113.6	123.8	124.6	3.1	16.4	2.0
30 µg/mL	3.4	18.4	5.7	124.7	151.1	129.3	3.4	22.9	3.2
25 µg/mL	7.2	18.3	10.7	110.1	147.3	123.9	5.5	24.6	4.9
20 µg/mL	6.9	22.6	12.9	116.2	135.8	122.2	8.2	30.4	7.6
15 µg/mL	32.4	32.1	82.4	124.5	137.0	113.9	16.8	37.8	13.7
10 µg/mL	84.2	79.2	134.4	111.2	126.9	102.6	42.8	69.9	46.6
5 µg/mL	98.1	118.2	135.5	104.0	129.0	88.1	114.0	101.2	101.7

21–24 h	ZnO NP			MgCl ₂			ZnCl ₂		
	1	2	3	1	2	3	1	2	3
100 µg/mL	2.8	3.5	2.9	120.2	153.5	115.9	3.3	3.5	3.1
50 µg/mL	10.9	4.1	6.5	116.8	143.1	110.4	4.9	3.4	4.0
40 µg/mL	4.7	9.9	4.7	139.2	130.5	134.8	2.9	3.8	2.5
35 µg/mL	12.9	14.8	16.8	139.6	108.7	137.1	3.6	4.3	2.7
30 µg/mL	33.1	26.4	38.9	123.2	131.6	124.8	6.6	7.1	5.7
25 µg/mL	35.1	31.1	41.0	108.1	127.1	112.5	10.2	10.2	8.7
20 µg/mL	37.5	30.9	48.0	121.4	122.9	109.3	30.2	20.1	32.3
15 µg/mL	45.0	39.9	75.4	114.1	119.8	115.0	43.2	26.8	44.1
10 µg/mL	90.3	93.0	108.9	114.1	112.8	111.2	68.1	56.4	47.7
5 µg/mL	91.6	101.3	125.0	86.5	109.4	91.8	106.6	98.9	110.8

Table 11 corresponding to Figure 29

To evaluate the toxicity of ZnO NP in contrast to the zinc ions that are released by the nanoparticles, A549 cells were incubated with the nanoparticles directly or with supernatant of ZnO NP from which all particulate material was separated by centrifugation. The cellular viability was measured via the cellular metabolic activity, after 4 h, after 7 h and after 24 h after beginning treatment. “1–4 h” refers to the timespan the alamar Blue® reagent was incubated with the cells in relation to the start point of the treatment. All values are stated in reference to untreated control cells (=100%) to correct for differences between the runs of the experiment.

	Untreated control cells			Supernatant (zinc ions only)		
	1	2	3	1	2	3
1–4 h	100.0	100.0	100.0	92.3	64.0	31.8
4–7 h	100.0	100.0	100.0	85.1	76.3	94.7
21–24 h	100.0	100.0	100.0	96.1	94.0	95.1
	100 µg/mL ZnO NP			Dead cells		
	1	2	3	1	2	3
1–4 h	93.6	64.2	27.2	24.7	-1.6	-1.2
4–7 h	40.9	62.5	34.2	18.8	-5.6	0.5
21–24 h	35.2	50.7	37.3	9.0	-2.3	0.2

Table 12 corresponding to Figure 31

To compare the toxicity of ZnO NP and ZnO@SiO₂ NP equimolar amounts of enclosed zinc oxide was used. A549 cells were incubated with the nanoparticles and their viability was measured via the cellular metabolic activity, after 4 h, after 6 h and after 24 h after beginning treatment. “1–4 h” refers to the timespan the alamar Blue® reagent was incubated with the cells in relation to the start point of the treatment. All values are stated in reference to untreated control cells (=100%) to correct for differences between the runs of the experiment.

	Untreated control cells			ZnO NP		
	1	2	3	1	2	3
1–4 h	100.0	100.0	100.0	45.8	44.3	51.0
3–6 h	100.0	100.0	100.0	38.6	30.8	25.6
21–24 h	100.0	100.0	100.0	31.3	11.7	22.8
	ZnO@SiO ₂ NP			Dead cells		
	1	2	3	1	2	3
1–4 h	101.1	110.2	95.9	0.4	0.3	0.4
3–6 h	64.3	75.7	55.4	0.5	0.4	0.7
21–24 h	41.4	20.2	35.9	0.6	0.5	0.4

Table 13 corresponding to Figure 35

To evaluate the toxicity of treatment with zinc ions (ZnCl_2), ZnO NP, irradiation (4 Gray), and combinations thereof, staining with propidium iodide and annexin V was performed and measured by flow cytometry at different time points in reference to the starting point of the treatment (4 h = 4 h after beginning treatment). Treatment with ZnCl_2 or ZnO NP lasted for four hours, irradiation was applied in parallel three hours after the beginning of the treatment with ZnCl_2 or ZnO NP. After four hours the medium was exchanged for fresh medium. Alive = PI negative and annexin V negative, apoptotic = PI negative, annexin V positive, dead = PI positive and annexin V positive, necrotic = PI positive and annexin V negative.

4 h	100 $\mu\text{g}/\text{mL}$ ZnCl_2						
	1	2	3	4	5	6	7
Alive	91.2626	86.2239	88.9063	92.074	91.19	90.60	90.90
Apoptotic	2.9646	7.0937	5.2203	3.772	2.58	3.50	1.50
Dead	5.6846	6.6602	5.8231	4.072	5.86	5.70	7.30
Necrotic	0.0882	0.0222	0.0502	0.082	0.37	0.30	0.40
	40 $\mu\text{g}/\text{mL}$ ZnCl_2						
	1	2	3	4	5	6	7
Alive	94.4558	92.1307	94.9849	94.4558	93.62	92.10	93.10
Apoptotic	1.6519	2.6939	2.657	1.6519	2.52	2.20	0.90
Dead	3.568	5.1514	2.34	3.568	3.57	5.50	5.40
Necrotic	0.3244	0.024	0.0181	0.3244	0.29	0.30	0.70
	Control						
	1	2	3	4	5	6	7
Alive	90.207	83.088	88.8332	92.57	92.36	91.00	94.70
Apoptotic	2.7946	7.3113	5.9599	2.78	3.49	3.50	1.00
Dead	6.1517	9.5006	5.1163	4.25	3.14	4.80	2.70
Necrotic	0.8468	0.1002	0.0906	0.40	1.01	0.70	1.60
	100 $\mu\text{g}/\text{mL}$ ZnO NP						
	1	2	3	4	5	6	
Alive	91.0182	90.2478	91.6413	90.64	93.20	94.00	
Apoptotic	3.2563	2.7466	3.9472	1.55	2.00	1.20	
Dead	5.6327	6.9673	4.3785	7.73	4.70	4.40	
Necrotic	0.0928	0.0384	0.033	0.08	0.20	0.40	
	100 $\mu\text{g}/\text{mL}$ ZnO NP + 4 Gray						
	1	2	3	4	5	6	
Alive	93.6442	89.9816	91.1903	93.64	95.15	93.30	
Apoptotic	2.4807	4.2293	4.5762	3.19	1.30	1.90	
Dead	3.8111	5.7388	4.2137	3.09	3.47	4.60	
Necrotic	0.0641	0.0503	0.0198	0.08	0.08	0.20	
	4 Gray						
	1	2	3	4	5	6	
Alive	93.2027	82.9701	88.6601	91.69	90.94	90.00	
Apoptotic	2.2858	10.0012	7.786	3.35	3.99	2.50	
Dead	4.3733	7.0006	3.4716	4.65	4.10	6.80	
Necrotic	0.1382	0.028	0.0823	0.31	0.97	0.70	
	100 $\mu\text{g}/\text{mL}$ ZnCl_2 + 4 Gray						
	1	2	3				
Alive	92.73	90.90	89.90				
Apoptotic	3.21	3.30	1.70				
Dead	3.86	5.70	8.20				
Necrotic	0.20	0.10	0.30				

12 h	100 µg/mL ZnCl ₂				
	1	2	3	4	5
Alive	7.9068	7.5228	10.2535	8.1800	15.8300
Apoptotic	7.4681	14.5908	10.0050	6.8300	5.7900
Dead	84.3667	77.8063	78.5853	84.8700	78.1700
Necrotic	0.2584	0.0801	1.1562	0.1200	0.2100
	40 µg/mL ZnCl ₂				
	1	2	3	4	5
Alive	4.2235	3.8697	2.4901	1.8400	3.8300
Apoptotic	4.1915	6.2990	9.6136	3.9300	12.1100
Dead	91.5109	89.8032	87.8662	94.1900	83.8800
Necrotic	0.0741	0.0281	0.0301	0.0400	0.1800
	control				
	1	2	3	4	5
Alive	5.7084	4.2818	3.5175	5.2200	4.1800
Apoptotic	2.0243	4.8771	2.8767	2.4000	3.5400
Dead	92.1192	90.7369	93.4974	91.7300	91.9400
Necrotic	0.1482	0.1042	0.1085	0.6500	0.3400
	100 µg/mL ZnO NP				
	1	2	3	4	5
Alive	8.4443	6.5307	10.9290	6.7700	24.6900
Apoptotic	10.3528	23.8873	22.9272	4.6900	5.8900
Dead	81.1067	69.5598	66.0792	88.4700	69.2300
Necrotic	0.0962	0.0222	0.0647	0.0700	0.1900
	100 µg/mL ZnO NP + 4 Gray				
	1	2	3	4	5
Alive	6.2345	6.9197	4.9621	7.4200	16.1800
Apoptotic	8.7848	10.5050	14.2415	3.9400	7.9000
Dead	84.8766	82.5372	80.7341	88.5500	75.7600
Necrotic	0.1042	0.0381	0.0623	0.0900	0.1600
	4 Gray				
	1	2	3	4	5
Alive	6.6599	8.1127	5.6930	5.8100	4.0700
Apoptotic	2.9080	9.3556	9.4184	4.3600	4.2800
Dead	90.1816	82.4792	84.8482	89.4900	91.2300
Necrotic	0.2505	0.0525	0.0404	0.3400	0.4200
	100 µg/mL ZnCl ₂ + 4 Gray				
	1	2	3		
Alive	8.3100	11.4300	9.8700		
Apoptotic	7.2000	6.7000	6.9500		
Dead	84.4100	81.2400	82.8250		
Necrotic	0.0800	0.1300	0.1050		

18 h	100 µg/mL ZnCl ₂					
	1	2	3	4	5	
Alive	5.8290	22.4412	24.6000	20.0400	12.0000	
Apoptotic	7.6758	11.9150	8.3100	5.8600	7.9000	
Dead	86.2465	65.4251	66.2800	73.3800	78.8000	
Necrotic	0.2486	0.2188	0.8100	0.7200	1.3000	
	40 µg/mL ZnCl ₂					
	1	2	3	4	5	
Alive	11.6399	4.6156	4.3300	5.7900	5.7000	
Apoptotic	8.4901	10.6145	10.6000	17.4700	9.4000	
Dead	79.5610	84.7216	84.7900	76.5000	83.7000	
Necrotic	0.3090	0.0482	0.2800	0.2400	1.3000	
	Control					
	1	2	3	4	5	6
Alive	3.1049	11.0271	3.9824	2.3200	2.0300	3.6000
Apoptotic	2.1790	13.6128	5.6898	3.0100	1.6300	1.0000
Dead	94.1960	75.2116	90.1848	93.9800	95.7300	94.4000
Necrotic	0.5202	0.1484	0.1429	0.6900	0.6100	0.9000
	100 µg/mL ZnO NP					
	1	2	3	4	5	6
Alive	18.0604	13.8179	15.7888	2.9400	23.5000	11.9000
Apoptotic	14.0613	23.6763	12.3847	5.6100	5.7200	3.8000
Dead	67.3829	62.4212	71.4366	91.0400	70.3200	83.7000
Necrotic	0.4954	0.0846	0.3898	0.4100	0.4700	0.7000
	100 µg/mL ZnO NP + 4 Gray					
	1	2	3	4	5	6
Alive	13.9264	10.1201	10.5910	5.7800	24.0200	8.9000
Apoptotic	12.0742	17.6578	15.7427	8.3400	5.2600	9.3000
Dead	73.7656	72.0190	73.5899	85.8100	70.1200	80.7000
Necrotic	0.2338	0.2031	0.0764	0.0700	0.6000	1.1000
	4 Gray					
	1	2	3	4	5	6
Alive	8.8933	17.1183	3.4446	3.5100	2.5300	2.8000
Apoptotic	6.2203	24.1508	7.7186	4.8400	4.0400	1.2000
Dead	84.6157	58.5903	88.7134	91.3100	92.4700	95.5000
Necrotic	0.2707	0.1406	0.1234	0.3400	0.9600	0.5000
	100 µg/mL ZnCl ₂ + 4 Gray					
	1	2	3			
Alive	23.77	16.20	10.00			
Apoptotic	7.59	6.90	9.90			
Dead	68.01	76.45	79.30			
Necrotic	0.63	0.45	0.90			

24 h	100 µg/mL ZnCl ₂						
	1	2	3	4	5	6	
Alive	88.5162	58.8499	68.9064	74.5660	60.7300	63.2100	
Apoptotic	4.5763	15.9153	12.6880	10.1700	13.1400	13.0400	
Dead	0.3044	0.0883	0.5792	0.5640	0.9400	1.1300	
Necrotic	6.6031	25.1465	17.8264	14.7000	25.1900	22.6200	
	40 µg/mL ZnCl ₂						
	1	2	3	4	5	6	
Alive	67.6032	81.3319	67.9949	59.6400	89.5200	70.0000	
Apoptotic	14.7926	12.5699	25.3363	22.0700	6.8300	18.6000	
Dead	0.2689	0.0303	0.0791	0.4900	0.2100	0.5200	
Necrotic	17.3353	6.0680	6.5897	17.8000	3.4400	10.8800	
	Control						
	1	2	3	4	5	6	7
Alive	86.73620	75.37110	90.53210	92.17000	92.17000	94.16000	92.40000
Apoptotic	3.33355	13.86910	4.43310	3.78000	3.05000	2.96000	2.00000
Dead	0.80580	0.06220	0.14740	0.30000	0.72000	0.58000	1.30000
Necrotic	9.12250	10.69770	4.88740	3.75000	4.06000	2.30000	4.40000
	100 µg/mL ZnO NP						
	1	2	3	4	5	6	7
Alive	59.1239	52.0379	33.0070	72.6500	63.0900	51.5300	70.0000
Apoptotic	13.0734	23.8628	18.4389	6.8000	10.2100	7.3400	12.8000
Dead	1.1012	0.0930	3.0417	0.5200	0.3600	1.9700	3.0000
Necrotic	26.7015	24.0063	45.5124	20.0300	26.3400	39.1600	16.9000
	100 µg/mL ZnO NP + 4 Gray						
	1	2	3	4	5	6	7
Alive	67.4404	66.8339	57.4133	67.5500	80.6000	61.2700	71.7000
Apoptotic	7.9393	21.7337	29.7079	12.0400	8.5000	7.0500	17.7000
Dead	0.5974	0.0789	0.0910	0.5000	0.3900	0.8700	0.3000
Necrotic	24.0229	11.3535	12.7877	19.9100	10.5100	30.8100	10.3000
	4 Gray						
	1	2	3	4	5	6	
Alive	87.0891	66.3566	76.5048	90.0900	91.5900	92.0300	
Apoptotic	4.9293	19.0113	15.1715	6.2600	5.3000	4.6500	
Dead	0.1487	0.1386	0.0495	0.1000	0.3400	0.7600	
Necrotic	7.8330	14.4935	8.2742	3.5500	2.7700	2.5600	
	100 µg/mL ZnCl ₂ + 4 Gray						
	1	2	3				
Alive	74.092	61.27	66.04				
Apoptotic	8.812	16.20	11.98				
Dead	0.834	0.64	1.44				
Necrotic	16.262	21.89	20.54				

48 h	100 µg/mL ZnCl ₂						
	1	2	3	4	5	6	
Alive	49.8931	48.3441	47.0519	39.7300	55.4500	47.3700	
Apoptotic	21.9824	22.4868	25.7365	24.6500	21.8700	23.6300	
Dead	1.4785	1.4208	0.8374	2.1600	1.8400	2.3000	
Necrotic	26.6460	27.7483	26.3742	33.4600	20.8400	26.7000	
	40 µg/mL ZnCl ₂						
	1	2	3	4	5	6	
Alive	88.6891	89.9445	79.6986	71.6800	93.3200	74.8600	
Apoptotic	4.9839	5.3963	15.1006	20.9100	4.3000	15.0900	
Dead	0.2114	0.1070	0.0987	0.5600	0.3500	1.0700	
Necrotic	6.1156	4.5522	5.1021	6.8500	2.0300	8.9800	
	Control						
	1	2	3	4	5	6	7
Alive	86.40370	91.20050	80.99510	89.27000	93.94000	96.38000	94.00000
Apoptotic	3.14980	3.55220	4.87940	6.81000	2.59000	1.30000	1.20000
Dead	0.37510	0.17420	0.42480	0.18000	0.65000	0.47000	0.70000
Necrotic	10.07140	5.07000	13.70070	3.74000	2.82000	1.85000	4.20000
	100 µg/mL ZnO NP						
	1	2	3	4	5	6	7
Alive	22.2724	30.6995	11.2840	40.5200	58.8300	22.1000	54.9000
Apoptotic	24.9410	16.6538	17.1784	17.4100	17.1500	24.8100	13.4000
Dead	1.7254	0.5890	1.9758	3.8300	1.6700	7.6300	2.7000
Necrotic	51.0612	52.0576	69.5618	38.2400	22.3500	45.4600	29.1000
	100 µg/mL ZnO NP + 4 Gray						
	1	2	3	4	5	6	7
Alive	43.0330	64.2390	51.0856	17.1800	71.0200	23.9600	67.1000
Apoptotic	16.9353	23.5194	32.8440	20.3800	17.6800	23.1400	18.2000
Dead	1.4955	0.3185	0.5408	6.1300	0.5900	5.6100	0.6000
Necrotic	38.5362	11.9231	15.5200	56.3100	10.7100	47.2900	14.1000
	4 Gray						
	1	2	3	4	5	6	
Alive	85.5929	84.2536	75.6302	80.5900	88.8400	93.5600	
Apoptotic	8.3077	11.3161	13.1473	14.3900	7.6600	3.7900	
Dead	0.3722	0.0863	0.1980	0.2800	0.5100	0.7000	
Necrotic	5.7273	4.3440	11.0245	4.7400	2.9900	1.9500	
	100 µg/mL ZnCl ₂ + 4 Gray						
	1	2	3				
Alive	39.04	51.61	47.91				
Apoptotic	21.63	22.05	20.93				
Dead	2.89	1.81	2.55				
Necrotic	36.44	24.53	28.61				

72 h	100 µg/mL ZnCl ₂						
	1	2	3	4	5	6	
Alive	33.7523	42.3638	31.5138	28.4100	62.7600	41.0400	
Apoptotic	42.1960	38.9712	43.8660	38.6800	27.6900	38.4900	
Dead	1.2611	1.3395	1.4514	7.8300	1.3500	2.9200	
Necrotic	22.7906	17.3255	23.1688	25.0800	8.2000	17.5500	
	40 µg/mL ZnCl ₂						
	1	2	3	4	5	6	
Alive	84.2007	86.9157	88.0814	57.9900	94.5700	78.3200	
Apoptotic	9.9525	5.7206	6.4106	26.9800	3.1400	14.7600	
Dead	0.2557	0.1223	0.2325	3.2700	0.3900	1.6700	
Necrotic	5.5911	7.2414	5.2755	11.7600	1.9000	5.2500	
	Control						
	1	2	3	4	5	6	7
Alive	88.09320	90.96110	91.39600	84.36000	94.46000	93.75000	91.90000
Apoptotic	5.40620	1.62270	3.39730	9.13000	2.25000	2.44000	3.10000
Dead	0.25190	0.24440	0.27070	0.49000	0.62000	0.80000	0.40000
Necrotic	6.24870	7.17180	4.93610	6.02000	2.67000	3.01000	4.60000
	100 µg/mL ZnO NP						
	1	2	3	4	5	6	7
Alive	8.8876	28.9871	17.0161	28.7800	15.1800	20.5200	26.4000
Apoptotic	32.7121	30.0197	17.7942	31.3600	27.3100	36.0000	33.4000
Dead	5.5712	4.6898	2.4353	11.7600	7.9200	6.5900	6.4000
Necrotic	52.8292	36.3035	62.7544	28.1000	49.5900	34.2400	33.8000
	100 µg/mL ZnO NP + 4 Gray						
	1	2	3	4	5	6	
Alive	15.0111	59.7930	42.5906	16.2300	13.8000	63.8000	
Apoptotic	34.0588	30.0666	38.3856	36.1200	37.3600	26.8000	
Dead	2.3961	0.4598	1.3648	11.3200	9.5100	1.2000	
Necrotic	48.5340	9.6807	17.6590	36.3300	39.3300	8.2000	
	4 Gray						
	1	2	3	4	5	6	
Alive	78.2458	84.2855	85.9018	85.5900	90.6600	87.8800	
Apoptotic	17.0584	4.9224	8.2661	9.1400	6.1500	7.3700	
Dead	0.1612	0.2389	0.2038	0.4700	0.6100	0.8800	
Necrotic	4.5346	10.5531	5.6283	4.8000	2.5800	3.8700	
	100 µg/mL ZnCl ₂ + 4 Gray						
	1	2	3				
Alive	32.18	52.62	38.38				
Apoptotic	35.63	32.74	38.30				
Dead	11.04	2.23	3.36				
Necrotic	21.15	12.41	18.96				

96 h	100 µg/mL ZnCl ₂				
	1	2	3	4	
Alive	20.9000	55.9300	39.8600	55.9000	
Apoptotic	54.6300	33.5900	44.5700	33.5000	
Dead	1.2000	2.6400	2.1200	2.1000	
Necrotic	23.2700	7.8400	13.4500	8.6000	
	40 µg/mL ZnCl ₂				
	1	2	3	4	
Alive	77.5900	90.1700	77.2900	88.8000	
Apoptotic	13.0500	5.4600	16.0000	7.2000	
Dead	0.6400	1.0200	1.8000	0.5000	
Necrotic	8.7200	3.3500	4.9100	3.6000	
	Control				
	1	2	3	4	5
Alive	89.27000	89.45000	93.10000	83.40000	78.50000
Apoptotic	7.13000	4.72000	2.53000	8.40000	12.00000
Dead	0.19000	1.36000	0.91000	0.60000	0.60000
Necrotic	3.41000	4.47000	3.46000	7.70000	8.90000
	100 µg/mL ZnO NP				
	1	2	3	4	5
Alive	25.7900	22.5200	36.1000	62.3000	22.5200
Apoptotic	43.4700	40.4500	43.4000	27.0000	40.4500
Dead	1.2300	6.5900	3.8000	2.1000	6.5900
Necrotic	29.5100	30.4400	16.7000	8.6000	30.4400
	100 µg/mL ZnO NP + 4 Gray				
	1	2	3	4	5
Alive	23.8000	60.6500	16.5300	52.4000	43.6000
Apoptotic	41.6300	30.4000	41.8400	37.3000	45.7000
Dead	1.9200	2.5500	7.6100	1.8000	1.3000
Necrotic	32.6500	6.4000	34.0200	8.6000	9.4000
	4 Gray				
	1	2	3	4	
Alive	76.8000	86.1500	89.0400	76.4000	
Apoptotic	18.8500	9.4700	5.4100	15.3000	
Dead	0.0700	1.1100	0.9400	0.4000	
Necrotic	4.2800	3.2700	4.6100	7.9000	
	100 µg/mL ZnCl ₂ + 4 Gray				
	1	2	3		
Alive	21.88	49.68	33.66		
Apoptotic	50.58	40.34	48.65		
Dead	1.31	2.16	2.86		
Necrotic	26.23	7.82	14.83		

Table 14 corresponding to Figure 36

The experiment was performed exactly identical to the one in Table 13 / Figure 35.

HNSCCUM-02T				
1	Apoptotic	Dead	Alive	Necrotic
Control	8.6	7.1	82.2	2.1
4 Gray	8.7	6.4	83.2	1.6
40 µg/mL ZnCl ₂	35.8	36.4	26.60	1.2
100 µg/mL ZnCl ₂	35.8	34.1	27.1	3.1
100 µg/mL ZnCl ₂ + 4 Gray	37	33.2	28.4	1.4
100 µg/mL ZnO NP	27.4	45.7	25.2	1.7
100 µg/mL ZnO NP + 4 Gray	22.8	50.6	24.9	1.7
2	Apoptotic	Dead	Alive	Necrotic
Control	7.1	8.3	82.4	2.2
4 Gray	7.5	7.2	83.2	2.1
40 µg/mL ZnCl ₂	7.9	12.9	55.50	23.8
100 µg/mL ZnCl ₂	21.2	30	29.7	19.1
100 µg/mL ZnCl ₂ + 4 Gray	36.1	44	15.7	4.2
100 µg/mL ZnO NP	20.4	34.6	40.1	4.8
100 µg/mL ZnO NP + 4 Gray	28.6	41.3	26.4	3.6
3	Apoptotic	Dead	Alive	Necrotic
Control	6.6	7.6	83.6	2.2
4 Gray	5.7	9.1	82	3.3
40 µg/mL ZnCl ₂	18.1	27.9	47.50	6.5
100 µg/mL ZnCl ₂	25.3	34.7	27.4	12.6
100 µg/mL ZnCl ₂ + 4 Gray	35.5	47.4	14.5	2.6
100 µg/mL ZnO NP	29.8	39.4	26.2	4.6
100 µg/mL ZnO NP + 4 Gray	17.8	24.8	49.8	7.7
4	Apoptotic	Dead	Alive	Necrotic
Control	5.1	11.9	80.6	2.4
4 Gray	4.2	7.4	83	5.5
40 µg/mL ZnCl ₂	5.4	9.7	52.60	32.3
100 µg/mL ZnCl ₂	18.8	27	30.9	23.4
100 µg/mL ZnCl ₂ + 4 Gray	22.2	32.4	39.7	5.7
100 µg/mL ZnO NP	9.2	29.5	36.4	24.8
100 µg/mL ZnO NP + 4 Gray	15.8	36.7	29.4	18.2
5	Apoptotic	Dead	Alive	Necrotic
Control	4.9	4.2	90	1
4 Gray	8.8	6.3	83	1.8
40 µg/mL ZnCl ₂	40	28.4	31.1	0.5
100 µg/mL ZnCl ₂	40.1	47.8	11.6	0.5
100 µg/mL ZnCl ₂ + 4 Gray	43.2	46.3	10.1	0.4
100 µg/mL ZnO NP	37.7	37.7	24.4	0.1
100 µg/mL ZnO NP + 4 Gray	39.5	35.4	24.9	0.2

HeLa				
1	Apoptotic	Dead	Alive	Necrotic
Control	7.4	4	87.9	0.6
4 Gray	13.5	13.9	70.7	1.9
40 µg/mL ZnCl ₂	16.6	20.9	57.7	4.8
100 µg/mL ZnCl ₂	5.3	24.6	66.9	3.2
100 µg/mL ZnCl ₂ + 4 Gray	4.1	28	64.1	3.8
100 µg/mL ZnO NP	10.4	36.2	33.3	20.1
100 µg/mL ZnO NP + 4 Gray	9.9	33	35.3	21.7
2	Apoptotic	Dead	Alive	Necrotic
Control	7.9	4.7	86.8	0.6
4 Gray	14.4	8.6	76.1	0.9
40 µg/mL ZnCl ₂	16.8	20.3	60.7	2.3
100 µg/mL ZnCl ₂	4.3	20.9	67.7	7.1
100 µg/mL ZnCl ₂ + 4 Gray	6.3	23.8	67.8	2
100 µg/mL ZnO NP	6.8	30	28.6	34.7
100 µg/mL ZnO NP + 4 Gray	3.4	9.1	42.2	45.3
3	Apoptotic	Dead	Alive	Necrotic
Control	2.7	3.4	93.3	0.5
4 Gray	5	6.4	84.3	4.3
40 µg/mL ZnCl ₂	5.3	8.4	69.2	17.1
100 µg/mL ZnCl ₂	0.3	7.8	61.3	30.6
100 µg/mL ZnCl ₂ + 4 Gray	1.2	18	67.7	13.1
100 µg/mL ZnO NP	1.1	3.5	40.8	54.6
100 µg/mL ZnO NP + 4 Gray	2.8	9.7	36.9	50.7
4	Apoptotic	Dead	Alive	Necrotic
Control	16	4.6	78.1	16
4 Gray	10.5	5.2	81.2	10.5
40 µg/mL ZnCl ₂	6.3	8.4	70.4	6.3
100 µg/mL ZnCl ₂	5.8	8.8	52.6	5.8
100 µg/mL ZnCl ₂ + 4 Gray				
100 µg/mL ZnO NP	4.7	10.3	48.7	4.7
100 µg/mL ZnO NP + 4 Gray	8	11	50.3	8
T24				
1	Apoptotic	Dead	Alive	Necrotic
Control	7.2	5.1	86.8	1
4 Gray	7.3	6.1	85.6	1
40 µg/mL ZnCl ₂	5.5	9.5	63.3	21.7
100 µg/mL ZnCl ₂	2.3	14.6	48	35.1
100 µg/mL ZnCl ₂ + 4 Gray	2.4	21.8	43.9	31.9
100 µg/mL ZnO NP	1.2	12.5	58.2	28
100 µg/mL ZnO NP + 4 Gray	1.6	14.1	57.9	26.3
2	Apoptotic	Dead	Alive	Necrotic
Control	4.7	4.6	89.9	0.9
4 Gray	12	12.7	73.4	1.8
40 µg/mL ZnCl ₂	3.3	4	70.1	22.6
100 µg/mL ZnCl ₂	4.9	27.8	47	20.3
100 µg/mL ZnCl ₂ + 4 Gray	3.9	30.2	44	21.9
100 µg/mL ZnO NP	1.8	17.8	39.6	40.8
100 µg/mL ZnO NP + 4 Gray	4.3	31	41.9	22.8
3	Apoptotic	Dead	Alive	Necrotic
Control	4.6	3.4	91.4	0.7
4 Gray	13.5	11.9	72.4	2.2
40 µg/mL ZnCl ₂	10.1	15.5	57.7	16.8
100 µg/mL ZnCl ₂	5	27	39.5	28.6
100 µg/mL ZnCl ₂ + 4 Gray	6	30.4	37.8	25.8
100 µg/mL ZnO NP	2.7	21.5	41.6	34.2
100 µg/mL ZnO NP + 4 Gray	2.9	24.7	42.7	29.7

Table 15 corresponding to Figure 37

To evaluate the cell cycle distribution, A549 cells were harvested at the indicated time points after beginning the corresponding treatment, permeabilized, and stained with propidium iodide. Shorter timepoints were also measured (data not shown) but no changes in the cell cycle distribution were seen. Staining was measured and analysed on linear scale and corrected for doublets.

1		G1	S	G2	Debris
24 h	4 Gray	66.5	2.2	24.5	1.9
	40 µg/mL ZnCl ₂	64.2	11.4	16.8	2.9
	100 µg/mL ZnCl ₂ + 4 Gray	51.8	16.8	10.9	11.8
	100 µg/ml ZnCl ₂	52	16.8	10.5	9.8
	Control	58.7	14.2	13.9	1.2
	100 µg/mL ZnO NP + 4 Gray	53.5	18.6	13.4	7.5
	100 µg/mL ZnO NP	58.6	14.2	14.1	5.7
48 h	4 Gray	78.1	3.6	10.6	1.4
	40 µg/mL ZnCl ₂	76.9	9.6	8.7	3.1
	100 µg/mL ZnCl ₂ + 4 Gray	37.8	11	15.2	25.8
	100 µg/ml ZnCl ₂	38.3	16.1	8.6	25.2
	Control	81.1	7.5	10.1	0.6
	100 µg/mL ZnO NP + 4 Gray	46.2	11.2	17.7	16
	100 µg/mL ZnO NP	54.8	15.3	12.8	15.1
72 h	4 Gray	69.5	5.3	5.1	8.4
	40 µg/mL ZnCl ₂	69.5	7.4	5.3	4.8
	100 µg/mL ZnCl ₂ + 4 Gray	29.8	13	12.3	29.5
	100 µg/ml ZnCl ₂	46.7	14.7	15.5	15.8
	Control	86.2	4.1	7.9	0.4
	100 µg/mL ZnO NP + 4 Gray	34.9	10.3	12.8	21.7
	100 µg/mL ZnO NP	34	16.6	10	24.2
96 h	4 Gray	74	4.9	12.4	2.8
	40 µg/mL ZnCl ₂	69.5	7.4	5.3	4.8
	100 µg/mL ZnCl ₂ + 4 Gray	29.8	9	2.6	41.1
	100 µg/ml ZnCl ₂	44.9	15.3	2.2	33.1
	Control	81.5	2.4	3	5.7
	100 µg/mL ZnO NP + 4 Gray	44.7	11.7	9.5	24.6
	100 µg/mL ZnO NP	14.7	4	3.7	64.8
2		G1	S	G2	Debris
24 h	4 Gray	70.3	7.1	19.3	0.9
	40 µg/mL ZnCl ₂	46.9	27.7	19.9	2.6
	100 µg/mL ZnCl ₂ + 4 Gray	77.5	7	3.6	10.7
	100 µg/ml ZnCl ₂	75.5	7.7	3.4	12.3
	Control	63.8	19.6	14.2	0.7
	100 µg/mL ZnO NP + 4 Gray	65.2	17	6.8	6.2
	100 µg/mL ZnO NP	73.1	11.9	3	10.4
48 h	4 Gray	63.2	11.3	7.6	13
	40 µg/mL ZnCl ₂	62.7	17.1	15.2	3.4
	100 µg/mL ZnCl ₂ + 4 Gray	58.3	10.2	3.5	24
	100 µg/ml ZnCl ₂	56.5	12.6	3.6	24.4
	Control	68.8	16.4	13.3	0.6
	100 µg/mL ZnO NP + 4 Gray	63.2	11.3	7.6	13
	100 µg/mL ZnO NP	48.1	17.7	3.9	25.5
72 h	4 Gray	74.3	5.2	15.1	1.7
	40 µg/mL ZnCl ₂	74.5	8.7	14.4	1.3
	100 µg/mL ZnCl ₂ + 4 Gray	38.5	10.8	1.8	45.1
	100 µg/ml ZnCl ₂	50.1	14.8	5.1	26
	Control	79	8.6	9.7	0.9
	100 µg/mL ZnO NP + 4 Gray	60.7	12.6	8.4	13.7
	100 µg/mL ZnO NP	33.6	9.8	3.1	47.9
96 h	4 Gray	73.3	4.1	15.7	3.6
	40 µg/mL ZnCl ₂	77.1	6.1	10.6	4.3

	100 µg/mL ZnCl ₂ + 4 Gray	37.9	8.1	4.4	46.4
	100 µg/ml ZnCl ₂	38.1	8.1	4.4	45.9
	Control	86.3	3	7.3	1.8
	100 µg/mL ZnO NP + 4 Gray	47.3	7.6	8	32.1
	100 µg/mL ZnO NP	49.9	12.3	6.3	29.8
	3	G1	S	G2	Debris
24 h	4 Gray	56	3.3	5.5	2.5
	40 µg/mL ZnCl ₂	39.9	10.2	9.3	8.1
	100 µg/mL ZnCl ₂ + 4 Gray	43.5	14.7	8.6	17.8
	100 µg/ml ZnCl ₂	44.1	18.7	8.5	16
	Control	48.7	15	6.9	2.5
	100 µg/mL ZnO NP + 4 Gray	46.6	10.6	18.3	9.2
	100 µg/mL ZnO NP	38.2	13.8	13.7	14.8
48 h	4 Gray	54.7	1.5	12.2	2.7
	40 µg/mL ZnCl ₂	55.3	8.8	8.4	7.5
	100 µg/mL ZnCl ₂ + 4 Gray	38.5	8.6	13	30.5
	100 µg/ml ZnCl ₂	33.9	12.7	6.9	33.7
	Control	70.3	14	4.9	1
	100 µg/mL ZnO NP + 4 Gray	31.2	8.9	11.5	33.8
	100 µg/mL ZnO NP	30.7	7.3	11.4	37.8
72 h	4 Gray	66.9	3.1	16.4	1.7
	40 µg/mL ZnCl ₂	62.3	4.3	8.6	2.6
	100 µg/mL ZnCl ₂ + 4 Gray	28.9	10.5	7.9	47.3
	100 µg/ml ZnCl ₂	30.5	11.2	8.6	45.9
	Control	52.6	2	3.7	1.8
	100 µg/mL ZnO NP + 4 Gray	23.5	3.1	11.7	25.4
	100 µg/mL ZnO NP	27.8	8.3	9.4	34.4
96 h	4 Gray	41.5	2.8	9.4	12.6
	40 µg/mL ZnCl ₂	45.6	2.6	8.5	7.9
	100 µg/mL ZnCl ₂ + 4 Gray	17.3	3.8	6	69.7
	100 µg/ml ZnCl ₂	14.2	5.2	4.6	71.5
	Control	45.3	0.7	2.3	4.3
	100 µg/mL ZnO NP + 4 Gray	19.6	5.9	6.5	63.2
	100 µg/mL ZnO NP	45.6	7.7	13.7	30.2

Table 16 corresponding to Figure 39

To measure the mitochondrial superoxide level after treatment with ZnO NP MitoSOX™ Red was used. In order to correct for differences between the runs all values are expressed in reference to untreated control cells (=100%).

	1	2	3	4	5	6	7	8
Untreated control	100.00	100.00	100.00	100.00	100.00	100.00	100.00	100.00
4 h	95.00	122.00	103.00					
8 h	77.00	102.00	134.00					
12 h	84.00	96.00	109.00	127.00	114.00	145.00	128.00	165.00
16 h	91.00	104.00	131.00	142.00				
20 h	142.00	176.00	238.00	161.00				
24 h	153.00	199.00	218.00	343.00	293.00	320.00	274.00	380.00
48 h	197.00	190.00	280.00	316.00				
72 h	315.00	142.00	268.00	230.00				
96 h	330.00	296.00	374.00	516.00				
Positive control	450.00	263.00	303.00	385.00	447.00	601.00	595.00	788.00

Table 17 corresponding to Figure 40

The release of cytochrome c from the mitochondria was measured as described in the materials and methods section. The values represent fluorescence in arbitrary units (AU). The higher the fluorescence is the greater is the cytochrome c release.

	1	2	3
Untreated control	3.38	1.58	1.22
12 h	13.82	16.40	20.98
16 h	26.44	21.38	32.90
20 h	33.35	14.10	36.06
24 h	45.70	25.57	49.45

Table 18 corresponding to Figure 41

The expression of the proteins was evaluated via western blot and SDS-PAGE. The expression levels are expressed in reference to the expression level in A549 cells in order to be able to compare between the different cell lines. In order to correct for loading difference between the lanes, stain-free gels were used as loading control.

	A549			HeLa		
	1	2	3	1	2	3
P53	100.0	100.0	100.0	48.0	27.0	13.0
Bax	100.0	100.0	100.0	31.0	24.0	57.0
Bcl-xL	100.0	100.0	100.0	27.0	24.0	46.0
Caspase-9	100.0	100.0	100.0	192.0	221.0	185.6
	HNSCCUM-02T			T24		
	1	2	3	1	2	3
P53	546.0	678.0	204.0	48.0	22.0	11.0
Bax	27.0	20.0	43.0	74.0	41.0	105.0
Bcl-xL	58.0	66.0	77.0	133.0	105.0	153.0
Caspase-9	75.0	89.0	45.1	141.0	118.0	60.3

Table 19 corresponding to Figure 42

The expression of the proteins was evaluated via western blot and SDS-PAGE. The expression levels are expressed in reference to the untreated control cells of the corresponding cell line. All samples (one run, all cell lines, three samples) were loaded onto one gel, to make values directly comparable. In order to correct for loading difference between the lanes, stain-free gels were used as loading control.

P53	Untreated control			4 h after treatment with 100 µg/mL ZnO NP			20 h after treatment with 100 µg/mL ZnO NP		
	1	2	3	1	2	3	1	2	3
A549	100.0	100.0	100.0	210.0	201.0	254.0	161.0	112.0	227.0
HeLa	100.0	100.0	100.0	123.0	358.0	347.0	95.0	175.0	197.0
HNSCCUM-02T	100.0	100.0	100.0	43.0	60.0	47.0	14.0	18.0	20.0
T24	100.0	100.0	100.0	71.0	66.0	123.0	57.0	40.0	92.0
Bax	Untreated control			4 h after treatment with 100 µg/mL ZnO NP			20 h after treatment with 100 µg/mL ZnO NP		
	1	2	3	1	2	3	1	2	3
A549	100.0	100.0	100.0	86.0	82.0	130.0	29.0	56.0	79.0
HeLa	100.0	100.0	100.0	97.0	93.0	69.0	21.0	32.0	23.0
HNSCCUM 02T	100.0	100.0	100.0	65.0	102.0	81.0	9.0	27.0	15.0
T24	100.0	100.0	100.0	104.0	73.0	92.0	43.0	38.0	76.0

Bcl-xL	Untreated control			4 h after treatment with 100 µg/mL ZnO NP			20 h after treatment with 100 µg/mL ZnO NP		
	1	2	3	1	2	3	1	2	3
A549	100.0	100.0	100.0	77.0	78.0	106.0	47.0	57.0	97.0
HeLa	100.0	100.0	100.0	79.0	106.0	89.0	35.0	71.0	35.0
HNSCCUM 02T	100.0	100.0	100.0	50.0	106.0	96.0	19.0	57.0	32.0
T24	100.0	100.0	100.0	115.0	97.0	92.0	55.0	95.0	81.0
Caspase-9	Untreated control			4 h after treatment with 100 µg/mL ZnO NP			20 h after treatment with 100 µg/mL ZnO NP		
	1	2	3	1	2	3	1	2	3
A549	100.0	100.0	100.0	63.0	80.0	56.3	37.0	69.0	110.5
HeLa	100.0	100.0	100.0	71.0	83.0	85.6	48.0	56.0	60.1
HNSCCUM 02T	100.0	100.0	100.0	47.0	65.0	40.9	20.0	24.0	10.4
T24	100.0	100.0	100.0	63.0	64.0	95.8	37.0	56.0	69.4

Table 20 corresponding to Figure 43

To evaluate the toxicity of ZnO NP in different cell types A549 cells, endothelial cells and fibroblasts were incubated with different amounts of nanoparticles, as indicated, and their viability was measured via the cellular metabolic activity, after 4 h, after 8 h, after 12 h, and after 24 h after beginning treatment. "1–4 h" refers to the timespan the alamar Blue® reagent was incubated with the cells in relation to the start point of the treatment. All values are stated in reference to untreated control cells (=100%) to correct for differences between the runs of the experiment.

100 µg/mL ZnO NP				
A549	1	2	3	4
1–4 h	31.1	30.2	14.9	15.0
5–8 h	49.6	19.6	42.6	36.2
9–12 h	51.9	20.7	29.2	21.1
21–24 h	37.1	18.3	20.5	6.1
Endothelial cells	1	2	3	4
1–4 h	23.8	15.2	11.5	8.4
5–8 h	21.4	12.5	13.7	10.2
9–12 h	8.9	2.6	2.7	2.0
21–24 h	2.5	0.2	0.7	0.2
Fibroblasts	1	2	3	4
1–4 h	29.4	28.4	15.9	18.8
5–8 h	60.4	7.0	29.7	9.2
9–12 h	45.0	1.2	3.5	2.1
21–24 h	23.7	0.8	1.2	0.8
50 µg/mL ZnO NP				
A549	1	2	3	4
1–4 h	46.7	43.1	20.6	29.3
5–8 h	67.0	76.3	80.3	88.7
9–12 h	84.6	84.7	68.6	39.7
21–24 h	69.3	94.7	43.1	47.8
Endothelial cells	1	2	3	4
1–4 h	42.4	62.7	27.9	31.7
5–8 h	67.7	79.2	90.3	52.0
9–12 h	30.8	69.6	9.6	9.8
21–24 h	57.3	62.2	18.7	10.5
Fibroblasts	1	2	3	4
1–4 h	53.3	57.2	40.7	24.5
5–8 h	84.2	80.7	135.6	96.8
9–12 h	103.2	86.7	169.1	76.6
21–24 h	68.4	90.8	173.1	84.5

10 µg/mL ZnO NP				
A549	1	2	3	4
1–4 h	100.0	74.2	91.9	107.3
5–8 h	101.3	98.7	108.9	108.8
9–12 h	107.8	97.8	108.3	111.2
21–24 h	87.1	109.4	107.1	100.3
Endothelial cells	1	2	3	4
1–4 h	61.9	64.0	61.2	53.6
5–8 h	88.8	99.4	174.2	107.9
9–12 h	97.9	107.1	155.2	90.1
21–24 h	99.4	101.2	121.7	107.9
Fibroblasts	1	2	3	4
1–4 h	96.8	86.0	99.4	94.0
5–8 h	94.7	95.2	177.6	106.4
9–12 h	103.0	93.9	174.9	129.9
21–24 h	99.5	100.3	185.5	110.5

Table 21 corresponding to Figure 44

The first part of the table shows the number of colonies that were counted ten days after the corresponding treatment and the second part shows the calculated surviving fractions.

Colonies	1	2	3	4
Untreated	716	632	617	539
4 Gray	562	399	331	280
NP	88	158	81	76
NP + 4 Gray	35	10	10	11
4 Gray -> NP	24	11	23	79
NP -> 4 Gray	23	19	9	32

Surviving Fraction	1	2	3	4
Untreated	1.000	1.000	1.000	1.000
4 Gray	0.785	0.632	0.536	0.520
NP	0.061	0.087	0.046	0.049
NP + 4 Gray	0.007	0.002	0.002	0.002
4 Gray -> NP	0.005	0.002	0.004	0.015
NP -> 4 Gray	0.004	0.003	0.001	0.006

R code for the computation of the beta regression:

```
# Install packages
install.packages("betareg")
install.packages("foreign")
# Load packages
library(betareg)
library(foreign)
# Load data
setwd("C:/Users/wiesm/Desktop/17 CFA Radiosensitizer/Regression Auswertung mit IMBEI")
data <- read.spss(file = "CFA_linear_regression_1.sav",
                 use.value.labels = TRUE,
                 to.data.frame = TRUE,
                 use.missings = TRUE)
# Surviving-fraction set to 0.999
data$SF_new <- data$SF
data$SF_new[data$SF_new==1] <- 0.999
# Beta regression
fit <- betareg(SF_new ~ Irrad_Gy + NP + Interact, data=data)
# How good is the model?
predict(fit, data)
# 4G, no NP
mean(c(0.7855,0.6318,0.5361,0.5200))
# Observed: 0.61835
# Predicted: 0.623952907
# 0G, NP
mean(c(0.0615,0.0873,0.0460,0.0491))
# Observed: 0.060975
# Predicted: 0.066602582
# 4G, NP
mean(c(0.0069,0.0015,0.0016,0.0020))
# Observed: 0.003
# Predicted: 0.008585491
# Coefficients and p-values?
summary(fit)
```


13 Acknowledgement

No doctoral thesis is created in a vacuum and finally handing in this work would not have been possible without the help of all the people who supported me.

First and foremost, I would like to thank my doctoral supervisor [REDACTED]. As my scientific mentor, he challenged as well as supported me and it was a great pleasure to work with him. He really lives an “open-door policy” and I was always welcome to come in—with good news as well as with bad news. He has experienced all the ups and downs of this doctoral thesis with me, pushing me constantly to the next level. [REDACTED] fulfilled the German term “Doktorvater” for the doctoral supervisor in every respect.

I sincerely also thank [REDACTED] my co-supervisor, for many fruitful discussions and the very good collaboration. Every meeting with him opened new perspectives and pushed the boundaries of my understanding of what holds the world together at its core.

A lab is nothing without its technical staff, our “good souls”. Special gratitude goes to [REDACTED]. Without their constant technical, methodological, and emotional support I would not stand where I am standing now. In good times, we celebrated our successes; and in bad times they reminded me that there is a life outside the lab as well—and that maybe I should go and get some sleep. Moreover, I want to express my special gratitude to my cooperation partners at the Institute of Inorganic Chemistry and Analytical Chemistry, [REDACTED]. [REDACTED] am very grateful that they both didn't think of “interdisciplinary cooperation” as just fine words; but rather a challenge that we took up together. In many instances their chemical understanding complemented by biological perspective and vice versa. I was blessed to have them by my side.

I acknowledge the Max Planck Graduate Center (MPGC) for the financial support of my doctoral thesis, especially for the possibility to attend conferences all around the world. Furthermore, the MPGC brought me into contact with an international and interdisciplinary crowd of other PhD students, creating an inspiring and scientifically fascinating environment for which I am very grateful.

Special thanks also go to [REDACTED] who constantly supported me as my mentor during the doctoral thesis. Her “view from the outside” was always a great help for not getting lost in the data jungle.

Throughout my thesis, I was fortunate to receive great support by [REDACTED] [REDACTED] at the CLSM and [REDACTED] at the flow cytometer for which I would like to sincerely thank them. [REDACTED] deeply advanced my skills at the flow cytometer and she was always available for troubleshooting, for which I want to thank her. Thanks also go to [REDACTED] who provided access to the CLSM in his working group.

I want to thank [REDACTED] especially, and also [REDACTED] [REDACTED] for many hours of fruitful discussion. They restored by faith in doctors in biomedical research. Thanks go to all current and former members of the working group of [REDACTED] [REDACTED] for the good cooperation.

Many thanks go to [REDACTED] who took up the challenge to fine-tune the wording of this thesis and to [REDACTED] was as pedantic as possible when proof-reading this document. They perfectly complemented my own perfectionism in a project this big where perfection cannot be profoundly achieved.

I want to thank all my close friends who constantly supported me and accepted the importance I assigned to this thesis, which might have been difficult to understand from time to time. Special thanks go to [REDACTED] for constantly renewing my faith in science and scientific work.

Finally, I want to express my deep gratitude to my parents [REDACTED] [REDACTED] for their ever-present loving support. By teaching me to get to the heart of things and curiously explore my environment, they paved the way to where I am standing now.

My path was accompanied by great teachers passionate about science, starting with my biology teacher [REDACTED] [REDACTED] during my studies, and finally my doctoral supervisor [REDACTED] They all inspired me to advance my scientific mindset and to all of them I wish to express my sincere thanks.

14 Conference contributions

1st International Conference on 3D Printing in Medicine, 15.–16. April 2016, Mainz, Germany

Poster: Potential Toxicity of Internalized Metal Ions

European Nanomedicine Meeting, 3.–4. April 2017, London, UK

Poster: Improvement of Irradiation Response of Tumor Cells by ZnO Nanoparticles

88th Annual Meeting of the German Society of Oto-Rhino-Laryngology, Head and Neck Surgery, 23.–27. May 2017, Erfurt, Germany

Poster: Zinkoxid-Nanopartikel als Strahlensensitizer in der Behandlung von Kopf-Hals-Tumoren

33. Joint Annual Meeting of the German Society for Minerals and Trace Elements (GMS) with Zinc-UK and Zinc-Net Training School, 28.–30. September 2017, Aachen, Germany

Poster: Analysis of the cellular mechanism of toxicity of zinc oxide nanoparticles aiming at their application in tumor therapy

Annual Meeting of the German Society for Biomaterials (DGBM), 9.–11. November 2017, Würzburg, Germany

Poster: Improvement of the Irradiation Response in Cancer Treatment by ZnO Nanoparticles

Annual Meeting of the American Association for Cancer Research (AACR), 9.–14. April 2018, Chicago, USA

Poster: Metal oxide nanoparticles as adjuvant for radiation therapy

34. Annual Meeting of the German Society for Minerals and Trace Elements (GMS), 7.–9. June 2018, Jena, Germany

Lecture: Zinc oxide nanoparticle convey tumor cell death via induction of oxidative stress and subsequent apoptosis

Annual Meeting of the German Society for Biomaterials (DGBM), 8.–10. November 2018, Braunschweig, Germany

Lecture and poster: Zinc oxide nanoparticles as innovative nanoparticle-based drug support for the improvement of the irradiation response in tumor therapy

20th EMBL PhD Symposium “Game changers - Taking life sciences to the next level”, 22.–24. November 2018, Heidelberg, Germany

Poster: Curing cancer with zinc oxide nanoparticles? - How metal oxide nanoparticles could supplement state-of-the-art cancer therapy.

15 Publications

- Hu, M.; Korschelt, K.; Viel, M.; **Wiesmann, N.**; Kappl, M.; Brieger, J.; Landfester, K.; Thérien-Aubin, H.; Tremel, W. (2018): Nanozymes in Nanofibrous Mats with Haloperoxidase-Like Activity to Combat Biofouling. In: *ACS Applied Materials & Interfaces*, pp. 44722-44730, DOI: 10.1021/acsami.8b16307.
- **Wiesmann, N.**; Gieringer, R.; Grus, F.; Brieger, J. (2018a): Phosphoproteome Profiling Reveals Multifunctional Protein NPM1 as part of the Irradiation Response of Tumor Cells. In: *Translational Oncology* 12 (2), pp. 308-319, DOI: 10.1016/j.tranon.2018.10.015.
- Kluenker, M.; Tahir, M.N.; Dören, R.; Deuker, M.; Komforth, P.; Plana-Ruiz, S.; Barton, B.; Shylin, S.I.; Ksenofontov, V.; Panthöfer, M.; **Wiesmann, N.**; Herzberger, J.; Möller, A.; Frey, H.; Brieger, J.; Kolb, U.; Tremel, W. (2018): Iron Oxide Superparticles with Enhanced MRI Performance by Solution Phase Epitaxial Growth. In: *Chemistry of Materials* 30 (13), pp. 4277-4288, DOI: 10.1021/acs.chemmater.8b01128.
- **Wiesmann, N.**; Kluenker, M.; Demuth, P.; Brenner, W.; Tremel, W.; Brieger, J. (2018b): Zinc overload mediated by zinc oxide nanoparticles as innovative anti-tumor agent. In: *Journal of Trace Elements in Medicine and Biology* 51, pp. 226-234, DOI: 10.1016/j.jtemb.2018.08.002.
- **Wiesmann, N.**; Strozynski, J.; Beck, C.; Zimmermann, N.; Mandler, S.; Gieringer, R.; Schmidtmann, I.; Brieger, J. (2017): Knockdown of hnRNPK leads to increased DNA damage after irradiation and reduces survival of tumor cells. In: *Carcinogenesis* 38 (3), pp. 321-328, DOI: 10.1093/carcin/bgx006.
- Strozynski, J.; Heim, J.; Bunbanjerdasuk, S.; **Wiesmann, N.**; Zografidou, L.; Becker, S.K.; Meierl, A.-M.; Gouveris, H.; Lüddens, H.; Grus, F.; Brieger, J. (2015): Proteomic identification of the heterogeneous nuclear ribonucleoprotein K as irradiation responsive protein related to migration. In: *Journal of Proteomics* 113, pp. 154-161, DOI: 10.1016/j.jprot.2014.09.017.

16 Curriculum Vitae

NADINE WIESMANN



PERSONAL DATA

Date of birth 

Nationality German

EDUCATION

09/2015 – EXPECTED 05/2019

DISSERTATION

Laboratory for Molecular Tumor Biology, Department of Otorhinolaryngology, University Medical Center Mainz

My doctorate dealt with the improvement of radiotherapy for tumor patients with the help of zinc oxide nanoparticles. The project was an interdisciplinary cooperation between the University Medical Center and the Institute of Inorganic Chemistry and Analytical Chemistry which involved close collaboration and teamwork between both disciplines.

10/2012 – 07/2015

MASTER OF SCIENCE BIOMEDICINE

Johannes Gutenberg-University, Mainz

The M. Sc. Biomedicine was especially focused on medical research and the specific requirements that must be met in this field. This involved training in safety in genetic engineering, good clinical practice, and carrying out of animal experiments.

I finalized the M. Sc. Biomedicine with the master thesis “Functional analysis of selected phosphorylation sites of NPM1”

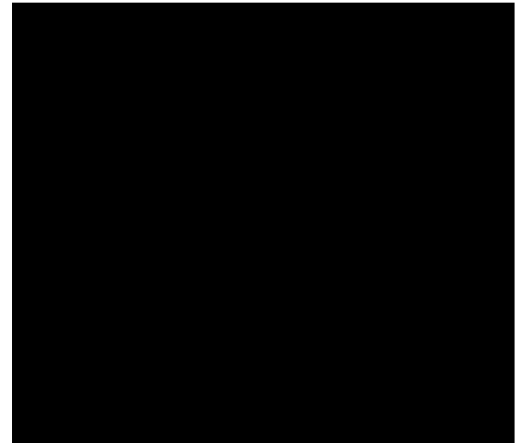
Grade 1.1

10/2012 – 10/2014

STUDY OF APPLIED BIOINFORMATICS

Johannes Gutenberg-University, Mainz

The M. Sc. Applied Bioinformatics was addressed at biologists who strive to deepen their knowledge in Informatics and its application to solve biological problems.



09/2011 – 09/2012

STUDY OF MOLECULAR BIOLOGY AND COMPUTER SCIENCES

Johannes Gutenberg-University, Mainz

While I deepened my knowledge in modern molecular biology, I immersed myself into computer sciences to widen my horizon which also involved training in mathematics and different programming languages.

10/2008 – 09/2011

BACHELOR OF SCIENCE BIOLOGY

Johannes Gutenberg-University, Mainz

The B. Sc. Biology provided me with a broad overview of all disciplines of modern biology.

I finalized the B. Sc. Biology with the bachelor thesis “Knockdown of hnRNP enhances the radiation sensitivity of tumor cells of the respiratory epithelium”

Grade: 1.7

09/2005 – 06/2008

ABITUR

Pestalozzischule, Idstein

I finished my school career with the high-school diploma.

Grade: 1.6

AWARDS AND FELLOWSHIPS

- Since 11/2015 I hold a doctoral fellowship of the Max Planck Graduate Center Mainz which—besides financial support—also includes a special educational curriculum for interdisciplinary exchange and soft skills training.
- 10/2015 I was awarded the Alexander-Karl-Award of the Foundation for Tumor Research Head and Neck endowed with 50'000 Euro as initial funding for young researchers in the field of tumor biology.

TEACHING EXPERIENCES

From 10/2011 until 07/2014 I repeatedly served as student research assistant for the Institute of Botany teaching different courses and supervising students.

FURTHER QUALIFICATIONS

Language skills

German (mother tongue)

English (fluently)

Spanish, French, Polish (basic knowledge)

IT skills

MS Office

Image editing software (Photoshop, Gimp, ImageG, Inkscape)

Basic knowledge of Python, C++, Java